

Inaugural dissertation
for
obtaining the doctoral degree
of the
Combined Faculty of Mathematics, Engineering, and Natural Sciences
of the
Ruprecht-Karls-University
Heidelberg

Presented by
M. Sc. Alexandra Katharina Schöne
born in: Heilbronn-Neckargartach, Germany
Oral examination: 17 December 2024

Living on the edge -
the evolutionary history, edaphic adaptations
and conservation prospects
of the
Cheddar Pink,
Dianthus gratianopolitanus

Referees: Prof. Dr. Marcus Koch
PD Dr. Mike Thiv

Abstract

The Cheddar Pink (*Dianthus gratianopolitanus* Vill., Caryophyllaceae) is an endangered, herbaceous perennial native to Central Europe, currently facing population decline. To understand its evolutionary history and biogeographic patterns, we sampled 130 populations and 1705 individuals across its entire distribution range, from southern France to Poland and the British Isles and used nuclear AFLP data, maternally inherited plastid haplotype variation, whole plastome sequence information, and cytological data.

The absence of spatial genetic variation, the high rate of mixed plastid haplotypes, and the lack of spatial structure in the plastome tree suggest postglacial gene flow, favoring a scenario of once widespread distribution with secondary fragmentation. While AFLP data revealed a genetic division between southern and northern groups, plastid haplotype variation did not show clear biogeographic patterns but did highlight southwestern richness. Differences in bedrock type, calcareous in the south and siliceous in the north, coincide with AFLP groupings, suggesting edaphic factors may influence the differentiation and adaptation of *D. gratianopolitanus*. Genetic and cytological data strongly support the existence of refugia in southern France: Although clear evidence for a northern German/Czech refugium is lacking, the survival of now-extinct small populations in western Germany near Belgium, with subsequent expansion, is a possibility. A third genetic group in Baden-Württemberg, located in the contact zone between northern and southern groups, might result from survival in unknown refugia or represent a melting pot scenario. The colonization of the British Isles likely originated from French populations, specifically from the (Pre-)Alps, expanding through Belgium and into the Isles, as supported by genetic assignment and plastid haplotypes.

To further investigate local adaptations, cuttings of *D. gratianopolitanus* from both calcareous and siliceous regions were cultivated and used in a reciprocal transplant experiment in the Botanical Garden in Heidelberg. After one year of growth on triassic shell limestone, porphyry, and serpentine soils, fitness parameters and leaf elemental composition were assessed. Additionally, flowering time and behavior were recorded for individuals from the entire distribution range, as well as *D. gratianopolitanus* subsp. *moravicus* cultivated in the Botanical Garden in 2022 and 2023, respectively. While the results revealed only small adaptations in elemental uptake they indicated that plants from calcareous bedrock invested more in vegetative growth, potentially enhancing vegetative reproduction and competitiveness on restricted limestone outcrops. In contrast, plants from siliceous origins exhibited higher flowering rates, promoting gene flow and faster colonization in more open habitats. Although a trend towards earlier flowering between 2013 and 2022/23 was observed, higher early spring and summer temperatures alone likely do not suffice to trigger the earlier flowering.

In addition, eleven metapopulations originating from both calcareous and siliceous regions were analyzed using nuclear AFLP data and plastid haplotypes. The genetic structuring revealed varying patterns of connectivity and degrees of isolation, that could indicate either recent gene flow or remnants of past connections. Ecological niche modeling under current and future climate scenarios revealed that southern populations are more affected by drought stress, while northern populations are limited by minimum temperatures. The siliceous group displayed a broader climatic niche, while the more specialized calcareous group might be more vulnerable to climate change. Although current climatic conditions predict a wider suitable area than presently occupied, future scenarios indicate a significant reduction in suitable habitats, with a trend towards higher elevations and northern migrations. These findings underscore the need for conservation strategies that target all subpopulations, preserve genetic variation, and potentially re-establish dispersal routes to ensure the survival of this species.

Zusammenfassung

Die Pfingstnelke (*Dianthus gratianopolitanus* Vill.) ist eine gefährdete, in Mitteleuropa beheimatete krautige mehrjährige Pflanze aus der Familie der Nelkengewächse, deren Bestände derzeit rückläufig sind. Um ihre Evolutionsgeschichte und biogeografischen Muster zu verstehen, wurden 130 Populationen und 1705 Individuen in ihrem gesamten Verbreitungsgebiet von Südfrankreich bis Polen und den Britischen Inseln beprobt und nukleare AFLP-Daten, maternal vererbte Plastiden-Haplotypen-Variationen, Plastom-Sequenzinformationen und zytologische Daten verwendet.

Das Fehlen einer räumlichen genetischen Variation, die hohe Rate gemischter Plastiden-Haplotypen und das Fehlen einer räumlichen Struktur im Plastom-Baum deuten auf einen postglazialen Genfluss hin, was für ein Szenario einer einst weit verbreiteten Verbreitung mit sekundärer Fragmentierung spricht. Während die AFLP-Daten eine genetische Trennung zwischen südlichen und nördlichen Gruppen erkennen lassen, zeigt die Variation der Plastidenhaplotypen keine klaren biogeografischen Muster, sondern weist auf eine erhöhte genetischen Diversität im Südwestens hin. Unterschiede im Substrat - kalkhaltig im Süden und silikathaltig im Norden - stimmen mit den AFLP-Gruppierungen überein, was darauf hindeutet, dass edaphische Faktoren die Differenzierung und Anpassung von *D. gratianopolitanus* beeinflussen können. Genetische und zytologische Daten sprechen für die Existenz von Refugien in Südfrankreich. Obwohl es keine klaren Beweise für ein norddeutsches/tschechisches Refugium gibt stellt das Überleben kleiner, heute ausgestorbener Populationen in Westdeutschland in der Nähe von Belgien mit anschließender Ausbreitung eine Möglichkeit dar. Eine dritte genetische Gruppe in Baden-Württemberg, die in der Kontaktzone zwischen nördlichen und südlichen Gruppen liegt, könnte aus dem Überleben in unbekanntem Refugien resultieren oder ein Schmelztiegelszenario darstellen. Die Besiedlung der britischen Inseln ging wahrscheinlich von französischen Populationen aus, insbesondere aus den (Vor-)Alpen, die sich über Belgien auf die Inseln ausbreiteten, wie die genetische Zuordnung und die Plastiden-Haplotypen belegen.

Zur weiteren Untersuchung lokaler Anpassungen wurden Stecklinge von *D. gratianopolitanus* aus kalk- und silikathaltigen Regionen im Botanischen Garten in Heidelberg kultiviert. Anhand eines reziproken Anzuchtversuchs wurden Anpassungen an verschiedene Substrattypen und Vorteile an das Heimatsubstrat analysiert. Nach einem Jahr Wachstum auf Muschelkalk-, Porphy- und Serpentinböden wurden die Fitnessparameter und die Elementzusammensetzung der Blätter untersucht. Zusätzlich wurden die Blütezeit und das Blühverhalten von Pfingstnelken mit Herkunft aus dem gesamten Verbreitungsgebiet sowie von *D. gratianopolitanus* subsp. *moravicus* im Botanischen Garten für die Jahre 2022 und 2023 erfasst. Während die Ergebnisse keine ausgeprägten Anpassungen bei der Elementaufnahme anzeigen, deuten sie darauf hin, dass Pflanzen aus kalkhaltigem Gestein mehr in das vegetative Wachstum investieren, was möglicherweise die vegetative Vermehrung und die Wettbewerbsfähigkeit auf begrenzten Kalkstein Felsköpfen verbessert. Im Gegensatz dazu zeigten Pflanzen aus silikathaltigem Untergrund eine höhere Blütfrequenz, was den Genfluss und die schnellere Besiedlung offenerer Lebensräume fördern kann. Obwohl zwischen 2013 und 2022/23 ein Trend zu einer früheren Blüte zu beobachten war, reichen die höheren Temperaturen im Frühjahr und Sommer allein nicht aus, um eine frühere Blüte auszulösen.

Darüber hinaus wurden elf Metapopulationen, die sowohl aus kalkhaltigen als auch aus silikathaltigen Regionen stammen, anhand von AFLP-Daten und Plastiden-Haplotypen analysiert. Die genetische Struktur innerhalb der Metapopulationen ergab unterschiedliche Muster der Konnektivität und des Isolationsgrads, die entweder auf einen kürzlichen Genfluss oder auf Überbleibsel früherer Verbindungen hindeuten könnten. Die Modellierung ökologischer Nischen unter aktuellen und zukünftigen Klimaszenarien ergab, dass die südlichen Populationen stärker von Trockenstress betroffen sind, während die nördlichen Populationen durch Mindesttemperaturen eingeschränkt werden. Während die Gruppe aus den Silikatarealen eine breitere klimatische Nische aufweist, könnte die stärker spezialisierte Gruppe aus dem Kalkgebiet möglicherweise anfälliger für den Klimawandel ist. Obwohl die derzeitigen Klimabedingungen ein größeres geeignetes Gebiet vorhersagen als das derzeit besiedelte Areal, deuten künftige Szenarien auf eine erhebliche Verringerung der geeigneten Lebensräume hin, mit einem Trend zu höheren Lagen und einer Verschiebung in den Norden. Diese Ergebnisse unterstreichen die Notwendigkeit von Erhaltungsstrategien, die auf alle Teilpopulationen abzielen, die genetische Variation erhalten und möglicherweise Ausbreitungswege wiederherstellen, um das Überleben dieser Art zu sichern.

Contents

General Introduction	3
The biodiversity crisis and the risk for rare, endemic species	3
The genus <i>Dianthus</i>	11
Aims and research questions	11
1 Bibliography	13
I Phylogeography and evolutionary history of <i>Dianthus gratianopolitanus</i> - where does the Cheddar Pink come from and how to interpret bedrock type association?	17
1 Introduction	21
2 Material and Methods	23
2.1 Field work and sampling efforts	23
2.2 DNA extraction	24
2.3 Generation of AFLP data	24
2.4 Amplification of plastid marker sequences and plastid type variation	26
2.5 AFLP data and plastid marker genetic data analysis	28
2.6 Plastome DNA sequencing, assembly, phylogenetic reconstruction, and divergence time estimates	30
2.7 Ploidy and genome size	33
3 Results	35
3.1 Population structure indicate two major gene pools	35
3.2 Plastid haplotype variation shows varying patterns of genetic diversity	38
3.3 Deep evolutionary splits in plastomes pre-date origin of species	42
3.4 Genome size differ among bedrock type, Structure cluster and latitude	43
4 Discussion	51
5 Bibliography	57
II The calcicole-calcifuge refugia idea revisited - insights from reciprocal cultivation experiments.	67
1 Introduction	71

2	Material and Methods	75
2.1	Reciprocal transplant experiment	75
2.2	Flowering time in 2022 and 2023	82
3	Results	85
3.1	Pre-evaluation of raw data	85
3.2	Treatment soil differs in element composition	86
3.3	Element composition in leaf material influenced by treatment soil - no strong home effect based on plant origin substrate	86
3.3.1	Element accumulation	92
3.4	Fitness parameter	92
3.4.1	Withering and Chlorosis unaffected by plant origin substrate and treatment soil	92
3.4.2	Growth and plant weight influenced by treatment and origin	94
3.4.3	Flowering is influenced by treatment and plant origin	96
3.5	Comparison of flowering behaviour of <i>D. gratianopolitanus</i> cultivated in the Botanical Garden Heidelberg in 2022 and 2023	100
4	Discussion	109
5	Bibliography	117
 III Genetic variation and structure within populations of Cheddar Pink, and future prospects under changing climate conditions		123
1	Introduction	127
2	Material and Methods	129
2.1	Analysis of selected (Meta-) populations using Structure, Splitstree and di- versity indices	129
2.2	Ecological niche modelling	130
3	Results	135
3.1	Genetic diversity and population structure within selected populations from calcareous and siliceous bedrock	135
3.2	Ecological niches and predicted distribution range differ between the cal- careous and siliceous groups	170
4	Discussion	175
5	Bibliography	181
 Synthesis and Conclusion		189
1	Bibliography	191
 Appendix		193
A	Appendix - Part I	195

B Appendix - Part II	209
C Appendix - Part III	223
D Digital Supplement	229
E Lists	235
Acknowledgements	253

General Introduction

The biodiversity crisis and the risk for rare, endemic species

Worldwide an estimated amount of one million animal and plant species are facing extinction within decades, an alarming high rate of species loss surpassing all rates in the past 10 million years (Drenckhahn et al., 2020). Europe is no exception here; here too 1,677 of 15,060 assessed species are threatened with extinction according to the International Union for Conservation of Nature (IUCN), among them approximately one-fifth of amphibians and reptiles but also over half of Europe's endemic trees (European Parliament, 2021). Two-thirds of species protected by EU habitat directives have poor conservation status and three-fourths of analysed habitats have a poor conservation status (European Environment Agency, 2024). The main drivers for the biodiversity loss and crisis include pollution, climate change, overexploitation, the spread of invasive species, and the loss, degradation, and alterations of habitats. Agricultural land use and advancing urbanization put additional pressure on species, habitats, and ecosystems (European Environment Agency, 2024). While some of these factors take immediate effect, the decline and later vanishing of populations takes time after a change in environmental conditions. This so-called extinction debt might lead to an underestimation of the number of endangered species and the effects of the drivers on biodiversity in total (Kuussaari et al., 2009). Effective conservation strategies therefore need to take several factors into account the understanding of the population structure and the distribution of genetic diversity, an understanding of requirements to and distribution of fitting habitats and possible restoration options, as well as of overall interactions and threats. To determine international importance and national responsibilities for the conservation of species factors like distribution range, dispersal ability, and endemism should be considered (Schmeller et al., 2008). Endemic and rare species are even more vulnerable to environmental changes and anthropogenic threats and hold a higher risk of extinction. In contrast to widespread, common species, these rare species often form smaller populations in their distribution area and colonize special habitats and/or geographically limited areas. An endemic species is naturally restricted to a specific area or region, while the size of the area can vary greatly ranging from "local endemics" that are restricted to a small area, to "continental endemics", that are restricted to a continent (Işik, 2011; Coelho et al., 2020). In addition, the isolation of the small populations as well as often low dispersal and reproductive capacity exacerbate the problem. Beyond this, rare and endemic species are often found in so-called biodiversity hotspots, regions with exceptionally high levels of biodiversity and endemism, further highlighting the importance of conservation (Myers et al., 2000; Marchese, 2015).

The genus *Dianthus*

Within the angiosperms, the flowering plants, the order Caryophyllales is a major lineage that includes around 12,500 species across 39 families (as of 2016), such as the Caryophyllaceae family. The Caryophyllaceae, also called Pink family, is a large family of mostly herbaceous plants with representatives all over the world, with about 2,625 known species across 81 genera (as of 2016, see [Christenhusz and Byng \(2016\)](#)), including well-known plants like pinks and carnations (*Dianthus* L.). The genus *Dianthus* is the second largest genus in the family Caryophyllaceae only surpassed in size by the genus *Silene* L. . While often quoted with a number of approximately 300 species within *Dianthus* a recent study estimates the number to be higher with over 500 accepted species and heterotypic subspecies. Due to a rising interest focusing on *Dianthus* species groups, 54 new species, and 18 subspecies were described within the last 15 years ([Fassou et al., 2022](#)). *Dianthus* is a predominantly temperate taxon with a natural distribution in the northern hemisphere in Europe and Asia as well as some species in southern and eastern Africa ([Fassou et al., 2022](#); [Valente et al., 2010](#)). In addition to and as a possible explanation for remarkably high species diversity and large numbers of endemic and range-restricted species, [Valente et al. \(2010\)](#) found the Eurasian part of the *Dianthus* lineage to have diversified at a rapid rate in the last 1-2 Myr exceeding even rates for the most rapid radiations known in plants from islands and tropical regions, making it a first evidence and an interesting model for complex evolutionary processes in the temperate flora of Eurasia. Furthermore, the diversity in different cytotypes both within as well as between species offers an interesting starting point for studies on polyploidy and species formation ([Weiss et al., 2002](#); [Balao et al., 2010](#)). Most of the plants are herbaceous perennials, although some annuals, biennials, and low shrubs are also known. The leaves are opposite, often linear to grass-like and gray-green to blue-green. The hermaphrodite flowers are characterized by five petals which are divided into blade and claw and are usually light to dark pink, in rare cases white or even yellow, often with a frilled or pinked margin. The Latin name *Dianthus* is derived from the Greek and means “Flower of Zeus” or “Divine Flower”. These striking, often fragrant flowers have also led to many *Dianthus* species being prized as ornamental plants. *Dianthus caryophyllus* L. is one of the most commercially valuable cut flowers traded worldwide and has been cultivated for 2000 years ([Panwar et al., 2020](#)). In addition, *Dianthus plumarius* L., the Garden Pinks, and *Dianthus barbatus* L., Sweet William, but also other *Dianthus* species like the China Pinks, *Dianthus chinensis* L., and Cheddar Pinks, *Dianthus gratianopolitanus* Vill., are cultivated as ornamental and garden plants with numerous cultivars ([Shekhdar, 2023](#)). Besides importance in horticulture, different *Dianthus* species find uses as medicinal plants in traditional Chinese medicinal systems and are tested in pharmacological studies for anticancer, antiviral, antibacterial, anti-fungal, and anti-insecticide properties ([Chandra et al., 2016](#)). Among the many *Dianthus* species *Dianthus gratianopolitanus*, is one of the *Dianthus* species with the farthest distribution range in Europe while still having fragmented and isolated populations living in a challenging habitat. It is endangered and of interest for

national and international conservation strategies. Nevertheless it has not been the focus of many studies so far, despite it being an interesting model for a species subjected to a high degree of isolation and harsh environmental conditions.

Dianthus gratianopolitanus

Dianthus gratianopolitanus Villars 1789 (synonym: *Dianthus caesius* J.E. Smith 1792), commonly known as the Cheddar Pink (German: Pfingstnelke or Grenobler Nelke), is a Central European herbaceous perennial with a disjunct distribution area ranging from south-east french prealps region towards the Ardennes and Brandenburg with the center of distribution in the Swiss Jura Mountains and the Swabian Alb. Populations can also be found in the French Massif-Central, Poland, the Czech Republic, and south-west England among others in the eponymous Cheddar gorge (Kovanda, 1982). In distribution maps from the Atlas Flora Europaeae (see Figure 1) a population in western Ukraine and uncertain populations in northern Italy are included (Jalas, 1988). Fedoronchuk (2023) states that while it is listed in the Ukrainian Flora, it was not possible to find evidence in nature or in herbaria and it is listed as extinct in nature in the Red Data Book of Ukraine (Didukh, 2010). In general, the Cheddar Pink can be found from lowlands to alpine regions like in the French Alps (Kovanda, 1982).

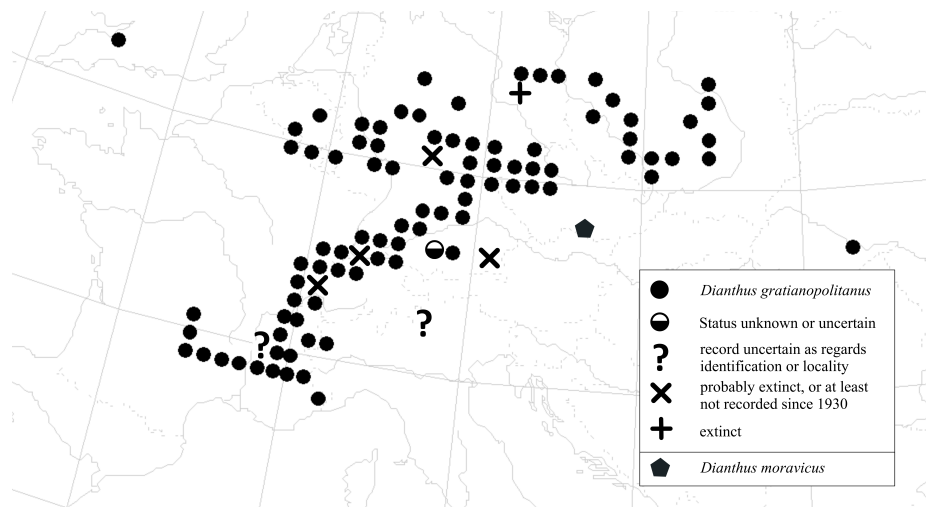


Figure 1: *Distribution area of Dianthus gratianopolitanus and D.gratianopolitanus subsp. moravicus adapted from the digital map generated by Atlas Flora Europaeae (version year 1999) (Jalas, 1988).*

The fragmented distribution of *D. gratianopolitanus* may indicate to be a relict originating from periods previous to the last glaciation (Erhardt, 1990) or a post-glacial relict that found preferable conditions during the post-glacial period (Banzhaf et al., 2009) comparable to the relict character of other xerotherm vegetation (Pott, 1996). Its typical habitat, the humus-poor, sunny ridges, rocky outcrops, and cliffs show themselves a fragmented distribution. While limestone bedrock is preferred in the center of distribution in the Swiss Jura

Mountains and Swabian Alb the Cheddar Pink is less particular towards the north and east and can be found on a variety of non-calcareous rocks like basalt, granite, diabase, porphyry, slate, gneiss, sandstone, sand and acid bedrocks (Kovanda, 1982) (see Figure 2 B-E). This variety of different substrate types also provides very different physical and chemical properties, e.g. element composition and soil pH, that often require adaptations to the specific conditions (Palacio et al., 2022). Soil pH requirements (or soil reaction R) are also included in Ellenbergs indicator values, a common way to characterize ecological requirements and niches of species with respect to e.g. light availability (L), temperature (T), moisture (M), or soil fertility (N). While originally invented in 1974 for Central Europe it has been adapted successfully for e.g. the UK and the Mediterranean region (Ellenberg, 1974; Zolotova et al., 2022). In addition indicator values for specific regions have been published like the indicator values for Switzerland (Landolt, 1977). Even though *D. gratianopolitanus* can tolerate heat and drought and is a full light plant (see Table 1) it tends to be missing in south-facing locations with full sun exposure but can be found in northern exposition if enough lightning is guaranteed (Banzhaf et al., 2009). It can often be found on the edges of the cliffs where humus accumulation is aggravated due to erosion processes lowering the competition from more demanding species.

Table 1: Ecological indicator values for *D. gratianopolitanus* after Ellenberg (Ellenberg et al., 1992) and Landolt (Landolt, 1977). Table adapted from (Banzhaf et al., 2009)

		Ellenberg		Landolt
light availability (L)	9	full light plant	4	light indicator
temperature (T)	7	heat indicator	4	lower forest level (colline level)
continentality (K)	4	suboceanic, main focus in central europe, reaching eastwards	4	main distribution in areas with continental climate
soil moisture (F)	2	(heavy) drought indicator	1	(heavy) drought indicator
soil reaction/ pH (R)	7	weak base indicator	4	base indicator (pH 5.5 -8)
nitrogen (N)	1	indicator of very low levels of soil nitrogen	2	indicator of low levels of soil nitrogen
Life form	C	herbaceous chamaephyte	h	hemicytopyte
leaf endurance	W	overwintering with green leaves, leaves are replaced in spring		
humus index			2	mineral soil indicator
dispersity			1	rockplant

The Cheddar Pink is the namesake and character species of the endangered plant society *Diantho-gratianopolitani-Festucetum pallentis* Gauckl. 1938 (German: Pfingstnelken-Blauschwingelflur), mostly small-scale pioneer grasslands in the extreme habitat of narrow rocky ledges and outcrops, dry sites that are often covered with ice in winter, are moist in spring and dry in summer (Schubert et al., 2001). It is characterized by a high occurrence of *Festuca pallens*, accompanied by e.g. *Aster alpinus* or *Sedum album* (Schubert et al., 2001; Rennwald, 2000). *Sesleria albicans* can be found replacing *Festuca pallens* on rugged calcareous bedrock that allow the roots to dig into cracks and in more shaded locations, indicating degradation of the *Diantho-Festucetum* (Banzhaf et al., 2009). While the vegetation cover of the *Diantho-Festucetum* is often patchy, Cheddar Pink populations can reach a coverage of 100% while facing optimal conditions and without much competition (Banzhaf

et al., 2009). The cushion-forming plant reaching 10-20 cm in height, features underground runners and overwintering leaf rosettes. The underground shoots also allow vegetative reproduction. Its leaves are opposite, linear-lanceolate to grass-like, measuring 15-70 mm in length, 1 - 3 mm in width, and ranging in color from gray-green to bluish-green, fused at the base into a short sheath. The flowering shoots, ranging from 10 cm to 30 cm in height, are glabrous and typically unbranched with a single flower. In rare cases, they can also branch with two to three flowers, as illustrated in Hess et al. (1976) (see Figure 2 A). The petals are pale to dark pink, deeply toothed, and hairy at the throat entrance, emitting a fragrant scent, attracting pollinators during the flowering period in May to June (Erhardt, 1990). The in Erhardt (1990) mentioned pollinators include a wide variety of butterflies, diurnal and nocturnal hawk moths, and other moths species which are not exclusively tied to the Cheddar Pink with *Macroglossum stellatarum* (Linnaeus, 1758) as one of the most effective pollinators. It is of additional interest due to its potential as a long-distance pollen vector with its ongoing migrations from its breeding area in the Mediterranean zone over the Alps up to Scandinavia and Iceland. However, the morphological characteristics of the flower and leaf features can vary, as can be seen in the example pictures from the Heidelberg Botanical Garden depicting *D. gratianopolitanus* from different localities (see Figure 2 F-O). Its capsules contain a large amount of small, 2.0-2.5 mm long, oval, flat, blackish-brown seeds that show no clear adaptations to certain types of dispersion and fall out of the capsules and disperse at short distances like other *Dianthus* species (Kovanda, 1982; Banzhaf et al., 2009; Rico and Wagner, 2016). Dispersal through animals and long-term soil-seed banks seem unlikely (Banzhaf et al., 2009). Seedlings have been rarely observed during observations from 2001 to 2008 at localities in the federal state of Baden-Württemberg and are often not surviving the harsh summer droughts. Due to its low dispersal potential with diaspores and the reproduction through vegetative growth the Cheddar Pink relies on its rather isolated outcrops as habitat and combined with its low competitiveness the colonization of new habitats is difficult and practically not observed (Banzhaf et al., 2009). The cushion-like growth, as well as the dense cuticle, a wax coating, water-storing cells rich in lipids, and vascular bundles surrounded by sclerenchymatous tissue all are xerophyte characteristics, adaptations that allow the overwintering leaf rosettes to endure both the drought and heat of summer but also the drying effects of winter frost. Banzhaf et al. (2009) also states in this context that unlike many plant species found in Central European xerothermic habitats, *D. gratianopolitanus* apparently does not originate from sub-Mediterranean, Mediterranean, or Pontic-Sarmatian regions.

In the east of the distribution range at the rivers Oslava, Jihlava, and Rokytna initially called Moravian *D. gratianopolitanus* (see Figure 1 and Figure 3) was discovered late, with the oldest surviving collections dating back to 1870 still labeled *D. plumarius*. It was transferred to *D. gratianopolitanus* by OBORNY (1885) and remained within this classification despite morphological differences noted by NOVAK (1926) (Kovanda, 1982). In 1982, after population studies and experimental cultivation Kovanda (1982) described a new distinct species *D. moravicus* (German: Mährische Nelke) comparing its morphology with *D. lum-*



Figure 2: **A** Drawing of *Dianthus gratianopolitanus* from Hess *et al.* (1976); **B** flowering *D. gratianopolitanus* in Kellerwald-Edersee, Hesse; **C** Klausberg near Hemfurth, Hesse; **D** Blossenberg, Kellerwald-Edersee, Hesse; **E** Bilsteinklippen, Bad Wildungen, Hesse, Photos B-E from Florian Michling 2013; **F** Bourscheid-Michelau, Luxembourg; **G** Near Blankenberg, Thuringia; **H** Wartburg, Thuringia; **I, J** Danube valley, Baden-Württemberg, **K, L** Ehrenbürg, Bavaria; **M** Lenninger Tal, Baden-Württemberg; **N** Near Blankenberg, Thuringia; **O** Wutachflüh, Baden-Württemberg; **P** Massif Central, France; Photos F-P from Botanical Garden Heidelberg April 2024

nitzeri Wiesb. and *D. gratianopolitanus*. Kovanda (1982) proposed the possibilities of *D. moravicus* to be either a surviving relict or a closely related species, from which *D. gratianopolitanus* evolved at the end of Tertiary, or that *D. moravicus* and *D. gratianopolitanus* share a common ancestor and represent parallel lines of evolution. In 1983 Holub (1983) is changing the rank from *Dianthus moravicus* to *Dianthus gratianopolitanus* Vill. subsp. *moravicus* (Kovanda) Holub, listing the Moravian Pink as a subspecies of the Cheddar Pink.

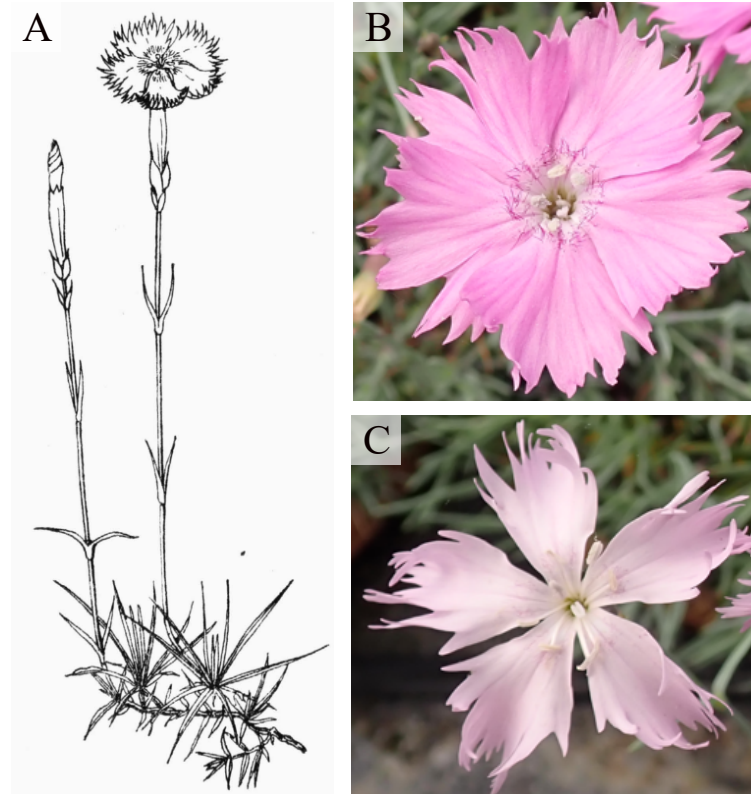


Figure 3: **A** *Dianthus gratianopolitanus* subsp. *moravicus* Drawing of plant from type locality, adapted from Kovanda (1982), (Orig. A. Chrtkova); **B** *Dianthus gratianopolitanus* subsp. *moravicus* from Bitov, CZ; **C** *Dianthus gratianopolitanus* subsp. *moravicus* from Ivancice, Pictures taken April 2024 in the Botanical Garden Heidelberg

While two ploidy levels are known for *Dianthus gratianopolitanus* subsp. *moravicus* ($2n = 60, 90$) three ploidy levels are documented ($2n = 30, 60, 90$) for *D. gratianopolitanus*, though some publications do not include clear information on localities as reviewed in Weiss et al. (2002). While $2n = 60$ and 90 are reported from different sources, e.g. by Kovanda (1982) throughout Bohemia, $2n = 30$ is reported only once in Puch (1941) from Garden Material of unknown origin (see (Weiss et al., 2002)).

D. gratianopolitanus is endangered throughout its distribution range with a decline in populations. While data from the IUCN is missing (as of 2024) national data is available. It is listed as endangered in Germany (Metzing et al., 2018) and the Czech Republic (Grulich, 2012), vulnerable in Switzerland (BAFU, 2016) and the UK (Stroh et al., 2014) and declining - critically endangered in Poland (Zarzycki and Szelag, 2006). In France, the species is listed

as of least concern, with little risk of disappearance (INPN, 2019). On the Swabian Alb, one of the core areas of distribution, this trend is also observable with known populations in sharp decline and with at least ten Messtischblatt-quadrants (ordnance survey map 1 : 25.000, 1010 km, MTB) where *D. gratianopolitanus* is now missing and most likely extinct. Herein also a significant decline based on 1m² permanent observation plots could be observed over the short period of four years from 2002 to 2006 (Banzhaf et al., 2009). Zoogenic damage such as feeding damage caused by the bank vole (*Myodes glareolus*, (Schreber, 1780)) or caterpillars of the owl moths (*Hadena* spec.; *Noctuidae*), as well as damage caused by common ravens (*Corvus corax* (Linnaeus, 1758)) or peregrine falcons *Falco peregrinus* (Tunstall, 1771)) are known, but can be ruled out as the cause of the drastic decline (Banzhaf et al., 2009). While collecting and digging up the plants may have played a greater role in the past, today the effect is considered to be of secondary importance. On the other hand, trampling by hikers and climbers can cause lasting damage to the cushions, especially on rocky outcrops used as vantage points (Banzhaf et al., 2009). Climate change will also affect the *D. gratianopolitanus* with its isolated populations, unique habitat on open sun-exposed rocky outcrops, and limited potential to move to and inhabit new habitats. Increased emissions of nitrogen and air pollution pose a further problem. The additional deposition of nitrogen leads to eutrophication of the substrate. Low competitive species in particular those that are adapted to low nutrient levels, such as those of rocky cliffs or dry grasslands, are now at risk of being displaced by more demanding and vigorous species. For the Cheddar Pink, the frequently observed companion species such as bluegrass (*Sesleria albicans* Kit. ex Schult.) and dwarf sedge (*Carex humilis* Willd. ex Kunth) could be mentioned here, which have similar general requirements to those of the Cheddar Pink, but with increased nitrogen requirements. *Sesleria albicans* forms dense tussocks that additionally capture foliage and thus further increase humus formation. In addition, overgrowth by bushes and shading shrubs can be observed, leading to lower light and temperatures, higher moisture and moisture retention capacities, increased humus formation due to foliage as well as lower erosion due to protection from harsh winds and rain (Banzhaf et al., 2009). Protection measures include the targeted fencing off of the rocky outcrops and the guidance of hikers, as well as targeted clearing measures and the removal of herbaceous competitors. Koch et al. (2021) analyzed two populations from the Swabian Alb also showing genetically mosaic patterns in the landscape indicating an often reduced genetic exchange and dispersal between individual growing sites within the valleys analyzed, thus highlighting the importance of protecting each individual rocky outcrop as well as of the creation of more suitable sites to increase exchange and dispersal possibilities.

Based on its distribution range Germany has a high responsibility for the protection of the species (Koch et al., 2021). *D. gratianopolitanus* is one of the selected species of high national responsibility and part of the project "Aufbau eines nationalen Netzwerkes zum Schutz gefährdeter Wildpflanzen in besonderer Verantwortung Deutschlands" (WIPs-De, <https://www.wildpflanzenenschutz.uni-osnabrueck.de/>, (Wöhrmann et al., 2020)) of the Federal Program on Biological Diversity of the German Federal Agency for Nature

Conservation (BfN) (Wöhrmann et al., 2020). In addition, the Federal state of Baden-Württemberg initiated the "Artenhilfsprogramm Pfingstnelke". First preparations for the research project concerning *Dianthus gratianopolitanus* in Heidelberg in the context of the "Artenhilfsprogramm Pfingstnelke", started already in the spring of 2009 with the extensive mapping and collection of plant material over the distribution range. In the following years, more sites were visited, material was collected and experiments conducted. In total six theses (Michling, 2011; Heck, 2011; Pöhl, 2013; Strobel, 2014; Winizuk, 2021; Kartal, 2022) were written in the context of this project and an extensive ex situ conservation culture is cultivated in the Heidelberg Botanical Garden.

Aims and research questions

In my study I aim to unravel the evolutionary history of *D. gratianopolitanus*, patterns of adaptations and putative speciation processes. I want to assess the distribution of genetic diversity within populations in order to gather information on contemporary threats and for developing effective conservation strategies. For this I will answer the following questions:

In Part I: What can we learn about the evolutionary and phylogeographic history of *D. gratianopolitanus* based on nuclear, plastid and cytological data? Can we see genetic footprints of adaptations and past migrations?

In Part II: How does different substrates influence and drive the differentiation of *D. gratianopolitanus*? Can we unravel home effects indicating adaptations bedrock type which may reflect past evolutionary history and may also provide guidance for nature protection policies?

In Part III: How is the distribution of genetic diversity and genetic structure within metapopulations of *D. gratianopolitanus* and does the bedrock type influence the genetic connectivity and structuring? Are there differences in the genetic make-up of metapopulation systems that need to be considered for conservation efforts? How are the future prospects of *D. gratianopolitanus* from calcareous and siliceous bedrock under changing climate conditions?

1 | Bibliography

- BAFU (2016). Rote Liste Gefäßpflanzen. *Bundesamt für Umwelt BAFU, Umwelt-Vollzug Bern, Switzerland.*
- Balao, F., Valente, L. M., Vargas, P., Herrera, J., and Talavera, S. (2010). Radiative evolution of polyploid races of the Iberian carnation *Dianthus broteri* (Caryophyllaceae). *New Phytologist*, 187(2):542–551.
- Banzhaf, P., Jäger, O., and Meisterhans, U. (2009). Artenhilfsprogramm für die Pfingstnelke *Dianthus gratianopolitanus* im Regierungsbezirk Stuttgart. *Jahreshefte der Gesellschaft für Naturkunde in Württemberg*, 165:73–115.
- Chandra, S., Rawat, D., Chandra, D., and Rastogi, J. (2016). Nativity, phytochemistry, ethnobotany and pharmacology of *Dianthus caryophyllus*. *Research Journal of Medicinal Plant*, 10(1):1–9.
- Christenhusz, M. J. and Byng, J. W. (2016). The number of known plants species in the world and its annual increase. *Phytotaxa*, 261(3):201–217.
- Coelho, N., Gonçalves, S., and Romano, A. (2020). Endemic plant species conservation: Biotechnological approaches. *Plants*, 9(3):345.
- Didukh, Y. (2010). "Red Data Book of Ukraine. Vegetable Kingdom" Afterword. *Biodiversity Research and Conservation*, 19(2010):87–92.
- Drenckhahn, D., Arneth, A., Filser, J., Haberl, H., Hansjürgens, B., Herrmann, B., Homeier, J., Leuschner, C., Mosbrugger, V., Reusch, T., Schäffer, A., Scherer-Lorenzen, M., and Tockner, K. (2020). Global biodiversity in crisis - what can Germany and the EU do about it? *Nationale Akademie der Wissenschaften Leopoldina, Diskussion Nr. 24, Halle (Saale).*
- Ellenberg, H. (1974). *Zeigerwerte der Gefäßpflanzen Mitteleuropa*. Universität Göttingen, Lehrstuhl für Geobotanik.
- Ellenberg, H., Weber, H. E., Düll, R., Wirth, V., Werner, W., Paulißen, D., et al. (1992). *Zeigerwerte von Pflanzen in Mitteleuropa*, volume 18. Goltze Göttingen.

- Erhardt, A. (1990). Pollination of *Dianthus gratianopolitanus* (Caryophyllaceae). *Plant Systematics and Evolution*, 170:125–132.
- European Environment Agency, E. (2024). Biodiversity: state of habitats and species. <https://www.eea.europa.eu/en/topics/in-depth/biodiversity?activeTab=fa515f0c-9ab0-493c-b4cd-58a32dfaae0a>. Accessed on: 18.06.2024, ISBN 978-92-79-19269-2, doi:10.2779/30669.
- European Parliament, E. P. (2021). Endangered species: facts and figures (infographic). <https://www.europarl.europa.eu/topics/en/article/20200519ST079424/endangered-species-in-europe-facts-and-figures-infographic>. Accessed on: 18.06.2024.
- Fassou, G., Korotkova, N., Nersesyan, A., Koch, M. A., Dimopoulos, P., and Borsch, T. (2022). Taxonomy of *Dianthus* (Caryophyllaceae)– overall phylogenetic relationships and assessment of species diversity based on a first comprehensive checklist of the genus. *PhytoKeys*, 196:91.
- Fedoronchuk, M. M. (2023). Ukrainian flora checklist. 5: family Caryophyllaceae (incl. Illecebraceae)(Caryophyllales, Angiosperms). *Chornomorski botanical journal*, 19(1):5–57.
- Grulich, V. (2012). Red List of vascular plants of the Czech Republic.
- Heck, E. M. (2011). Evolution der Pfingstnelke in den Randarealen. Staatsexamens Arbeit, Ruprecht-Karls University Heidelberg.
- Hess, H. E., Landolt, E., and Hirzel, R. (1976). *Flora der Schweiz und angrenzender Gebiete: Band I: Pteridophyta bis Caryophyllaceae*. Springer.
- Holub, J. (1983). Reclassifications and new names for some European Phanerogams. *Folia geobotanica & phytotaxonomica*, 18:203–206.
- INPN (2019). Liste Rouge de la flore vasculaire de France metropolitaine (liste *Dianthus gratianopolitanus* Vill.). https://inpn.mnhn.fr/espece/cd_nom/94756/tab/statut. Accessed on 19.06.2024.
- Işık, K. (2011). Rare and endemic species: why are they prone to extinction? *Turkish Journal of Botany*, 35(4):411–417.
- Jalas, Jaakko; Suominen, J. (1988). *Atlas Florae Europaeae. Distribution of vascular plants in Europe. III: Caryophyllaceae*. Cambridge University Press,.
- Kartal, M.-G. (2022). Geographic differentiation in *Dianthus gratianopolitanus* cytotypes: Clinal variation versus taxonomic units. Bachelor’s thesis, Ruprecht-Karls University Heidelberg.

- Koch, M. A., Winizuk, A., Banzhaf, P., and Reichardt, J. (2021). Impact of climate change on the success of population support management and plant reintroduction at steep, exposed limestone outcrops in the German Swabian Jura. *Perspectives in Plant Ecology, Evolution and Systematics*, 53:125643.
- Kovanda, M. (1982). *Dianthus gratianopolitanus*: variability, differentiation and relationships. *Preslia*, 54(3).
- Kuussaari, M., Bommarco, R., Heikkinen, R. K., Helm, A., Krauss, J., Lindborg, R., Öckinger, E., Pärtel, M., Pino, J., Rodà, F., et al. (2009). Extinction debt: a challenge for biodiversity conservation. *Trends in ecology & evolution*, 24(10):564–571.
- Landolt, E. (1977). Ökologische Zeigerwerte zur Schweizer Flora.
- Marchese, C. (2015). Biodiversity hotspots: A shortcut for a more complicated concept. *Global Ecology and Conservation*, 3:297–309.
- Metzing, D., Garve, E., Matzke-Hajek, G., Adler, J., Bleeker, W., Breunig, T., Caspari, S., Dunkel, F., Fritsch, R., Gottschlich, G., Gregor, T., Hand, R., Hauck, M., Korsch, H., Meierott, L., Meyer, N., Renker, C., Romahn, K., Schulz, D., Täuber, T., Uhlemann, I., Welk, E., Weyer, K. v. d., Wörz, A., Zahlheimer, W., Zehm, A., and Zimmermann, F. (2018). *Rote Liste und Gesamtartenliste der Farn- und Blütenpflanzen (Tracheophyta) Deutschlands*, volume 70 of *Naturschutz und Biologische Vielfalt*. Landwirtschaftsverlag, Münster.
- Michling, F. (2011). Conservation genetics of *Dianthus gratianopolitanus*. Staatsexamens Arbeit, Ruprecht-Karls University Heidelberg.
- Myers, N., Mittermeier, R. A., Mittermeier, C. G., Da Fonseca, G. A., and Kent, J. (2000). Biodiversity hotspots for conservation priorities. *Nature*, 403(6772):853–858.
- Palacio, S., Cera, A., Escudero, A., Luzuriaga, A. L., Sánchez, A. M., Mota, J. F., Pérez-Serrano Serrano, M., Merlo, M. E., Martínez-Hernández, F., Salmerón-Sánchez, E., et al. (2022). Recent and ancient evolutionary events shaped plant elemental composition of edaphic endemics: a phylogeny-wide analysis of Iberian gypsum plants. *New Phytologist*, 235(6):2406–2423.
- Panwar, S., Gupta, Y. C., Kumari, P., Thakur, N., and Mehraj, U. (2020). *Carnation*, pages 1–22. Springer Singapore, Singapore.
- Pott, R. (1996). Die Entwicklungsgeschichte und Verbreitung xerothermer Vegetationseinheiten in Mitteleuropa unter dem Einfluss des Menschen. *Tuexenia: Mitteilungen der Floristisch-Soziologischen Arbeitsgemeinschaft*, 16:337–369.
- Puch, E. (1941). Kariologija nekotorych vidov gvozdiki (karyology of selected species of Caryophyllaceae). *Sovetskaja Botanika*, 1941:178–180.

- Pöhl, S. (2013). Evolution der Pfingstnelke - Klinale Variation oder multiple Zentren genetischer Diversität? Staatsexamens Arbeit, Ruprecht-Karls University Heidelberg.
- Rennwald, E. (2000). Rote Liste der Pflanzengesellschaften Deutschlands mit Anmerkungen zur Gefährdung.
- Rico, Y. and Wagner, H. (2016). Reduced fine-scale spatial genetic structure in grazed populations of *Dianthus carthusianorum*. *Heredity*, 117(5):367–374.
- Schmeller, D. S., Gruber, B., Budrys, E., Framsted, E., Lengyel, S., and Henle, K. (2008). National responsibilities in European species conservation: a methodological review. *Conservation Biology*, 22(3):593–601.
- Schubert, R., Hilbig, W., and Klotz, S. (2001). Bestimmungsbuch der Pflanzengesellschaften Deutschlands.
- Shekhdar, K. (2023). <https://horticulture.co.uk/dianthus/>. Accessed on 22.04.2024.
- Strobel, K. A. (2014). Substrate adaptation of *Dianthus gratianopolitanus*: Local effect or evolutionary footprint? Staatsexamens Arbeit, Ruprecht-Karls University Heidelberg.
- Stroh, P., Leach, S., August, T., Walker, K., Pearman, D., Rumsey, F., Harrower, C., Fay, M., Martin, J., Pankhurst, T., et al. (2014). A vascular plant red list for England. *BSBI News*, 9:1–193.
- Valente, L. M., Savolainen, V., and Vargas, P. (2010). Unparalleled rates of species diversification in Europe. *Proceedings of the Royal Society B: Biological Sciences*, 277(1687):1489–1496.
- Weiss, H., Dobeš, C., Schneeweiss, G. M., and Greimler, J. (2002). Occurrence of tetraploid and hexaploid cytotypes between and within populations in *Dianthus* sect. *Plumaria* (Caryophyllaceae). *New Phytologist*, pages 85–94.
- Winizuk, A. (2021). The evolutionary history of Cheddar Pink. Master's thesis, Ruprecht-Karls University Heidelberg.
- Wöhrmann, F., Burkart, M., Lauterbach, D., et al. (2020). WIPS-DE II Wildpflanzenschutz Deutschland Botanische Gärten übernehmen Verantwortung. *Gärtnerisch Botanischer Brief*, 2:24–36.
- Zarzycki, K. and Szelaġ, Z. (2006). Red list of the vascular plants in Poland. *Red list of plants and fungi in Poland*, pages 9–20.
- Zolotova, E., Ivanova, N., and Ivanova, S. (2022). Global overview of modern research based on Ellenberg indicator values. *Diversity*, 15(1):14.

Part I

Phylogeography and evolutionary
history of *Dianthus*
gratianopolitanus - where does the
Cheddar Pink come from and how to
interpret bedrock type association?

Abstract

Cheddar Pink (*Dianthus gratianopolitanus* Vill., Caryophyllaceae) is an endangered, herbaceous perennial of Central Europe, facing population decline. We sampled 130 populations and 1705 individuals across the entire distribution range from southern France to Poland and the British Isles and used nuclear AFLP data, maternally inherited plastid haplotype variation, whole plastome sequence information as well as cytological data to infer biogeographic patterns as well as the species' evolutionary history. The distribution-wide missing spatial structure of genetic variation, high rate of the mixture of plastid haplotypes, and lack of spatial and species structure in the plastome tree indicate postglacial gene flow favoring a scenario of once area-wide distribution with secondary fragmentation. Although a genetic division in a southern and northern group is revealed by the AFLP data, the plastid haplotype variation shows no clear biogeographic pattern but exemplifies southwestern richness. The observed AFLP groups coincide with differences in bedrock type, with calcareous bedrock to the south and siliceous bedrock to the north, highlighting the possible influence of edaphic factors on the differentiation and adaptation of *D. gratianopolitanus*. While a refugia in the South of France is highly supported by genetic and cytological data, clear evidence for a northern German/Czech refugia is still missing. Yet the survival of now-extinct small populations in western Germany near Belgium with later expansion could be possible. The third genetic group, in Baden-Württemberg, the contact zone of the northern and southern groups, could be the result of survival in unknown refugia or of a melting pot scenario with a contact zone of a northern and southern gene pool. Colonization of the nowadays isolated British Isles originating from populations in the French (Pre-)Alps, expanding to Belgium and the Isles is supported by the genetic assignment and plastid haplotypes.

Zusammenfassung

Die Pfingstnelke (*Dianthus gratianopolitanus* Vill., Caryophyllaceae) ist eine gefährdete, krautige mehrjährige Pflanze in Mitteleuropa, deren Populationen vom Rückgang bedroht sind. In dieser Arbeit wurden 130 Populationen und 1705 Individuen im gesamten Verbreitungsgebiet von Südfrankreich bis Polen und Großbritannien beprobt und AFLP-Daten, maternal vererbte Plastiden-Haplotypen-Variationen, Plastomsequenz sowie zytologische Daten verwendet, um biogeografische Muster sowie die Evolutionsgeschichte der Art zu ermitteln. Die verbreitungsweit fehlende räumliche Struktur der genetischen Variation, die hohe Rate der Vermischung von Plastidenhaplotypen und das Fehlen einer räumlichen und artenspezifischen Struktur im Plastomenbaum deuten auf einen postglazialen Genfluss hin, der ein Szenario einer einst flächendeckenden Verbreitung mit sekundärer Fragmentierung begünstigt. Obwohl die AFLP-Daten eine genetische Unterteilung in eine südliche und eine nördliche Gruppe erkennen lassen, zeigt die Plastiden-Haplotyp-Variation kein klares biogeografisches Muster, jedoch höhere Diversität in den südlichen Regionen. Die beobachteten AFLP-Gruppen decken sich mit Unterschieden in den zugrundeliegenden Bodentypen, mit kalkhaltigem Boden im Süden und silikathaltigem Gestein im Norden, was den möglichen Einfluss edaphischer Faktoren auf die Differenzierung und Anpassung von *D. gratianopolitanus* unterstreicht. Während ein Refugium in Südfrankreich durch genetische und zytologische Daten sehr gut unterstützt wird, fehlen noch eindeutige Beweise für ein norddeutsches/tschechisches Refugium. Das Überleben kleiner, heute ausgestorbener Populationen in Westdeutschland in der Nähe von Belgien mit späterer Ausbreitung könnte jedoch möglich sein. Die dritte genetische Gruppe in Baden-Württemberg, der Kontaktzone zwischen den nördlichen und südlichen Gruppen, könnte das Ergebnis eines Überlebens in unbekanntem Refugien oder eines sogenannten "Melting pot" Szenarios mit einer Kontaktzone zwischen einem nördlichen und südlichen Genpool darstellen. Die Besiedlung der heute isolierten Britischen Inseln, die von Populationen in den französischen (Vor-)Alpen ausging und sich nach Belgien und nach Großbritannien ausbreitete, wird durch die genetische Zuordnung und die Plastiden-Haplotypen unterstützt.

1 | Introduction

The climatic fluctuations of the Pleistocene and the recolonization following the LGM shaped today's plant distribution

The Pleistocene, commonly known as the Ice Age, was Earth's most recent period of glacial cycles, lasting from approximately 2.58 million to 11,700 years ago. During the last glacial period in northern Europe (around 115,000 to 11,700 years ago), known as the Weichselian glaciation, large ice sheets covered areas such as the east coast of Schleswig-Holstein, and northern parts of Poland and Russia. The corresponding glacial period in the Alpine region is called the Würm glaciation. During these often cold and dry glacial periods, where the mountain ranges were covered by ice sheets, the plains were defined by cold steppes and tundra (Hewitt, 1996, 1999). Following the Last Glacial Maximum (LGM, around 25,000 to 17,000 years ago), ice sheets receded, leaving new habitats to colonize (Petit et al., 2003). The climatic fluctuations during these glaciation and deglaciation cycles, particularly the strong oscillations dating back 700,000 years, significantly impacted plant distribution patterns (Comes and Kadereit, 1998) by dramatically altering environmental conditions like changing sea levels that formed or erased migration corridors via land bridges or changes in soil types, sediments, or even whole landscapes. To survive these changes species had to adapt to them or migrate to more suitable habitats, leading to the formation of southern glacial refugia, with the biggest in the Italian and Iberian peninsulas and the Balkans (Hewitt, 2000; Petit et al., 2003). North European refugia have been suggested in many studies (Stewart and Lister, 2001; Petit et al., 2003), but often lack sufficient evidence, such as fossil data, to support continuous survival of temperate taxa north of the Alps during the LGM (Hošek et al., 2024). In addition to cryptic glacial refugia (Tzedakis et al., 2013), coastal areas (Kadereit et al., 2007) or refugia associated with mountain islands (Brochmann et al., 2003) more recent proposals suggest hot spring oases that could have maintained humid and warm microclimates locally, providing the necessary conditions for survival north of the Alps (Hošek et al., 2024). During the interglacials and following the melting of glaciers and the warming climate after the LGM, surviving populations from refugia could recolonize the now available habitats (Petit et al., 2003). Differing rates of range expansions due to dispersal mechanisms and the availability of suitable habitats led to complex biogeographic distributions and genetic diversity across Europe. As a result, populations close to refugia

are expected to be highly divergent, with intraspecific diversity declining with increasing distance from the refugia due to consecutive founder events during postglacial colonization (Comes and Kadereit, 1998; Hewitt, 2000; Petit et al., 2003). As species expanded their ranges, hybrid zones likely formed in regions where previously isolated populations came into contact (Hewitt, 1996). The genetic exchange in these zones can lead to increased genetic diversity and the emergence of new genotypes (Petit et al., 2003) that may be better adapted to changing environmental conditions. The formation of hybrid zones thus contributed to the dynamic evolutionary processes that have shaped the current patterns of plant diversity and distribution in Europe. While Erhardt (1990) suggests the present-day distribution of the Cheddar Pink to be a relict from periods previous to the last glaciation, Banzhaf et al. (2009) presumed that *D. gratianopolitanus* survived the past ice ages in refugia and recolonized suitable habitats during warmer phases of the interglacials and the postglacial period. Such over long time periods stable populations, either in refugia or long time relict population, can retain a higher genetic diversity compared to the populations from interglacial and postglacial spread that were subjected to repeated population bottlenecks (Comes and Kadereit, 1998; Hewitt, 2000). This strong isolation of refugia during the Pleistocene with a possible gene flow only during the warmer periods of the interglacials allowed an independent evolution of these relic populations (Reisch et al., 2003). The nowadays fragmented distribution could be due to the survival of *D. gratianopolitans* in several disjoint refugia, long-distance dispersal, or the secondary fragmentation of an area-wide postglacial distribution (Reisch, 2008; Schneeweiss and Schönswetter, 2010). Using present-day population structure, genetic differentiation, and diversity and relating them to the geographical context evolutionary processes can be inferred. The use of nuclear and plastid data as well as cytological information collected from the whole distribution range allows to obtain a comprehensive picture of the phylogeographic history of *D. gratianopolitanus*.

Contributions

Plant material collection was done by Prof. Dr. Koch and Florian Michling, starting in 2009. The experimental ground work was first done in the context of state examination theses from 2011 to 2013 including work on primer generation for plastid marker amplification (Michling, 2011), first amplification of plastid marker sequences (Heck, 2011) and the generation of AFLP data (Pöhl, 2013). In the following years additional plastid marker data as well as AFLP data was generated (Koch, Kretz, unpublished). Data analysis of the whole data sets was conducted by myself. DNA extraction for genome skimming sequencing of the *Dianthus* plastomes was done by Anna Loreth. Plastome sequence assembly as well as analysis was done by myself. Genome sizes via Flowcytometry was measured by Florian Michling and Dr. Peter Sack as well as in the context of a bachelors thesis including the preparation and counting of chromosome numbers using root tips by Kartal (2022) with the help of Helena Greifzu. I sorted and analysed all data.

2 | Material and Methods

2.1 Field work and sampling efforts

Data on the present-day occurrence of *D. gratianopolitanus* across its distribution range was collected from various databases [e.g., Infoflora (<https://www.infoflora.ch/en/>), NHMS floristic mapping (<http://www.flora.naturkundemuseum-bw.de/>), BSBI distribution database (<https://database.bsbi.org/>)] (see Koch et al., 2021). During the fieldwork starting in 2009, the majority of sites have been visited, monitored, and sampled collecting leaf material, cuttings, or plants (see Figure 2.1). Necessary permits were acquired (see Appendix Table A.1 and Digital Supplement "S_ I.1-Permits"). In addition, a representative set of populations of various closely related species from Central Europe has been sampled (See Digital Supplement "S_ I.0-Dianthus.Summary.xlsx") including the *Dianthus gratianopolitanus* subsp. *moravicus*.

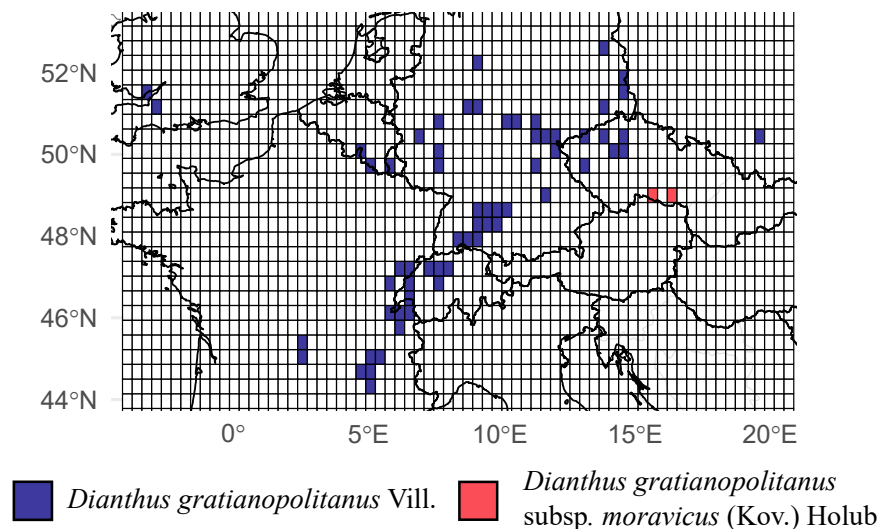


Figure 2.1: Sample locations included in the genetic analysis. Grid size indicates 4 MTB, MTB = Messtischblatt = ordnance survey map 10 x 10 km, colors indicate sample locations from *D. gratianopolitanus* and *D. gratianopolitanus* subsp. *moravicus* from the Czech Republic.

2.2 DNA extraction

Genomic DNA was extracted from fresh as well as dried leaf material following the protocol described in [Doyle and Doyle \(1987\)](#) with minor modifications ([Gong et al., 2008](#)). Approximately ~ 25 mg leaf material was ground in the Precellys 24 Homogenisator (Bertin Technologies, Montigny-le-Bretonneux, France). After centrifugation at 5500x g at room temperature the pellet was washed twice with 70% ethanol and dried and dissolved in 50 μ L TE buffer. 2U of RNase A were added and incubated at 37 °C for 1h. The concentration and quality of the extracted DNA were measured using Qubit fluorometer (Thermo Fisher Scientific, Waltham, US) and each sample was diluted with ddH₂O to a final DNA concentration of 100 ng/ μ L. The extracted DNA was centrifuged and stored at -20 °C until further use.

2.3 Generation of AFLP data

Genetic information needs to be collected to infer the genetic structure of populations and to reveal biogeographical distribution patterns of genetic diversity. While genome sequencing for big datasets can still be quite expensive, alternatives like multilocus fingerprinting prove to be a viable alternative for the genotyping of a high number of individuals ([Meudt and Clarke, 2007](#)).

The Amplified Fragment Length Polymorphism (AFLP) method has been used in a broad range of applications since its development in the 1990s ([Bonin et al., 2007](#); [Vos et al., 1995](#)). No previous sequence information is required and a high amount of polymorphic molecular markers can be generated in a rather short time resulting in a genetic fingerprint of each individual ([Mueller and Wolfenbarger, 1999](#)). The good resolution of even small genetic differences between individuals facilitates its use in intraspecific studies ([Meudt and Clarke, 2007](#)). The AFLP procedure can be summarized in i) a restriction step, ii) a ligation step, iii) preselective polymerase chain reaction (PCR) followed by iv) the selective PCR using fluorescent-labeled primer. The resulting fragments can be analyzed using Capillary electrophoresis. The presence and absence of fragments are recorded in a 0-1 matrix. These differences in fragment occurrences can be the result of the gain or loss of restriction sites or insertion-deletions (Indels) within the fragments changing their length ([Meudt and Clarke, 2007](#)). This procedure does not require prior knowledge of the sequences and amplifies fragments covering the whole genome allowing an assessment of genetic variation within the whole genome ([Vos et al., 1995](#); [Meudt and Clarke, 2007](#)). In studies with plants, the total error rate is usually less than 5%, which in turn also suggests a high reproducibility ([Bonin et al., 2004](#)).

The dominant marker system has on the other hand also disadvantages. The distinction between the mere presence and absence of fragments does not allow for a differentiation between homozygous and heterozygous alleles ([Meudt and Clarke, 2007](#)). In order to compensate for this lower information content (compared to codominant markers such as e.g.

microsatellites), approximately ten times as many markers should be generated as would be necessary for comparable experiments with microsatellites (Bonin et al., 2004; Evanno et al., 2005). Another problem is the information content of the presence and absence signal. The presence of a band does not necessarily mean that it is the same fragment in two individuals that have arisen homologous, but can also result from fragments of the same size but different fragments by chance. The absence of a band can have various reasons and is, therefore, more susceptible due to homoplasy that can distort the true genetic fingerprint and influence the following analysis based on the 0-1 matrix (Bonin et al., 2007). AFLP also allows for interploidal comparisons [e.g. (Kolář et al., 2012; Jiménez et al., 2008; Guo et al., 2005)] though keeping in mind that ploidy and genome size might influence the number of AFLP fragments generated (Meudt and Clarke, 2007; Fay et al., 2005), which has to be tested.

Keeping these limitations in mind the AFLP procedure still provides a valuable tool in phylogenetic studies and is used in studies on plants (Brand et al., 2022; Kropf et al., 2020; Jian et al., 2018; Koch and Bernhardt, 2004), animals (Milá et al., 2013) and fungi (Roberto et al., 2021). In my study, the AFLP data allowed to have genomic fingerprints of *D. gratianopolitanus* covering its whole distribution range. To analyze patterns of genomic variation in space the AFLP data provided a sufficient resolution and depth and a comparison to closely related species like *D. gratianopolitanus* subsp. *moravicus* was also possible.

In total 1676 *D. gratianopolitanus* from 120 populations, covering its whole distribution, were genotyped for AFLP. In addition, 36 *D. gratianopolitanus* subsp. *moravicus* as well as individuals of several closely related *Dianthus* species were genotyped (see Digital supplement "S_ I.2.1-AFLP.Dg.morav.xlsx" and "S_ I.2.2-AFLP.additional.species.xlsx"). While *D. gratianopolitanus* subsp. *moravicus* was included here the other *Dianthus* species are not further analyzed and discussed here. To obtain a sufficient amount of AFLP bands within a reasonable fragment size range, suitable primer pairs for selective PCR were chosen after primer screening. The AFLP procedure was performed according to (Vos et al., 1995).

Restriction Ligation. The restriction ligation reaction was performed in a final volume of 15 μ L, containing 200 ng genomic DNA, 2 U T4 DNA ligase in 1 \times T4 ligase buffer, 10 U *Mse*I, 75 pmol *Mse*I-adapter pair (5'-GACGATGAGTCCTGAG-3' and 5'-TACTCAGGACTCAT-3'), 10 U *Eco*RI and 75 pmol *Eco*RI-adapter pair (5'-CTCGTAGACTGCGTACC-3' and 5'-AATTGGTACGCAGTC-3'). The genomic DNA was digested at 37 °C for 3 h in a thermal cycler (MJ Research PTC 200 Peltier) followed by 65 °C for 15 min and was held at 4 °C. The resulting product was diluted 10-fold with sterile ddH₂O.

pre-selective PCR. The pre-selective PCR mix (50 μ L) contained 2.5 μ L diluted restriction ligation product, 1 \times PCR buffer, 2.5 U *Taq* DNA polymerase, 1.5 mM MgCl₂, 200 μ M dNTP, and 40 pmol of each primer. As preselective primers *Mse*I +C(5'-GACGATGAGTCCTGAGTAAC-3') and *Eco*RI +A(5'-GACTGCGTACCAATTCA-3') were used. The pre-selective PCR amplification was performed following the program: 72 °C, 2 min; 30x (94 °C, 30 s; 56 °C, 30 s; 72 °C, 2 min); 72 °C, 60 min; hold at 8 °C.

selective PCR. The three 5' fluorescence-labeled primer pairs for selective PCR amp-

lification were : *EcoRI*-AAC (5'-GACTGCGTACCAATTCAAC-3') (FAM)/*MseI*-CTT (5'-GACGATGAGTCCTGAGTAACTT-3'), *EcoRI*-AGC (5'-GACTGCGTACCAATTCACC-3') (TET)/*MseI*-CTA(5'-GACGATGAGTCCTGAGTAACTA-3'), and *EcoRI*-AGT (5'-GACTGCGTACCAATTCAGT-3') (TAMRA)/*MseI*-CTC (5'-GACGATGAGTCCTGAGTAACTC-3'). For each pair a reaction mix with a volume of 25 μL was prepared, containing 2.5 μL diluted pre-selective products, 1 \times PCR buffer, 1 U *Taq* DNA polymerase, 1.5 mM MgCl_2 , 300 μM dNTP, and 4 pmol of each *EcoRI* fluorescence-labeled primer, 25 pmol *MseI* primer. Amplification was performed following the program: 94 $^\circ\text{C}$, 5 min; 13x (94 $^\circ\text{C}$, 30 s; 65 $^\circ\text{C}$, 30 s; 72 $^\circ\text{C}$, 2 min); 21x (94 $^\circ\text{C}$, 30s; 56 $^\circ\text{C}$, 30s; 72 $^\circ\text{C}$, 2 min); 72 $^\circ\text{C}$, 30 min; hold at 8 $^\circ\text{C}$.

Genotyping and evaluation. The selective PCR products were pooled for each accession and a length standard (MegaBACETM ET550-R) was added. The genotyping was performed using a MegaBACETM 1000 instrument (GE Healthcare GmbH, Solingen, Germany) and raw data were scored and exported as a presence/absence matrix using GeneMarker v1.95 (SoftGenetics LLC, State College, USA). Fragment sizes were restricted from 60 to 450 nucleotides to improve the reliability of the data set. The resulting presence/absence matrix was inspected manually. 249 sample duplicates (for 147 accessions \sim 9%) were included to calculate the experimental error rate (Bonin et al., 2004).

2.4 Amplification of plastid marker sequences and plastid type variation

While the nuclear genome is affected by sexual recombination during reproduction, the mitochondrial and plastid genomes are unaffected and inherited only uniparentally, usually maternally in angiosperms, allowing the investigation of the matrilineal history of a species (Avisé, 2009). cpDNA has a high structural stability, meaning it is highly conserved with respect to gene content and arrangement and the high number of plastid genome copies per plant cell facilitates PCR amplification of specific cpDNA regions using universal PCR primers (Small et al., 2004). Especially noncoding and fast evolving genomic regions like the introns and intergenic regions of the plastid genomes find wide-range use in botanical studies (Shaw et al., 2005; Avisé, 2009). In my study these maternally inherited marker regions are used to assess genetic diversity and reveal the footprint for past seed dispersal. Primer pairs and PCR settings were chosen based on Shaw et al. (2005) and adjusted for the work with *D. gratianopolitanus*. The nomenclature of plastid DNA segments follows Shaw et al. (2005). Three plastid intergenic spacer regions were chosen based on amplification success and sufficient sequence variability (*trnL-trnF*, *trnC-ycf6*, *psbA-trnH*).

***trnL-trnF* region (430 bp).** The *trnL-trnF* region is a commonly used marker for phylogenetic as well as population genetic studies in plants to infer intra-, as well as interspecies relationships (Koch et al., 2007; Bellstedt et al., 2001). The *trnL-F* region was amplified using the primer pair 3'*trnL*^{UAA}R (GGTTCAAGTCCCTCTATCCC) and *trnF*gaa (ATTGAACTGGTGACACGAG) (Shaw et al., 2005; Taberlet et al., 1991). The reaction was

performed in a final volume of 25 μL containing 1x reaction buffer (5x Mango *Taq*TMColorless Reaction Buffer, (Bioline, Luckenwalde, Germany)), 0.5 U Mango *Taq*TMDNA polymerase (Bioline), 4 mM MgCl_2 , 0.16 μM of each primer, 0.2 mM dNTPs and 50 ng of template DNA. The touchdown PCR was performed with a PTC-200 thermocycler (MJ Research) following the program: 94 °C, 2 min; 3x (94 °C, 45 s; 69.3 °C, 40s; 72 °C, 35 s); 3x (94 °C, 45 s; 69.1 °C, 40 s; 72 °C, 35 s); 3x (94 °C, 45 s; 68.9 °C, 40 s; 72 °C, 35 s); 19x (94 °C, 45 s; 68.7 °C, 40 s; 72 °C, 35 s); 72 °C, 10 s; hold at 4 °C. Length and concentration of the PCR product was checked using a 1.5% agarose gel.

***trnC-ycf6* region (529 bp).** *trnC-ycf6* has been utilized primarily for haplotype identification and network analysis in order to infer phylogenetic history and evolutionary relationships in plants (Carlsen and Croat, 2013). The *trnC-ycf6* region was amplified using the primer pair *trnC*^{GCAF} (CCA GTT CRA ATC YGG GTG) and *ycf6R*(GCC CAA GCR AGA CTT ACT ATA TCC AT) (Shaw et al., 2005). The reaction was performed in a final volume of 25 μL containing 1x reaction buffer (5x Mango *Taq*TMColourless Reaction Buffer, (Bioline)), 0.5 U Mango *Taq*TMDNA polymerase (Bioline), 3 mM MgCl_2 , 0.16 μM of each primer and 0.2 mM dNTPs. The PCR was performed with the program 94 °C, 2 min; 30x (94 °C, 45 s; 67 °C, 40 s; 72 °C, 22 s); 72 °C, 1 min; 4 °C till program stop. Length and concentration of the PCR product was checked using a 1.5% agarose gel.

***trnH-psbA* region (224 bp).** The *trnH-psbA* is used for DNA barcoding and species identification (Telford et al., 2011; Kress et al., 2005; Hebert et al., 2003) as well as population genetic and phylogenetic analysis also, for example, in other *Dianthus* species like *D. broteri* Boiss. & Reut. (Balao et al., 2010) or in the comparison of different European *Dianthus* species (Valente et al., 2010). For the amplification of the intergenic spacer *trnH-psbA* the mix was prepared as for *trnC-ycf6* using the according primer pair: *trnH*^{GUG} (CGC GCA TGG TGG ATT CAC ATT CC) and *psbA* (GTT ATG CAT GAA CGT AAT GCT C) (Shaw et al., 2005). A touchdown PCR was performed following the program: 94 °C, 2 min; 3x (94 °C, 45 s; 62 °C, 40 s; 72 °C, 28 s); 3x (94 °C, 45 s; 61 °C, 40 s; 72 °C, 28 s); 3x (94 °C, 45 s; 60 °C, 40 s; 72 °C, 28 s); 3x (94 °C, 45 s; 59 °C, 40 s; 72 °C, 28 s); 25x (94 °C, 45 s; 58 °C, 40 s; 72 °C, 28 s); 72 °C, 1 min; 4 °C till program stop. Length and concentration of the PCR product was checked using a 1.5% agarose gel. Due to the contamination with a unspecific by-product of shorter length the *trnH-psbA* region PCR fragments were amplified after cloning. A 1.5% agarose gel was run and the corresponding band of the *trnH-psbA* PCR fragment was purified using either the NucleoFast 96 PCR Cleanup Kit (Macherey-Nagel, Düren, Germany) or the Wizard SV Gel and Clean-Up System (Promega, Mannheim, Germany) following the manufacturers specifications. The *E. coli* strain JM109 (F'[traD36 proA+B+ lacIq (lacZ)M15] (lac-proAB) glnV44 (supE44) e14- (McrA-) thi gyrA96 (NalR) endA1 hsdR17(rk- mk+) relA1 recA1, Promega, Mannheim, Germany) was prepared for ligation using the Competent *E. coli* Transformation Kit and Buffer Set, (Zymo Research Europe GmbH, Freiburg, Germany) following the manufacturers specifications.

For ligation a pGEM-T vector (pGEM-T vector system I, Promega) was used. The 10 μL reaction mix contained 6 μL 2x Rapid Ligation Buffer, 50 ng vector, 2 μL Insert and

3 U T4 DNA-ligase (Promega) and was kept at 4 °C overnight. 2 μL of ligation mix was added to the prepared cell aliquot (100 μL), incubated on ice for 10-20 min and plated on LB/Ampicillin/IPTG/X-Gal plates (Ampicillin Sodium Salt Ultrapure 100 $\mu\text{g}/\text{mL}$ (USB Corporation, Cleveland, USA); IPTG (0,5 M) 1 $\mu\text{L}/\text{mL}$ (Roth; Karlsruhe, Germany); X-Gal 50 mg/mL^{-1} (Bioline)). The plates were incubated at 37 °C overnight. Four to eight white colonies were picked and dissolved in 10 μL ddH₂O. The correct insertion of the fragment was verified using a colony PCR using the SP6 (5'-ATTTAGGTGACACTATAGAA-3') and T7 (5'-TAATACGACTCACTATAGGG-3') primer in the mix: 1x reaction buffer (5x Mango *Taq*TM Coloured Reaction Buffer), 0.2 mM dNTPs, 1 mM MgCl₂, 0.2 μM of each primer, 1 U Mango *Taq*TM DNA-polymerase and 5 μL of colony batch. The PCR reaction was performed following the program: 95 °C, 5 min; 40x (95 °C, 1 min; 50 °C, 1 min; 72 °C, 1 min); 72 °C, 5 min; hold at 4 °C. The reaction result was verified on a 1.5% agarose gel. Overnight cultures of promising colonies were prepared in 3 mL LB medium containing 0.1 mg/mL^{-1} ampicillin at 37 °C and 200 rpm on a shaker. The plasmids were extracted from the overnight culture using the Isolationkit Nucleo Spin Plasmid (Macherey-Nagel, Düren, Germany). The results were verified using restriction enzymes (*Apa*I-HF and *Sac*I, *Pst*I-HF and *Apa*I-HF, *Sph*I-HF and *Pst*I-HF (Biolabs, Frankfurt, Germany)). For each reaction a mix was prepared that contained 2 μL NEBuffer 4 (Biolabs), 0.2 μL BSA (100x Bovine Serum Albumin; Biolabs), 0.3 μL of the two corresponding restriction enzymes, 16.2 μL ddH₂O and 1 μL of the isolated plasmid. The reaction mix was incubated at 37 °C for one to two hours and the results were verified on a 1.5% agarose gel. The promising plasmids were sequenced. The forward and reverse sequences were reviewed and edited in Seqman 4.00 (DNASTAR, USA). The consensus sequences for each individual were created and compared with known sequences from NCBI using BLAST (Basic Local Alignment Search Tool) (Camacho et al., 2009).

Haplotype concatenation. I generated haplotype codes for each of the three markers and concatenated them into one final haplotype combination (Kiefer et al., 2009). I filtered individuals for either a complete sequence for all three marker haplotypes or for sequences that allowed an unambiguous assignment to a haplotype combination based on the regional occurrence of haplotypes (see Digital Supplement "S_I.3.1-plastid_marker_Dg_Dgm.xlsx" and "S_I.3.2-plastid_marker_additional_species.xlsx").

2.5 AFLP data and plastid marker genetic data analysis

AFLP data analysis. I calculated different metrics to evaluate the distribution of diversity and overall structure of the AFLP data using R (script: AFLP metrics.R, (R Core Team, 2023; Wickham et al., 2023)): average number of bands (F_{bands}), average number of polymorphic sites ($F_{polymorph}$), average number of occurrence of rare alleles (F_{rare}) as well as number of different rare alleles per region (F_{rare} total), average number of different fragments found (F_{tot}), as well as number of fragments unique to one region were counted (F_{unique}). I defined rare alleles as those that occur with a frequency of < 0.01 in the entire

dataset, as the often used threshold of 0.05 results in approximately 208 of the 362 loci being classified as rare (compared to 96 with a cut-off of 0.01). In addition the frequency-down-weighted marker (DW) following [Schönswetter and Tribsch \(2005\)](#) was calculated based on the formula:

$$DW = \sum_{i=1}^n \frac{n_pop_i}{n_all_i} \quad (2.1)$$

with n_pop the number of occurrences of a AFLP marker at locus i in the population and n_all the number of occurrences at said locus in the whole dataset. The values obtained for each locus are summed over the number of loci n . The obtained DW value is said to be higher in populations where rare markers could accumulate due to mutations over longer periods of time, indicating long-term isolated populations while in contrast newly established populations would show lower DW values. To consider unequal sample size random subset of n individuals per region or population were generated with n being the number of sampled individuals in the smallest group. The parameters were calculated, and a new subset generated. After 1000 repetitions means and standard deviations were computed. In addition mean values for populations were calculated for $n = 5$ and 100 repetitions. Neis' average gene diversity (H) was calculated for regions using the software Arlequin v.3.5.2.2 (Average gene diversity over loci) ([Excoffier and Lischer, 2010](#)). In order to correct for sample size differences subset of 10 individuals per region were generated. Neis' gene diversity was calculated for each subset and the mean as well as standard deviation was calculated based on 100 subsets. I calculated Jaccard distances from the AFLP data using the R function [`dist(x, method = "binary")`] ([R Core Team, 2023](#)), geographical distances using the function [`distm(x, fun = distHaversine)`] ([Hijmans et al., 2022](#)) and a Mantel correlogram (`vegan` package, ([Oksanen et al., 2022](#))) using Spearman correlation (`r.type = "spearman"`) and a correction for multiple testing using the Holm method (`mult = "holm"`). I chose distance classes of varying sizes to ensure equal distribution of distances in each group. A total of 1000 permutations were used for test of significance ($nperm = 1000$). Genetic variation among regions, localities and substrate types was analysed by AMOVA using Arlequin v.3.5.2.2 ([Excoffier and Lischer, 2010](#)). To infer population structure and assign individuals to populations or genetic clusters I used STRUCTURE version 2.3 ([Pritchard et al., 2000](#)) using settings appropriate for dominant markers defining a ploidy of one, without the admixture option (`NOADMIX = 1`) and with correlated allele frequencies (`FREQSCORR = 1`) ([Pritchard et al., 2010](#)), as well as the *locprior* setting, providing prior information on sampling location without influencing the optimal K value ([Hubisz et al., 2009](#)). Ten runs with 100,000 iterations were performed with a burn-in of 10,000 iterations for the number of clusters ranging from $K = 1$ to 9. I calculated mean estimates of posterior probabilities for each number of clusters K , as well as the statistic ΔK ([Evanno et al., 2005](#)) to estimate the most significant and meaningful number of clusters to consider using STRUCTURE HARVESTER ([Earl and VonHoldt, 2012](#)) and CLUMPP ([Jakobsson and Rosenberg, 2007](#)). In addition I used pophelper ([Francis, 2017](#)) to further process the structure results, confirming

the $L(K)$ and ΔK and the group mean values of regions and localities. The results were visualized using `ggplot2` (Wickham, 2016). Based on the STRUCTURE results individuals were assigned to groups if the proportion of a cluster in the genetic composition of the individual exceeds 75%. Using these groups and the information on origin bedrock I performed a Chi²-test and Fisher test using the `Crosstable` function from the R package "gmodels" (Warnes et al., 2022) to test the independence of Structure cluster assignment/distribution and bedrock type.

Plastid haplotype analysis. Based on an alignment of the resulting plastid haplotype sequences TCS ver.1.21 (Clement et al., 2000) was used to create a statistical parsimony network. For this a manually generated SNP matrix was used extracting all Single Nucleotide Polymorphisms (SNPs) as well as coding insertions/deletions longer than one base pair as a single mutations (Simmons and Ochoterena, 2000). The SNP matrix is given for each marker in the Appendix Table A.2, Table A.3 and Table A.4. Due to the exclusion of two sites, one in the *trnL-trnF* marker and one in the *trnH-psbA* marker, exhibiting complicated combinations of SNPs and Indels, where the underlying mutation steps leading to the final result are unclear, some haplotypes were missing differences in the SNP matrix while differences were present in the total alignment (see Digital Supplement "S_I.3.3-Datamatrix_Indel_SNPs.xlsx" and "S_I.3.4-haplotypes_Dg_Dm.fas"). TCS calculates these networks based on the maximum parsimony principle creating a network requiring the least number of evolutionary steps. I calculated gene diversity indices and hierarchical AMOVA using Arlequin v.3.5.2.2 (Excoffier and Lischer, 2010) based on the whole alignment. Gene diversity was calculated following the same logic as for the AFLP data, generating subsets of $n = 5$ individuals and calculating mean and standard deviation for 100 subsets. The four individuals from Brandenburg (Ger BB) were included in the Central German data set. I visualized the geographical distribution and variation of the haplotypes using the package "ggplot2" in R (Wickham, 2016). Chi²-test and Fisher test was performed using the `Crosstable` function from the R package "gmodels" (Warnes et al., 2022) to test the independence of haplotype groups inferred from the TCS network and bedrock type as well as region.

2.6 Plastome DNA sequencing, assembly, phylogenetic reconstruction, and divergence time estimates

The phylogenetic network based on the plastid haplotypes was used to select a diverse set of haplotypes and the respective plants from the Botanical Garden for a phylogenetic reconstruction and the calculation of divergence time estimates. The use of high-throughput techniques like the shallow sequencing genome skimming method, allows for a cost efficient analysis of high-copy fractions of the total genomic DNA like repetitive elements and organelle genomes like those of plastomes and mitochondria. Plastid genomes as well as plastid markers like *rbcL* and *matK* genes are used for phylogenetic studies and as DNA barcodes

(Dodsworth, 2015). In addition to fresh, green leaf material this method also yields good results for dried leaf material from herbaria vouchers by focusing on the still higher abundance of plastome DNA and repetitive elements (Nevill et al., 2020). In my study, the fresh leaf tissue of 23 individuals from the genus *Dianthus* was selected from plants cultivated at the Botanical Garden Heidelberg as well as dried leaf material from a voucher (HEID 813086) based on the plastid haplotype characterization (Table 2.1). Genomic DNA was extracted using the Invisorb® Spin Plant Mini Kit (STRATEC Biomedical, Birkenfeld, Germany), DNA quality was checked on a 1% agarose gel and concentrations were measured using the Invitrogen Qubit® 2.0 fluorometer kit (Thermo Fisher, Freiburg, Germany). Library preparation and Illumina sequencing was performed by the CellNetworks Deep Sequencing Core Facility (Heidelberg, Germany) using the SMARTer® ThruPLEX® Tag-seq Kit (Takara Bio Inc, Saint-Germain-en-Laye, France). Sequencing was done on Illumina NextSeq 550 sequencing system in 150bp paired-end mode. Raw reads were filtered for quality only retaining reads longer than 50 bp and a Phred score >30. I removed adapter sequences using the program trimmomatic (Bolger et al., 2014) and only reads where both paired reads passed the filtering process were used I then mapped the trimmed reads to a published *D. gratianopolitanus* plastid genome (LN877387.1) using BWA (mem algorithm; (Li, 2013)) to generate reference-based assemblies. To reduce secondary alignments due to duplicated sequences in the reference one copy of the inverted repeat region was removed. Penalty for unpaired reads in BWA was set to 15. I filtered the mapping for reads with mapping quality >1 and removed duplicate reads using MarkDuplicates from Picard (<http://broadinstitute.github.io/picard/>) and samtools (Li et al., 2009). To improve alignment quality and for variant calling gatk3 tools (McKenna et al., 2010) was used. I used FastaAlternateReferenceMaker, a gatk3 tool, to generate sequences including detected SNPs and indels. Regions with a coverage <10 and a mapping quality of <30 were marked using gatk3 and masked using bedtools (Quinlan and Hall, 2010). I realigned the obtained reference-based mapped sequences to the reference and transferred gene annotations using cpanno (Kiefer et al., 2024). For phylogenetic reconstruction I included additional plastomes from NCBI (see Table 2.2). An additional *Dianthus longicalyx* plastome (MT001881) used in the study of Meng et al. (2023) on differentiation *Dianthus* species and varieties based on plastome sequences is available from NCBI but was not included in my study, due to later publication.

In total I extracted 110 coding regions, regions encoding tRNAs or rDNAs bedtools (Quinlan and Hall, 2010) and concatenated the gene alignments using the script catfasta2phym1 (<https://github.com/nylander/catfasta2phym1>). I used PartitionFinder 2.1.1 (Lanfear et al., 2017) to find a suitable molecular evolutionary model and partitioning schemes for phylogenetic reconstruction. I tested models implemented in RAxML-ng (Kozlov et al., 2019) and BEAST2 (Bouckaert et al., 2014) in a greedy search, with allowed linked branch lengths using the corrected Akaike Information Criterion (AICc) for model selection. The alignment, partitions and suitable models were used as input for the phylogenetic reconstruction using RAxML-ng (see Digital Supplement "S_I.4.1-Raxml_tree.pdf"). The algorithm started using 20 parsimony trees, branch length was set to linked and a total

Table 2.1: *Dianthus* species included in plastome analysis List of species, their sample origin, Lab-internal LabID and official HEID-number under which they can be found in the database of the Botanic garden Heidelberg (gartenbank.cos.uni-heidelberg.de)

HEID	LabID	GenBank accession	Species	locality
1000551	1369	OR939655	<i>Dianthus serotinus</i> Waldst. & Kit.	HU: Kiskunsag NP : Magyarorszag
1000541	1363	OR911458	<i>Dianthus hyssopifolius</i> L.	IT: Abruzen: Gran Sasso: Tre Valloni
1000533	1361	OR915882	<i>Dianthus hyssopifolius</i> subsp. <i>gallicus</i> (Pers.) M. Lainz & Munoz Garm	BA (Bosnia and Herzegovina) : Trebevic (seeds)
1000532	1360	OR915883	<i>Dianthus petraeus</i> Waldst. & Kit.	FR: Botanical Garden Nantes (seeds)
1000531	1358	OR915884	<i>Dianthus alpinus</i> L.	AUT: Noe: Ybbstaler Alpen: Oetscher
1000526	1356	OR915885	<i>Dianthus waldsteini</i> Sternb. (syn. <i>D. sternbergii</i> Sieber ex Capelli)	AUT: K: Baerental
1000554	1348	OR939652	<i>Dianthus arenarius</i> L.	DE : BB : near Oder river, same latitude as Berlin
1000553	1300	OR939656	<i>Dianthus broteri</i> Boiss. & Reut.	ES: El Maimo y Montcabrer
1000010	4383	OR915886	<i>Dianthus cintranus</i> Boiss. & Reut.	PT: Lisboa: Parque Natural de Sintra-Cascais, Cabo da Roca
1000507	2652	OR939659	<i>Dianthus superbus alpestris</i> Kablk. ex Čelak.	AUT: Hohe Tauern, Glocknergruppe, Kaprun, Stausee Mooserboden, Ebmaten
1000002	2649	OR915887	<i>Dianthus blandus</i> (Rchb.) Hayek	AUT: Steiermark: Liezen: Gesäuse, Schuttkar östlich der Gsängscharte: Dolomitschutt
1000452	439	OR939654	<i>Dianthus lumnitzeri</i> Wiesb.	AUT: Noe: BL: Braunsberg 0
1000453	1161	OR939653	<i>Dianthus lumnitzeri</i> Wiesb.	AUT: Noe: BL: Hundsheimer Berg
1000491	1419	OR939660	<i>Dianthus neitreichii</i> Hayek	AUT: Noe: MD: Anninger
1000477	1241	OR915888	<i>Dianthus moravicus</i> Kovanda	CZ: Jihomoravsky kraj: okres Znojmo: Vrch Vinohrady (Tabor) SE Rokytna
1000142	464	OR939661	<i>Dianthus gratianopolitanus</i> Vill.	DE : BW : HDH : Eselsburger Tal : Jungfrauen
1000251	459	OR915889	<i>Dianthus gratianopolitanus</i> Vill.	DE : BY : HO : Wurlitzer Serpentin : Wojaleite
1000358	447	OR939662	<i>Dianthus gratianopolitanus</i> Vill.	FR: Massif Central: Auvergne: Puy-de-Dome: Monts Dore: Puy-de-Sancy
1000423	441	OR939663	<i>Dianthus gratianopolitanus</i> Vill.	UK: SOM: Mendip Hills: Cheddar Gorge
1000014	3634	OR939657	<i>Dianthus gratianopolitanus</i> Vill.	CH: AG: Saeliflue
1000421	392	OR915890	<i>Dianthus gratianopolitanus</i> Vill.	LU: Diekirch: Bourscheid-Michelau
	8106913	OR939665	<i>Dianthus gratianopolitanus</i> Vill.	GER: Lower Saxony: Süntelfelsen
	813086	OR939664	<i>Dianthus praecox</i> Willd. ex Spreng. subsp. <i>Praecox</i>	SLO: Velka Fatra
	3286	OR939658	<i>Dianthus pavonius</i> Tausch.	FR: Rhone-Alpes: Haute-Savoie : Mt. Cenis

Table 2.2: Species and GenBank accession numbers

List of additional species from the genus *Dianthus* as well as representatives from the family Caryophyllaceae used as outgroup for the plastome analysis and their corresponding accession numbers.

Species	GenBank
<i>Dianthus gratianopolitanus</i> Vill.	LN877387.1
<i>Dianthus gratianopolitanus</i> Vill.	LN877388.1
<i>Dianthus gratianopolitanus</i> Vill.	LN877389.1
<i>Dianthus gratianopolitanus</i> Vill.	LN877390.1
<i>Dianthus gratianopolitanus</i> Vill.	LN877391.1
<i>Dianthus gratianopolitanus</i> Vill.	LN877392.1
<i>Dianthus gratianopolitanus</i> Vill.	LN877393.1
<i>Dianthus gratianopolitanus</i> Vill.	LN877394.1
<i>Dianthus gratianopolitanus</i> Vill.	LN877395.1
<i>Dianthus moravicus</i> Kov.	LN877396.1
<i>Dianthus longicalyx</i> Miq.	KM668208.1
<i>Dianthus caryophyllus</i> L.	NC039650.1
<i>Silene vulgaris</i> (Moench) Garcke	NC016727.1
<i>Agrostemma githago</i> L.	NC023357.1
<i>Gymnocarpos przewalskii</i> Maxim	NC036812.1
<i>Gypsophila vaccaria</i> (L.) Sm.	NC040936.1

of 1000 bootstrap replicates were calculated. The penalized likelihood approach as implemented in treePL (Smith and O’Meara, 2012) was used for divergence-time analysis using the optimal maximum likelihood tree and the 1000 bootstrap replicates. I analysed the bootstrap support with RAxML-ng followed by the dating with treePL using calibration points from Frajman et al. (2009) (*Gypsophila-Dianthus*: ~20,18 mya; *Silene-Gypsophila/Dianthus*: ~29,76 mya) and visualized the resulting tree using FigTree v1.4.2 (<http://tree.bio.ed.ac.uk/software/figtree/>). I determined the corresponding haplotypes based on the three plastid marker (*trnL-trnF*, *trnC-ycf6*, *trnH-psbA*) and visualized the geographic distribution as well as location within the network. I transferred the divergence time estimates to the TCS network to add a time estimation to both the network and geographical distribution of the marker haplotypes.

2.7 Ploidy and genome size

Karyological analyses - Chromosome counting in root tips. Somatic chromosome numbers are typically counted in cells in mitotic metaphase. Due to the high mitotic activity in healthy root tips there is a high abundance of cells in different stages of cell division including stages with high condensed chromosomes that facilitates observation and counting of chromosomes. The method is used in studies investigating ploidy and polyploids like in a study on the European *Dianthus* sect. *Plumaria* by Weiss et al. (2002) or as an additional tool in studies involving both ploidy as well as genome size (e.g. (Hu et al., 2023)). The haploid chromosome number in *D. gratianopolitanus* is 15, leading to $2n = 60$ chromosomes in tetraploids and $2n = 90$ chromosomes in hexaploids. 39 *D. gratianopolitanus* (see Table A.5) were chosen to represent a transect throughout the distribution range with a special focus on the southern french regions. 10-20 root tips per plant were collected and pre-treated in 8-hydroxyquinolin at room temperature in darkness for 3 h. The material was fixed in 3 : 1 ethanol-acetic acid overnight at 6°C, transferred to 70% ethanol and kept at -80 °C for long-time storage.

Eight root tips per plant were transferred to a dyeing dish, washed three times with dd H₂O followed by a final washing step for 5 min in 1 mM Citrate buffer (10 mM Trisodium citrate, 10 mM citric acid, in H₂O). To enzymatically digest the cells and expose only the nuclei an enzyme stock solution (1% cellulase, 1% pectolyase, 1% cytohelicase in citrate buffer) was diluted 1:10 with citrate buffer. The root tips were digested in 2 mL diluted enzyme solution for 2.5 h at 37°C. The root meristem of the digested root tips was transferred onto a microscopy slide, excess fluid was removed, and the cells were macerated using a dissection needle. After adding a drop of acidic acid, the slide was incubated on a heating plate with 42 °C for 1 min. The slide was washed with 3:1 ethanol-acetic acid to remove leftover cell debris and dried on the heating plate. The slides were fixed and stained using 25 µL VECTASHIELD®HardSet™ Antifade Mounting Medium with DAPI and left to dry overnight in darkness at room temperature. Pictures were taken with a Zeiss Axioskop and the Zen software.

Flow Cytometry (FCM). The term "genome size" covers two main aspects. Firstly, it refers to the total amount of DNA contained within a single set of chromosomes, known as the Cx-value. Secondly, it describes the DNA content of the unreplicated haploid genome, the so called C-value, which essentially means half of the total DNA content regardless of an organism's ploidy. On the other hand the 1Cx-value is calculated by dividing the 2C-value by the organism's ploidy level. In diploid organisms, C-value and Cx-value are the same, but in polyploids where there's more than one set of chromosomes in the haploid state, they differ (Greilhuber et al., 2005; Kron et al., 2007). Flow Cytometry (FCM) is a valuable tool for genome size and ploidy measurement in systematics and evolutionary biology and allows a fast and uncomplicated but reliable estimation of DNA content (Hu et al., 2023; Nora et al., 2013; Doležel et al., 2007). Nuclei stained with fluorochromes are focused into a stream of single nuclei and guided to cross a laser beam of defined wavelength. The excited particles emit light themselves and by comparing the relative amount of light emitted by a sample nucleus compared to nuclei of an included standard with known DNA content the nuclear DNA amount in a sample nucleus can be inferred (Kron et al., 2007).

The DNA content was measured for 287 *D. gratianopolitanus* and 13 *D. gratianopolitanus* subsp. *moravicus*. Approximately the size of 0.5 cm² of fresh leaf material per plant was collected avoiding leaf tips, to minimize noise due to nuclei caught during cell division. The preparation was performed following the sysmex CyStain PI Absolute P protocol. The fresh leaf material was covered in 500 µL Nuclei Extraction Buffer and finely chopped using fresh razor blades. After 5 minutes incubation the nuclei were filtered through CellTrics™ disposable filters (30 µm) and stained using 2 ml freshly prepared sysmex Staining Solution (60 µL RNase A, 120 µL Propidium Iodide, 20 mL Staining buffer, kept on ice) for one hour in the dark at room temperature. Pea (*Pisum sativum*, 2C = 9.09 pg) (Doležel et al., 1998) was used as standard. Samples were measured using the CyFlow Space (Sysmex-ParTec GmbH, Münster/Görlitz, Germany) flow cytometer equipped with a green (532 nm) solid state laser at a rate of 30 particles per second and a total count of 10,000 particles per sample. The data was evaluated with the software FloMax FCS 2.0 (Sysmex-ParTec GmbH, Münster/Görlitz, Germany).

Plants with determined ploidy level from chromosome counting were used to calibrate the 1Cx value range for *D. gratianopolitanus*. I grouped the individuals by substrate of origin and clustering based on the AFLP Structure results. I calculated boxplots and linear regressions using ggplot2 (Wickham, 2016) and nonparametric significance tests using ggpubr.

3 | Results

3.1 Population structure indicate two major gene pools

AFLP data from 1676 *D. gratianopolitanus* and 36 *D. gratianopolitanus* subsp. *moravicus* individuals were used for a genetic and population structural assessment throughout the whole species distribution range. The total AFLP error rate is $< 2\%$ over all 362 loci according to Bonin et al. (2004). A comparison between the average number of bands between ploidy levels within the Massif Central suggests no statistical difference in number of bands between hexaploid ($n = 11$) and tetraploid ($n = 13$) individuals (Mann-Whitney U test, $p = 0.08 > 0.05$, Appendix Figure A.1), allowing the inclusion of tetraploids in further analysis. Of the 362 generated AFLP fragments between 108 ($\sim 30\%$, Poland) and ~ 167 ($\sim 46\%$, Swabian Alb, Germany) were found (F_{tot} Table 3.1). The mean number of bands per individual, F_{bands} , varied between ~ 53 in the French Massif Central and ~ 67 in Belgium and Luxembourg (overall mean = 62.51, SD = 6.65). The mean number of polymorphic bands per region, F_{poly} , ranged from 76 ($\sim 21\%$) in Poland to ~ 139 ($\sim 38\%$)(Swabian Alb). Of the 362 fragments 96 were classified as rare, occurring in $< 1\%$ of accessions. Mean values of found rare alleles, F_{rare} , varied between 1 in Poland and the Bavarian serpentine population and 11 in the French Diois region, while in total the most rare alleles, F_{rare} total, can be found in the biggest subset originating from the Swabian Alb (F_{rare} total = 63, $n = 629$). As an additional marker for divergence the number of unique fragments, F_{unique} , was calculated. In total 29 unique fragments were found with zero in the French Jurassic, the Bodensee region, Bavarian Jurassic and serpentine populations, populations from Brandenburg, the Czech Republic, Poland, and Belgium and Luxembourg. Ten unique fragments are found in the Swabian Alb. The frequency-down-weighted marker (DW) varied between 1.79 in the Bavarian serpentine population and 4.87 in the Diois region. Average gene diversity over loci ranged between 0.0648 (± 0.0315) in the French Massif Central and 0.107 (± 0.0516) in the Bavarian Jurassic. The genetic assignment using STRUCTURE analysis indicates three clusters ($K = 3$) as the optimal number of genetic clusters according to ΔK (Appendix Figure A.2 and Digital Supplement "S_I.2.4-evanno.pdf" and "S_I.2.5-evanno.txt"). $K = 2$ displays a division into two major gene pools: the first one in the southwest ranging from southern France towards Switzerland and a second one located in Northern Germany and the Czech Republic. With $K = 3$ a transition zone, connecting the two clusters, in the French Jurassic, Luxembourg, Switzerland, and

Southern Germany, is emerging (Figure 3.1). Populations in England show a mixed signal but with a high proportion assigned to the third cluster. The included *D. gratianopolitanus* subsp. *moravicus* accessions were mainly assigned to the Northern German and Czech cluster. The overview for different numbers of clusters is given in Appendix Figure A.3. The structure results per population is given in the Appendix Figure A.4 and a more detailed visualization of $K = 3$ is given in the Appendix Figure A.5 and Figure A.6. The two major clusters align well with substrate variations with a more calcareous bedrock throughout the Swabian Alb, the Prealps and Alps, and the siliceous bedrocks of Northern Germany and the Bohemian Massif. The χ^2 was used to examine the relationship between substrate type (limestone, serpentine, siliceous+) and Structure cluster assignment ($K = 3$, Clusters one (orange cluster), two (blue cluster) and three (pink cluster)). Only accessions of *D. gratianopolitanus* with an assignment of $> 75\%$ to one Structure cluster and with known bedrock are considered for the test. The results show a significant association between bedrock type and cluster assignment ($\chi^2(4, N = 1628) = 1076.892, p < 0.001$). Because of possible inaccuracy due to low expected frequencies the recommended Fisher's test was performed in addition, confirming the association of substrate and Structure cluster ($p < 0.001$). While the siliceous+ group showed more individuals assigned to cluster two than expected (residual $res = 20.143$), the limestone group had significantly fewer individuals assigned to cluster two than expected (residual $res = -15.222$). On the other hand, the limestone group had more individuals assigned to group one than would have been expected (residual $res = 11.115$) and the siliceous+ group had significantly fewer assigned to cluster one (residual $res = -14.803$). The ten included individuals from serpentine bedrock were assigned to cluster two. Cluster three in the contact zone includes mostly individuals from the limestone bedrock (residual $res = 4.465$) and is underrepresented in the siliceous+ group (residual $res = -5.762$). In summary, the siliceous+ group showed higher proportions of individuals assigned to cluster two (blue) while the limestone group had individuals primarily assigned to cluster one (orange) and three (pink).

I also calculated the summary statistics on population level with a subsampling size $n = 5$ without considering individual gene pool assignment, resulting in data for 111 populations (see Digital Supplement, "S_I.2.3-AFLP_Stats_Populations.xlsx"). If meta-populations of sufficient sizes were divided by possible barriers to gene flow, e.g. rivers, they were considered to be separate populations. While the precise numeric values differed between regional level and single populations the overall trends for regional differences can be confirmed on a population level, with e.g. overall higher values of the DW in Diois. Total number of fragments ranged between 79.54 ± 2.20 (*Dianthus gratianopolitanus* subsp. *moravicus*, Suche skaly) and 122.89 ± 6.81 (Altmühltal, Ger_BY_Jura) and number of polymorphic bands per population varied between 29 (Jägerstein, Swabian Alb) and 87 ± 7.05 (Altmühltal, Ger_BY_Jura). Rare alleles could be found in nearly all analysed populations ranging between 0 and 10 mean number of rare alleles found in the population of Nägelesstein on the Swabian Alb that also showed the highest frequency-down-weighted marker ($DW = 3.63, n = 5$). While most populations did not exhibit unique fragments the population from Les

Moucherolles (Switzerland) and Les Grand Delmas (Diois) showed in total 2 unique fragments each. While Les Moucherolles is also the biggest population ($n = 51$) Les Grand Delmas is rather small ($n = 12$) but still also shows high rates of rare alleles (4.56 ± 1.3) and a high DW (2.25 ± 0.71). Indeed besides the population from Nägelesstein, the rate of rare alleles is only surpassed by other populations from Diois (Notre Dame de Beauvoir and Le Roche Colombe), while the DW is only surpassed by the population from Nägelesstein. To compare the genetic structure and longitudinal and latitudinal trends that might reflect footprints of past migrations of the three Structure Clusters, mean cluster assignment values per population were calculated. For further analysis a population was considered to belong to one of the three gene pools if it were assigned to one of the three clusters with a threshold of an assignment of $> 75\%$. Populations with no clear assignment were not further considered (UK, Altmühltal (Swabian Alb), La Chatelaine, Le Chatelet, Rocher de Chatard, Rochers du Chateau Lorient (French Jurassic), Balmfluechöpfli, Chruetzflue, Le Chasseron, Lehnfluh, Ravellenflue (Switzerland)). [Figure 3.2](#) shows the comparisons of and the linear relationships to longitudinal changes of the mean number of bands (F_{bands}), number of polymorphic bands (F_{poly}), and the DW per population. In cluster one (blue) and cluster three (orange) mean number of bands and number of polymorphic bands are higher towards the center of distribution and decrease towards the periphery. Especially in cluster one, whose distribution also follows the east-west axis, this trend can be confirmed by linear models ([Figure 3.2](#), F_{bands} , adj. $R^2 = 0.232$, $p < 0.01$; F_{poly} , adj. $R^2 = 0.222$, $p < 0.01$) with higher numbers at its western border. Overall populations assigned to cluster two (pink) have significantly more mean bands per individual (Mann-Whitney U, $p < 0.01$) while those from clusters one and two did not differ significantly (Mann-Whitney U, $p > 0.05$). Cluster one has a significantly lower number of polymorphic sites compared to clusters two and three (Mann-Whitney U, $p < 0.01$). Cluster two and three do not differ significantly (Mann-Whitney U, $p > 0.05$). The DW does not show a significant relationship with Longitude in clusters two and three but decreases towards the east in cluster one (adj. $R^2 = 0.118$, $p < 0.05$). Here the populations from cluster three have significantly higher DW values followed by those from cluster and cluster one having the overall lowest DW values (Mann-Whitney U, $p < 0.01$).

The latitudinal trends do indicate significant increase of mean number of bands for the blue cluster for populations further north (adj. $R^2 = 0.199$, $p < 0.01$, [Appendix Figure A.7 A](#)), and an significant decreases in the orange cluster the DW in population further to the north (adj. $R^2 = 0.285$, $p < 0.05$ [Figure A.7 C](#)). The pink cluster did not show any significant variation with latitude. To further test the relationship of genetic and spatial distances as well as overall genetic structure a Mantel test and Analysis of Molecular Variance (AMOVA) were performed. The Mantel test reveals a significant correlation (Mantel $r = 0.234$, $p < 0.01$) indicating a decreasing genetic similarity with increasing geographic distance, suggesting isolation by distance [IBD, ([Wright, 1943](#))]. For a more detailed analysis, I calculated a Mantel correlogram with ten distance classes ([Figure 3.3](#)) that shows a significant positive correlation at shorter distances ($\sim 21\text{km}$, $r = 0.129$, $p < 0.001$). The

correlation coefficient gradually decreases and becomes negative at around $\sim 350 - 400\text{km}$ with a significant negative correlation of $r = -0.136$ ($p < 0.01$) at $\sim 1142\text{km}$. In addition the AMOVA (Table 3.2) reveals the genetic variations within populations to be the major contributor with around $\approx 83\%$ (fixation index, $F_{ST} = 0.17036$, $p < 0.01$). Moderate levels of genetic variation are found among populations within regions ($\approx 13\%$, fixation index, $F_{SC} = 0.13080$, $p < 0.01$). Only a small proportion ($\approx 5\%$) of genetic variation is attributed to differences between regions (fixation index, $F_{CT} = 0.04552$, $p < 0.01$).

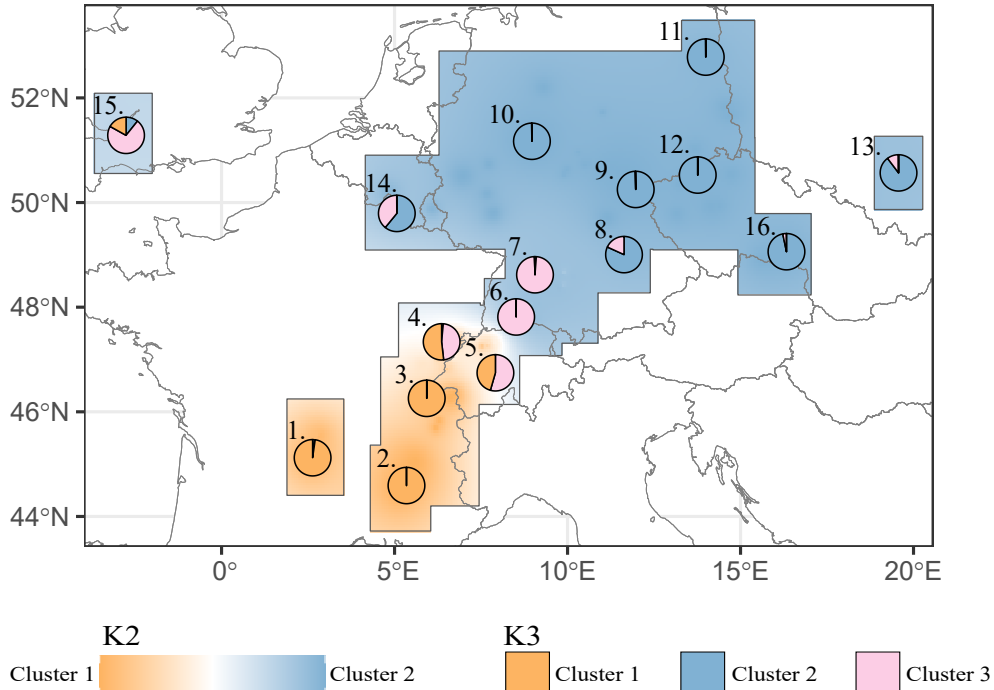


Figure 3.1: *Distribution of spatial AFLP genetic structure STRUCTURE analysis results are given for $K = 2$ as inverse distance weighted (idw) interpolation as background and $K=3$ as region mean for the different regions. Numbers indicate regions according to Table 3.1.*

3.2 Plastid haplotype variation shows varying patterns of genetic diversity

The sequence information of the three plastid intergenic regions was obtained for 857 *D. gratianopolitanus*. The 454 individuals with complete sequences and 206 individuals with incomplete but unambiguous sequences, that allowed for a safe assignment to a haplotype, resulted in a total of 660 individuals of *D. gratianopolitanus* used for further analysis. In addition 12 *D. gratianopolitanus* subsp. *moravicus* were included. 20 different sequences were found for the *trnL-trnF* region, 17 different sequences were found for *trnC-ycf6* region and 21 for the *trnH-psbA* region and concatenated into 39 unique plastid haplotypes with a total alignment length of 1183 bp (*trnL-trnF*: 430 bp, *trnC-ycf6*: 529 bp, *trnH-*

Table 3.1: Summary statistics of AFLP data of *D. gratianopolitanus* per region. Numbering of regions, number of investigated individuals per region (N), number of AFLP fragments (F_{tot}), number of polymorphic sites (F_{poly}), mean number of bands per individual (F_{bands}), number of unique alleles (F_{unique}), mean number of rare alleles (F_{rare}), total number of rare alleles found in the population ($F_{rare\ total}$), frequency-down-weighted marker values (DW) and Average gene diversity over loci (Arlequin) H . To take different sample sizes into account mean values and standard deviation were calculated by repeated subsampling. * Minimum subsample size was set to $n = 13$ the number of individuals from Poland.

Region (N)	F_{tot}	F_{poly}	F_{bands}	F_{unique}	$F_{rare\ total}$	F_{rare}	DW	H
1 FRA_MC (44)	118.90 ± 6.46	93.70 ± 6.51	52.93 ± 1.10	1	9	4.59 ± 1.34	2.75 ± 0.60	0.064813 ± 0.031518
2 FRA_Diois (52)	156.96 ± 7.21	128.41 ± 7.20	59.26 ± 1.41	4	24	11.13 ± 2.00	4.87 ± 0.76	0.077080 ± 0.037303
3 FRA_preAlpes (147)	159.21 ± 6.58	128.91 ± 6.74	62.88 ± 1.43	6	32	6.57 ± 2.34	3.54 ± 0.74	0.091611 ± 0.044156
4 FRA_Jura (53)	146.64 ± 6.43	118.28 ± 6.65	60.85 ± 1.50	0	9	3.32 ± 1.60	2.42 ± 0.37	0.084760 ± 0.040925
5 CH (101)	157.08 ± 7.04	129.49 ± 6.95	61.72 ± 1.62	1	24	5.36 ± 2.21	2.70 ± 0.59	0.079345 ± 0.038372
6 GER_BW_Bodensee (49)	146.28 ± 5.89	119.37 ± 6.30	63.63 ± 1.33	0	6	2.11 ± 1.20	2.26 ± 0.19	0.082218 ± 0.039727
7 GER_BW_Alb (629)	167.36 ± 7.29	138.75 ± 8.37	65.11 ± 1.75	10	63	4.85 ± 2.37	2.76 ± 0.51	0.083765 ± 0.040456
8 GER_BY_Jura (48)	146.78 ± 8.72	116.30 ± 9.16	62.64 ± 1.69	0	10	3.87 ± 1.49	2.22 ± 0.29	0.107414 ± 0.051608
9 GER_BY_Serp (26)	127.20 ± 4.61	98.08 ± 5.27	60.46 ± 0.91	0	2	1.00 ± 0.71	1.79 ± 0.10	0.073101 ± 0.035427
10 GER_Central (399)	150.25 ± 7.21	121.70 ± 7.28	61.42 ± 1.71	5	33	3.77 ± 1.77	2.17 ± 0.47	0.071609 ± 0.034723
11 GER_BB (18)	122.71 ± 3.32	94.48 ± 3.76	65.30 ± 0.99	0	4	3.45 ± 0.61	2.55 ± 0.17	0.090451 ± 0.043609
12 CZ (108)	133.93 ± 6.48	104.82 ± 6.91	59.60 ± 1.35	0	13	3.38 ± 1.76	1.96 ± 0.27	0.067521 ± 0.032795
13 PL (13)*	108.00 ± 0.00	76.00 ± 0.00	58.69 ± 0.00	0	1	1.00 ± 0.00	2.45 ± 0.00	0.065918 ± 0.032039
14 BEL_LU (24)	149.90 ± 5.65	118.84 ± 6.81	67.03 ± 0.89	0	5	3.90 ± 0.87	2.97 ± 0.21	0.099955 ± 0.048091
15 UK (22)	135.26 ± 5.10	108.32 ± 5.73	61.36 ± 1.25	1	5	4.10 ± 0.89	3.14 ± 0.62	0.080892 ± 0.039101
16 <i>D. gratianopolitanus</i> subsp. moravicus (36)	128.08 ± 6.44	99.88 ± 6.25	57.23 ± 1.16	1	6	2.74 ± 1.57	2.07 ± 0.24	0.073985 ± 0.035844

Table 3.2: Analysis of Molecular Variance (AMOVA) for genetic variation in *D. gratianopolitanus* based on AFLP data Significance test were performed in Arlequin v.3.5.2.2. with 1023 permutations ($p < 0.01$). Fixation indices were calculated: $F_{SC} = 0.13080$, $F_{ST} = 0.17036$, $F_{CT} = 0.04552$

Source of variation	degrees of freedom	Sum of squares	Percentage of Variation
Among regions	15	2256.799	4.55 %
Among populations in regions	83	4825.577	12.48 %
Within populations	1632	27036.545	82.96 %
Total	1730	34117.921	

psbA: 224 bp). The plastid marker haplotypes are made available at NCBI, the respective GenBank accession numbers and combinations are given in the Digital Supplement "S_I.3.5-Genbank_accessions_and_haplotype_combinations.xlsx". The two most common haplotypes, ht16 (found in $\sim 27\%$ accessions, see Appendix Table A.6) and ht19 (in $\sim 24\%$), are found throughout the whole distribution range in *D. gratianopolitanus* as well as in *D. gratianopolitanus* subsp. *moravicus*. The more common ht01 (in $\sim 10\%$), ht02 (in $\sim 5\%$), ht03 (in $\sim 7\%$), and ht21 (in $\sim 7\%$) also show a broader distribution over France, Switzerland, Baden-Württemberg, Central Germany, the Czech Republic, and Belgium. In addition, a high amount of unique haplotypes can be found in the South French regions exhibiting a high rate of unique haplotypes with a total of 19 of the 39 haplotypes being exclusive to Southern French regions (Table 3.3). In the TCS network (Figure 3.4) these unique haplotypes from Southern France make up a large proportion of Group 2 and Group 3 but ht29 and ht30 from Group 3 can be found in Baden-Württemberg and Central Germany. A clear geographical separation based on the network layout can not be observed (Figure 3.5) but the χ^2 test indicates an overall pattern when comparing the network groups to either regions or substrate class (limestone and siliceous+). While the χ^2 test indicates a significant link between the haplotype group inferred by the TCS network and geographical region ($\chi^2(df = 70, N = 674) = 490.0847, p < 0.01$) the cell counts were often very small possibly influencing the significance of the test. The Fisher's test was performed but due to computational limitations only simulated p-values were used. However, the simulated p-values (based on 2000 replicates) confirmed the connection between the region and haplotype group ($p < 0.001$). Here we could also observe the strong link between haplotypes in Group 3 with the southern French Dios region ($res = 10.088$). Group 1 has a wider spread distribution over multiple regions, while Group 2 has a higher representation within the Czech Republic ($res = 4.656$), Poland ($res = 4.143$) but also in the Massif Central ($res = 3.345$). The haplotypes ht02 and ht03 from Group 5 show a higher occurrence within Switzerland ($res = 7.306$), the German Bodensee region ($res = 5.899$) but also in Central German regions ($res = 3.869$). They are underrepresented on the Swabian Alb ($res = -4.848$). Group 6 (ht41 and ht43) are linked to a higher degree to the Massif Central ($res = 2.805$) and French Prealpes ($res = 3.632$). The test also indicates a significant association between the haplotype group and substrate class ($\chi^2(df = 5, N = 636) = 14.81, p < 0.05$). Because of possible inaccuracy due to low expected frequencies the recommended Fisher's test was performed in addition. Due to computational limitations only simulated p-values were used which also confirms the association of substrate and haplotype group ($p < 0.001$). While Group 2 ($res = 0.591$) and Group 4 ($res = 1.44$) show a slight over-representation in individuals from limestone bedrock, Group 1 ($res = -0.420$) and Group 5 ($res = -1.339$) show an under-representation. On the other hand, Group 4 is underrepresented in the siliceous+ group ($res = -2.182$) and overrepresented in Group 5 ($res = 2.028$). Gene diversity ranged between 0.3836 (UK) and 0.8456 (Diois), excluding the Bavarian Jurassic, where only one haplotype was found, not allowing for a calculation of gene diversity. The Southern French regions all indicate high genetic diversity, with the Diois region being the hotspot of gene

diversity, followed by the Central German area (0.8319) (Table 3.3). As in the nuclear AFLP data, the source for higher genetic variation is attributed to variation within regions (82%) and within substrates (93%) compared to among regions (18%) and substrates (7%) (Table 3.4).

Table 3.3: Summary on found plastid haplotypes per region. For each region the number of analysed individuals (N), number of different haplotypes (N_{ht_total}), number (N_{ht_unique}) and name of plastid haplotypes unique to this region as well as the gene diversity (Arlequin) is given. Especially the three French regions, from the Massif Central (MC), Diois and the prealps show high amounts of unique haplotypes and high gene diversity. One haplotype (ht14) is restricted to *D. gratianopolitanus* subsp. *moravicus*.

	Region (N)	N_{ht_total}	N_{ht_unique}	name of unique haplotypes	Gene diversity
1	FRA_MC (23)	9	6	ht06, ht07, ht08, ht22, ht44, ht48	0.8116 ± 0.0095
2	FRA_Diois (17)	8	8	ht04, ht05, ht11, ht12, ht33, ht34, ht35, ht47	0.8456 ± 0.0050
3	FRA_prealpes (53)	11	5	ht10, ht37, ht38, ht43, ht46	0.8357 ± 0.0099
4	FRA_Jura (19)	4	0		0.6112 ± 0.0176
5	CH (53)	6	1	ht13	0.6853 ± 0.0158
6	GER_BW_Bodensee (24)	5	0		0.6861 ± 0.0140
7	GER_BW_Alb (240)	10	1	ht09	0.7331 ± 0.0123
8	GER_BY_Jura (9)	1	0		0.0 ± 0.0
9	GER_BY_Serp (12)	3	1	ht39	0.4810 ± 0.0208
10	GER_Central* (140)	9	1	ht18	0.8319 ± 0.0064
12	CZ (34)	4	1	ht15	0.4180 ± 0.0235
13	PL (7)	2	1	ht25	0.4923 ± 0.0060
14	BEL_LU (8)	3	1	ht17	0.6558 ± 0.0054
15	UK (21)	2	1	ht24	0.3836 ± 0.0190
16	<i>D. gratianopolitanus</i> subsp. <i>moravicus</i> (12)	3	1	ht14	0.6670 ± 0.0021

Table 3.4: AMOVA of plastid haplotypes Analysis of molecular variance calculated using Arlequin for (a) by regions, (b) by bedrock type

(a) **AMOVA of plastid haplotypes by region.** Groups based on region of origin. Results indicate the within region variation to be the major contributor reflected by the corresponding $F_{ST} = 0.17905$.

Source of variation	degrees of freedom	Sum of squares	Percentage of Variation
Among regions	15	628.497	17.91 %
Within regions	644	3096.085	82.09 %
Total	659	3724.582	

(b) **AMOVA of plastid haplotypes by substrate.** Groups based on bedrock types: limestone, serpentine, siliceous, sand, volcanic and other unspecified bedrocks. 93.03% of variation can be contributed to within substrate differences ($F_{ST} = 0.06970$).

Source of variation	degrees of freedom	Sum of squares	Percentage of Variation
Among substrates	5	164.073	6.97 %
Within substrates	654	3560.509	93.03 %
Total	659	3724.582	

3.3 Deep evolutionary splits in plastomes pre-date origin of species

A phylogenetic tree and divergence times estimates were calculated based on 15 plastome sequences of *D. gratianopolitanus* as well as plastome sequences of an additional 20 individuals of additional *Dianthus* species (Figure 3.6). In total 110 coding regions, regions encoding tRNAs or rDNAs were used for calculations. The *Dianthus* group is supported as a clade and separated by the outgroup consisting of *Silene vulgaris*, *Agrostemma githago*, *Gymnocarpus przewalskii* and *Gypsophila vaccaria* (Bootstrap support = 100%, see Digital Supplement "S_I.4.1-Raxml_tree.pdf"). Within the *Dianthus* clade, no clear division into species or geographical origin can be observed. The oldest node within the *Dianthus* clade between *D. alpinus* and the remaining *Dianthus* species date back to approximately 1.2 million years ago, the oldest split between two *D. gratianopolitanus* dates back to $\sim 765,000$ years ago. The divergence time estimates for tree tips range between $\sim 711,000$ years (*D. longicalyx*) and $\sim 17,000$ years (*D. gratianopolitanus* OR915890 - *D. blandus* OR915890). Plastid marker haplotypes were inferred for the plastomes of *D. gratianopolitanus* and *D. gratianopolitanus* subsp. *moravicus* and are indicated by colors according to the TCS network position and group. Divergence time estimates connecting the plastid marker haplotypes are included in Figure 3.4. Grouping within the TCS network is reflected within the phylogenetic tree. Individuals located more at the basis of the *Dianthus* clade have marker haplotypes that are not part of the main network (ht02, ht03 (Group 5, purple) and ht10 (Group4, blue)). Group 5 appears as the sister to all others with their divergence dating back to $\sim 765,000$

years ago. Their distribution is focused in the French (Pre-)Alps, Switzerland, and at the Bodensee also occurring in Central Germany. One haplotype from Group 3 (ht06, red) is included in the phylogenetic tree and is located as a sister to Group 2 (yellow) and Group 1 (petrol) with an estimated divergence time of $\sim 493,000$ years. The split between Group 1 and Group 3 dates back to $\sim 338,000$ years ago.

3.4 Genome size differ among bedrock type, Structure cluster and latitude

Chromosome numbers for a transect of the distribution range of *D. gratianopolitanus* (n=39) were counted manually (Appendix Table A.5). In addition, ploidy and genome size were measured via flow cytometry (FCM) for *D. gratianopolitanus* (n=287) as well as *D. gratianopolitanus* subsp. *moravicus* (n=13)(Table A.7). Data is available at flowrepository.org under the ID FR-FCM-Z52A. The comparison of ploidy inferred by chromosome counting and by flow cytometry showed good agreement. On two occasions ploidy levels differed (LabID 760 from CZ and LabID 1706 from the Rhone-Alpes) but due to good accordance of 1Cx-values with other individuals of the same ploidy level inferred by FCM, the ploidy from FCM was trusted. The majority of analyzed accessions showed a hexaploid genome while a small number of tetraploids (n=16) can be found in the French Massif Central and Diois region. In addition, decaploids occurred on four occasions and were estimated using flow cytometry, but need confirmation by chromosome counting.

Comparing the 1Cx of tetra- and hexaploid individuals over the whole range indicates bigger genome sizes in tetraploids (median $1Cx_{tetra} = 0.678$ pg, median $1Cx_{hexa} = 0.632$ pg; Mann-Whitney U test, $p < 0.001$, Figure 3.7 A). To exclude latitudinal effects on genome sizes to assess differences between tetraploid and hexaploid individuals only accessions from the Massif Central and Dios were compared, showing no statistical significance (median $1Cx_{tetra} = 0.678$ pg, median $1Cx_{hexa} = 0.682$ pg; Mann-Whitney U test, $p = 0.48 > 0.05$, Figure 3.7 B) though the sample sizes in both cases were comparable small ($n_{hex} = 13$, $n_{tet} = 14$) hindering a meaningful conclusion.

To exclude the possible influence of the ploidy level on genome sizes only hexaploid individuals were used for further analysis. Linear regression of latitudinal distribution and monoploid genome size (1Cx) grouped by substrate of origin reveals a decrease in genome size with increasing latitude in individuals originating from limestone bedrock, while the serpentine and siliceous+ group does not show this trend (Figure 3.8 A). Accessions from siliceous bedrock as well as volcanic and sandy bedrock were combined in a siliceous+ group. While $\sim 41\%$ of variability in the limestone group ($R^2 = 0.412$, $p < 0.001$) can already be explained by the simple linear regression this can not be shown for the serpentine and siliceous+ groups. Overall, the genome size for accession originating on limestone bedrock (median $1Cx_{lime} = 0.638$ pg) is statistically significantly higher compared to the serpentine (median $1Cx_{serp} = 0.622$ pg, Mann Whitney U Test, $p = 0.001$) and siliceous+ group

(median $1Cx_{sil+} = 0.622$ pg, Mann Whitney U Test, $p < 0.001$), respectively (Figure 3.8 B). A comparison of the genome size of plants originating from serpentine and siliceous bedrock shows no statistically significant differences (Mann Whitney U test, $p = 0.93$). Serpentine plants all originate from Wojaleite in Bavaria, which leads to a smaller sample size as well as no differences in latitudinal distribution hindering a robust statement of their behavior. The linear regression of longitudinal distribution and monoploid genome size (1Cx) shows a significant relationship for the limestone group, where a decrease in genome size could be observed with increasing longitude ($R^2 = 0.286$, $p < 0.001$, Appendix Figure A.8 A).

Following the idea of separated gene pools the linear regression based on the genetic Structure cluster was analysed in Figure 3.9. Individuals were assigned to a cluster if their assignment exceeded the threshold of $> 75\%$. The three clusters are separated by latitude and 1Cx overlaps but show significant differences. The cluster from northern Germany on siliceous bedrock has a smaller Genome size (median $1Cx_{one} = 0.621$ pg) compared to the second cluster in the transition zone (median $1Cx_{two} = 0.634$ pg, Mann Whitney U Test, $p < 0.001$) and third cluster in Switzerland and southern France (median $1Cx_{three} = 0.657$ pg, Mann Whitney U Test, $p < 0.001$). The second and third clusters also differ significantly (Mann Whitney U Test, $p < 0.001$). The linear regression of latitude and 1Cx shows significant trends in the third cluster, where $\sim 25\%$ of variance is explained (adj. $R^2 = 0.279$, $p < 0.01$). In both the first and second clusters explained variation is negative and not statistically significant (adj. $R^2 < 0$, $p > 0.35$). The individual assigned to cluster three (orange) at $\sim 51.25^\circ N$ is from the Cheddar Gorge (UK, limestone) while the one assigned to cluster one (blue) at $\sim 46^\circ N$ is from the French Massif Central (volcanic). The longitudinal trend indicates a weak significant decrease in genome size with increasing longitude for the blue cluster from Northern Germany and the Czech Republic ($R^2 = 0.082$, $p = 0.011$, Appendix Figure A.8 B).

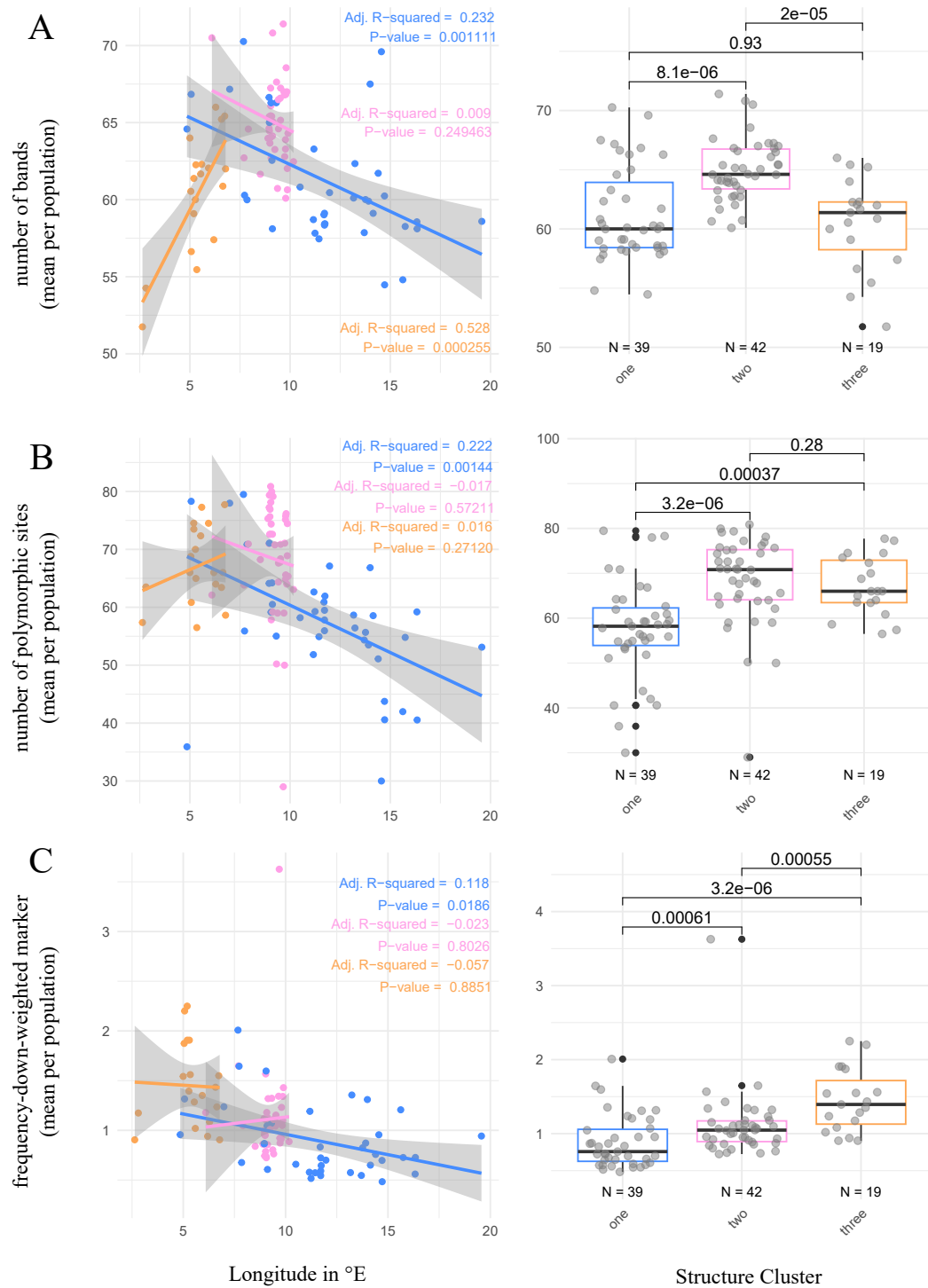
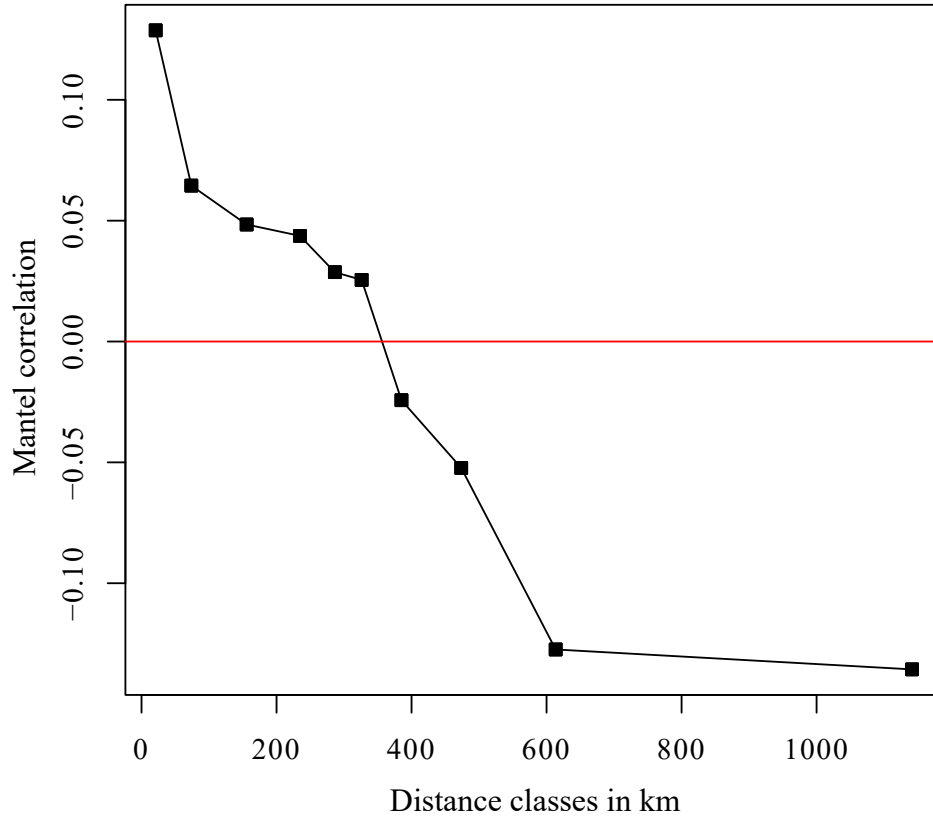


Figure 3.2: Linear relationship of longitude and AFLP statistics (mean) for populations and corresponding boxplots. To ensure sufficient sample sizes and correct for population size, mean values were calculated on basis of $n = 5$ subsamples per population. Colors refer to the respective *STRUCTURE* cluster were populations were grouped by the structure assignment with a threshold of $> 75\%$ population mean assignment to a cluster. Three different statistics are included: **A** number of bands, **B** number of polymorphic sites and **C** frequency-down-weighted marker.



(a) **Figure: Mantel correlogram** filled squares indicate significance ($p < 0.01$)

Distance classes	upper limit of the Distance classes [km]	N of pairwise comparisons	Mantel correl. coefficient	corr. P-value (holm)
1	41.9	2.8100e+05	1.2873e-01	0.000999
2	106	2.8067e+05	6.4512e-02	0.001998
3	206	2.8089e+05	4.8416e-02	0.002997
4	264	2.8079e+05	4.3714e-02	0.003996
5	309	2.8115e+05	2.8686e-02	0.004995
6	343	2.7997e+05	2.5503e-02	0.005994
7	427	2.8089e+05	-2.4286e-02	0.006993
8	520	2.8053e+05	-5.2294e-02	0.007992
9	707	2.8073e+05	-1.2741e-01	0.008991
10	1,580	2.8069e+05	-1.3565e-01	0.009990

(b) **Table: Mantel test results**

Figure 3.3: Mantel correlogram (a) and mantel test results (b) for AFLP data Jaccard-distances for AFLP data was used as genetic distance matrix, ten geographic distance classes were adjusted to contain the same amount of pairwise comparisons, upper distance class limit is given. Calculation of Mantel correlation coefficients was done using Spearman correlation, p-values were adjusted for multiple testing using the Holm method.

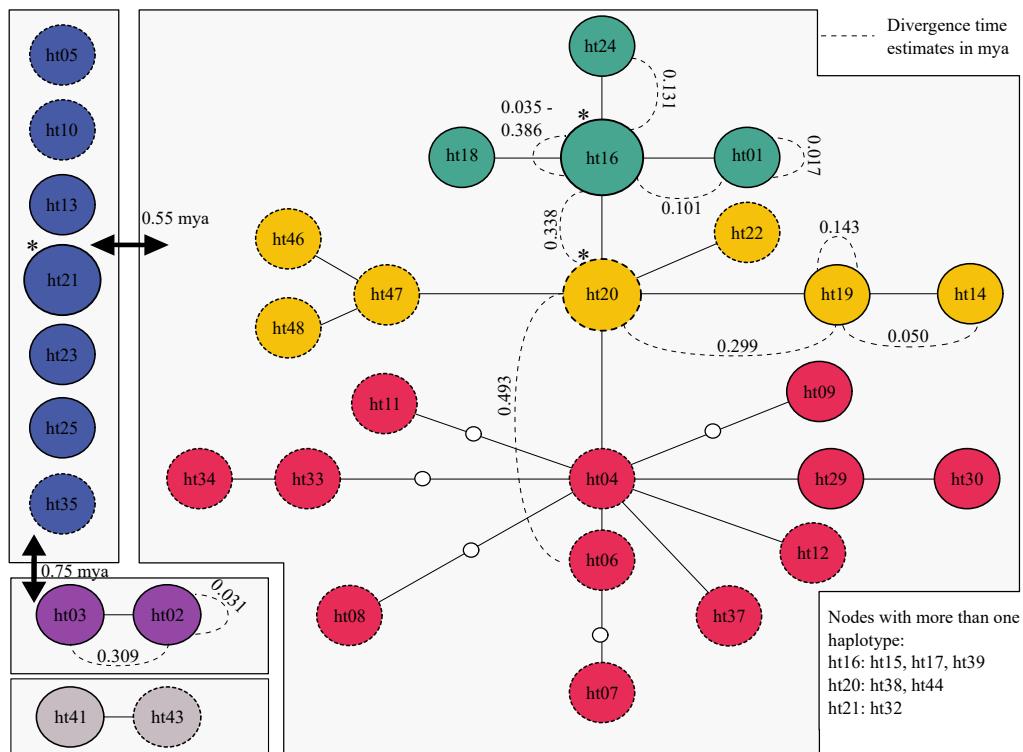


Figure 3.4: TCS network based on plastid marker haplotypes. Network is calculated based on a total of 47 SNPs, single nucleotide gaps and longer indels. Lines represent one mutational step, small circles indicate intermediate (unsampled or extinct) haplotypes. * Additional haplotypes were assigned to the nodes of ht16, ht20 and ht21 due to missing resolution of the SNP matrix. Haplotypes unique to the Southern France regions are indicated by dashed circle outlines. While ht20 is not exclusive to France the ht38 and ht44 are. Dashed lines indicate divergence time estimates in mya from Figure 3.6. Representatives of Group 6 were missing from the plastome tree. Geographical distribution is given in Figure 3.5.

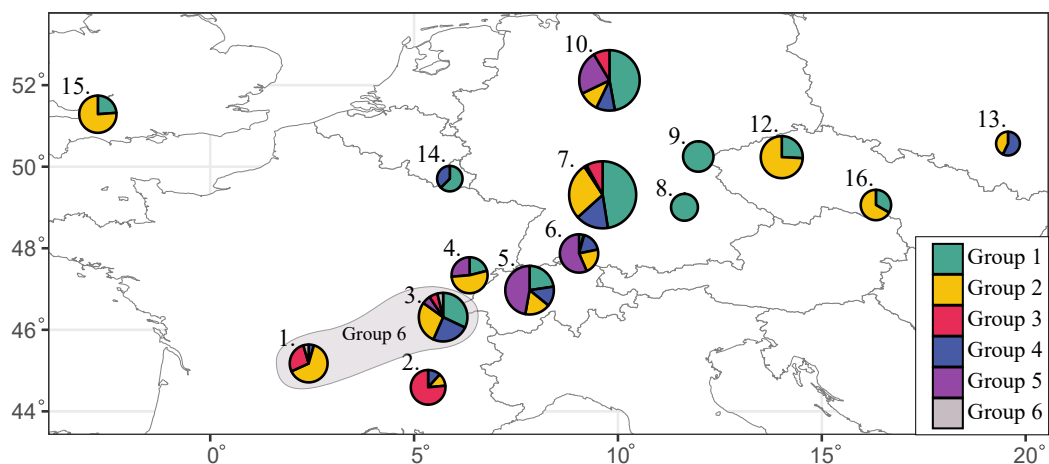


Figure 3.5: Distribution of plastid marker haplotypes over Europe. Haplotypes are grouped and colored based on their position in the TCS network (Figure 3.4). Regions are numbered based on Table 3.3. Size reflects sampling sizes.

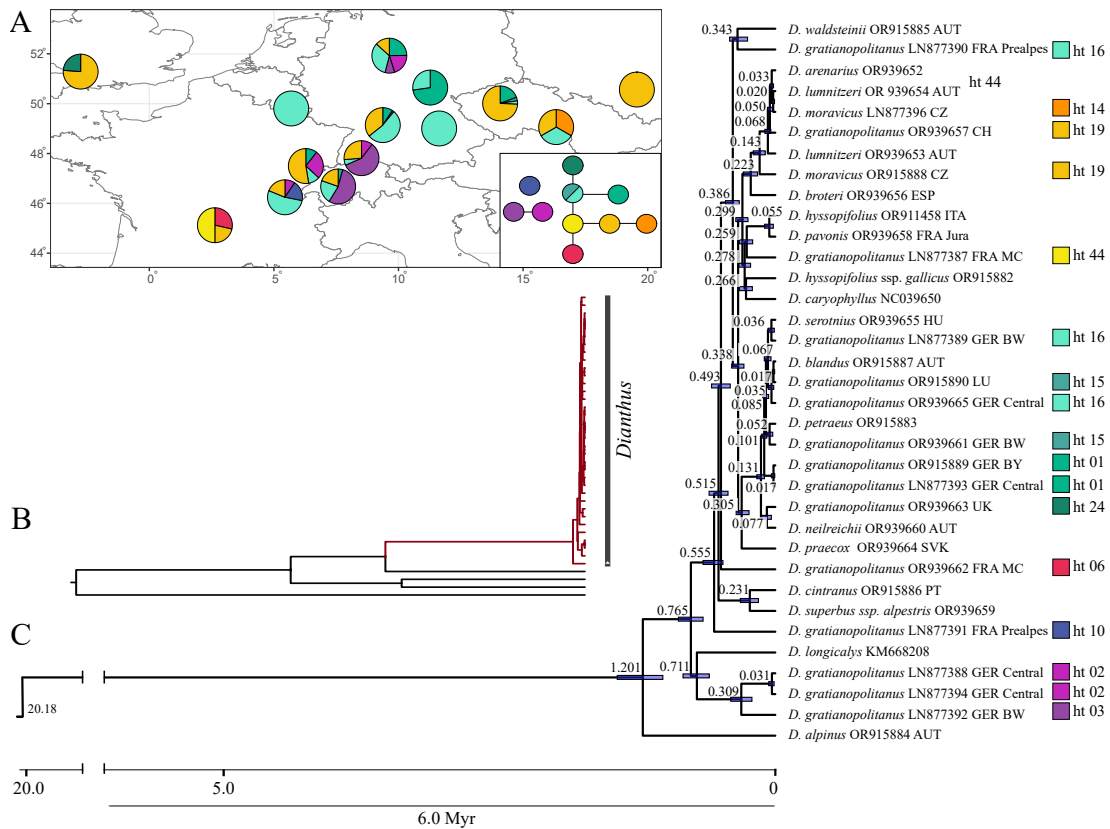


Figure 3.6: Time calibrated phylogenetic tree and divergence time estimates of 15 *D. gratianopolitanus* and 20 additional *Dianthus* using plastome sequences. Divergence times are indicated by blue bars and given in million years ago (Myr). The maximum-likelihood tree was constructed using RAXM-ng and dated using treePL. Colored blocks indicate position in the TCS network based on the inferred haplotype. Geographical occurrence of haplotypes is given in **A** including the reduced outline of the TCS network. **B** Complete phylogenetic tree including outgroup branches. The *Dianthus* clade is given in more detail in **C**

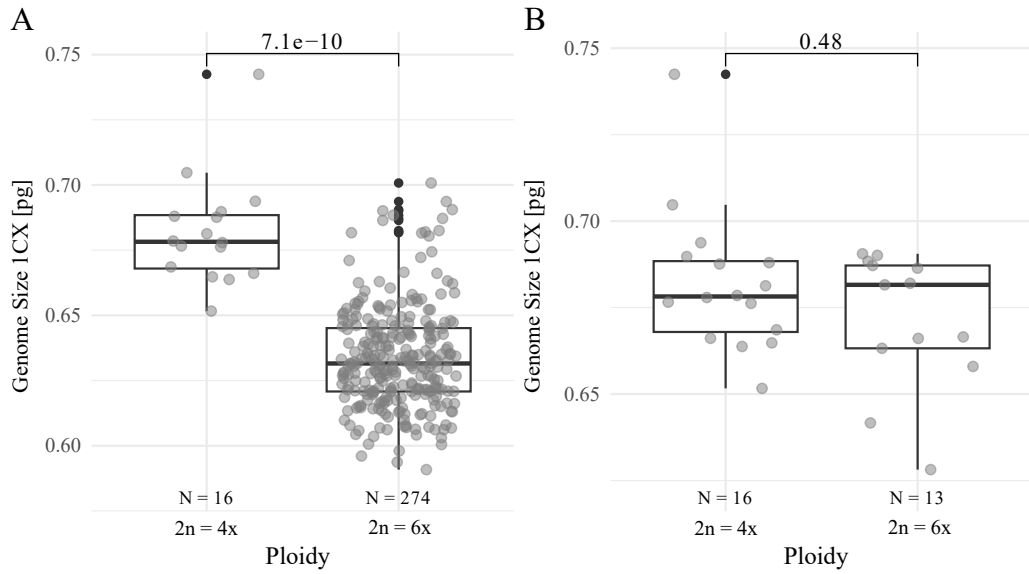


Figure 3.7: Comparison of genome size by ploidy level. Comparison of **A** tetra- and hexaploids from the whole distribution range, **B** tetra- and hexaploids from the French Massif Central and Diois region including significance from Mann-Whitney U test

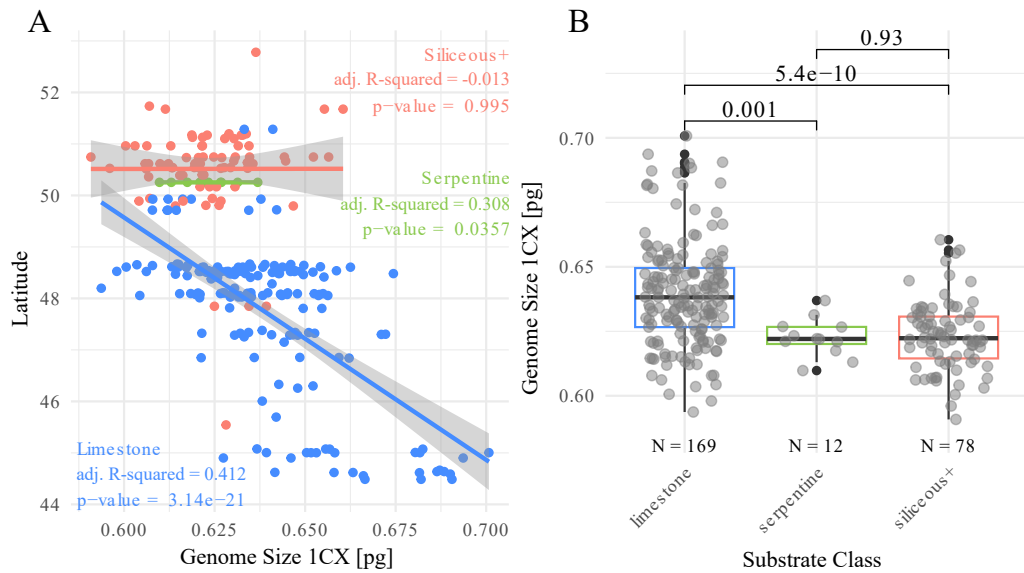


Figure 3.8: Linear relationship of latitude and genome size (1Cx) and corresponding boxplots. **A** Linear regression. Colors indicate bedrock types (limestone, serpentine and siliceous+ including siliceous, volcanic and sandy bedrock). Adjusted R^2 and corresponding p-values are given. **B** Corresponding boxplots comparing genome size based on substrate types. Statistical significance (Mann-Whitney U test with Bonferroni correction) for pairwise comparisons are given.

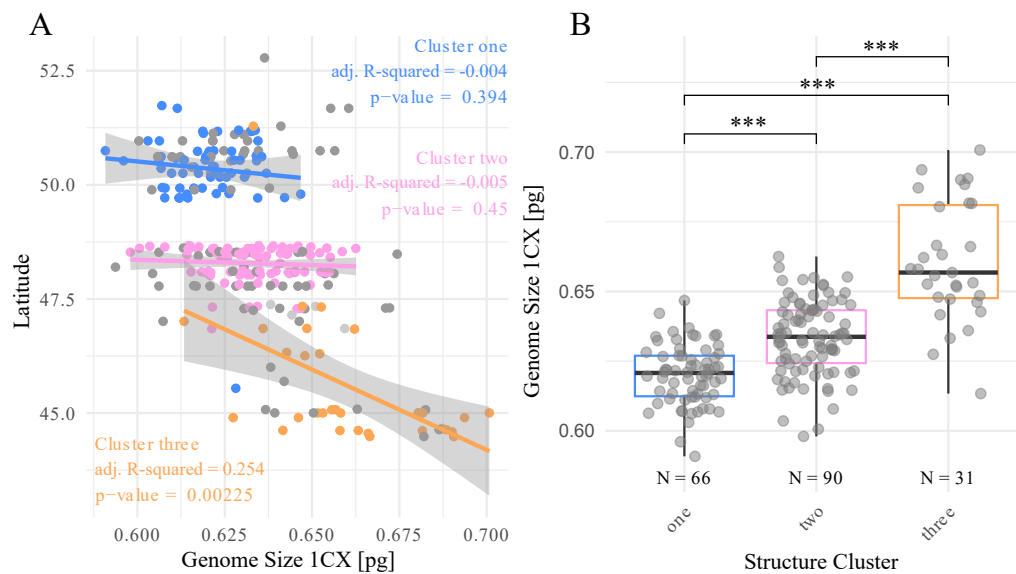


Figure 3.9: Linear relationship of latitude and genome size (1Cx) and corresponding boxplots. **A** Linear regression. Colors indicate the assignment to a Structure cluster ($K = 3$). Grey colored points indicate either no available Structure data or no possible assignment to a cluster to more than 75%. Adjusted R^2 and corresponding p-values are given. **B** Corresponding boxplots comparing genome size based on structure clusters. Statistical significance (Mann-Whitney U test with Bonferroni correction) for pairwise comparisons are given.

4 | Discussion

The quaternary ice ages, with its glaciation and deglaciation cycles, have shaped the present day distribution of plant species and their genetic diversity. In this study I analysed the structure of the genepool of *Dianthus gratianopolitanus* in Europe by AFLP and plastid sequencing along with cytological data.

Overall genetic diversity distribution suggest postglacial geneflow The high percentage of genetic variation attributed to within-population variation by the hierarchical AMOVA based on the nuclear AFLP data (Table 3.2) and within-region variation for the plastid haplotypes (Table 3.4), as well as the low values of the corresponding F -statistic indicate high levels of diversity within populations with less variation between them. In Gabrielsen et al. (1997) this missing genetic variation is also observed in northern populations of *Saxifraga oppositifolia* where it is interpreted as extensive gene flow among the nearly area-wide distributed populations during the Weichselian (115,000-10,000 BC). Here it is also suggested that the comparable small time scale following a fragmentation into the more isolated populations did not yet result in a high degree of differentiation between populations. Still, it could do so in the future with increasing isolation. Indeed missing differentiation of isolated populations is known for various different species like *Howellia aquatilis* (Lesica et al., 1988), *Cirsium canescens*, and *C. pitcheri* (Loveless and Hamrick, 1988), *Pinus resinosa* (Fowler and Morris, 1977), where the requirement of many thousand generations for the differentiation is proposed. While high levels of present gene flow between the isolated populations of *D. gratianopolitanus* seems unlikely it would have been possible in a more or less continuous distribution following the postglacial colonization. Postglacial colonization and later increased isolation and fragmentation into the present-day observed distribution pattern could therefore explain the missing geographical structure of genetic variation in the Cheddar Pink. On the other hand, this missing differentiation would also disfavor the scenario, where the present-day distribution of *D. gratianopolitanus* is indeed a relict of (pre-)glaciation times, as we would expect higher rates of differentiation for long time stable but isolated populations that evolved independently (Schönswetter and Tribsch, 2005). These relict plant species often show strong geographic patterns in genetic diversity as observed for relict species from the Alps like *Saxifraga paniculata* (Reisch et al., 2003) or *Eritrichum namum* (Stehlik et al., 2001, 2002). Yet small isolated populations could also be subject to a decrease in genetic variation and fitness (Leimu et al., 2006), and post-

glacial gene flow could have also swamped any genetic differentiation (Gabrielsen et al., 1997). The Mantel correlogram of ten distance classes of spatial distances between all *D. gratianopolitanus* also indicates a clinal structure of the genetic variation with small positive autocorrelations for smaller distance classes and small negative ones for the bigger distance classes, indicating isolation by distance [IBD, (Wright, 1943)] and an accumulation of genetic differences at least for distances $< 350 - 400\text{km}$, that would indeed cover the distances of each region to its closest neighbors. The rapid radiation of European *Dianthus* in the last 1-2 Myr described in Valente et al. (2010) might lead to a high rate of ancestral shared polymorphism and missing resolution, that in combination with the gene flow between populations and species during the past glaciation and deglaciation cycles in the quaternary could also explain the insufficient division of plastomes between species as well as missing differentiation between geographical regions, as seen in Figure 3.6. They might indicate older ancestral genetic variation and shared ancestral polymorphisms pre-dating the origin of the species. In previous studies on *Caryophyllaceae* so-called haplotype sharing between species in the genus *Silene* was observed and interspecific hybridization and introgression are proposed as possible origin (Hathaway et al., 2009; Rautenberg et al., 2010). The lack of geographical structure can also be observed in the plastid marker haplotypes where no clear geographical distribution pattern and direction is observable. Statistical tests indicate a significant association of certain regions and haplotype groups although no group is restricted to one region. Also here the lack of genetic structuring and separate gene pools could be evidence for the proposed area-wide postglacial colonization with gene flow between populations and even species with later fragmentation. Exceptional here are the South French regions that show high levels of unique haplotypes and gene diversity (Table 3.3). In addition, the oldest, most basal marker haplotypes have a high occurrence in the French and Swiss Alps and the Bodensee region as well as in Central Germany. Following the indicated divergence time estimates a migration to the French Prealps and the Massif Central could be traced. From here the other haplotypes differentiated (Figure 3.6). Due to only a fraction of all observed haplotypes being represented in the plastome tree, this might only pose a preliminary result and could change with higher coverage, but again, it highlights the French region as an older region from where migration could have occurred.

Genetic diversity and population structure indicate a Southern French refugia

The distribution of genetic diversity of nuclear AFLP data as well as plastid marker haplotypes also highlights the Southern French regions, namely the Massif Central, Diois, and Prealps, as areas of high genetic richness, possibly indicating refuge areas. The high *DW* values in Diois and the Prealps (Table 3.1) suggest long-term isolated populations where rare alleles could accumulate over time as suggested by Schönswetter and Tribsch (2005). This is further supported by the high rate of unique plastid haplotypes found in South France alongside higher levels of plastid haplotype gene diversity (Table 3.3). The idea of a possible refugia in the French (Pre-)Alps and Jura is indeed not new and has already been proposed for e.g. *Erinus alpinus* (Shehlik et al., 2002), for various other species around

the Aost valley, Como Lake and Nice (Schönswetter et al., 2005) or based on climate data (Ohlemüller et al., 2012). Comparable high levels of rare alleles, unique haplotypes, and *DW* are missing in northern Germany, consistent with the 'southern richness, northern purity' paradigm often observed in European species, indicating a survival in southern refugia with a recolonization of the north (Hewitt, 1999). Yet even though only one unique haplotype was found in Central Germany, the gene diversity of plastid haplotypes is comparable to the South France regions. The next highest rates of AFLP rare fragments were found in Switzerland, the Swabian Alb, and the UK. Only the latter also showed a higher *DW* while the Swabian Alb showed increased levels of polymorphic sites and a mean number of bands also indicating higher levels of diversity and possible old refuge areas (Table 3.1).

The STRUCTURE analysis revealed two stable clusters, one centred in southern France and one in Central Germany and the Czech Republic, that could indicate two separate genetic groups originating from a proposed French refugia and an unknown refugia in the north or east (Figure 3.1 and Appendix Figure A.4). On closer inspection of $K = 2$ (see Appendix Figure A.3) the northern Cheddar Pink show indeed a mixture of the two clusters while the Baden-Württemberg cluster shows a uniform pure signal, hinting towards a Baden-Württemberg refugia. The geographical location of the first two genetic clusters inferred with STRUCTURE coincides well with the difference in calcareous and siliceous bedrock. Besides the putative role of edaphic factors in speciation processes (Rajakaruna, 2004) the bedrock preferences could have also influenced the survival and migration during the past glaciation periods influencing present-day biogeographic patterns (Alvarez et al., 2009). The emergence of the third cluster in the contact zone of the first two clusters at the Bodensee region and in Baden-Württemberg, could, on one hand, indicate a separate gene pool originating from additional, so far unknown refugia in the Swabian Alb or Switzerland or could be explained by a so-called melting pot scenario, where the two gene pools from the South and North met and hybridized in the past forming a new cluster. This new cluster would, like an old refugium, also show increased levels of genetic diversity (Petit et al., 2003). The higher levels of bands per individual in the Swabian Alb exceed those from the French or the Central German/Czech regions. This geographical trend is even more pronounced when looking at the separate populations (Figure 3.2). The number of bands as well as the number of polymorphic sites decrease with distance to the distribution center in Switzerland and Baden-Württemberg. For the French cluster, the higher values of the mean number of bands and polymorphic sites further to the East might also be influenced by an introgression of the contact zone cluster into populations from the Swiss and French Alps (Figure A.5) that is mostly missing for populations in the northern cluster (Figure A.6). In contrast to the northern cluster, the French cluster has the highest *DW* that peaks at 5°E, the Diois region, with slightly lower values to the west and east (Figure 3.2 C), and higher *DW* towards the south (Appendix Figure A.7). The decline with increasing longitude to the east in all three parameters, as well as the decline observed towards the south (Appendix Figure A.7) in the northern cluster indicates a west to south-east migration with lower gene diversity in the younger populations due to consecutive founder effects as described in Comes and

Kadereit (1998) or Hewitt (2000). This would also imply older populations and possibly now extinct refugia at the western border of the present-day distribution. From here colonization could have led to the contact to the South French cluster and the formation of the contact zone in Baden-Württemberg. However, this hypothesis is complicated by the fact that the glaciers of the Alps only receded within the Boreal (7-6 kya) hindering a first north migration from the French refugia (Pott, 1996). While the northern populations could of course expand and colonize new habitats the contact with the southern populations would have been delayed. Even though no clear evidence for Baden-Württemberg refugia is known so far, speculations on refugia in or north of the Alps are proposed and part of ongoing research (e.g. (Hošek et al., 2024)). The Cheddar Pink could have survived in a Nunatak scenario in Switzerland or the Swabian Alb, where they could have survived on small ice-free rocky outcrops as proposed for the survival of *Eritrichium nanum* (Stehlik, 2000; Stehlik et al., 2001), *Arabis alpina* (Koch et al., 2006) or *Draba aizoides* (Vogler and Reisch, 2013). Due to postglacial migrations and gene flow the clear signs of these refugia could have been diluted and swamped (Gabrielsen et al., 1997).

Latitudinal effect on genome size traces back postglacial migration The declining genome size with increasing latitude for the calcareous bedrock plants could indicate a size reduction accompanying the postglacial migration from southern French refugia to Southern Germany, while the west-east migration from the siliceous+ range was not affected by latitudinal effects (Figure 3.8). The proposed migration direction of the calcareous group towards the north-east can also be observed in the genome size reduction with increasing longitude towards the east (Appendix Figure A.8). The genome size change with increasing latitude and therefore often changing climatic conditions is disputed and evidence for both directions, an increase as well as decrease, is published (Knight et al., 2005). On the other hand, the observed differences could also be evidence for the three different gene pools assigned by STRUCTURE (Figure 3.9), although also here the decrease in genome size for the South France gene pool with increasing latitude can be observed. Differences in genome sizes in hybrid or melting pot zones are not well understood and studied so far. In *Helianthus* hybridization by itself did not lead to increased DNA content (Baack et al., 2005). Yet the genome size differences between the assigned genetic clusters (Figure 3.9), with the northern Central German cluster having the smallest genome sizes, and the southern French cluster the biggest genome sizes, could, in theory, lead to a mixture of the two parent zones resulting in a transition zone with a medium genome size. The restriction of tetraploid individuals to southern France could be another evidence for the older age of the Massif Central and Diois populations.

The colonisation of the British Isles The most isolated populations can be found in southwest England (Cheddar Gorge, Somerset). In Koch et al. (2020) the postglacial colonization of the British Isles by the Bristol rock cress (*Arabis scabra*, Brassicaceae) via a migration corridor from the French Prealps is suggested. Considering the similar ecological

niches of both species and the genetic assignment of the British Cheddar Pink populations to the contact zone cluster present in the Alps, a similar migration route from the French Prealps and Alps, over Belgium to the southwest of the UK as the origin of the British populations is a possible explanation. The most common plastid haplotype found in the UK, ht19, is also one of the most common haplotypes in general and can be found in the French Jurassic. In addition, the British Isles have a unique haplotype, ht24, derived from ht16 based on the TCS network (Figure 3.4). Ht16 is also very common and can be found in the French and Swiss Alps. According to the divergence time estimates of whole plastome sequences, this split dates back to $\sim 131,000$ years though here the sister accessions originated from Germany and Luxembourg. The split to the accession from Switzerland (ht 19, $\sim 338,000$ years ago) and a ht16 from the French Prealps ($\sim 386,000$ years ago) are even older, all falling into the glacial periods of the Pleistocene. Ht24 could have evolved from ht16 before the postglacial migration to the British Isles and subsequently went extinct on the mainland. Assuming a once area-wide distribution, a colonization scenario where intermediate populations on the migration route went extinct is also in accordance with the present-day fragmented distribution.

No distinction between *D. gratianopolitanus* and *D. gratianopolitanus* subsp. *moravicus* based on genetic data The included individuals from *D. gratianopolitanus* subsp. *moravicus* were not differentiated from *D. gratianopolitanus* based on the herein-used AFLP data, plastid marker haplotypes, plastomes, or genome sizes. In the genetic assignment, the individuals were assigned to the northern German/Czech cluster (Figure A.6) and showed similar behavior in gene diversity on regional and population levels. Based on the position of individuals of *D. gratianopolitanus* subsp. *moravicus* in the plastome tree, the missing differentiation between the *Dianthus* species and the presence of a shared plastid haplotype further highlights the close relationship of the species.

Summary and Outlook The missing spatial structure of genetic variation, high rate of the mixture of plastid haplotypes, and lack of spatial and species structure in the plastome tree indicate postglacial gene flow favoring a scenario of once area-wide distribution with secondary fragmentation. Here a French refugia is highly supported by genetic and cytological data. While clear evidence for a northern German/Czech refugia is still missing, the survival of now-extinct small populations in the west of Germany near Belgium with later expansion could be possible. The third genetic group suggested in Baden-Württemberg could be the result of survival in unknown refugia or of a melting pot scenario with a contact zone of a northern and southern gene pool. The colonization of the British Isles originating from populations in the French (Pre-)Alps, expanding to Belgium and the Isles is supported by the genetic assignment and plastid haplotypes.

The here found high genetic variation that is attributed to within populations can lead to interesting findings for within-population diversity. The genetic structuring, genetic connectivity, or signs of isolation within populations are analyzed in detail in Part III. As

indicated by the accordance of genetic assignment and bedrock type a possible adaptation of different genotypes to the specific conditions of their home substrates might be a first step towards further differentiation and highlights edaphic factors as putative drivers of speciation processes. This question of edaphic influences, possible adaptations, and the plasticity in *D. gratianopolitanus* to react to different environmental conditions is the topic of the next part.

5 | Bibliography

- Alvarez, N., Thiel-Egenter, C., Tribsch, A., Holderegger, R., Manel, S., Schönswetter, P., Taberlet, P., Brodbeck, S., Gaudeul, M., Gielly, L., et al. (2009). History or ecology? Substrate type as a major driver of patial genetic structure in Alpine plants. *Ecology Letters*, 12(7):632–640.
- Avise, J. C. (2009). Phylogeography: retrospect and prospect. *Journal of biogeography*, 36(1):3–15.
- Baack, E. J., Whitney, K. D., and Rieseberg, L. H. (2005). Hybridization and genome size evolution: timing and magnitude of nuclear DNA content increases in *Helianthus* homoploid hybrid species. *New Phytologist*, 167(2):623–630.
- Balao, F., Valente, L. M., Vargas, P., Herrera, J., and Talavera, S. (2010). Radiative evolution of polyploid races of the Iberian carnation *Dianthus broteri* (Caryophyllaceae). *New Phytologist*, 187(2):542–551.
- Banzhaf, P., Jäger, O., and Meisterhans, U. (2009). Artenhilfsprogramm für die Pfingstnelke *Dianthus gratianopolitanus* im Regierungsbezirk Stuttgart. *Jahreshefte der Gesellschaft für Naturkunde in Württemberg*, 165:73–115.
- Bellstedt, D. U., Linder, H. P., and Harley, E. H. (2001). Phylogenetic relationships in *Disa* based on non-coding *trnL-trnF* chloroplast sequences: evidence of numerous repeat regions. *American Journal of Botany*, 88(11):2088–2100.
- Bolger, A. M., Lohse, M., and Usadel, B. (2014). Trimmomatic: a flexible trimmer for Illumina sequence data. *Bioinformatics*, 30(15):2114–2120.
- Bonin, A., Bellemain, E., Bronken Eidesen, P., Pompanon, F., Brochmann, C., and Taberlet, P. (2004). How to track and assess genotyping errors in population genetics studies. *Molecular ecology*, 13(11):3261–3273.
- Bonin, A., Ehrlich, D., and Manel, S. (2007). Statistical analysis of amplified fragment length polymorphism data: a toolbox for molecular ecologists and evolutionists. *Molecular ecology*, 16(18):3737–3758.

- Bouckaert, R., Heled, J., Kühnert, D., Vaughan, T., Wu, C.-H., Xie, D., Suchard, M. A., Rambaut, A., and Drummond, A. J. (2014). BEAST 2: a software platform for Bayesian evolutionary analysis. *PLoS computational biology*, 10(4):e1003537.
- Brand, M. H., Obae, S. G., Mahoney, J. D., and Connolly, B. A. (2022). Ploidy, genetic diversity and speciation of the genus *Aronia*. *Scientia Horticulturae*, 291:110604.
- Brochmann, C., Gabrielsen, T. M., Nordal, I., Landvik, J. Y., and Elven, R. (2003). Glacial survival or tabula rasa? The history of North Atlantic biota revisited. *Taxon*, 52(3):417–450.
- Camacho, C., Coulouris, G., Avagyan, V., Ma, N., Papadopoulos, J., Bealer, K., and Madden, T. L. (2009). Blast+: architecture and applications. *BMC bioinformatics*, 10:1–9.
- Carlsen, M. M. and Croat, T. B. (2013). A molecular phylogeny of the species-rich Neotropical genus *Anthurium* (Araceae) based on combined chloroplast and nuclear DNA. *Systematic Botany*, 38(3):576–588.
- Clement, M., Posada, D., Crandall, K. A., et al. (2000). TCS: a computer program to estimate gene genealogies. *Molecular ecology*, 9(10):1657–1659.
- Comes, H. P. and Kadereit, J. W. (1998). The effect of quaternary climatic changes on plant distribution and evolution. *Trends in plant science*, 3(11):432–438.
- Dodsworth, S. (2015). Genome skimming for next-generation biodiversity analysis. *Trends in Plant Science*, 20(9):525–527.
- Doležel, J., Greilhuber, J., Lucretti, S., Meister, A., Lysák, M., Nardi, L., and Obermayer, R. (1998). Plant genome size estimation by flow cytometry: inter-laboratory comparison. *Annals of botany*, 82(suppl_1):17–26.
- Doležel, J., Greilhuber, J., and Suda, J. (2007). Estimation of nuclear DNA content in plants using flow cytometry. *Nature protocols*, 2(9):2233–2244.
- Doyle, J. J. and Doyle, J. L. (1987). A rapid DNA isolation procedure for small quantities of fresh leaf tissue. *Phytochemical bulletin*.
- Earl, D. A. and VonHoldt, B. M. (2012). STRUCTURE HARVESTER: a website and program for visualizing STRUCTURE output and implementing the Evanno method. *Conservation genetics resources*, 4:359–361.
- Erhardt, A. (1990). Pollination of *Dianthus gratianopolitanus* (Caryophyllaceae). *Plant Systematics and Evolution*, 170:125–132.
- Evanno, G., Regnaut, S., and Goudet, J. (2005). Detecting the number of clusters of individuals using the software STRUCTURE: a simulation study. *Molecular ecology*, 14(8):2611–2620.

- Excoffier, L. and Lischer, H. E. (2010). Arlequin suite ver 3.5: a new series of programs to perform population genetics analyses under Linux and Windows. *Molecular ecology resources*, 10(3):564–567.
- Fay, M. F., Cowan, R. S., and Leitch, I. J. (2005). The effects of nuclear DNA content (C-value) on the quality and utility of AFLP fingerprints. *Annals of Botany*, 95(1):237–246.
- Fowler, D. P. and Morris, R. W. (1977). Genetic diversity in red pine: evidence for low genic heterozygosity. *Canadian Journal of Forest Research*, 7(2):343–347.
- Frajman, B., Eggens, F., and Oxelman, B. (2009). Hybrid origins and homoploid reticulate evolution within *Heliosperma* (*Sileneae*, Caryophyllaceae)—a multigene phylogenetic approach with relative dating. *Systematic Biology*, 58(3):328–345.
- Francis, R. M. (2017). pophelper: an R package and web app to analyse and visualize population structure. *Molecular ecology resources*, 17(1):27–32.
- Gabrielsen, T., Bachmann, K., Jakobsen, K., and Brochmann, C. (1997). Glacial survival does not matter: RAPD phylogeography of Nordic *Saxifraga oppositifolia*. *Molecular Ecology*, 6(9):831–842.
- Gong, W., Chen, C., Dobeš, C., Fu, C.-X., and Koch, M. A. (2008). Phylogeography of a living fossil: Pleistocene glaciations forced *Ginkgo biloba* L.(Ginkgoaceae) into two refuge areas in China with limited subsequent postglacial expansion. *Molecular Phylogenetics and Evolution*, 48(3):1094–1105.
- Greilhuber, J., DOLEŽEL, J., Lysák, M. A., and Bennett, M. D. (2005). The origin, evolution and proposed stabilization of the terms ‘genome size’ and ‘C-value’ to describe nuclear DNA contents. *Annals of botany*, 95(1):255–260.
- Guo, Y.-P., Saukel, J., Mittermayr, R., and Ehrendorfer, F. (2005). AFLP analyses demonstrate genetic divergence, hybridization, and multiple polyploidization in the evolution of *Achillea* (Asteraceae-Anthemideae). *New Phytologist*, 166(1):273–290.
- Hathaway, L., Malm, J. U., and Prentice, H. C. (2009). Geographically congruent large-scale patterns of plastid haplotype variation in the European herbs *Silene dioica* and *S. latifolia* (Caryophyllaceae). *Botanical Journal of the Linnean Society*, 161(2):153–170.
- Hebert, P. D., Cywinska, A., Ball, S. L., and DeWaard, J. R. (2003). Biological identifications through DNA barcodes. *Proceedings of the Royal Society of London. Series B: Biological Sciences*, 270(1512):313–321.
- Heck, E. M. (2011). Evolution der Pfingstnelke in den Randarealen. Staatsexamens Arbeit, Ruprecht-Karls University Heidelberg.
- Hewitt, G. (2000). The genetic legacy of the Quaternary ice ages. *Nature*, 405(6789):907–913.

- Hewitt, G. M. (1996). Some genetic consequences of ice ages, and their role in divergence and speciation. *Biological journal of the Linnean Society*, 58(3):247–276.
- Hewitt, G. M. (1999). Post-glacial re-colonization of European biota. *Biological journal of the Linnean Society*, 68(1-2):87–112.
- Hijmans, R. J., Bivand, R., Forner, K., Ooms, J., Pebesma, E., and Sumner, M. D. (2022). Package ‘terra’. *Maintainer: Vienna, Austria*.
- Hošek, J., Pokorný, P., Storch, D., Kvaček, J., Havig, J., Novák, J., Hájková, P., Jamrichová, E., Brengman, L., Radoměřský, T., et al. (2024). Hot spring oases in the periglacial desert as the Last Glacial Maximum refugia for temperate trees in Central Europe. *Science Advances*, 10(22):eado6611.
- Hu, L., Tate, J. A., Gardiner, S. E., and MacKay, M. (2023). Ploidy variation in rhododendron subsection maddenia and its implications for conservation. *AoB Plants*, 15(3):plad016.
- Hubisz, M. J., Falush, D., Stephens, M., and Pritchard, J. K. (2009). Inferring weak population structure with the assistance of sample group information. *Molecular ecology resources*, 9(5):1322–1332.
- Jakobsson, M. and Rosenberg, N. A. (2007). CLUMPP: a cluster matching and permutation program for dealing with label switching and multimodality in analysis of population structure. *Bioinformatics*, 23(14):1801–1806.
- Jian, H., Li, S., Guo, J., Li, S., Wang, Q., Yan, H., Qiu, X., Zhang, Y., Cai, Z., Volis, S., et al. (2018). High genetic diversity and differentiation of an extremely narrowly distributed and critically endangered decaploid rose (*Rosa praelucens*): implications for its conservation. *Conservation genetics*, 19:761–776.
- Jiménez, J. P., Brenes, A., Fajardo, D., Salas, A., and Spooner, D. M. (2008). The use and limits of AFLP data in the taxonomy of polyploid wild potato species in *Solanum* series *Conicibaccata*. *Conservation Genetics*, 9:381–387.
- Kadereit, J., Westberg, E., et al. (2007). Determinants of phylogeographic structure: a comparative study of seven coastal flowering plant species across their European range. *Watsonia*, 26(3):229–238.
- Kartal, M.-G. (2022). Geographic differentiation in *Dianthus gratianopolitanus* cytotypes: Clinal variation versus taxonomic units. Bachelor’s thesis, Ruprecht-Karls University Heidelberg.
- Kiefer, C., Dobeš, C., Sharbel, T. F., and Koch, M. A. (2009). Phylogeographic structure of the chloroplast DNA gene pool in North American *Boechera*—a genus and continental-wide perspective. *Molecular phylogenetics and evolution*, 52(2):303–311.

- Kiefer, M., Kiefer, C., and Koch, M. A. (2024). Versatile tools for masking and annotation of plastid genomes: cpanno and masker. Mendeley Data, V1.
- Knight, C. A., Molinari, N. A., and Petrov, D. A. (2005). The large genome constraint hypothesis: evolution, ecology and phenotype. *Annals of Botany*, 95(1):177–190.
- Koch, M. and Bernhardt, K.-G. (2004). Comparative biogeography of the cytotypes of annual *Microthlaspi perfoliatum* (Brassicaceae) in Europe using isozymes and cpDNA data: refugia, diversity centers, and postglacial colonization. *American Journal of Botany*, 91(1):115–124.
- Koch, M. A., Dobeš, C., Kiefer, C., Schmickl, R., Klimeš, L., and Lysak, M. A. (2007). Supernetwork identifies multiple events of plastid *trnF* (gaa) pseudogene evolution in the Brassicaceae. *Molecular Biology and Evolution*, 24(1):63–73.
- Koch, M. A., Kiefer, C., Ehrich, D., Vogel, J., Brochmann, C., and Mummenhoff, K. (2006). Three times out of Asia Minor: the phylogeography of *Arabis alpina* L. (Brassicaceae). *Molecular Ecology*, 15(3):825–839.
- Koch, M. A., Möbus, J., Klöcker, C. A., Lippert, S., Ruppert, L., and Kiefer, C. (2020). The Quaternary evolutionary history of Bristol rock cress (*Arabis scabra*, Brassicaceae), a Mediterranean element with an outpost in the north-western Atlantic region. *Annals of Botany*, 126(1):103–118.
- Koch, M. A., Winizuk, A., Banzhaf, P., and Reichardt, J. (2021). Impact of climate change on the success of population support management and plant reintroduction at steep, exposed limestone outcrops in the German Swabian Jura. *Perspectives in Plant Ecology, Evolution and Systematics*, 53:125643.
- Kolář, F., Fér, T., Štech, M., Trávníček, P., Dušková, E., Schönswetter, P., and Suda, J. (2012). Bringing together evolution on serpentine and polyploidy: spatiotemporal history of the diploid-tetraploid complex of *Knautia arvensis* (Dipsacaceae). *PLoS One*, 7(7):e39988.
- Kozlov, A. M., Darriba, D., Flouri, T., Morel, B., and Stamatakis, A. (2019). RAxML-NG: a fast, scalable and user-friendly tool for maximum likelihood phylogenetic inference. *Bioinformatics*, 35(21):4453–4455.
- Kress, W. J., Wurdack, K. J., Zimmer, E. A., Weigt, L. A., and Janzen, D. H. (2005). Use of DNA barcodes to identify flowering plants. *Proceedings of the National Academy of Sciences*, 102(23):8369–8374.
- Kron, P., Suda, J., and Husband, B. C. (2007). Applications of flow cytometry to evolutionary and population biology. *Annu. Rev. Ecol. Evol. Syst.*, 38:847–876.

- Kropf, M., Bardy, K., Höhn, M., and Plenk, K. (2020). Phylogeographical structure and genetic diversity of *Adonis vernalis* L. (Ranunculaceae) across and beyond the Pannonian region. *Flora*, 262:151497.
- Lanfear, R., Frandsen, P. B., Wright, A. M., Senfeld, T., and Calcott, B. (2017). Partition-Finder 2: new methods for selecting partitioned models of evolution for molecular and morphological phylogenetic analyses. *Molecular biology and evolution*, 34(3):772–773.
- Leimu, R., Mutikainen, P., Koricheva, J., and Fischer, M. (2006). How general are positive relationships between plant population size, fitness and genetic variation? *Journal of ecology*, 94(5):942–952.
- Lesica, P., Leary, R. F., Allendorf, F. W., and Bilderback, D. E. (1988). Lack of genic diversity within and among populations of an endangered plant, *Howellia aquatilis*. *Conservation biology*, 2(3):275–282.
- Li, H. (2013). Aligning sequence reads, clone sequences and assembly contigs with BWA-MEM. *arXiv preprint arXiv:1303.3997*.
- Li, H., Handsaker, B., Wysoker, A., Fennell, T., Ruan, J., Homer, N., Marth, G., Abecasis, G., Durbin, R., and Subgroup, . G. P. D. P. (2009). The sequence alignment/map format and SAMtools. *bioinformatics*, 25(16):2078–2079.
- Loveless, M. and Hamrick, J. (1988). Genetic organization and evolutionary history in two North American species of *Cirsium*. *Evolution*, 42(2):254–265.
- McKenna, A., Hanna, M., Banks, E., Sivachenko, A., Cibulskis, K., Kernytsky, A., Garimella, K., Altshuler, D., Gabriel, S., Daly, M., et al. (2010). The Genome Analysis Toolkit: a MapReduce framework for analyzing next-generation DNA sequencing data. *Genome research*, 20(9):1297–1303.
- Meng, D., Yang, L., Yunlin, Z., Guiyan, Y., Shuwen, C., and Zhenggang, X. (2023). Distinguish *Dianthus* species or varieties based on chloroplast genomes. *Open Life Sciences*, 18(1):20220772.
- Meudt, H. M. and Clarke, A. C. (2007). Almost forgotten or latest practice? AFLP applications, analyses and advances. *Trends in plant science*, 12(3):106–117.
- Michling, F. (2011). Conservation genetics of *Dianthus gratianopolitanus*. Staatsexamens Arbeit, Ruprecht-Karls University Heidelberg.
- Milá, B., Surget-Groba, Y., Heulin, B., Gosá, A., and Fitze, P. S. (2013). Multilocus phylogeography of the common lizard *Zootoca vivipara* at the Ibero-Pyrenean suture zone reveals lowland barriers and high-elevation introgression. *BMC Evolutionary Biology*, 13:1–15.

- Mueller, U. G. and Wolfenbarger, L. L. (1999). AFLP genotyping and fingerprinting. *Trends in ecology & evolution*, 14(10):389–394.
- Nevill, P. G., Zhong, X., Tonti-Filippini, J., Byrne, M., Hislop, M., Thiele, K., Van Leeuwen, S., Boykin, L. M., and Small, I. (2020). Large scale genome skimming from herbarium material for accurate plant identification and phylogenomics. *Plant Methods*, 16:1–8.
- Nora, S., Castro, S., Loureiro, J., Gonçalves, A. C., Oliveira, H., Castro, M., Santos, C., and Silveira, P. (2013). Flow cytometric and karyological analyses of *Calendula* species from Iberian Peninsula. *Plant systematics and evolution*, 299:853–864.
- Ohlemüller, R., Huntley, B., Normand, S., and Svenning, J.-C. (2012). Potential source and sink locations for climate-driven species range shifts in Europe since the Last Glacial Maximum. *Global Ecology and Biogeography*, 21(2):152–163.
- Oksanen, J., Simpson, G. L., Blanchet, F. G., Kindt, R., Legendre, P., Minchin, P. R., O’Hara, R., Solymos, P., Stevens, M. H. H., Szoecs, E., Wagner, H., Barbour, M., Bedward, M., Bolker, B., Borcard, D., Carvalho, G., Chirico, M., De Caceres, M., Durand, S., Evangelista, H. B. A., FitzJohn, R., Friendly, M., Furneaux, B., Hannigan, G., Hill, M. O., Lahti, L., McGlinn, D., Ouellette, M.-H., Ribeiro Cunha, E., Smith, T., Stier, A., Ter Braak, C. J., and Weedon, J. (2022). *vegan: Community Ecology Package*. R package version 2.6-4.
- Petit, R. J., Aguinagalde, I., de Beaulieu, J.-L., Bittkau, C., Brewer, S., Cheddadi, R., Ennos, R., Fineschi, S., Grivet, D., Lascoux, M., et al. (2003). Glacial refugia: hotspots but not melting pots of genetic diversity. *science*, 300(5625):1563–1565.
- Pott, R. (1996). Die Entwicklungsgeschichte und Verbreitung xerothermer Vegetationseinheiten in Mitteleuropa unter dem Einfluss des Menschen. *Tuexenia: Mitteilungen der Floristisch-Soziologischen Arbeitsgemeinschaft*, 16:337–369.
- Pritchard, J. K., Stephens, M., and Donnelly, P. (2000). Inference of population structure using multilocus genotype data. *Genetics*, 155(2):945–959.
- Pritchard, J. K., Wen, X., and Falush, D. (2010). Documentation for structure software: Version 2.3. *University of Chicago, Chicago, IL*, pages 1–37.
- Pöhl, S. (2013). Evolution der Pfingstnelke - Klinale Variation oder multiple Zentren genetischer Diversität? Staatsexamens Arbeit, Ruprecht-Karls University Heidelberg.
- Quinlan, A. R. and Hall, I. M. (2010). BEDTools: a flexible suite of utilities for comparing genomic features. *Bioinformatics*, 26(6):841–842.
- R Core Team (2023). *R: A Language and Environment for Statistical Computing*. R Foundation for Statistical Computing, Vienna, Austria.

- Rajakaruna, N. (2004). The edaphic factor in the origin of plant species. *International Geology Review*, 46(5):471–478.
- Rautenberg, A., Hathaway, L., Oxelman, B., and Prentice, H. C. (2010). Geographic and phylogenetic patterns in *Silene* section *Melandrium* (Caryophyllaceae) as inferred from chloroplast and nuclear DNA sequences. *Molecular Phylogenetics and Evolution*, 57(3):978–991.
- Reisch, C. (2008). Glacial history of saxifraga paniculata (saxifragaceae): molecular biogeography of a disjunct arctic-alpine species from europe and north america. *Biological Journal of the Linnean Society*, 93(2):385–398.
- Reisch, C., Poschlod, P., and Wingender, R. (2003). Genetic variation of *Saxifraga paniculata* Mill.(Saxifragaceae): molecular evidence for glacial relict endemism in central Europe. *Biological Journal of the Linnean Society*, 80(1):11–21.
- Roberto, T., De Carvalho, J., Beale, M., Hagen, F., Fisher, M., Hahn, R., de Camargo, Z., and Rodrigues, A. (2021). Exploring genetic diversity, population structure, and phylogeography in *Paracoccidioides* species using AFLP markers. *Studies in Mycology*, 100:100131.
- Schneeweiss, G. and Schönswetter, P. (2010). The wide but disjunct range of the European mountain plant *Androsace lactea* L.(Primulaceae) reflects Late Pleistocene range fragmentation and post-glacial distributional stasis. *Journal of Biogeography*, 37(10):2016–2025.
- Schönswetter, P., Stehlik, I., Holderegger, R., and Tribsch, A. (2005). Molecular evidence for glacial refugia of mountain plants in the European Alps. *Molecular Ecology*, 14(11):3547–3555.
- Schönswetter, P. and Tribsch, A. (2005). Vicariance and dispersal in the alpine perennial *Bupleurum stellatum* L. (Apiaceae). *Taxon*, 54(3):725–732.
- Shaw, J., Lickey, E. B., Beck, J. T., Farmer, S. B., Liu, W., Miller, J., Siripun, K. C., Winder, C. T., Schilling, E. E., and Small, R. L. (2005). The tortoise and the hare II: relative utility of 21 noncoding chloroplast DNA sequences for phylogenetic analysis. *American journal of botany*, 92(1):142–166.
- Shehlik, I., Schneller, J. J., and Bachmann, K. (2002). Immigration and in situ glacial survival of the low-alpine *Erinus alpinus* (Scrophulariaceae). *Biological Journal of the Linnean Society*, 77(1):87–103.
- Simmons, M. P. and Ochoterena, H. (2000). Gaps as characters in sequence-based phylogenetic analyses. *Systematic biology*, 49(2):369–381.

- Small, R. L., Cronn, R. C., and Wendel, J. F. (2004). Use of nuclear genes for phylogeny reconstruction in plants. *Australian Systematic Botany*, 17(2):145–170.
- Smith, S. A. and O’Meara, B. C. (2012). treePL: divergence time estimation using penalized likelihood for large phylogenies. *Bioinformatics*, 28(20):2689–2690.
- Stehlik, I. (2000). Nunataks and peripheral refugia for alpine plants during quaternary glaciation in the middle part of the Alps. *Botanica Helvetica*, 110:25–30.
- Stehlik, I., Blattner, F., Holderegger, R., and Bachmann, K. (2002). Nunatak survival of the high Alpine plant *Eritrichium nanum* (L.) Gaudin in the central Alps during the ice ages. *Molecular Ecology*, 11(10):2027–2036.
- Stehlik, I., Schneller, J., and Bachmann, K. (2001). Resistance or emigration: response of the high-alpine plant *Eritrichium nanum* (L.) Gaudin to the ice age within the Central Alps. *Molecular ecology*, 10(2):357–370.
- Stewart, J. R. and Lister, A. M. (2001). Cryptic northern refugia and the origins of the modern biota. *Trends in Ecology & Evolution*, 16(11):608–613.
- Taberlet, P., Gielly, L., Pautou, G., and Bouvet, J. (1991). Universal primers for amplification of three non-coding regions of chloroplast DNA. *Plant molecular biology*, 17:1105–1109.
- Telford, A., O’Hare, M. T., Cavers, S., and Holmes, N. (2011). Can genetic bar-coding be used to identify aquatic *Ranunculus* L. subgenus *Batrachium* (DC) A. Gray? A test using some species from the British Isles. *Aquatic Botany*, 95(1):65–70.
- Tzedakis, P., Emerson, B. C., and Hewitt, G. M. (2013). Cryptic or mystic? Glacial tree refugia in northern Europe. *Trends in ecology & evolution*, 28(12):696–704.
- Valente, L. M., Savolainen, V., and Vargas, P. (2010). Unparalleled rates of species diversification in Europe. *Proceedings of the Royal Society B: Biological Sciences*, 277(1687):1489–1496.
- Vogler, F. and Reisch, C. (2013). Vital survivors: low genetic variation but high germination in glacial relict populations of the typical rock plant *Draba aizoides*. *Biodiversity and Conservation*, 22:1301–1316.
- Vos, P., Hogers, R., Bleeker, M., Reijans, M., Lee, T. v. d., Hornes, M., Friters, A., Pot, J., Paleman, J., Kuiper, M., et al. (1995). AFLP: a new technique for DNA fingerprinting. *Nucleic acids research*, 23(21):4407–4414.
- Warnes, G. R., Bolker, B., Lumley, T., from Randall C. Johnson are Copyright SAIC-Frederick, R. C. J. C., by the Intramural Research Program, I. F., of the NIH, Institute, N. C., and for Cancer Research under NCI Contract NO1-CO-12400., C. (2022). *gmodels: Various R Programming Tools for Model Fitting*. R package version 2.18.1.1.

- Weiss, H., DobeS, C., Schneeweiss, G. M., and Greimler, J. (2002). Occurrence of tetraploid and hexaploid cytotypes between and within populations in *Dianthus* sect. *Plumaria* (Caryophyllaceae). *New Phytologist*, pages 85–94.
- Wickham, H. (2016). *ggplot2: Elegant Graphics for Data Analysis*. Springer-Verlag New York.
- Wickham, H., François, R., Henry, L., Müller, K., and Vaughan, D. (2023). *dplyr: A Grammar of Data Manipulation*. R package version 1.1.3.
- Wright, S. (1943). Isolation by distance. *Genetics*, 28(2):114.

Part II

The calcicole-calcifuge refugia idea revisited - insights from reciprocal cultivation experiments.

Abstract

Cuttings of 57 *D. gratianopolitanus* were cultivated from plants from the calcareous distribution range in Baden-Württemberg and the siliceous range in Central Germany and the Czech Republic, collected in the wild between 2009 and 2011. The cuttings were cultivated and propagated and used for a reciprocal transplant experiment in the Botanical Garden in Heidelberg. Fitness parameters and the elemental composition of leaf material were scored after the growth for one year on three treatment soils: triassic shell limestone, porphyry, and serpentine soil. In addition flowering time and growth behaviour of 269 and 255 *D. gratianopolitanus* from the whole distribution range and cultivated in the greenhouses of the Botanical Garden Heidelberg, were scored in 2022 and 2023, respectively. In addition flowering behaviour of 17 and 14 *D. gratianopolitanus* subsp. *moravicus* were scored in 2022 and 2023. The Cheddar Pink from calcareous and siliceous bedrock form distinct groups that indicate adaptations to their home conditions. While differences in elemental uptake did only show small differences an adaptation in growth and flowering strategies is shown. While the plants from calcareous bedrock invested more in vegetative growth, possibly facilitating vegetative reproduction and leading to higher competitiveness for space on the spatially restricted limestone outcrops, plants with siliceous origin showed higher flowering rates allowing more gene flow and faster colonization of the more open habitats. The adaptation of increased flowering could be confirmed based on the flowering behavior of the different regions, while the cushion sizes showed a more differentiated picture where the bigger cushions of the Baden-Württemberg plants could be observed, but plants from limestone bedrock in France did not follow this trend. While a shift towards earlier flowering between 2013 and 2022/23 could be shown, higher temperatures in the early spring and summer alone are likely not enough to trigger earlier flowering.

Zusammenfassung

Von 2009 bis 2011 wurden lebend Pflanzen von *D. gratianopolitanus* aus dem Verbreitungsgebiet auf Kalkgestein in Baden-Württemberg und dem silikathaltigen Verbreitungsgebiet in Mitteldeutschland und der Tschechischen Republik gesammelt. Davon wurden 57 Stecklinge kultiviert und vermehrt und für ein Reziproken Anzuchtversuch im Botanischen Garten in Heidelberg verwendet. Fitnessparameter wie Anzeichen von Chlorosis, Polstergröße oder Blühverhalten und die Elementkonzentrationen im Blattmaterial wurden nach einjährigem Wachstum auf drei Substrattypen bewertet: Porphy-, Muschelkalkstein- und Serpentinboden. Außerdem wurden die Blütezeit und das Blühverhalten von 269 bzw. 255 *D. gratianopolitanus* aus dem gesamten Verbreitungsgebiet und 17 bzw. 14 *D. gratianopolitanus* subsp. *moravicus*, die in den Gewächshäusern des Botanischen Gartens Heidelberg kultiviert wurden, im Jahr 2022 bzw. 2023 bewertet. Die Pfingstnelken von kalkhaltigem und silikathaltigem Gestein gehört zu unterschiedlichen Physiotypen, die auf Anpassungen an ihre Heimatbedingungen hinweisen. Während die Elementaufnahme nur geringe Unterschiede aufwies, zeigt sich eine Anpassung in den Wachstums- und Blühstrategien. Während die Pflanzen von kalkhaltigem Untergrund mehr in das vegetative Wachstum investierten, was möglicherweise die vegetative Vermehrung erleichterte und zu einer größeren Konkurrenzfähigkeit beim Kampf um den Platz auf den räumlich begrenzten Kalksteinaufschlüssen führte, zeigten Pflanzen mit Ursprung im Silikatareal höhere Blühraten und eine höhere Blütenproduktion, was einen größeren Genfluss und eine schnellere Besiedlung der offeneren Lebensräume ermöglichte. Die Anpassung an die verstärkte Blüte konnte anhand des Blühverhaltens der verschiedenen Regionen bestätigt werden, während die Polstergrößen ein differenzierteres Bild zeigten, bei dem die größeren Kissen der baden-württembergischen Pflanzen zu beobachten waren, während die Pflanzen von Kalksteinfelsen in Frankreich diesem Trend nicht folgten. Es konnte zwar eine Verschiebung hin zu einer früheren Blüte zwischen 2013 und 2022/23 festgestellt werden, jedoch scheinen die höheren Temperaturen im Frühjahr und Sommer allein nicht auszureichen, um eine frühere Blüte auszulösen.

1 | Introduction

Environmental influences on species distribution and differentiation

Differences between the vegetations on limestone and siliceous bedrock as well as differing distribution patterns based on different bedrock types were already published nearly two hundred years ago (Unger, 1836) and have since raised the attention of botanists and ecologists (Ellenberg, 1958; Lee, 1999; Bothe, 2015; Cross and Lambers, 2021). Indeed the distribution and biogeographic patterns of plant species are shaped by a complex interplay of factors, with ecology and climatic history playing crucial roles (Alvarez et al., 2009). Among ecological factors, edaphic conditions have emerged as one of the most significant determinants of plant distribution (Rajakaruna, 2004). For example, species distribution in the European Alps is influenced by soil and land cover to the same degree as by climate (Chauvier et al., 2021). The edaphic conditions involve a complex interplay of physical, chemical, and biotic soil properties (Ellenberg, 1958; Rajakaruna, 2004). Silicate soils have lower pH values, lower heat retention, and higher water content when compared to calcareous soils (Bothe, 2015). The differing soil pH can especially influence the solubility and availability of mineral nutrients like iron (Fe), manganese (Mn), phosphorus (P), or zinc (Zn). For instance, calcium-rich soils have higher rates of calcium (Ca) and lower available levels of Fe, Mn, and Zn, as well as copper (Cu) and boron (B). The higher levels of calcium might also exacerbate phosphor sensitivity and hinder potassium (K) uptake (Lee, 1999; Cross and Lambers, 2021). Siliceous or acidic soils show lower levels of Ca, magnesium (Mg), molybdenum (Mo), and K but higher levels of possible toxic aluminum (Al) and lower P availability (Cross and Lambers, 2021). When these edaphic conditions become extreme, they can act as agents of natural selection and lead to speciation through adaptation to different substrate characteristics (Rajakaruna, 2004; Anacker, 2014). Many examples of so-called vicarious plants, meaning closely related species that occur on either limestone or siliceous bedrock, like the pairs *Rhododendron hirsutum*/*R. ferrugineum*, *Gentiana clusii*/*G. acaulis* or *Achillea atrata*/*A. moschata* are known in alpine areas (Bothe, 2015). So-called calcicole and calcifuge plant strategies refer to the ability to grow on calcium-rich or acidic soils. While calcifuge species are restricted to acidic soils and show increased tolerances to high concentrations of Al, Mn, and Fe (Lee, 1999), calcicole species are, by definition, associ-

ated with Ca-rich habitats, and are typically insensitive to Fe and P deficiencies (Lee, 1999). On the other hand, it has been shown, that calcifuge species are unable to solubilize P and Fe with sufficient amounts and develop chlorosis when cultivated on calcareous soils (Zohlen and Tyler, 2000, 2004). To analyze local adaptations to encountered home conditions as well as the extent to which the distribution of a species is determined by environmental factors transplantation experiments remain a well-established method (Kawecki and Ebert, 2004; Ellis and Weis, 2006; Johnson et al., 2022). These experiments aim to identify variations in the fitness of genotypes from different populations across different environments and have been used to e.g. compare the influence of edaphic conditions (Rajakaruna et al., 2003), the relationship of soil bacteria communities (Lazzaro et al., 2011), adaptations to elevation levels and presence of other vegetation (Sumner et al., 2022), and different climate conditions and climate warming (Cui et al., 2018).

While edaphic conditions can change on smaller spatial scales the climate zones generally span over greater areas, yet both influence the vegetation, species distribution patterns, or even whole ecosystems. Furthermore, climate itself can directly impact soil pH, texture, and nutrient availability, e.g. via changes in the nutrient cycling due to altered moisture or increased erosion due to exposure to strong winds or high-intensity rainfalls, which in turn affect vegetation patterns and ecosystem dynamics (Hamidov et al., 2018). The influence of climate change on soil functions has been assessed by several studies during the past decades (Xiong et al., 2014; Coyle et al., 2016), linking, for example, increased temperatures and decreased soil moisture to a reduction of carbon storage capacity (Ostle et al., 2009). Indeed soil plays a crucial role in the global nutrient cycles, like the carbon and nitrogen cycle, serving as major reservoir and regulator. Here especially changes in mean temperature and precipitation due to global warming can influence the soil organic matter content, which in turn can affect e.g. the water holding capacity or soil nutrients, further altering the edaphic conditions (Brevik, 2013). Increasing erosion and degradation of the land can lead to the complete collapse of soil functions, with already an estimated proportion of 8% of areas in southern, central, and eastern Europe being at very high risk of desertification (European Commission, 2011).

Climate warming can also directly influence the vegetation period and flowering behavior. Within the period from 2001-2015, the mean flowering phenology in North America showed an average shift of 25 days to an earlier flowering (Pearse et al., 2017). Earlier flowering is also documented for Germany, where *Forsythia*, as an indicator for early spring, showed a median of 10 days earlier flowering in the period from 1991-2009 when compared to data from 1961-1990 (Holz et al., 2010). A shift towards earlier flowering was also confirmed using old flowering records (Panchen et al., 2012), as well as so-called "resurrection, approaches" using seeds from present day populations and stored seeds sampled from the same populations (Thomann et al., 2015; Rauschkolb et al., 2023). "Hopkins' bioclimatic law" proposed by Hopkins (1918) over a century ago, hypothesized a delay of spring and summer phenology by 4 days for each increase of either 1° of latitude or 122m in elevation when all other conditions remained the same. Richardson et al. (2019) used the "green-up" and "green-down"

dates from North America to evaluate Hopkins' law and found a 2.7 days delay per °N as well as 0.6 days per °E.

For *D. gratianopolitanus* a previous study by Koch et al. (2021) showed a shift in the flowering onset of Cheddar Pink from the Lenninger and Eselsburger Tal during the period from 2016 to 2019 in the Green houses of the Botanical Garden in Heidelberg. Here, a shift to an earlier flowering of three to six weeks from 1990 onwards based on observed shifts between 2016 and 2018 was proposed. These shifts together with a shortening of the peak flowering period and a possible asynchrony between flowering and pollinator availability might lead to a reduction in successful pollinations and seed set development (Koch et al., 2021). The Europe-wide distribution from *D. gratianopolitanus* ranges from southern France to southern England covering $\sim 10^\circ\text{N}$ and over 20°E , from France to Poland and the Czech Republic, leading to possible local adaptations. The cultivation of *D. gratianopolitanus* originating from different regions in Europe in the greenhouses allows a comparison of fitness parameters between regions and years, revealing possible local adaptations of different regions. In its distribution range *D. gratianopolitanus* occurs on calcareous and siliceous bedrock, as well as on ultramafic soil. Possible adaptations to the different bedrock types can be analyzed using a reciprocal transplant experiment.

Contributions

The reciprocal transplant experiment was conducted and data was collected by Kathrin Strobel in the context of a state examination thesis in 2011 (Strobel, 2014). ICP OES was performed by Kathrin Strobel at the University of Bochum with the help of Prof. Dr. Ute Krämer, Dr. Ricardo J. Stein and Petra DÜchting. Plant material and samples were collected by Marcus Koch and Florian Michling. Following the pre-evaluation of data by Kathrin Strobel the final data analysis was conducted by myself. The study was designed as reciprocal transplant experiment in the greenhouses of the Botanic Garden Heidelberg with a duration of 15 months. Flowering time documentation in 2022 and 2023 was done by myself with the help of Jonas Silbermann.

2 | Material and Methods

2.1 Reciprocal transplant experiment

Reciprocal transplant experiments are used in evolutionary and ecological biology to study local adaptations and possible fitness differences under different environmental conditions. By cross-transplanting populations to each other's native conditions, differences in fitness under the home versus away conditions as well as the behaviour of native versus foreign populations can be compared (Johnson et al., 2022). These conditions can vary for example in climatic or edaphic conditions. In this experiment *D. gratianopolitanus* from different home substrates were used to test for adaptations to different bedrock types. In order to unravel the evolutionary past of *D. gratianopolitanus* throughout its distribution range we sampled several populations covering wide areas of the calcareous and most of the siliceous range. While the small number of sampled individuals per population does not allow the comparison on population level the general evolutionary footprint of adaptation to calcareous and siliceous bedrock can be unravelled.

Plant sampling, mother plants and plant material from natural habitats

From 2009 to 2011, 57 individuals across main areas in both the calcareous distribution area ($n = 31$), and the siliceous distribution area ($n = 26$), which includes the Czech Republic were collected (Table 2.1). All individuals involved in the transplant experiment were confirmed to be hexaploid ($2n = 6x = 90$) (see Part I and Digital Supplement "SI.0-Dianthus.Summary.xlsx"). In addition individuals from atypical bedrock types were sampled: individuals from the Wutachschlucht in Baden-Württemberg that, while in the calcareous distribution range grow on siliceous bedrock, plants from Střevíc, in the Czech Republic, growing on limestone bedrock while surrounded by siliceous bedrock, as well as some individuals from the ultramafic serpentine bedrock from Wojaleite, but were not included in further analysis. The leaf material of plants from their natural habitats as well as leaf material of so called mother plants, meaning the plants the cuttings were made of, was collected and dried for 3 days at 60 °C. The leaf element concentrations were measured but not further analysed here (See Digital Supplement "S_II.1.0-Transplant_experiment_overview_all_leafmaterial.xlsx").

Table 2.1: List of individuals included in analysis List of *Dianthus gratianopolitanus* with lab-internal LabID, sampling origin and substrate of origin. Table adapted from (Strobel, 2014). The geographic locations are given in Figure 2.1.

LabID	origin	substrate of origin
dg01243	GER : BW : Lenninger Tal : nördlicher Nachbar Müllerfels	limestone
dg00969	GER : BW : Lenninger Tal : Müllerfels	limestone
dg00974	GER : BW : Lenninger Tal : Müllerfels	limestone
dg00466	GER : BW : Lenninger Tal : Sylphenwand	limestone
dg01242	GER : BW : Lenninger Tal : zweiter südlicher Nachbar Müllerfels	limestone
dg00463	GER : BW : Eybtal	limestone
dg01296	GER : BW : Eybtal : Drehfels	limestone
dg01295	GER : BW : Eybtal : Spielerwand	limestone
dg01163	GER : BW : Eybtal : Donaldfels	limestone
dg01164	GER : BW : Eybtal : Donaldfels	limestone
dg01160	GER : BW : Eybtal : Nadelfels	limestone
dg01172	GER : BW : Eybtal : Schulterfels	limestone
dg01291	GER : BW : Eybtal	limestone
dg01286	GER : BW : Eybtal	limestone
dg00461	GER : BW : Große Hausener Wand	limestone
dg00462	GER : BW : Große Hausener Wand	limestone
dg01027	GER : BW : Große Hausener Wand	limestone
dg01022	GER : BW : Große Hausener Wand	limestone
dg01066	GER : BW : Kleine Hausener Wand	limestone
dg01350	GER : BW : Kleine Hausener Wand	limestone
dg01071	GER : BW : Eselsburger Tal : Bachfelsen	limestone
dg01086	GER : BW : Eselsburger Tal : Bindstein	limestone
dg01088	GER : BW : Eselsburger Tal : Bindstein	limestone
dg00465	GER : BW : Eselsburger Tal : Jungfrauen	limestone
dg01082	GER : BW : Eselsburger Tal : Falkenstein	limestone
dg01083	GER : BW : Eselsburger Tal : Falkenstein	limestone
dg01084	GER : BW : Eselsburger Tal : Himmel und Hölle	limestone
dg00661	GER : BW : Obere Donau	limestone
dg00665	GER : BW : Obere Donau	limestone
dg00666	GER : BW : Obere Donau	limestone
dg00667	GER : BW : Obere Donau	limestone
dg00942	CZ : Ústecký kraj : Lipská hora	siliceous
dg00852	CZ : Liberecký kraj : okres Česká Lípa : Velký Bezděz	siliceous
dg00759	CZ : Plzeňský kraj : okres Plzeň-sever : S. of Lipno	siliceous
dg00760	CZ : Plzeňský kraj : okres Plzeň-sever : S. of Lipno	siliceous
dg00926	CZ : Praha kraj : okres Praha-západ : Homole	siliceous
dg00927	CZ : Praha kraj : okres Praha-západ : Homole	siliceous
dg00866	CZ : Ústecký kraj : okres Teplice : Bořeň	siliceous
dg00966	CZ : Ústecký kraj : Úhošť	siliceous
dg00454	GER : BY (Oberfranken): Höllental	siliceous
dg00455	GER : BY (Oberfranken): Höllental	siliceous
dg00335	GER : He : Kellerwald-Edersee	siliceous (argillite)
dg00336	GER : He : Kellerwald-Edersee	siliceous (argillite)
dg00385	GER : RP : NSG Gans und Rheingrafenstein	siliceous (porphyry)
dg00429	GER : RP : NSG Gans und Rheingrafenstein	siliceous (porphyry)
dg00401	GER : Th : Wartburg	siliceous
dg00414	GER : Th : Wartburg	siliceous
dg00415	GER : Th : Wartburg	siliceous
dg00934	GER : Th : Steinigt "Nelkenstein"	siliceous
dg00432	GER : Th : Falkenstein am Schmalwasser	siliceous (porphyry)
dg00438	GER : Th : Falkenstein am Schmalwasser	siliceous (porphyry)
dg00928	GER : Th : Zimmerberg, Kaulsdorf	siliceous (argillite)
dg00929	GER : Th : Zimmerberg, Kaulsdorf	siliceous (argillite)
dg00930	GER : Th : Zimmerberg, Kaulsdorf	siliceous (argillite)
dg00338	GER : Th : Bleiberg	siliceous
dg00339	GER : Th : Bleiberg	siliceous
dg00932	GER : Th : Bleiberg	siliceous

Soil sampling and measurement of substrates pH

Three substrate types present within the distribution range of *D. gratianopolitanus* were included: i) a calcareous, limestone substrate, ii) a siliceous, porphyritic substrate and iii) an ultramafic substrate with higher levels of heavy metals. The substrate for the limestone treatment (L) a calcareous substrate was a triassic shell limestone from the quarry in Nussloch. As a typical representative for limestone locations throughout the Jura mountains an alkaline bedrock high in CaCO_3 was predicted. As the siliceous or porphyritic treatment (P) a siliceous-porphphyritic substrate was chosen to represent the diverse types of siliceous soils in Central Germany and the Czech Republic. The porphyry was collected from a quarry near Wojaleite and is a rhyolite; a highly heterogenic, fine grained volcanic rock with kaolintic clays. Despite rhyolites typically being acidic (Kruckeberg, 2002), it was predicted that the porphyritic treatment would exhibit a neutral to alkaline response, owing to the secondary inclusion of CaCO_3 . Ultramafic soils, or serpentine, arise from the weathering of igneous or metamorphic rocks rich in ferromagnesian minerals, typically constituting over 70% of their composition (Kruckeberg, 2002). While the term "serpentine" encompasses a diverse range of soils with varying chemical and physical properties they share common characteristics such as a low Ca:Mg ratio inherited from the magnesium-rich origin substrates, elevated levels of heavy metals like Fe, Ni, Cr and Co, as well as deficiencies in macronutrients like K and P. Furthermore physical properties like low moisture retention, dearth of organic matter, and overall susceptibility to erosion add to the inhospitable conditions for most plant species. The chosen serpentine substrate for the serpentine treatment (S) in the transplant experiment marked an extreme substrate type colonized by *D. gratianopolitanus*, characterized by elevated levels of the potentially toxic heavy metals and lower contents of Ca. The used serpentine rock was collected from Wojaleite (for permit see Digital Supplement "S_II.1.1-Permit-Germany_Bavaria_55.1-8622_Substrate.pdf") and prepared for the use as treatment substrate (Koch et al., 2021). Despite the typical lack of organic matter, the now used serpentine soil contained a notable proportion of organic material, which may mitigate the low moisture retention capacity.

For pH measurement of each soil type used, 3 g of each substrate was mixed in TPP centrifuge tubes with 7.5 mL of CaCl_2 (0.01 M, Merck, calcium chloride dehydrate crystalline, for analysis) and shaken overnight on a overhead shaker. The samples were centrifuged and pH was measured (Knick Calimatic 766 Laboratory pH meter equipped with a Mettler Toledo InLab Easy pH combination electrode).

Transplant experiment

All sampled individuals were cultivated in the open greenhouses for a minimum of six months prior to the experiment to acclimate and minimize non-genetic influences due to handling or maternal effects. Between 26 March and 29 March 2012, 10 cuttings of equal size of each individual were made, planted in potting soil in multi-cell plant trays and placed in propagators equipped with sodium vapour lamps. For the transplant experiment six

clay pots per individual containing the three soil treatments, with two pots per treatment, limestone (L), porphyry (P), and serpentine (S) were prepared.

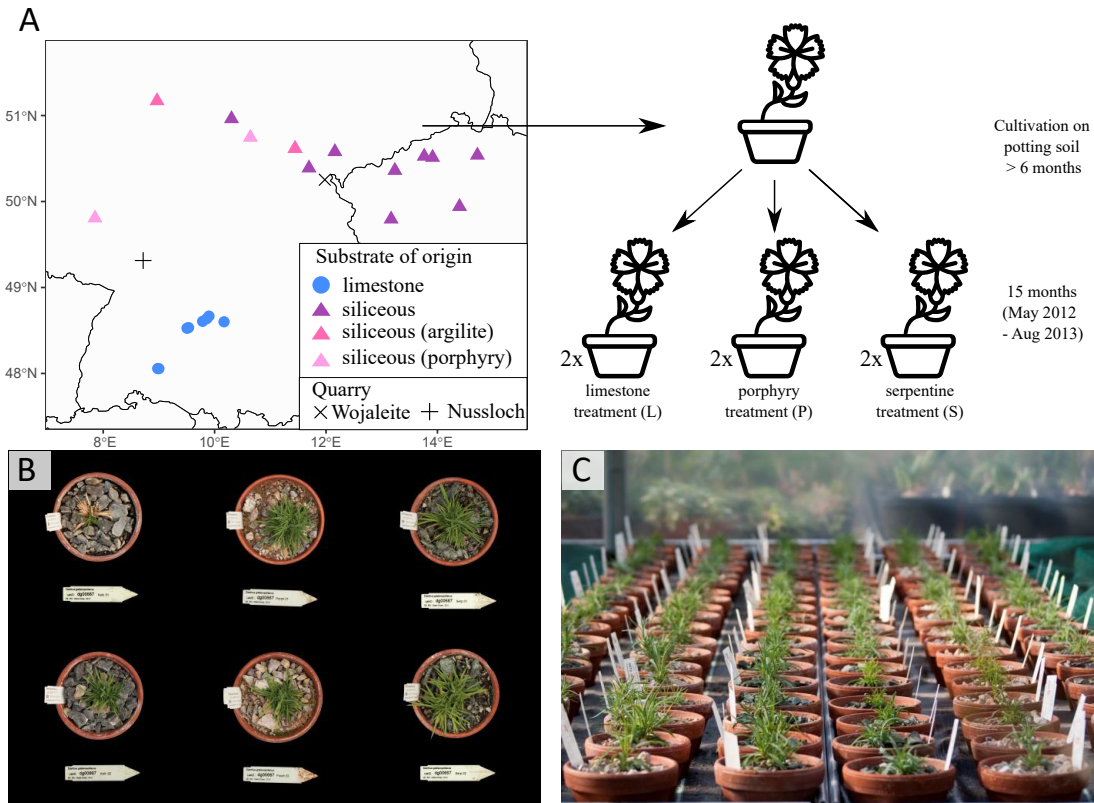


Figure 2.1: **A:** Plant sampling and outline of transplant experiment. Limestone substrate was triassic shell limestone from the quarry in Nussloch, the porphyry as well as serpentine substrate were collected from quarries in Wojaleite. Plants were acclimatized on potting soil for a minimum of 6 months prior to the transfer of cuttings to the treatment soils. Duration of the transplant experiment was from May 2012 to August 2013. **B:** Pot arrangement per individual. From left to right: limestone, porphyry and serpentine. Replicates are arranged accordingly in a second row. **C:** Arrangement in the greenhouse at the start of the experiment in May 2012 (Photos: Florian Michling)

Between 21 March and 23 May 2012 six cuttings per individual in similar conditions and development stages were chosen and transferred. The pots of one individual were placed next to each other on nylon fleece covers and the pots were not moved during the duration of the experiment to avoid possible contamination (see Figure 2.1). The plants were grown under common garden condition in the greenhouse for 15 months. During the third August week in 2013 leaf material was harvested, put in paper bags, weighed and dried to constant weight for three days at 60 °C. To avoid contamination fresh pairs of nitril gloves were used per pot. On August 19th 2013 all above-ground plant material was harvested and the greenhouse experiment was finished.

Element analysis using ICP OES

ICP-OES is short for Inductively Coupled Plasma Optical Emission Spectroscopy and describes an analytical method for the measurement of elemental composition of a sample. It is based on the principles of atomic emission spectroscopy, where the atoms in a sample are first excited to higher energy levels followed by the emission of element characteristic wavelengths of light when dropping back to their basic energy state. These so called spectral or analytical lines are specific to certain energy transitions in the analysed atom leading to possibly several different analytical lines for each element. These lines allow for the identification as well as quantification of the element in the sample. The key components for ICP-OES include a high energy plasma (e.g. composed of argon), a sample aerosolizer and the spectrometer for the measurement of the emitted light.

The experiment was performed at the Department of Plant Physiology at Ruhr University Bochum with the help of Prof. Dr. Ute Krämer, Dr. Ricardo J. Stein and Petra DÜchting. For measurement a Thermo Scientific iCAP DUO 6500 spectrometer equipped with an EMT torch (diameter 2 mm), a concentric glass nebuliser and a cyclone nebuliser chamber was used. The setup included a CID detector of 540×540 pixels and an Echelle grating optical system. For plasma generation as well as rinsing of the system, argon of the highest purity level (5.0) was used. For system calibration five internal calibration standards (Std-0 to Std-5, see Appendix [Table B.1](#)) were used with each run. In addition to a blank sample, Std-3 also served as an internal quality check.

Soil sample preparation, measurement and analysis

Sample preparation Soil samples of the three treatment substrates, were sampled after the soil preparation for the transplant experiment before the distribution to individual pots. The samples were dried for five days at room temperature, sieved through a 2 mm nylon mesh sieve followed by an additional drying step for seven days at room temperature. Two different approaches were chosen to either measure i) total element concentrations or ii) plant available element concentrations.

For the measurement of total element concentrations at least four replicates per treatment soils were used. 0.25 g of soil sample and 3 mL of "Aqua regia" (0.75 mL HNO₃, Sigma-Aldrich $\geq 65\%$; 2.25 mL HCL, Merck, 37%, for analysis) were mixed in acid-washed borosilicate DURAN glass tubes (0.2 M HCL solution overnight, rinsed three time with ultrapure water) and left overnight. The samples were heated to 100 °C in three consecutive steps: two hours at 60 °C, two hours at 75 °C, five hours at 100 °C and left to cool down at room temperature. Ultrapure water was added to a final volume of 10 mL, sealed with lamellar plugs and stored at 4 °C until further use.

For the analysis of plant available element concentrations two replicates per treatment soil were used. 1 g of soil sample was mixed with 10 mL 0.01 M BaCl₂ (BaCl₂ X 2H₂O, Merck, for analysis) in TPP cetrifuge tubes, shaken on an overhead shaker overnight and filtered through Whatman syringe filters FP 300.2 CA-S before adding 1 mL of HNO₃ (Sigma-

Aldrich $\geq 65\%$). 6.5% HNO₃ was added to a final volume of 10 mL and stored at 4 °C until further use.

Measurement For soil element concentration measurement, the concentrations of Ag, Al, As, B, Ca, Cd, Co, Cr, Cu, Fe, Hg, K, Mg, Mn, Mo and Ni were analysed. As additional quality check *San Joaquin soil CRM (NIST 2709a)*, a certified reference material, was used. Measurement of plant available element concentration for the three substrate types, started with porphyry samples, followed by serpentine and limestone samples. Following the calibration by interposition of Std-3 the samples prepared for total element concentration analysis were analysed sequentially in the same order. After completing the first run for plant available element concentrations as well as total element concentrations, dilutions were made if needed and analysed again.

Raw data analysis and evaluation Data clean up and first evaluation of data quality was done by Kathrin Strobel. To obtain the final element concentration, c_f [$\mu\text{g g}^{-1}$], for each sample the offset of the raw element concentration values c_{raw} [mg L^{-1}] by i) the weighed portions of soil m [mg], ii) the dilution factor f_d , and iii) the final analysis volume of 10 mL V must be taken into account (Formula 2.1).

$$\frac{c_r \cdot V \cdot f_d \cdot 1000}{m} = c_f \quad (2.1)$$

Lines displaying interference, instability, or malfunction, like negative values or oscillations, were omitted from further analysis, as were lines known to be insensitive within the sample's measuring range. Mean values of the remaining elements' analytical lines were calculated.

Plant sample preparation, measurement and analysis

Sample preparation The leaf material harvested of plants included in the transplant experiment at the end of the of the experiment in August 2013 was dried for three days at 60°C followed by at least three days of equilibration at room temperature. The leaves were ground using yttrium-stabilised zirconium oxide beads (SiLibeads type ZY 3.0-3.3 mm) in a Precellys24 homogenizer (PEQLAB) and digested according to the protocol provided by the Department of Plant Physiology at Ruhr University, Bochum. 0.20 - 0.25 g of ground leaf material were mixed with 2 mL HNO₃ (Sigma-Aldrich $\geq 65\%$) in acid-washed borosilicate DURAN glass tubes (0.2 M HCL solution overnight, rinsed three times with ultrapure water), covered and left overnight. The samples were heated stepwise to 120 °C and left to cool down at room temperature. After adding 1 mL H₂O₂ (AppliChem, 30%) the samples were heated to 100 °C. Ultrapure water was added to a final volume of 10 mL, sealed with lamellar plugs and stored at 4 °C until further use.

In addition the dried leaf material of the mother plants as well as silica dried leaf material of sampled plants from visited natural sites were included and processed as described.

Measurement For plant element concentration measurement, the concentrations of Al, B, Ca, Cd, Co, Cr, Cu, Fe, K, Mg, Mn, Mo, Ni, P, Pb, S, Se and Zn were analysed. Analytical lines for Al and Pb were added as control for sample contamination. While they can be naturally be present in plants, elevated levels can be toxic and can indicate a contamination. By comparing measured concentrations to background levels it can be assessed whether the Al and Pb levels are within expected ranges or hint towards contamination. As additional quality check the certified reference material, *tobacco CRM (INCT-PVTL 6)*, was used. To prevent contamination of samples with materials from other treatments or measurement bias caused by consecutive measurements of different treatment groups, the three treatments were measured as distinct sets, with replicates measured consecutively to reduce the risk of bias. At the start of each measurement of a treatment group, the standards, a set of blanks and the quality check reference material sample was inserted beforehand. In addition the quality check standard (Std-3) was introduced at the start of each analysis set, every 45-50th sample, and in the end of every treatment group to control for fluctuations in the measurement.

Raw data analysis and evaluation As a first step the raw data from the leaf material's ICP OES output (measured in CTS/s, or counts per second) was compared with the output data of calibration standards utilized in the analysis. Analytical lines of each element with measurement values not exceeding values obtain by the measurement of Std-O for any treatment group were excluded from further analysis. Raw concentrations were calculated using the CTS/s data and the Thermo Scientific iTEVA ICP Software accompanying the iCAP DUO 6500 spectrometer. The total element concentrations, c_f [$\mu\text{g g}^{-1}$], was calculated according to Formula 2.1 the raw concentration data, c_{raw} [mg L^{-1}], was offset against i) the weighed portions of leaf material m [mg], ii) the dilution factor f_d , and iii) the final analysis volume V of 10 mL. Values of Al and Pb exceeding a critical limit ($\geq 300 \mu\text{g g}^{-1}$, Ricardo J. Stein, personal communication with Kathrin Strobel, October 2013) were considered as indication of contamination and samples were excluded from further analysis. Mean values for all remaining analytical lines per sample were calculated. Individual element accumulation ratios, acc_{ind} , per plant were calculated as sum of i) the individual element accumulation ratio per treatment, $\text{acc}_{\text{treat}}$, and ii) the individual element accumulation ratio across all treatment groups, acc_{tot} divided by acc_{tot} :

$$\frac{\text{acc}_{\text{treat}} + \text{acc}_{\text{tot}}}{\text{acc}_{\text{tot}}} = \text{acc}_{\text{ind}} \quad (2.2)$$

The acc_{ind} indicates the ratio of individual element concentration within a treatment compared the individual element accumulation across the three different treatment groups.

Fitness parameters

To assess plants overall fitness response four parameters were recorded: i) the flowering status documenting if they flowered or not, ii) the size and growth of above ground plant material including signatures of chlorosis and withering, and iii) the biomass of above ground plant material. The signs of chlorosis were scored as either i) healthy plants indicating no signs of chlorosis, ii) mild signs of chlorosis or iii) severe signatures of chlorosis. The withering was scored using two categories with either i) healthy plants without withering or ii) clear signs of withering. Plant flowering was documented in the flowering period from April to June 2013. Size, growth and plant appearance was assessed by image analysis of top view photographs taken at two time points during the experiment: i) in the third week of April 2013 and ii) in the third week of August 2013. Constant distance to the objects and identical camera settings were used for photo documentation. Image analysis and measurements were done using Adobe Photoshop CS4 and KLONK Image Measurement. For the measurement of above-ground growth the difference between initial and final sizes of above-ground plant material was calculated for each individual excluding flowers and flowering stems in the measurement. The above ground plant and leaf material was harvested and weighed. In addition the leaf material was dried to constant weight for 3 days at 60 °C. The dry weight was calculated based on the fresh weight and the individual withering factor inferred from the water loss of leaf material during the elemental analysis experiment.

Data analysis

Data analysis was done using R (version 4.3.2). I used the principal component analysis (PCA) to assess overall patterns in element accumulation comparing for example the different treatments or the substrate origin. I assessed differences in elemental uptake between the soil treatments using Mann-Whitney U and Kruskal-Wallis test to assess the statistical significance of possible differences. In addition I calculated the effect sizes and corresponding 95% confidence intervals (CI) using the `wilcox_effsize()` function from the "rstatix" package (Kassambara, 2023). Dependencies were tested using the Chi² and Fisher test (`Crosstable()`, R package "gmodels" (Warnes et al., 2022)).

2.2 Flowering time in 2022 and 2023

To assess the influence of genetic background and climatic conditions on the flowering behaviour of *D. gratianopolitanus* the plants collected over the years are grown in the Botanical Garden Heidelberg under full-light outdoor conditions in greenhouses with lower able side walls to allow for good air circulation. Plants were sheltered from rain to simplify and control optimal watering conditions. They were grown in a well-draining substrate (25% TKS®1 (Floragard, Oldenburg, Germany), 25% pumice, 25% expanded slate, 12.5% lava, 6.25% sand (Rhine River sediments), 6.25% quartz sand, bentonite clay powder) in identical pots and were distributed randomly on the designated greenhouse tables to avoid

bias due to the plants position within the greenhouse. During the flowering period in 2022 and 2023 I documented the total amount of flowers as well as start of flowering (opening of the first flower) and end of flowering (wilting of last flower) per plant. The number of flowers were sorted into 5 categories ranging from 1 - small number of flowers to 5 - very high number of flowers (See Digital Supplement "S_II.2.2-Dianthus_Blütendoku_2022.xlsx" and "S_II.2.3-Dianthus_Blütendoku_2023.xlsx"). In addition the size of each plant was documented using three classes: S for for small cushions not reaching the pot edge, M for cushions that fill the pot, and L for all those that exceed the pot rim. In the autumn of 2022 the cushions were reduced to the same size, repotted and additional replicates were made. Temperature data (mean temperature every 30 min) as well as total global radiation (W/m, mean every 30 min) was collected from the weather station at Berliner Straße (Landesanstalt für Umwelt, Messungen und Naturschutz Baden-Württemberg (LUBW)) in addition on site temperature was measured in 2022 using three thermometers (testo 174H, Testo SE & Co. KGaA, Lenzkirch, Germany) distributed within the green house. During winter (November to February) minimum temperature was 4 °C to avoid uncontrolled frost damage. I corrected the temperature data from LUBW accordingly. I also compared the collected data on flowering time and number of flowers with data derived from the transplant experiment in 2013.

Data analysis

Data analysis was done using R (version 4.3.2). I compared the half monthly temperature sum of the first half of the year, for 2013, 2022 and 2023. I scored the flowering frequency, meaning the percentage of flowering plants of all plants, for the plants included in the transplant experiment in 2013 and for the same plants present in the garden in 2022 and 2023. For each year I grouped the plants by substrate of origin into a calcareous and siliceous group. In order to avoid a possible influence of substrate treatment in 2013, only plants grown on their home substrate were used. In addition I also analysed the available replicates for 2022 and 2023 separately. To analyse the influence of temperature differences at the start of the year on flowering behaviour, I calculated the cumulative mean daily temperature sum starting at the first day of flowering counting backwards to the start of the year for 2013, 2022 and 2023, as described in [Koch et al. \(2021\)](#).

I analysed the influence of different origins in geographical regions on the flowering behaviour by comparing the start of flowering between regions using boxplots and Mann-Whitney U test. I compared the overall trend observed in differences in number of flowers and cushion sizes between regions as well as years and tested possible dependencies using the Chi² and Fisher test (Crosstable(), R package "gmodels" ([Warnes et al., 2022](#))). In addition the number of flowers in correspondence to cushion sizes were analysed using linear regression as well as Chi² and Fisher test. 1

3 | Results

3.1 Pre-evaluation of raw data

Plant samples

Element analysis of leaf material of plants collected at the natural site, leaf material of the original mother plants, as well as leaf material of plants from atypical sites (Wutachschlucht, Wojaleite, and Střevíc) are available but not further analysed herein.

Elemental lines

Element concentration - Soil samples

The analytical lines showing signs of interference, malfunction or lines that are known to be insensible in the measuring range were removed from further analysis leading to the exclusion of: Al167.0, Cd214.4, Cd219.4, Cd226.5, Cd228.8, Fe238.3, and Fe259.9. Additionally, the analytical line for detecting Bor (B) concentrations (B208.9) was not used because the measured B concentrations might be influenced by the acid treatment of the borosilicate DURAN glass tubes used in preparing the samples for ICP OES analysis, and did not reflect the actual concentrations in the soils. For the analysis of plant-available element concentrations, Ag328.0, Al396.1, Cr205.5, Cr267.7, Cu324.7, Cu327.3, Fe208.4, and Fe217.8 were excluded because the measured values were too close to the null level (i.e., lower detection limit) to reflect the actual concentrations of these elements in the soil.

Element concentration - Leaf material

No sample was excluded due to signs of contamination since Al and Pb values did not exceed the critical limits. Even if Al was slightly elevated no suspicious accumulation of other elements was visible, giving no indication of contamination. The analytical lines Al237.3, Al396.1, Pb220.3, and Pb283.3 were further excluded from the analysis. As for the soil samples, the elemental lines used to measure B concentrations (B208.9, B249.7) were excluded due to the usage of B in the preparation of the borosilicate DURAN glass tubes for the ICP OES analysis. The analytical lines for Cr and Se detection (Cr205.5, Cr267.7, Se196.0) were excluded from analysis due to measured values close to zero.

3.2 Treatment soil differs in element composition

The measurements of the three substrates used as treatment groups did not show significant differences. The pH of the substrates ranged from 6.7 to 7.9 (Table 3.1), indicating that all three were neutral to slightly alkaline. Only the filtered solution of ground serpentine non-organic matter showed a tendency toward an acidic reaction.

Table 3.1: pH measurement of the treatment soils pH measurement of the used treatment soils including ground serpentine and measurement of unfiltered and filtered solutions. All samples show neutral to slightly alkaline reaction, with the only exception in the slightly acidic reaction of the filtered ground serpentine.

	limestone	porphyry	serpentine	ground serpentine
pH	7.9	7.3	7.0	7.5
pH (filtered)	7.4	7.3	7.5	6.7

Total soil element concentrations as well as plant available element concentrations were measured for the three treatment soils as well as ground serpentine treatment (Figure 3.1, Table 3.2 and Digital Supplement "S_II.1.2-Substrat_ICP-OES.xlsx"). The limestone treatment shows higher levels of total Ca, K, and Mo. While the higher concentrations of Ca and Mo are also present in the measurement of plant-available element concentrations, K can be found in higher concentrations in the used porphyry soil. The used triassic shell limestone also has a comparable high amount of Fe exceeding the amount of Fe within the porphyry treatment. The porphyry treatment has the highest concentration of As in the measurement of both total and plant available concentrations but shows great differences in Mn when comparing the measurements. While it has the lowest content of Mn in the total measurement it has the highest concentration within the plant available concentration when compared to the other substrates. As the used bedrock is a rhyolite the higher amount of Ca is also visible in both measurements. The serpentine treatment shows elevated levels of Ag, Cr, Mg, Co, Cu, Fe, Mn, and Ni in total element concentration, and higher levels of Mg and Ni in the plant available element analysis. The Ca: Mg ratio based on plant-available element concentrations differs between limestone (5.85), porphyry (10.97), and serpentine (0.63).

3.3 Element composition in leaf material influenced by treatment soil - no strong home effect based on plant origin substrate

The mean element content in the leaf material based on the three treatment groups and based on the plant origin is given in Table 3.3. A summary of the statistical analysis of differences in element content per substrate and treatment groups is given in the Appendix Table B.2 and Table B.3. The overview of results per individual including the replicates is

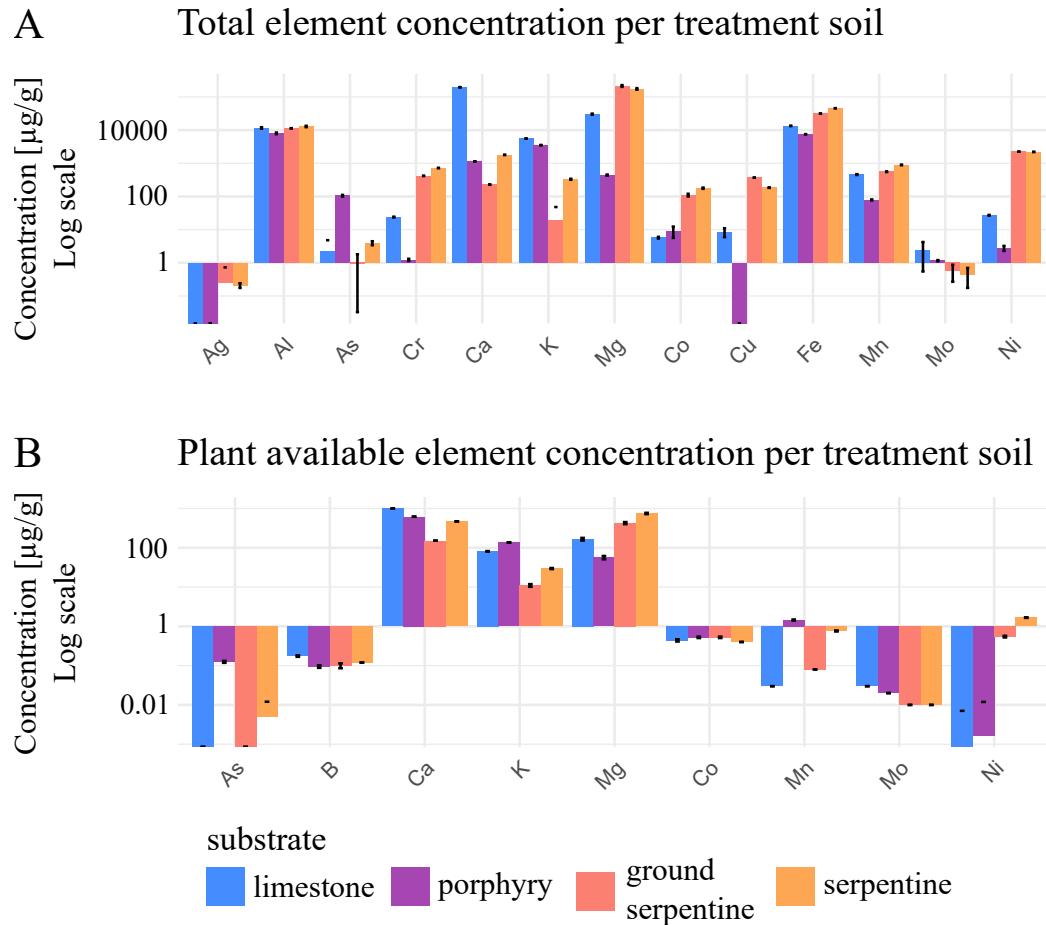


Figure 3.1: Element concentrations of treatment soils including ground serpentine. A: Total element concentration. B: Plant available (exchangeable) element concentrations. The corresponding table is given in [Table 3.2](#).

given in the Digital Supplement "S_II.1.3-Transplant_experiment_overview_plants.xlsx" as well as differences between replicates in "S_II.1.4-replicates_summary_table.xlsx".

Element concentrations between plant origins and treatment groups Comparing element concentration between plants from calcareous and siliceous bedrock sites across all treatments reveals significant differences in the concentrations of Mo, and S (Mann-Whitney U test with Bonferroni corrected orig. $\alpha = 0.05$, $\alpha' = 0.00031$, $p < 0.0001$) with plants from calcareous bedrock accumulating higher concentrations ([Table 3.3](#) and Appendix, [Table B.2](#)). Effect sizes indicate small to medium effects for Mo ($r = 0.31$, 95% CI [0.18, 0.45]), and S ($r = 0.383$, 95% CI [0.25, 0.5]). Element concentrations between the three treatment groups of plants from all origins showed bigger differences. Mean values and standard deviations are given in [Table 3.3](#), and results of the Bonferroni corrected Wilcoxon rank sum test with corresponding effect size are given in the Appendix, [Table B.2](#). Between limestone and porphyry treatment only Ca, Fe, Mo, and S showed no statistically significant difference (Mann-Whitney U test, $\alpha' = 0.00031$) in concentrations. Biggest effect sizes can be found

Table 3.2: Mean Element Concentrations in Treatment Soil Total element concentration and plant available (exchangeable) element concentrations measured for all treatment soils as well as ground serpentine soil. The number of replicates N per treatment soil is given in brackets. The corresponding plot is given in [Figure 3.1](#).

Total Element Concentrations [$\mu\text{g/g}$]				
	Limestone (N=8)	Porphyry (N=4)	Serpentine (N=5)	Ground Serpentine (N=8)
Ag	0 \pm 0.00	0 \pm 0.00	0.208 \pm 0.03	0.26 \pm 0.47
Al	11640 \pm 599.05	7997 \pm 438.40	12906.4 \pm 579.38	11313.5 \pm 136.68
As	2.21 \pm 2.59	105.43 \pm 6.01	3.924 \pm 0.54	0.92 \pm 0.89
Cr	23.835 \pm 0.65	1.23 \pm 0.09	720.9 \pm 0.46	417.42 \pm 0.43
Ca	196223.33 \pm 1866.12	1136.43 \pm 5.95	1791.89 \pm 13.20	228.79 \pm 2.96
K	5561.25 \pm 35.75	3529 \pm 28.90	329.99 \pm 10.58	19.56 \pm 28.39
Mg	30308 \pm 1083.50	440.36 \pm 17.15	175106 \pm 9178.00	214868.75 \pm 12921.25
Co	5.735 \pm 0.32	8.98 \pm 3.34	177.492 \pm 7.26	110.24 \pm 10.19
Cu	8.4825 \pm 2.51	0 \pm 0.00	184.38 \pm 2.82	369.67 \pm 2.41
Fe	13402.75 \pm 87.75	7505.5 \pm 45.50	45839.8 \pm 1.80	31670.75 \pm 31.00
Mn	457.1 \pm 11.85	78.64 \pm 2.73	892.37 \pm 16.69	557.1 \pm 12.05
Mo	2.39 \pm 1.84	1.16 \pm 0.05	0.436 \pm 0.26	0.57 \pm 0.30
Ni	27.08 \pm 0.61	2.76 \pm 0.47	2201.01 \pm 8.34	2244.6 \pm 5.18

Plant Available Element Concentrations [$\mu\text{g/g}$]				
	Limestone (N=2)	Porphyry (N=2)	Serpentine (N=2)	Ground Serpentine (N=2)
As	0.0 \pm 0.0	0.125 \pm 0.007	0.005 \pm 0.007	0.0 \pm 0.0
B	0.175 \pm 0.007	0.095 \pm 0.007	0.12 \pm 0.0	0.1 \pm 0.014
Ca	996.215 \pm 1.579	617.797 \pm 2.460	468.27 \pm 2.200	151.36 \pm 0.412
K	81.0175 \pm 1.213	136.345 \pm 1.320	29.518 \pm 0.913	10.998 \pm 0.858
Mg	165.2475 \pm 12.623	56.303 \pm 5.423	745.553 \pm 27.913	424.38 \pm 25.465
Co	0.44 \pm 0.028	0.525 \pm 0.021	0.4 \pm 0.0	0.525 \pm 0.021
Mn	0.03 \pm 0.0	1.443 \pm 0.048	0.763 \pm 0.023	0.08 \pm 0.0
Mo	0.03 \pm 0.0	0.02 \pm 0.0	0.01 \pm 0.0	0.01 \pm 0.0
Ni	0.0 \pm 0.007	0.002 \pm 0.010	1.67 \pm 0.025	0.548 \pm 0.026

for Cd ($r = 0.86$, 95% CI [0.84, 0.86]), Mn ($r = 0.795$, 95% CI [0.73, 0.84]) and Zn ($r = 0.846$, 95% CI [0.82, 0.86]) while the smallest yet significant are found in K ($r = 0.348$, 95% CI [0.16, 0.5]). Between limestone and serpentine treatment Cd, Cu, Fe, K, P, and S showed no statistically significant difference (Mann-Whitney U test, $\alpha' = 0.00031$) in concentrations. Biggest effect sizes can be found for Ca ($r = 0.776$, 95% CI [0.7, 0.83]), Co ($r = 0.85$, 95% CI [0.82, 0.86]) and Ni ($r = 0.86$, 95% CI [0.84, 0.86]) while the smallest but significant are found in Zn ($r = 0.39$, 95% CI [0.21, 0.52]). Comparing element concentrations in the porphyry and the serpentine treatment non-significant differences are only found in P and S (Mann-Whitney U test, $\alpha' = 0.00031$). Effect sizes indicate a large effect for Cd ($r = 0.86$, 95% CI [0.84, 0.86]), Mg ($r = 0.85$, 95% CI [0.47, 0.7]), Ni ($r = 0.86$, 95% CI [0.85, 0.86]) and Zn ($r = 0.86$, 95% CI [0.84, 0.86]) while the smallest yet significant effect sizes are found in Fe ($r = 0.38$, 95% CI [0.2, 0.53]). The principal component analysis of plant elemental concentrations indicates that the first two components accounted for $\sim 55.23\%$ of the total variance. While there is no clear separation between the substrate

of origin (see [Figure 3.2 A](#)), the treatment groups can be distinguished from one another. The serpentine group forms a dense, separated cluster whereas the limestone and porphyry clusters show a small overlap. Especially Mg and Ni contribute to the clear separation of the plants from serpentine treatment. Mg concentrations are on average nearly twice as high in the serpentine treatment when compared to limestone and even 2.7 times bigger than concentrations in porphyry. For Ni, this difference is even stronger with concentrations in the serpentine treatment being nearly 10 times greater than in those from limestone and porphyry treatment ([Table 3.3](#)). For closer analysis of differences and possible patterns in element concentrations macro and micro element concentrations are analysed separately.

Table 3.3: Mean element concentration in leaf material. Results are grouped either by origin: with calcareous ($n = 31 * 3 = 93$, plants from the calcareous range in all three treatments) or siliceous origin ($n = 26 * 3 = 78$), or per treatment with the limestone ($n = 57$), porphyry ($n = 57$) and serpentine treatment ($n = 57$).

element	substrate of origin		treatment		
	calcareous (C) [$\mu\text{g/g}$]	siliceous (S) [$\mu\text{g/g}$]	limestone (L) [$\mu\text{g/g}$]	porphyry (P) [$\mu\text{g/g}$]	serpentine (S) [$\mu\text{g/g}$]
Ca	15040.98 \pm 6499.06	16121.59 \pm 5862.31	19307.04 \pm 4970.78	17927.40 \pm 4981.72	9367.23 \pm 2995.69
Cd	1.61 \pm 1.90	1.42 \pm 1.62	0.45 \pm 0.23	3.63 \pm 1.63	0.49 \pm 0.23
Co	0.46 \pm 0.66	0.48 \pm 0.77	-0.10 \pm 0.17	0.51 \pm 0.78	1.00 \pm 0.53
Cu	9.63 \pm 4.22	8.11 \pm 4.45	7.60 \pm 3.20	12.47 \pm 4.70	6.72 \pm 2.53
Fe	30.36 \pm 7.88	31.36 \pm 8.26	29.75 \pm 7.34	34.66 \pm 9.12	28.04 \pm 5.97
K	15829.89 \pm 3885.02	15121.23 \pm 4081.05	15262.56 \pm 3283.97	18121.35 \pm 4006.10	13136.00 \pm 2916.21
Mg	4731.85 \pm 2568.72	4308.59 \pm 2255.97	3733.09 \pm 1220.82	2693.14 \pm 949.82	7190.12 \pm 2073.19
Mn	139.87 \pm 97.74	121.36 \pm 73.07	71.67 \pm 25.29	213.69 \pm 100.21	108.92 \pm 39.69
Mo	3.40 \pm 1.90	2.41 \pm 1.74	3.56 \pm 1.88	3.44 \pm 2.10	1.86 \pm 1.03
Ni	9.54 \pm 9.54	9.98 \pm 11.59	2.58 \pm 0.46	2.08 \pm 0.32	24.56 \pm 6.49
P	2540.53 \pm 540.39	2596.74 \pm 497.10	2325.59 \pm 459.04	2698.61 \pm 463.79	2674.32 \pm 554.45
S	2454.53 \pm 1227.56	1669.76 \pm 901.18	1928.18 \pm 950.66	2373.47 \pm 1380.97	1988.05 \pm 1062.59
Zn	269.49 \pm 269.49	276.99 \pm 214.14	164.66 \pm 64.03	534.74 \pm 198.06	119.32 \pm 58.97

Macro and micro element concentrations The PCA of macro element concentrations (Ca, K, Mg, P, S) suggest that the first two component axes account for $\sim 58.99\%$ of variation ([Figure 3.2, B](#)). Treatment groups are closer in factor-plane and more overlapping, with the limestone and porphyry treatment overlapping to a higher degree than with the serpentine treatment. Groups based on the substrate of origin have a large intersection but are separated along axis 2 influenced by differences in Mg, P and S concentrations, with S concentrations showing significant differences between the two groups (Mann-Whitney U, $p < 0.0003$, see Appendix [Table B.2](#)). The PCA of microelement (Cd, Co, Cu, Fe, Mn, Mo, Ni, Zn) concentrations suggest that the first two components account for $\sim 67.4\%$ of variance ([Figure 3.2, C](#)). Here the treatment groups are again separated more clearly with close to no overlap but groups based on the substrate of origin are nearly completely overlapping and indistinguishable.

Element concentration per substrate of origin within the three treatment groups PCA of element concentrations within the limestone treatment reveals that the first two components account for $\sim 48.48\%$ of variance ([Figure 3.3, A](#)). The siliceous group is more

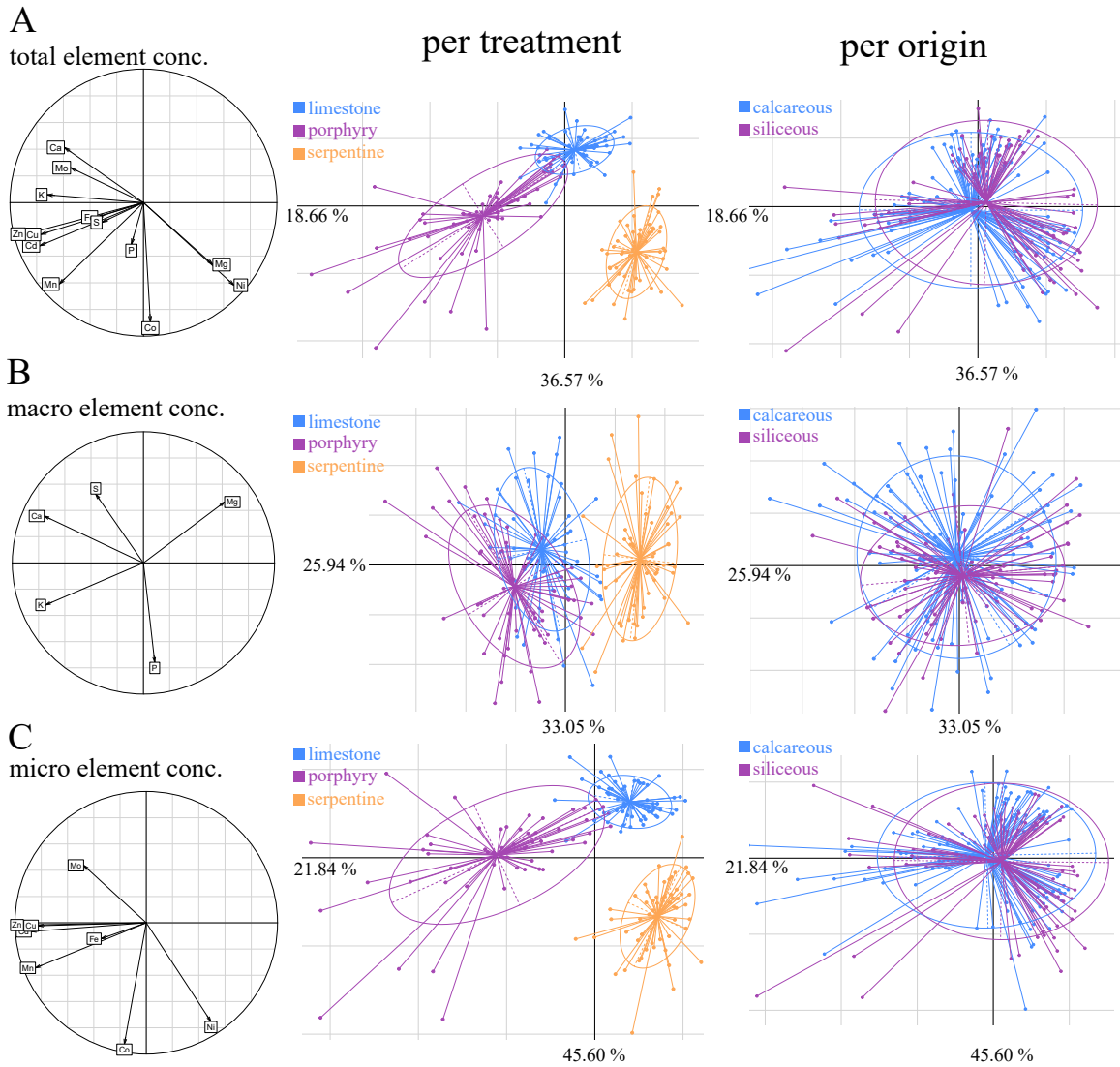


Figure 3.2: Principal component analysis of element concentrations in the trans-plant experiment grouped by treatment and substrate of origin **A** total element concentrations, **B** macro element concentrations and **C** micro element concentrations with correlation circle, biplot of the first two axes with point classes as representation of the three treatments (limestone (blue), porphyry (purple), serpentine (orange)) and as representation of substrate of origin (calcareous (blue) and siliceous (purple)). Centroids indicate the mean position of the groups and the respective ellipsoid each groups variability.

densely packed and completely included in the area spanned by the calcareous group. Comparing elemental concentrations significant differences can be found in the concentrations of Mo, and S (Mann-Whitney U, $\alpha' = 0.00031$, $p < 0.0003$) with plants from calcareous bedrock showing higher concentrations and effect sizes indicating a medium to large effect ($0.27 < r < 0.7$) (Appendix Table B.3). Within the porphyry treatment the first two components of the PCA account for $\sim 54.32\%$ of variance (Figure 3.3, B). No separation of origin groups can be observed. No significant differences in element concentrations between

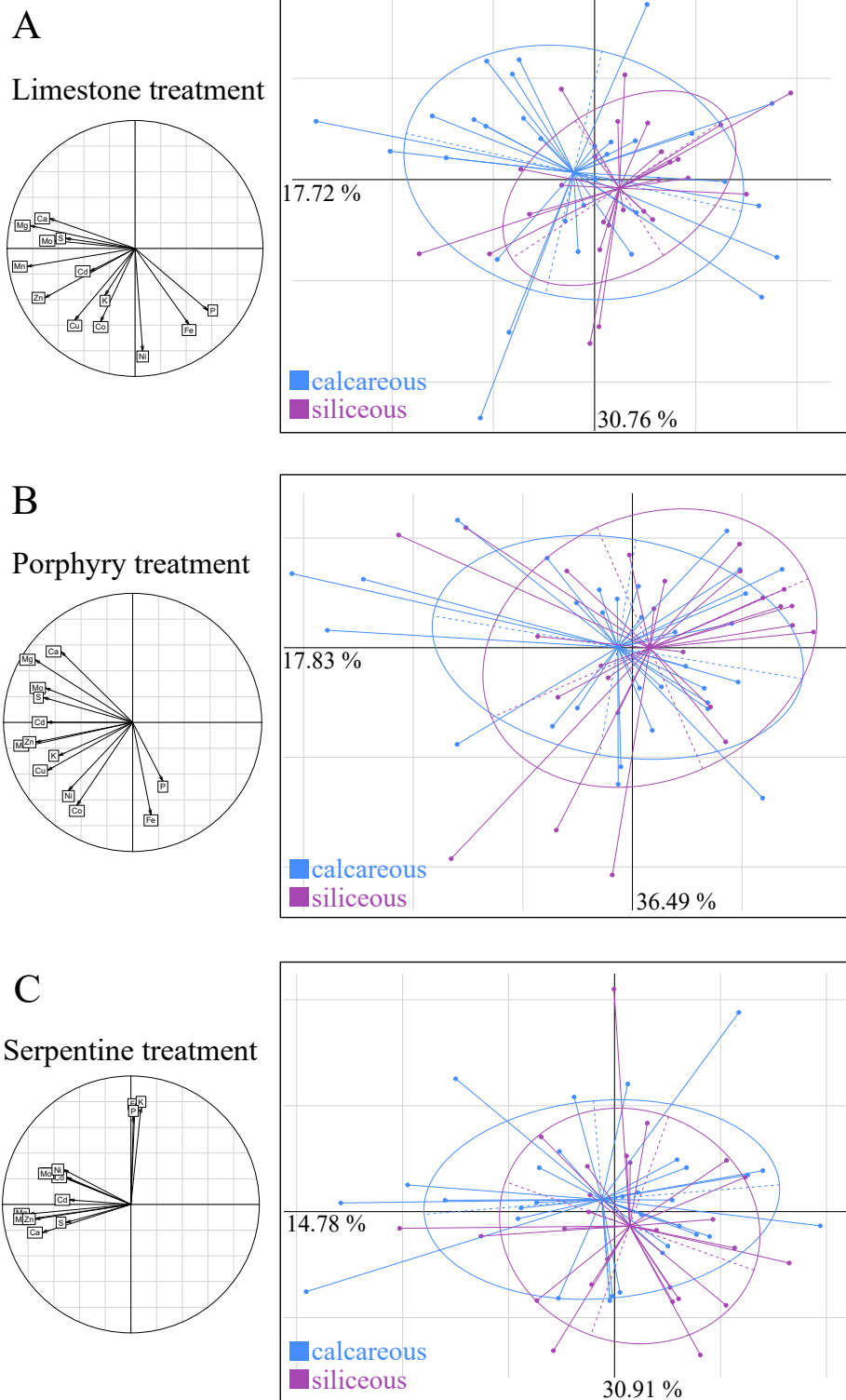


Figure 3.3: Principal component analysis of element concentrations within each treatment grouped by substrate of origin **A within the limestone treatment, **B** the porphyry treatment and **C** the serpentine treatment with correlation circle and biplot of the first two axes with point classes as representation of substrate of origin (calcareous (blue) and siliceous (purple)). Centroids indicate the mean position of the groups and the respective ellipsoid each groups variability.**

the two groups could be observed (Appendix Table B.3). The first two components of the PCA of element concentrations in the serpentine treatment account for $\sim 45.69\%$ of variance (Figure 3.3, C). No clear separation of substrate of origin groups is visible with both groups overlapping to a high degree. Plants from calcareous bedrock sites showed higher concentrations in Mo, and S (Mann-Whitney U, $\alpha' = 0.00031$, $p < 0.0003$) than those from siliceous bedrock sites with medium effect sizes ($0.25 < r < 0.72$) (Appendix Table B.3).

3.3.1 Element accumulation

Differences in total, micro (Cd, Co, Cu, Fe, Mn, Mo, Ni, Zn), and macro (Ca, K, Mg, P, S) element accumulation ratios are determined for the different substrate of origins between and within treatment groups as well as between the treatments (Figure 3.4, Appendix Table B.4). Total element accumulation shows a similar signal to macro element accumulation. No significant differences between the substrate of origins were found across and within the different treatment groups for total element accumulation ratio as well as for the macro and microelement accumulation ratios. Comparing the three treatment groups shows significant differences in total and macro element accumulation rates only between the serpentine treatment and the limestone and porphyry treatment, respectively (Mann-Whitney U test, $\alpha' = 0.00031$, $p < 0.00001$), with plants in the serpentine treatment accumulating significantly smaller amounts of elements. The Wilcoxon test revealed large effect sizes ($0.55 < r < 0.8$, see Appendix Table B.4) with the corresponding 95% confidence intervals, that indicate meaningful differences in total and macro element accumulation rates to the serpentine treatment. The microelement accumulation rate is significantly higher within the porphyry treatment compared to both limestone and serpentine treatment (Mann-Whitney U test, $\alpha' = 0.00031$, $p < 0.0001$). The effect sizes (limestone x porphyry $r = 0.86$, 95% CI [0.84, 0.86]; porphyry x serpentine, $r = 0.86$, 95% CI [0.84, 0.86]) also indicate a large effect and the narrow confidence intervals suggest a high precision.

3.4 Fitness parameter

Fitness parameters were scored using the photo documentation from April 2013 and August 2013 as well as weight from above-ground plant material measured at the end of the experiment in August 2013. Due to missing data four individuals were excluded from further analysis resulting in a total of 167 used plants out of 171.

3.4.1 Withering and Chlorosis unaffected by plant origin substrate and treatment soil

A marginally statistically significant association between withering and substrate of origin (Chi-squared test $p = 0.0228$, Fisher's exact test $p = 0.0254$, Kruskal-Wallis test $p = 0.0232$) but not within treatment groups (Chi-squared test $p = 0.2077$, Fisher's exact test $p = 0.2179$, Kruskal-Wallis test $p = 0.2097$) could be observed. There is a slight trend where

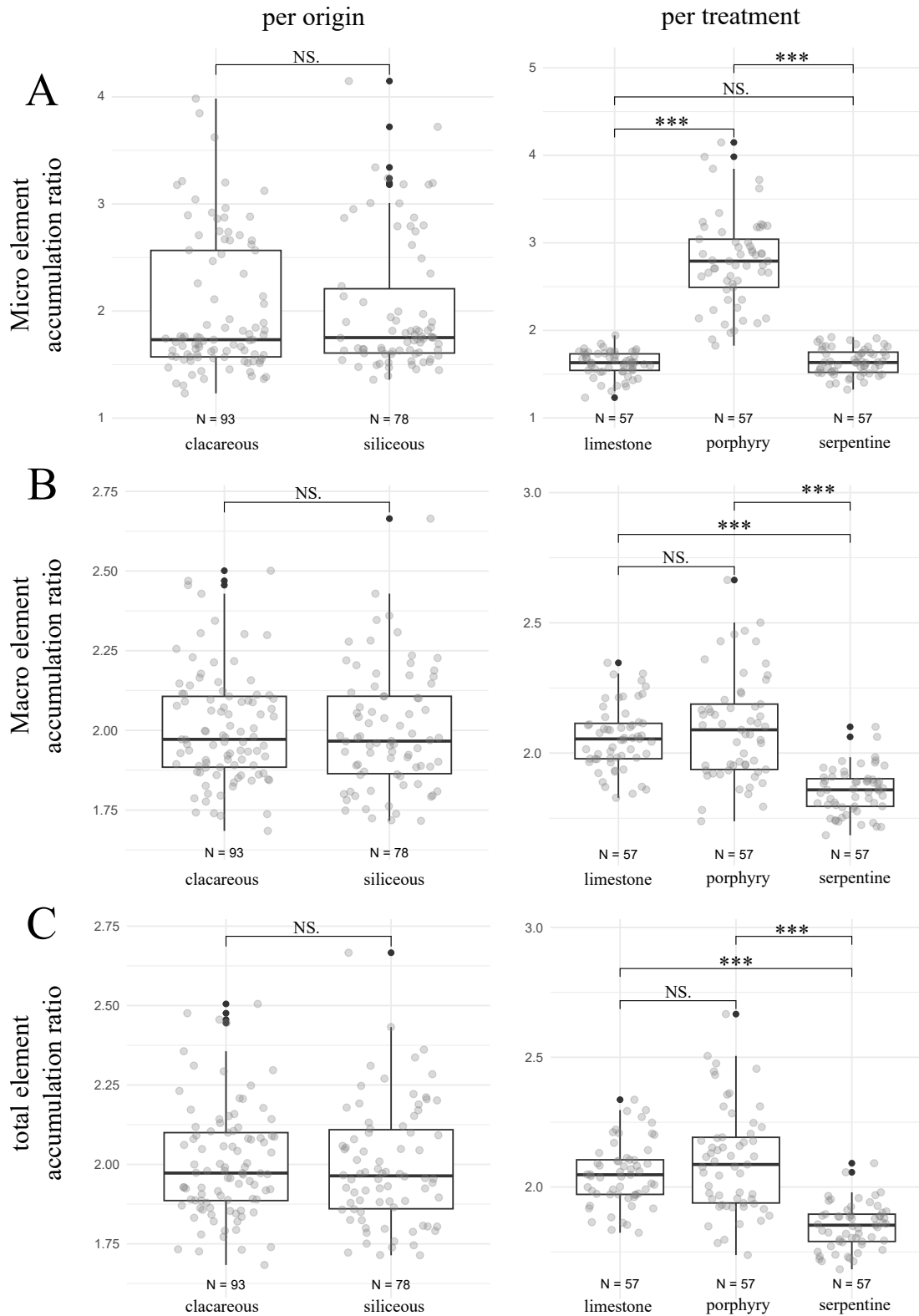


Figure 3.4: Element accumulation rate by origin and treatment group. Micro element accumulation ratio (Cd, Co, Cu, Fe, Mn, Mo, Ni, Zn), Macro element accumulation ratio (Ca, K, Mg, P, S) and total accumulation ratio indicate the ratio by which an individual accumulated elements within a treatment compared to how much it accumulated over all treatments.

fewer plants from calcareous soil showed signs of withering ($n = 28$, $\sim 30\%$, $res = -1.196$) than those from siliceous soil ($n = 35$, $\sim 47\%$, $res = 1.341$, see [Figure 3.5, A](#)). A similar trend could be observed between the different treatments where a slight trend towards a higher proportion of withered plants can be observed within the limestone treatment (26, $\sim 46\%$) than in the porphyry (17, $\sim 30\%$) or serpentine (20, $\sim 36\%$) treatment, yet here the differences are not significant. The residuals also suggest a higher amount of withered plants in the limestone treatment ($res = 1.060$) and fewer withered plants in the porphyry ($res = -0.8.98$) and serpentine ($res = -0.164$) treatment than expected although also here the differences are not statistically significant. The analysis of signatures of chlorosis indicates no significant association of substrate of origin and signs of chlorosis as indicated by the Chi-squared test ($p = 0.0974$), Fisher's test ($p = 0.0945$) and the Kruskal-Wallis test ($p = 0.0648$). Plants originating from calcareous bedrock tend to show signs of chlorosis more often with 33 ($\sim 35\%$, $res = 1.213$) showing signs of mild and 3 ($\sim 3\%$) showing signs of severe chlorosis than those from siliceous bedrock where 15 ($\sim 20\%$, $res = -1.359$) showed signs of mild and 3 ($\sim 4\%$) showed signs of severe chlorosis ([Figure 3.5, B](#)). The different treatments are not associated with the occurrence of chlorosis (Chi-squared $p = 0.9934$, Fisher's exact test $p = 0.9854$, Kruskal-Wallis test $p = 0.9022$).

3.4.2 Growth and plant weight influenced by treatment and origin

Mean cushion sizes in April and August, the growth factor (size Aug./size Apr.), as well as mean dry and fresh weight including the water loss factor (fresh/dry weight), are given in [Table 3.4](#). A summary statistic including results Mann-Whitney U test ($\alpha' = 0.00031$), effect sizes and confidence intervals are given in [Table B.5](#) (Appendix). Cushion sizes differed significantly between plants from calcareous and plants from siliceous sites, across all treatments. The plants from calcareous bedrock were on average $\sim 24\%$ bigger in April and $\sim 29\%$ bigger in August than the plants from siliceous bedrock ($\alpha' = 0.00031$, $p < 0.0001$) ([Table 3.4a](#), Appendix [Table B.5](#)). Effect sizes of $\sim 0.19 - 0.48$ indicate a medium-size effect. These differences could not be confirmed within treatments, were differences in mean and median between the two origin groups could be observed but did not yield significant test results (Appendix [Table B.5](#)). Differences in cushion size are also observable between the serpentine treatment and the limestone and porphyry treatment, respectively ($p < 0.0001$, Appendix [Table B.5](#)). The differences are also observable within one substrate of origin between two treatments ([Table 3.4a](#)) with e.g. plants from siliceous bedrock being on average nearly 40 to 50% bigger in the serpentine treatment compared to those in the porphyry treatment. Effect sizes ($r > 0.4$) also indicate a stronger effect between the treatments when compared to the substrate of origins ($r < 0.4$). While sizes differed the growth factor showed no differences, neither between substrates of origins nor between treatment groups. Cushion sizes of all plants increased by $\sim 47\%$ from April to August [Table 3.4a](#). Linear regressions comparing overall micro and macro element accumulation and growth rate indicate only weak predictive power and no statistically significant linear relationships ([Figure B.1](#)). A

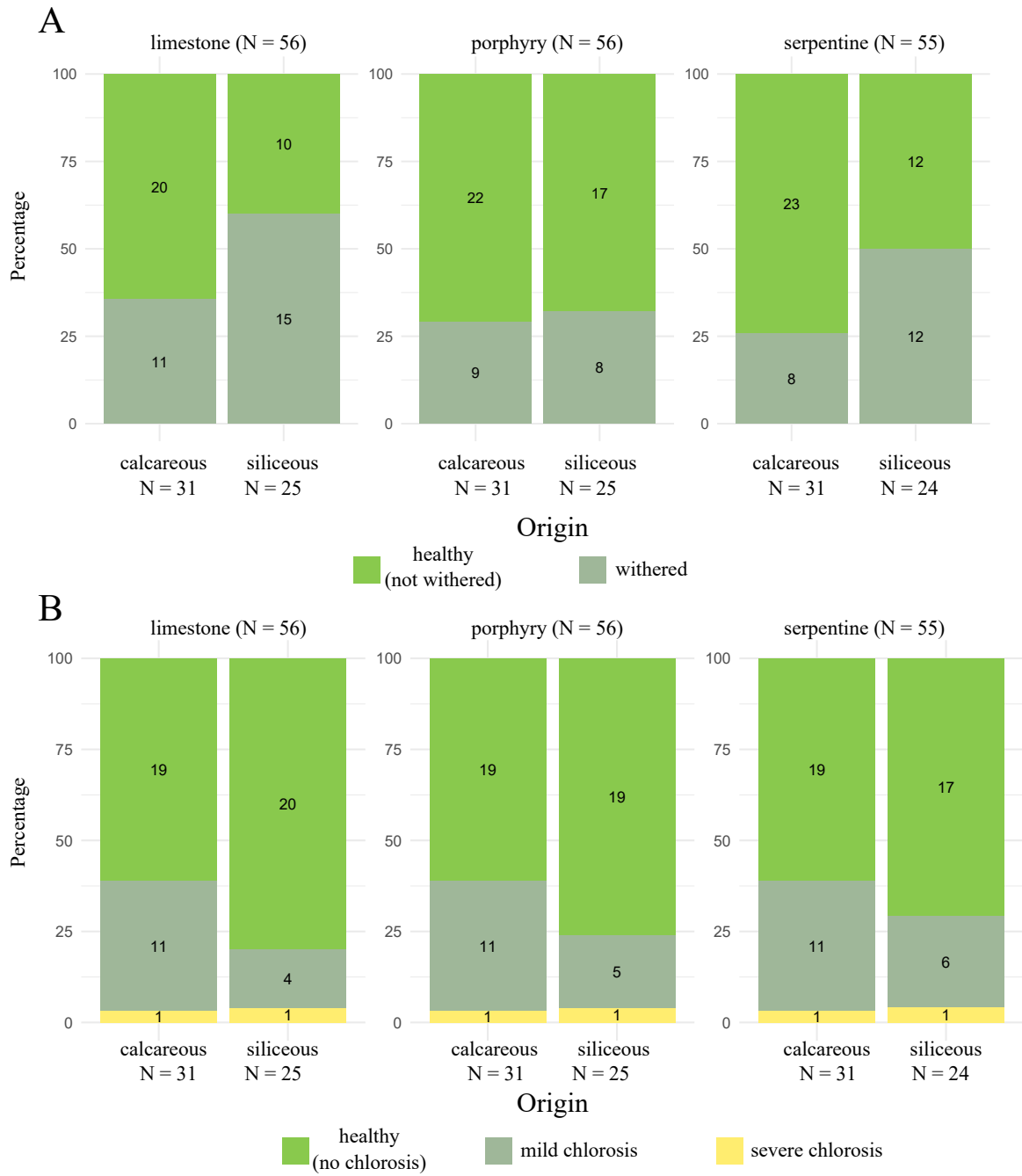


Figure 3.5: Signs of withering and chlorosis based on substrate of origin and treatment group. Numbers indicate the number of plants showing signs of **A** withering, categorized as either healthy or withered and **B** chlorosis categorized as either healthy or showing signatures of mild or severe chlorosis, grouped by treatment and substrate of origin.

more detailed correlation analysis between element accumulation, size, and growth indicates no significant correlation between the growth factor and element accumulation based on the substrate of origin and treatment groups (Table B.6). Plant cushion sizes in April and August show a statistically significant weak to moderate negative correlation to macro and total element accumulation rates ($-0.28 < r < -0.2$, $p < 0.001$) over all plants. This negative correlation can also be observed within the substrate of origin groups across all treatments for macro element accumulation rates. Within the three treatment groups, no correlations of cushion sizes and element accumulation could be observed (Table B.6). Size in August and above-ground plant material weight showed a strong correlation in both fresh ($R^2 = 0.669$, $p < 0.001$) and dry weight ($R^2 = 0.683$, $p < 0.001$) (Figure B.3). The same trends that have been observed for cushion sizes can also be found for fresh and dry weight, where plants from calcareous bedrock are significantly heavier ($\sim 43\%$, fresh weight) than those from siliceous bedrock ($p < 0.0001$, Appendix Table B.5). Plants from the serpentine treatment are also heavier than those from the limestone and porphyry treatments across and within the two substrates of origin groups ($p < 0.0001$, Appendix Table B.5, Figure B.2 and Table 3.4b). The water loss factor indicates no significant differences between the two substrates of origin groups or the three treatment groups (Figure B.2).

3.4.3 Flowering is influenced by treatment and plant origin

Of the 167 plants across all treatments and origins with complete fitness data $\sim 78\%$ flowered starting on April 22nd until June 9th 2013. Across all treatments $\sim 67\%$ of plants from calcareous bedrock sites and $\sim 93\%$ of plants from siliceous bedrock produced flowers (Table 3.5, Figure 3.6 A, flowering detail per individual is given in the Digital Supplement "S_II.1.5-Aufbluehzeiten_Mittelwert_Herkunft_T-Substrat.xlsx"). The association of flowering behavior and plant origin substrate could further be confirmed by a Chi-squared test ($\chi^2 = 38.32$, $p < 0.001$) and Fisher's exact test ($p < 0.001$) both indicating a highly significant relationship. This difference could also be observed within the separate treatments where plants from siliceous bedrock showed higher flowering rates (Table 3.5, Figure 3.6 A). In addition to higher flowering rates plants originating from siliceous bedrock also produced significantly more flowers (Mann-Whitney U test, $\alpha' = 0.00031$, $p < 0.0003$, Appendix Table B.5) than those from calcareous bedrock, yet this observed difference can not be confirmed when only comparing flowering plants (Figure 3.6 B). While the differences in the number of produced flowers of all plants between the two origin groups within each treatment can be observed in median values, the differences are not statistically significant ($p > 0.0003$, Appendix Table B.5). The three treatments did not differ significantly in the number of flowers when taking all plants, flowering and non flowering, into account (Mann-Whitney U test, $\alpha' = 0.00031$, Appendix Table B.5). While a trend towards higher numbers of flowers within the serpentine treatment can be observed including flowering as well as non flowering plants, these differences are deemed statistically not significant ($p > 0.0003$, Appendix Table B.5). Yet they are statistically significant differences when taking only

Table 3.4: Growth behaviour of plants in the experiment, based on origin and treatment groups). a) Mean cushion sizes measured in April and August 2013, b) Mean fresh and dry weight of above ground plant matter harvested at the end of the experiment in 2013.

(a) Mean cushion sizes in April and August 2013 as well as the growth factor (size August/ size April).

origin	treatment	n	mean size April [cm ²]	mean size Aug. [cm ²]	mean growth factor
all	all	167	24.42 ± 9.38	35.92 ± 15.94	1.49 ± 0.39
all	limestone	56	21.16 ± 6.78	32.08 ± 14.12	1.52 ± 0.38
all	porphyry	56	22.41 ± 8.13	32.15 ± 13.39	1.46 ± 0.39
all	serpentine	55	29.80 ± 10.57	43.69 ± 17.43	1.49 ± 0.40
calcareous	all	93	26.67 ± 9.57	39.89 ± 16.85	1.53 ± 0.45
calcareous	limestone	31	23.56 ± 7.65	36.36 ± 16.32	1.55 ± 0.43
calcareous	porphyry	31	24.95 ± 8.14	36.26 ± 13.33	1.51 ± 0.45
calcareous	serpentine	31	31.51 ± 10.90	47.07 ± 18.61	1.53 ± 0.48
siliceous	all	74	21.60 ± 8.38	30.94 ± 13.21	1.44 ± 0.28
siliceous	limestone	25	18.19 ± 3.93	26.78 ± 8.4	1.47 ± 0.31
siliceous	porphyry	25	19.25 ± 7.07	27.05 ± 11.82	1.41 ± 0.30
siliceous	serpentine	24	27.59 ± 9.92	39.32 ± 15.02	1.43 ± 0.25

(b) Mean fresh and dry weight at the end of the Experiment in August 2013, as well as the water loss factor (dry weight/ fresh weight).

origin	treatment	n	mean fresh weight [g]	mean dry weight [g]	mean water loss factor
all	all	167	5.86 ± 2.95	2.24 ± 1.20	2.67 ± 0.46
all	limestone	56	5.09 ± 2.44	1.97 ± 0.97	2.62 ± 0.42
all	porphyry	56	5.13 ± 3.12	1.97 ± 1.24	2.68 ± 0.50
all	serpentine	55	7.39 ± 2.70	2.80 ± 1.19	2.72 ± 0.46
calcareous	all	93	6.76 ± 3.16	2.55 ± 1.32	2.74 ± 0.49
calcareous	limestone	31	5.96 ± 2.81	2.28 ± 1.14	2.67 ± 0.49
calcareous	porphyry	31	5.96 ± 3.49	2.20 ± 1.40	2.82 ± 0.51
calcareous	serpentine	31	8.37 ± 2.56	3.16 ± 1.21	2.74 ± 0.46
siliceous	all	74	4.73 ± 2.22	1.86 ± 0.91	2.59 ± 0.41
siliceous	limestone	25	4.01 ± 1.27	1.58 ± 0.51	2.57 ± 0.31
siliceous	porphyry	25	4.11 ± 2.26	1.67 ± 0.96	2.52 ± 0.43
siliceous	serpentine	24	6.11 ± 2.37	2.34 ± 1.02	2.69 ± 0.47

flowering plants into account (Figure 3.6 C) The linear regression comparing the cushion size in April 2013, at the start of the flowering period, with the number of flowers counted per flowering plant indicates a significant relationship, where bigger cushions produced more flowers ($R^2 = 0.3$, $p < 0.001$, Figure 3.6 D). In contrast, non flowering plants showed a significantly higher growth rate between April and August 2013 (Appendix Figure B.5) that can be observed when considering all plants (Med_{flower}: 1.39 x Med_{non flower}: 1.61, $p < 0.0001$; Mann-Whitney U test with Bonferroni corrected orig. $\alpha = 0.05$, $\alpha' = 0.0023$, see Digital Supplement "S_II.1.6-Stats_flowering_vs_nonflowering.xlsx"), the plants from calcareous bedrock (Med_{flower}: 1.35 x Med_{nonflower}: 1.72, $p < 0.0001$; Mann-Whitney U) and within the serpentine treatment (Med_{flower}: 1.39 x Med_{nonflower}: 1.75, $p = 0.0004$; Mann-Whitney U). A comparison within the group from siliceous bedrock was not possible due to the small number of non flowering plants.

Table 3.5: Flowering frequency overview based on origin bedrock and treatment group. The total number of plants as well as the number and percentage of flowering and non flowering *D. gratianopolitanus* grouped by substrate of origin and treatment is given. The result is also given in Figure 3.6 A

origin substrate	treatment	total number of plants	number of flowering plants	number of non flowering plants
all	all	167	131 (78.4%)	36 (21.6%)
calcareous	all	93	62 (66.7%)	31 (33.3%)
siliceous	all	74	69 (93.24%)	5 (6.8%)
all	limestone	56	42 (75%)	14 (25%)
calcareous	limestone	31	19 (61.3%)	12 (38.7%)
siliceous	limestone	25	23 (92%)	2 (8%)
all	porphyry	56	42 (75%)	14 (25%)
calcareous	porphyry	31	19 (61.3%)	12 (38.7%)
siliceous	porphyry	25	23 (92%)	2 (8%)
all	serpentine	55	47 (85.5%)	8 (14.6%)
calcareous	serpentine	31	24 (77.4%)	7 (22.6%)
siliceous	serpentine	24	23 (95.83%)	1 (4.2%)

In order to compare the elemental composition of flowering and non flowering plants and analyse the possible influence of element composition on flowering over all treatments and origins I calculated a PCA (Appendix Figure B.4). The first two axes account for $\sim 55.23\%$ of variation, but no clear separation of floriferous and non-floriferous plants can be observed. Yet the Fe concentration over all plants, in the plants from calcareous origin as well as within the limestone treatment differed significantly between flowering and non flowering plants (overall Med_{flower}: 29.61 x Med_{nonflower}: 24.57, $p < 0.001$; calcareous Med_{flower}: 30.47 x Med_{nonflower}: 24.25, $p < 0.001$; limestone Med_{flower}: 31.10 x Med_{nonflower}: 23.36, $p < 0.001$; Mann-Whitney U test with Bonferroni corrected orig. $\alpha = 0.05$, $\alpha' = 0.0023$, Digital Supplement "S_II.1.6-Stats_flowering_vs_nonflowering.xlsx"). In addition Mo concentration (overall Med_{flower}: 2.12 x Med_{non flower}: 3.53, $p = 0.001$) and S concentration

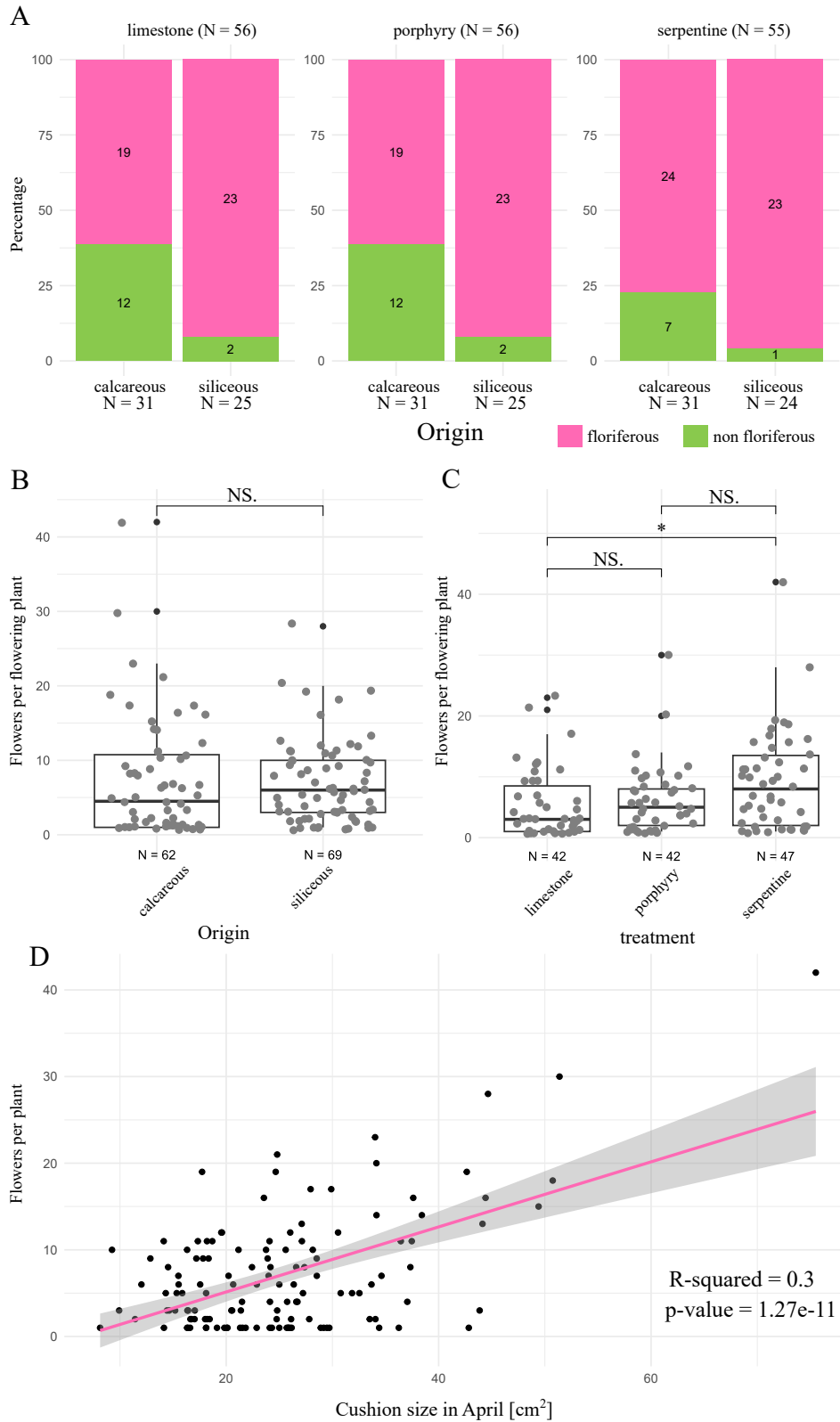


Figure 3.6: Flowering of *D. gratianopolitanus* in the flowering period 2013. A Summary of number of flowering and non flowering plants per origin in each treatment. **B** Number of flowers per flowering plant of calcareous and siliceous origin. **C** Number of flowers per flowering plant in each treatment. **D** Correlation of number of flowers per plant and cushion size at the start of the flowering period in April 2013.

(overall $\text{Med}_{\text{flower}}$: 1626.73 x $\text{Med}_{\text{non flower}}$: 2776.36, $p < 0.001$) differed between all plants. In the porphyry as well as the serpentine treatment no significant differences in element concentration could be observed between the flowering and nonflowering plants. The number of flowers in flowering plants of all origins and treatments showed a weak negative correlation with Mo concentration ($r = -0.234$, $p < 0.007$) Table B.7. In addition the concentration of Ca showed a weak negative correlation with number of flowers in all plants ($r = -0.357$, $p < 0.0001$), in those from calcareous ($r = -0.372$, $p = 0.003$) and siliceous bedrock ($r = -0.354$, $p = 0.003$), while its concentration within each treatment did not correlate with the number of flowers. The concentration of Ni showed a weak positive correlation to the number of flowers within the group from the siliceous bedrock. Within treatment element concentrations did not show a significant correlation with the number of flowers, with the only exception being the Mg concentration within the serpentine treatment indicating a negative correlation ($r = -0.436$, $p = 0.002$). Microelement accumulation rates did not differ significantly between flowering and nonflowering plants (Mann-Whitney U test $\alpha' = 0.0023$, Digital Supplement "S_II.1.6-Stats_flowering_vs_nonflowering.xlsx")

3.5 Comparison of flowering behaviour of *D. gratianopolitanus* cultivated in the Botanical Garden Heidelberg in 2022 and 2023

The half-monthly temperature sum from the nearby weather station (LUBW, Berliner Straße) for the years 2022 and 2023 are given in Figure 3.7. The temperatures from the LUBW were corrected to reflect the frost-free cultivation within the green houses, where temperature data from LUBW was corrected to 4°C for all temperature measurements $> 4^{\circ}\text{C}$. In addition, the half-monthly temperature sum for 2022 measured within the greenhouse is given (see Digital Supplement "S_II.2.1-BoGa_Temp_Messung_2022.xlsx"), with an overall daily mean temperature difference of $\sim 1.3^{\circ}\text{C}$ between in-house measurement and data from the LUBW. In order to compare the flowering behaviour documented during the transplant experiment in 2013 the climate data for the weather station (LUBW, Berliner Straße) in 2023 are included Figure 3.7. While 2022 and 2023 indicate a similar temperature curve for the first half of the year, 2013 is nearly always colder in comparison, only exceeding the temperatures from 2022 and 2023 in the second half of March and in July.

The flowering frequencies of *D. gratianopolitanus* and *D. gratianopolitanus* subsp. *mora-vicus* originating from different geographical regions for the years 2022 and 2023 differ with the flowering starting on April 9th in 2022 and April 13th in 2023 (Figure 3.8, Appendix Table B.8 and Digital Supplement "S_II.2.2-Dianthus_Blütendoku_2022.xlsx" and "S_II.2.3-Dianthus_Blütendoku_2023.xlsx"). *D. gratianopolitanus* from all regions started to flower within 17 days in 2022 and 21 days in 2023. The first to flower in both years were Cheddar Pink from Central Germany while those from the United Kingdom flowered at the latest in 2022, and those from Switzerland flowered latest in 2023. The Swiss group, French

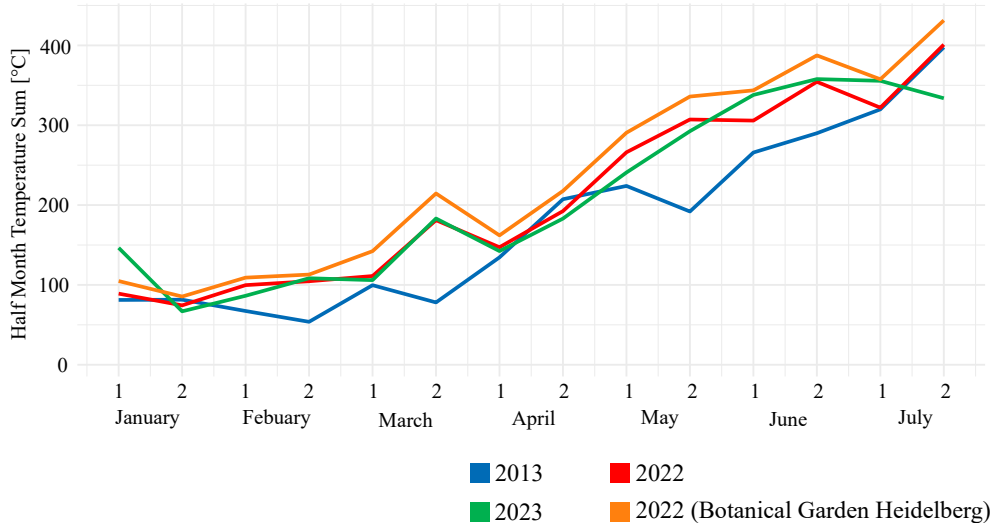


Figure 3.7: *Half monthly temperature sum for the years 2013, 2022 and 2023 as well as in green house data for 2022.* The half-monthly sum for the crucial months during spring and early summer documented at the weather station at Berliner Straße (LUBW) as well as in house temperature is given. Due to the frost-free cultivation within the green houses, the data from LUBW was corrected to 4°C for all temperature measurements > 4°C.

Diois, French Jura, and those from the Swabian Alb started to flower at the same time in 2022 and within eleven days in 2023. The *D. gratianopolitanus* from the French Massif Central showed an early flowering onset in 2022 but started to flower next to the latest in 2023. *D. gratianopolitanus* subsp. *moravicus*' flowering onset in 2022 is comparable to the *D. gratianopolitanus* from the Czech Republic. Maximum flowering, as the date when most plants per region flowered, reached its maximum at the beginning or mid of May. Flowering ended at the start of the middle of June. The within-region variation of flowering start reaches up to 34 days (Central Germany 2022) or 43 days (Central Germany 2023)(Figure 3.9). The differences in flowering start in 2022 and 2023 per region as well as per substrate of origin, are not statistically significant (pairwise Wilcoxon test, Bonferroni corrected, $p < 0.01$).

Flowering and growth behavior per region and year is given in Figure 3.10 and Figure 3.11. The Chi-squared test analyzing the relationship of flowering behavior (given as categories 1-5) and region indicates a significant relationship for both analyzed years (2022 $\chi^2(36, N = 286) = 67.06108, p < 0.01$; 2023 $\chi^2(36, N = 269) = 65.76081, p < 0.01$). The French regions showed varying signals in 2022 with the Massif Central being missing in the highest category ($res = -1.446$) with otherwise only minor differences to the expected values, and the French Jura being slightly overrepresented in the highest category 5 ($res = 3.480$). In 2023 this trend towards a higher number of flowers was not observed in the French Jura. In 2023, the Swiss plants were slightly overrepresented in the lowest categories (category 1, $res = 0.539$; category 2, $res = 2.056$), but under-represented in the mid-level category 3($res = -1.502$) and the higher category (category 4, $res = -1.267$),

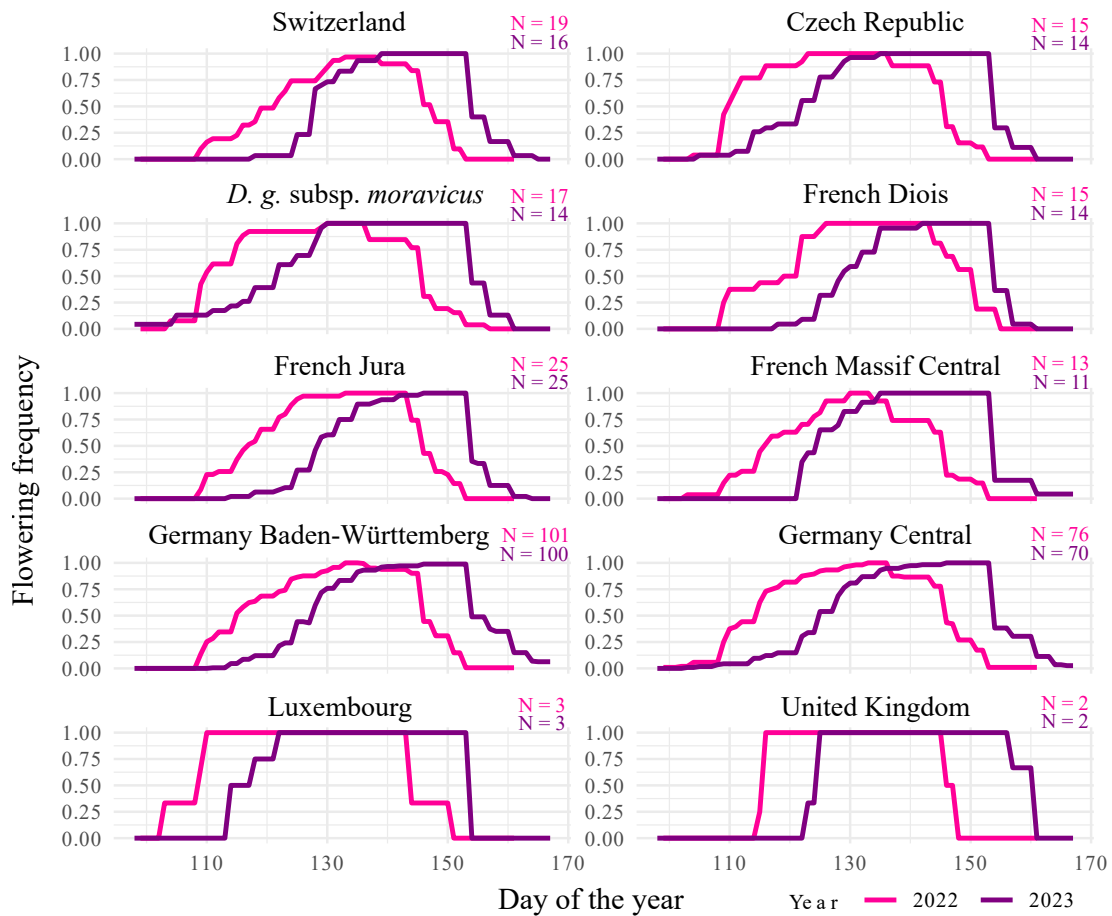


Figure 3.8: Flowering frequency of *D. gratianopolitanus* per region in 2022 and 2023. The flowering frequency (percentage of flowering plants per region) of Cheddar Pink cultivated in the Botanical Garden in Heidelberg grouped by origin region as well as *D. gratianopolitanus* subsp. *moravicus* plants is given at the corresponding day of the year. Overall flowering started on the 9th April in 2022 (99th day of the year) and on the 13th April 2023 (103rd day of the year) and reached its peak on the 13rd May 2022 and 26th May 2023, respectively. The regions of Luxembourg and the United Kingdom are represented by only 3 (LU) and 2 (UK) plants, hindering a meaningful results but still indicating the same overall trend. A detailed overview is given in the Appendix [Table B.8](#).

while the distribution in 2022 did not differ much from the expected values. In 2022 plants from Baden-Württemberg were slightly overrepresented in the mid-level flowering category (category 3, residual $res = 2.396$) and an under-representation in the highest categories (category 4, residual $res = -1.314$; category 5, residual $res = -2.790$). In 2023, it is slightly over-represented in category 5 ($res = 1.457$), although here the overall expected plants per regions are < 1 leading to a high weighting of each single plant. While in 2022 the Central German group deviates from the expected values mainly in the under-representation in low flowering plants (category 1, $res = -1.516$), it is overrepresented in this category in 2023 (category 1, $res = 1.508$). The Czech group showed an over-representation in category 5 in

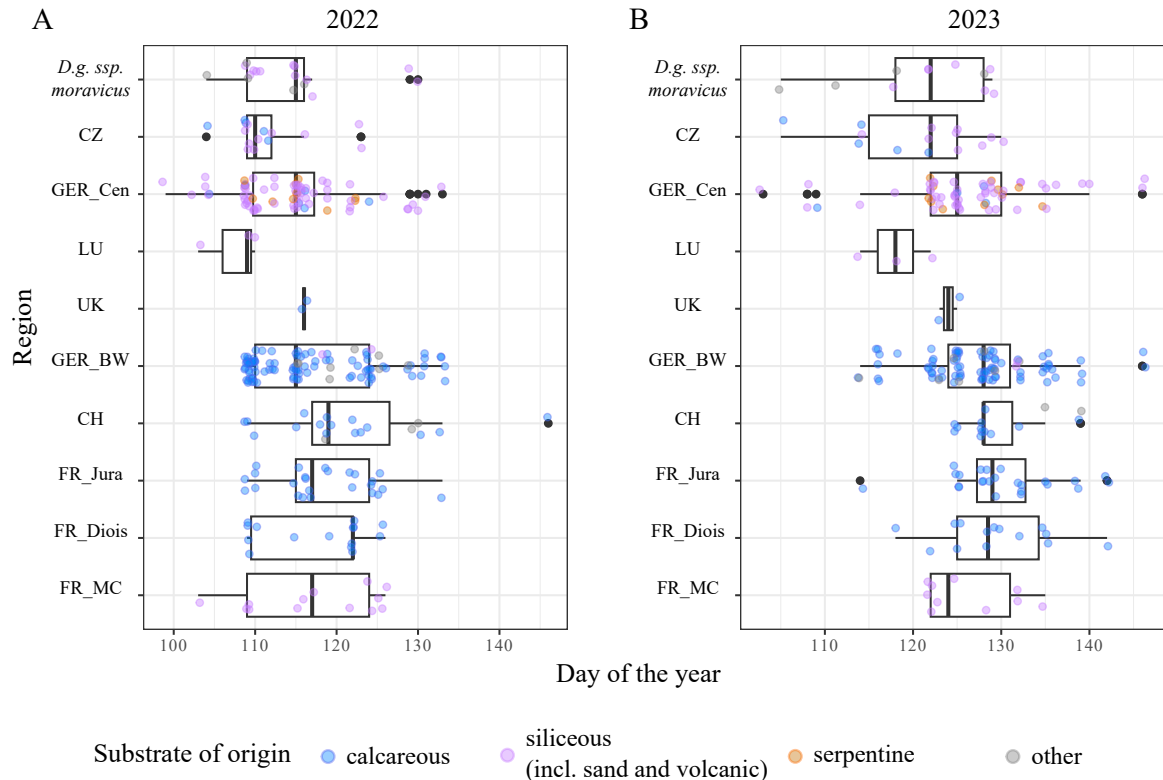


Figure 3.9: Flowering start of *D.gratianopolitanus* per region in 2022 and 2023. The flowering start was scored for each individual cultivated in the Botanical Garden in Heidelberg during the flowering period in 2022 and 2023. Points indicate individual start of flowering, with the color indicating the origin substrate of the plant. The variation of within region starting date varies for up to 34 days in 2022 and 43 days in 2023 (e.g. in Central Germany) and no significant differences between regions and substrates were found.

2022 ($res = 1.666$) and in category 4 in 2023 ($res = 3.033$). While in 2022 *D. gratianopolitanus* subsp. *moravicus* shows a slight over-representation in the highest category (category 5, residual $res = 1.975$), the distribution for 2023 is more evenly with only minor deviation from the expected values.

Analyzing the relationship of cushion size and the region also indicates a significant relationship for both analyzed years using a Chi-squared test (2022 $\chi^2(18, N = 286) = 76.3300, p < 0.001$; 2023 $\chi^2(18, N = 269) = 76.94785, p < 0.001$). The French regions showed an over-representation in smaller and medium-sized cushion sizes but were under-represented in the number of large cushion sizes in 2022 (e.g. French Jura, S: $res = 1.391$, L: $res = -0.659$; Diois, M: $res = 1.078$, L: $res = -2.612$). The same trend is also observable for 2023 (e.g. French Jura, S: $res = 1.378$, L: $res = -1.780$). While the Swiss plants showed an even distribution in 2022, they were slightly overrepresented in the medium category and under-represented in the small and large category in 2023 (S: $res = -1.025$, M: $res = 1.761$, L: $res = -1.245$). In 2022 plants from Baden-Württemberg were under-represented in the small and medium cushion size levels and showed an over-representation in the largest

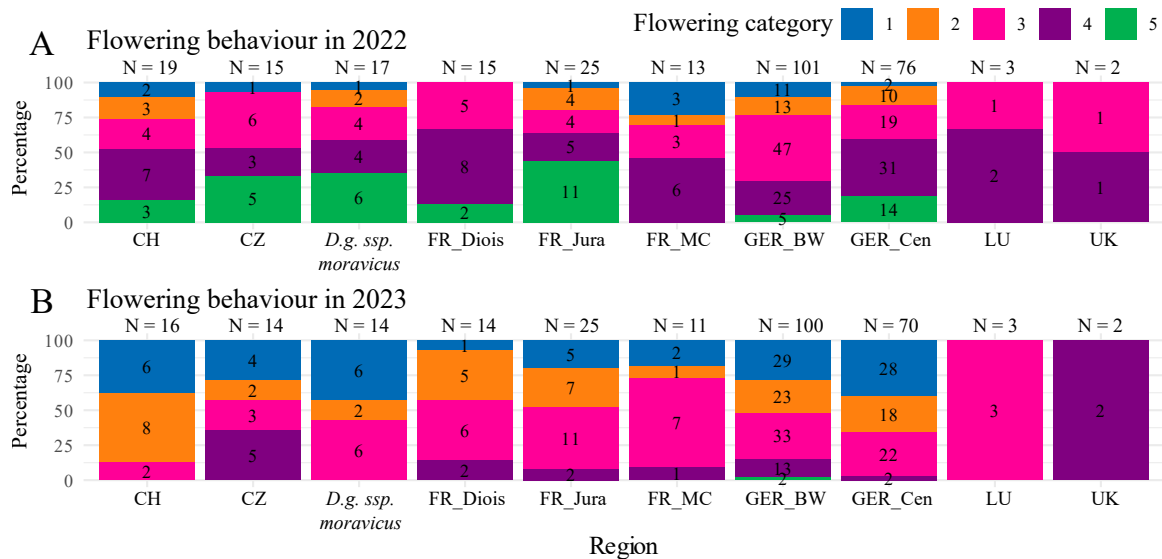


Figure 3.10: Categorical number of flowers per region. The flowering categories range from 1 - indicating only few flowers to 5 with exceptional high number of flowers. The numbers in each stacked barplot segment indicate the number of individuals in each category. The change in flowering between the years 2022 and 2023 is influenced by horticultural measures in fall 2022.

category (S: $res = -2.402$, M: $res = -2.752$, L: $res = 3.053$). This trend is even stronger in 2023 (S: $res = -2.623$, M: $res = -2.280$, L: $res = 4.236$). Plants from Central Germany showed a tendency to smaller cushion sizes in 2022 (S: $res = 1.659$, L: $res = -1.673$) and 2023 (S: $res = 3.007$, L: $res = -2.046$). The Czech group showed an under-representation in small cushions in 2022 (S: $res = -1.275$) and in 2023 (S: $res = -1.530$). *D. gratianopolitanus* subsp. *moravicus* shows a trend towards larger cushions in 2022 (S: $res = -1.357$, M: $res = -1.865$, L: $res = 1.952$) and also indicated an slight under-representation in small cushions in 2023 (S: $res = -0.877$).

To set the number of produced flowers in context with cushion sizes a Chi-squared test as well as linear regression was calculated (Figure 3.12 and Appendix Figure B.6). The Chi-squared test shows a statistically significant relationship (2022 $\chi^2(8, N = 286) = 18.46388, p < 0.05$; 2023 $\chi^2(8, N = 269) = 22.2982, p < 0.01$). In 2022 the low flowering plants were overrepresented in the small cushion sizes (category 1, S: $res = 1.805$, M: $res = -1.383$; category 2, S: $res = 2.339$), and in 2023 this can also be observed for category 1 (category 1, S: $res = 2.839$, M: $res = -1.606$). Higher flowering categories are missing from the small cushion sizes in 2022 (category 5, S: $res = -1.785$) and 2023 (category 4, S: $res = -2.125$), but are overrepresented in bigger cushion sizes in both 2022 (category 5, M: $res = 1.238$) and 2023 (category 4, L: $res = 1.488$). This trend is also observable in the linear regression in Appendix Figure B.6 where a slight increase in the flowering category with higher cushion sizes can be observed but did not yield high explanatory power and p-values for 2022 (adj. R-squared = 0.009, $p = 0.061$) and 2023 (adj. R-squared = 0.05,

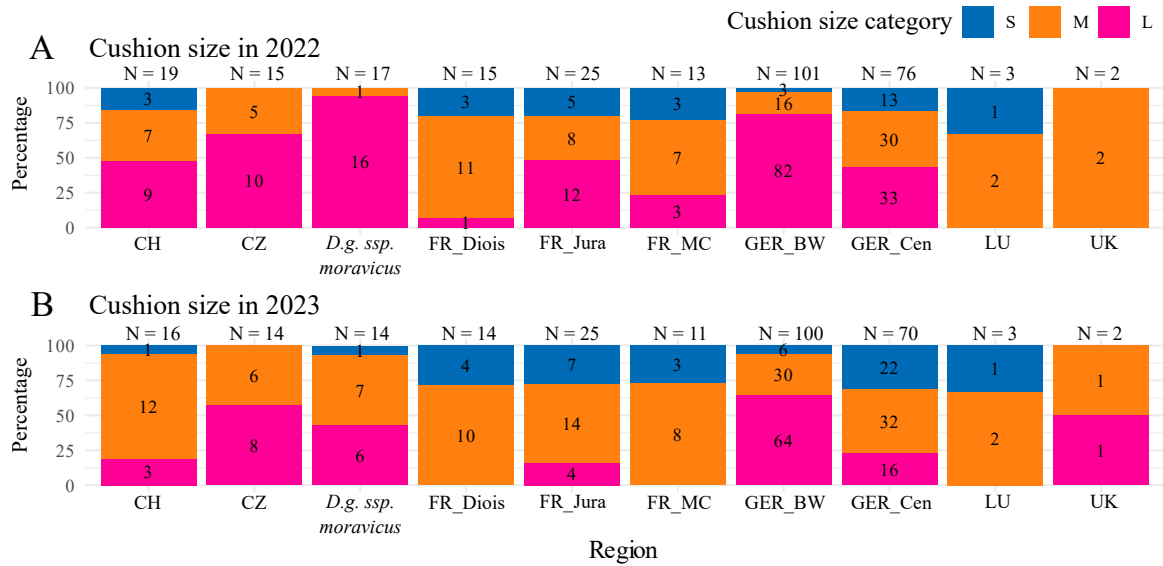


Figure 3.11: Categorical cushion size per region. The cushion size categories range from S indicating a small cushion to L indicating cushions that reach over the pot edges. The numbers in each stacked barplot segment indicate the number of individuals in each category. The change in cushion size between the years 2022 and 2023 is influenced by horticultural measures in fall 2022.

$p < 0.01$).

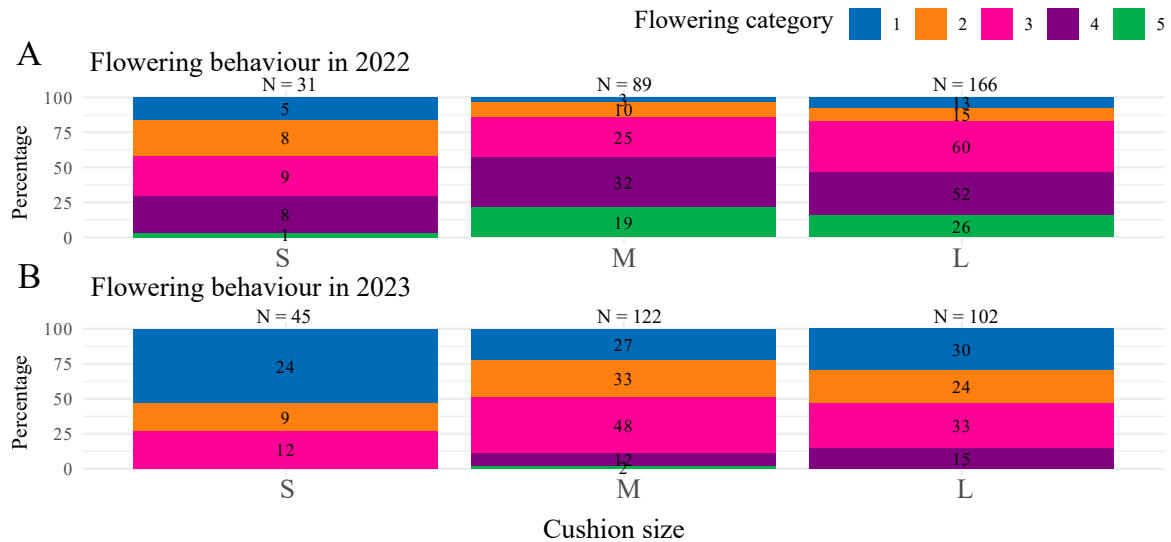


Figure 3.12: Categorical number of flowers per cushion size. The flowering categories range from 1 - indicating only few flowers to 5 with exceptional high number of flowers and the cushion size categories range from S indicating a small cushion to L indicating cushions that reach over the pot edges. The numbers in each stacked barplot segment indicate the number of individuals in each category.

Plants included in the transplant experiment 2013 were grouped by home bedrock and

the corresponding substrate treatment, calcareous (N = 31 plants) siliceous (N = 26). The used accessions and replicates were subsetting for the flowering data from 2022 (N = 89) and 2023 (N = 93). The plants were also grouped by bedrock of origin and only one set of replicates was analysed resulting in 30 plants from the calcareous and 26 for the siliceous group. A comparison of flowering time between the years is given in [Figure 3.13](#). Differences between genetic replicates in 2022 and 2023 were checked ([Appendix Figure B.7](#)). The start of flowering for the year 2013 was May 5th and April 27th, for the siliceous and calcareous groups, respectively. They reached their maximum flowering on June 3rd. In comparison flowering in 2022 started at April 19th (siliceous April 14th) and reached its maximum at May 13th, flowering in 2023 started at April 24th with the maximum reached at May 19th (calcareous May 16th).

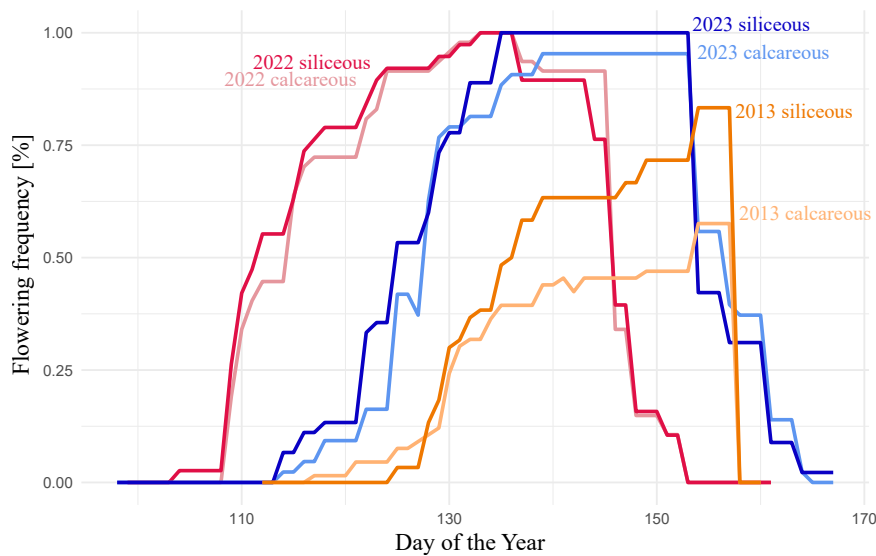


Figure 3.13: Flowering time comparison 2013, 2022 and 2023 for plants from calcareous and siliceous bedrock. Plants from the transplant experiment 2013 were extracted from the years 2022 and 2023. Plants from 2013 were grouped by home bedrock and the corresponding home substrate treatment.

To analyze the effect of temperature variation between years the cumulative temperature sums of mean daily temperatures were calculated for the three years starting at the date of peak flowering counting backward to the start of the year [Figure 3.14](#). While the sums for 2022 and 2023 have a parallel curve, 2013 and 2023 cross at $\sim 825^{\circ}\text{C}$ at March 25th.

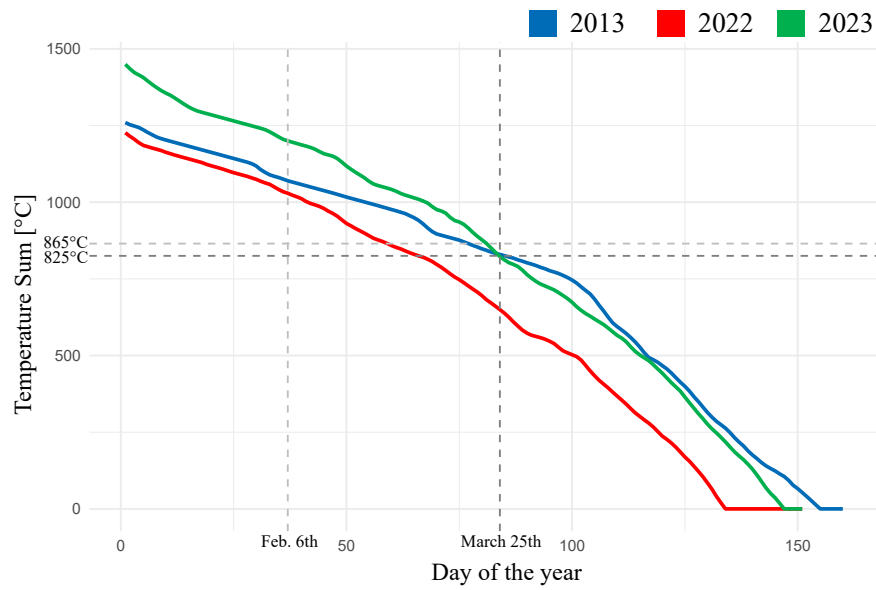


Figure 3.14: Cumulative temperature sum between start of the year and maximum flowering of *D. gratianopolitanus*. Maximum flowering was taken from [Figure 3.13](#) and the 4°C corrected climate data from the weather station at Berliner Straße was used for calculations. The cumulative sum of mean daily temperature values was calculated and plotted for 2013, 2022 and 2023. The in [Koch et al. \(2021\)](#) observed convergence at a temperature sum of 865°C the therein resulting starting date, February 6th, as well as the in my study observed temperature sum of 825°C at the convergence of the lines from 2013 and 2023 and corresponding date, March 25th, are indicated by dashed lines.

4 | Discussion

Differences in bedrock types influence and shape the local vegetation and are a major determinant of plant distribution. Adaptations to the local edaphic and climatic conditions can lead to physiologically distinct groups or even species. Herein I analyzed the influence of three treatment substrates on *D. gratianopolitanus* from calcareous and siliceous bedrock, revealing possible adaptations of the two groups to their home substrate as well as their plasticity in dealing with foreign conditions. In addition flowering behaviour in the years 2022 and 2023 were compared for plants from different geographical regions.

Three treatment soils show distinct elemental composition The used treatment substrates showed overall neutral to slightly alkaline pH values (Table 3.1), differing from the expected slightly acidic and alkaline reaction reported for siliceous and calcareous bedrocks (Kinzel, 1983). In addition, the elemental composition indicated deviations from typical calcareous and siliceous bedrock, with higher Fe content in the limestone treatment as well as higher Ca content in the porphyry treatment, due to the used triassic shell limestone with higher levels of Fe content and secondary incorporations of CaCO₃ within the used rhyolite. The serpentine shows the expected higher Ni content and a low Ca:Mg ratio (Brady et al., 2005). Due to missing analytical lines, the overall element composition of the three treatments is missing information but yielded enough to show the separation in elemental content of the three treatment soils. Moreover one has to keep in mind the variety of soils and bedrock summarised under the name "siliceous" all characterized by high silica (SiO₂) content. Nevertheless, conditions on granite, volcanic rhyolite, argillite, sandstone, and quartz sand still contribute to differing conditions. Igneous substrates for example can include variable proportions of minerals and other constituents and can provide acidic to highly alkaline pH conditions (Jenny, 1994). In addition, the inhabited cliffs and rocky outcrops are subjected to higher degrees of erosion and provide a very heterogeneous habitat themselves (Larson et al., 2000).

No strong signal for home effect in elemental composition based on origin substrate but clear differences between treatment groups Plants originating from calcareous bedrock showed higher leaf elemental concentrations of Mo, and S over all treatments as well as within the limestone and serpentine treatment while no differences could be observed in the porphyry treatment (Appendix Table B.2, Table B.3). These higher

concentrations of Mo and S could indicate a higher efficiency or upregulation of the sulfate transporter, that due to the similarity between molybdate and sulfate ions, would lead to higher accumulation of both S and Mo (Harvey et al., 2024). Yet these differences could not influence the micro and macro element accumulation rates and did not lead to a group distinction in the PCA, in each treatment, and in the overall analysis (Figure 3.2, Figure 3.3). Nevertheless, the differences in element accumulation observed in the calcareous plants indicate that present-day *D. gratianopolitanus* from calcareous and siliceous bedrock are indeed forming two distinct groups. Keeping the genetic background (See Part I) in mind these coincide with a genetic division. The origin of the Baden-Württemberg populations could either indicate old refugia in Baden-Württemberg with plants surviving the Pleistocene on calcareous bedrock or could indicate a colonization involving the northern siliceous populations. In this case, the Baden-Württemberg plants, although living on and adapting to the calcareous bedrock, could have retained their ability to live on siliceous soil. Siliceous substrates provide high small-scale as well as large-scale heterogeneity in physical and chemical properties. To survive and thrive under these conditions the populations either need to adapt to or be indifferent to these conditions. *D. gratianopolitanus* forms larger populations in the siliceous area than in the calcareous area (Personal communication, Marcus A. Koch, August 2024). Larger population sizes and higher genetic diversity can facilitate the adaptation to heterogeneous conditions (Kawecki and Ebert, 2004; Leimu and Fischer, 2008). In addition, polyploidy can help with adaptations and expansion of ecological niches due to the duplicated gene copies that can assume new or varied functions, while also posing disadvantages due to e.g. the increased complexity of chromosome pairing and segregation during meiosis and mitosis (Madlung, 2013). This higher variability and adaptation potential within the siliceous range could also have allowed the initial migration to the calcareous substrate. Yet such fine-scale local adaptations can not be properly assessed with the herein used setup, where a finer grouping by home conditions, and higher number of samples per population would have been needed, swamping a possible home effect indicating adaptations from siliceous plants to the porphyry treatment.

While the chemical differences between the origin bedrock groups were only minor, clear differences between each treatment could be observed. Plants from the limestone treatment showed the highest concentration of Ca that, while significantly larger than the concentrations in the serpentine treatment, did not differ significantly from those from the porphyry treatment. High Ca concentration can also lead to an impairment of cell signaling due to high Ca^{2+} in the cytosol (Bothe, 2015). Plants from calcareous bedrock often contain higher amount of free Ca^{2+} in the cytosol while plants from acidic soil often precipitate the excessive Ca as calcium oxalate. This strategy is also known for *D. lumnitzeri* that, while growing on limestone, also precipitates the surplus Ca as calcium oxalate (Bothe, 2015). While the plants from calcareous bedrock are familiar with high Ca concentrations, plants from siliceous bedrock are not necessarily adapted to high Ca concentrations. Yet no significant difference in Ca was observed between plants from calcareous and siliceous bedrock in the limestone treatment. The handling of higher Ca concentrations is not due

to local adaptations made in the calcareous area but seems to be a general capability of *D. gratianopolitanus*. As discussed earlier, the used rhyolite indeed showed high Ca content in total and as well as plant available concentrations. Including the comparable pH values observed in the limestone and porphyry treatment, this leads to similar conditions in these normally differing parameters, leading to similar Ca leaf concentrations in the limestone and porphyry treatment.

On the other hand, the higher plant-available micro elements in the porphyry treatment are also shown in their higher accumulation rate in the porphyry treatment compared to the other treatments. P concentrations were lowest within the limestone treatment, a trend that can naturally be observed in calcareous and karst regions where CaCO_3 can reduce P solubility by producing Ca phosphates and therefore limiting available P (Jiang et al., 2020).

Plants grown in the serpentine treatment soil showed, as expected, higher concentrations of Mg and Ni as well as lower amounts of Ca when compared to the other treatments. The median Ni concentration of $\sim 24\mu\text{g/g}$ does indicate a higher accumulation and possible tolerance but no hyperaccumulator capabilities of *D. gratianopolitanus* ($> 1000\mu\text{g/g}$, (Brady et al., 2005)). The Ca:Mg ratio affects plant growth, where high levels of one ion can affect the uptake of the other. The typical low ratios in serpentine substrates are attributed as one of the main stress factors of the serpentine syndrome and Loew (1901) stated that a ratio >1 is needed for optimal growth (Brady et al., 2005). Plants from calcareous bedrock faced high Ca abundance in their home substrate, and although they accumulated less Ca than plants from siliceous bedrock within the serpentine treatment, this difference was not statistically significant, indicating no clear adaptation targeting Ca uptake.

In addition, plants from the serpentine treatment also showed lower levels of total and macro element accumulation ratios when compared to the other treatments, which would also suggest worse growth and fitness rates within the serpentine treatment.

Cheddar Pink from calcareous bedrock formed bigger cushions while those from siliceous bedrock showed a higher flowering rate The basic demands of plants regarding element and water availability were met in all treatments, with no significant differences in signs of chlorosis between treatments or origins (Figure 3.5). Nevertheless, an overall marginally significant trend towards less withering in plants from calcareous bedrock as well as a non-significant trend to slightly higher rates in limestone treatment could be observed. This could indicate a small adaptation in plants from calcareous bedrock to the often drier conditions on the home calcareous bedrock that is more prone to low water retention capabilities (Jiang et al., 2020). While the limestone treatment could also be affected by these drier conditions leading to more signs of withering, this should also be observed in the serpentine treatment, which is also known for its drought in serpentine habitats (Brady et al., 2005). In contrast, the water loss factor did not differ between origins or treatment, indicating no deficiency in water supply in plants from siliceous bedrock, or on the other hand no adaptation of calcareous plants that would lead to a better water supply.

In addition, plants from calcareous bedrock formed bigger cushions in April that persisted

until the end of the experiment, indicated also by the bigger fresh weight of above-ground material (Appendix Table B.5). Indeed equal growth rates from April to August between plants from different origins and within treatments suggest that differences in cushion sizes are due to first-year growth. This high investment into forming big cushions early on could indeed be an adaptation to compete with other plants for space in the very space-limited habitat on rocky outcrops. In addition, this could also allow for easier reproduction via shoots, skipping the vulnerable seedling phase. The tendency towards higher investment in vegetative growth could also be observed in the flowering comparison from 2022 and 2023, where plants from Baden-Württemberg show an over-representation in the number of big cushion sizes while those from Central Germany were smaller. But in contrast, plants from southern France, while growing on calcareous bedrock did not show a higher number of bigger cushions while plants from the Czech Republic and *D. gratianopolitanus* subsp. *moravicus* revealed a trend towards bigger cushions. This indicates a more complex connection that needs further insight, but could reflect the differences in the three gene pools observed in this work.

On the other hand plants from siliceous bedrock showed a higher flowering rate than those from calcareous bedrock (Figure 3.6). A trend towards higher number of flowers could be observed for 2022 and 2023 where plants from Baden-Württemberg showed medium flower numbers in 2022 while those from Central Germany and the Czech Republic showed an increased number of flowers. While the calcareous Cheddar Pink grows bigger cushions to compete with their surrounding vegetation on the rocky outcrops, this increase in flowering together with the bigger *D. gratianopolitanus* populations observed on siliceous bedrock could also be the result of local adaptation, where the higher flowering allows for a higher gene flow within the population. The higher numbers of produced seeds could facilitate the colonization of the often more open habitats (Personal communication, Marcus A. Koch, August 2024).

A positive correlation between the cushion size of flowering plants and the number of flowers was observed in the transplant experiment and confirmed in 2022 and 2023. Non-flowering plants showed increased growth between April and August.

An increased flowering rate does not necessarily reflect a genetic adaptation and enhanced fitness. In addition, the increased flowering could also be a response to stress factors like poor nutrition or drought (Takeno, 2016). Especially the serpentine treatment, a condition that can be classified as foreign to the plants from siliceous and calcareous bedrock, provides harsh conditions, that are characterized by e.g. a low Ca:Mg ratio and drought (Brady et al., 2005). Indeed as described earlier, plants grown under the serpentine conditions show overall lower total and macro element accumulation rates when compared to other treatments with significantly higher concentrations of Ni and Mg, indicating a poorer supply of essential elements and overall poorer nutrition status, that could have induced flowering. Mg concentration in particular shows a negative correlation with the number of flowers within the serpentine treatment. In contrast to this are the increased cushion sizes and weight both during the flowering phase in April but also at the end of the experiment

contradicting an overall malnutrition of the plants.

The flower morphology of *D. gratianopolitanus* showed a high variation in the cultivated individuals in the Botanical Garden in Heidelberg (Figure B.8), with differences in colors and color patterns, petal forms and in the degree of frilled or pinked margins. These parameters could also show different expressions within a metapopulation, posing an interesting future research topic.

The flowering period is unaffected by substrate of origin but shifts with changing temperatures. In this study, I compared the flowering of the plants included in the transplant experiment 2013 with plants cultivated in the Botanical Garden from all over the distribution range of *D. gratianopolitanus*. To minimize substrate effects in 2013 only calcareous plants grown on limestone and siliceous plants grown in the porphyry treatment were used and flowering time was compared. While in 2013 the plants from calcareous bedrock started to flower nine days before those from siliceous bedrock, the large variation within each group as well as the similar starting date of both groups observed in 2022 and 2023 suggest no differences based on the plants substrate of origin (Figure 3.13). The differences in flowering behavior observed between the siliceous and calcareous group in the transplant experiment is therefore not influenced by differences in the flowering period due to the plants origin. Koch et al. (2021) analysed flowering behaviour of *D. gratianopolitanus* from the Baden-Württemberg metapopulations from Lenninger Tal and Eselsburger Tal and could show a shift of three weeks between 2016 and 2018. Between 2013 and 2022 a total shift of 13 days was observed, with one individual in 2022 flowering five days before the rest exacerbating the shift. The later flowering in 2023 compared to 2022 despite similar mean temperatures is an artefact that can be explained by reduction, propagation, and repotting in Autumn 2022. At the start of the vegetation period in 2023 plants first invested in vegetative growth to reach sufficient sizes for flowering before producing flowers that lead to a delay in maximum flowering of 3 to six days in 2023. The flowering time observed in 2023 should therefore be handled with caution. On the other hand, while the maximum flowering period lasted only 4 days in 2022 it lasted for 15 in 2023, indicating either greater variation in individual flowering time in 2022 or shorter flowering times per individual in 2022. Plants from Central Germany started flowering earliest in both years although also here the time from the first plant opening a flower to the last plant started flowering (reaching maximum flowering) was 34 days in 2022 indicating a high plasticity within the region. The fact that all regions showed similar flowering times under the same climatic conditions further indicates that accumulated temperature sum is more important than genetic background for the triggering of flowering. Indeed flowering data from Lenninger and Eselsburger Tal from Koch et al. (2021) indicated that with an accumulated temperature sum of 865°C the starting point coincided with the start of the vegetative growth on February 6th. While the similar mean temperature sum curves for 2022 and 2023 with delayed flowering in 2023 did not lead to convergence, 2013 and 2023 converge at March 25th with a total accumulated temperature sum of 825°C. Due to the observed artefact resulting in delayed flowering in

2023 this convergence is unreliable and should be handled with caution. The cumulative temperature sum of 2013 and 2022 could converge dating back to winter 2021 reaching a total temperature sum of approximately 1250°C. The previously proposed sum of 865°C was reached on February 28th 2022 and March 22th 2023 reducing the period to accumulate the sum from the proposed 80 (2018, peak flowering 26-28th April) or 95 (2016, peak flowering 12-17th May) to 75 days (2022) and 59 days (2023). The fact that the overall flowering period, including start and peak flowering, did only differ by e.g. 9 days earlier peak flowering in 2022 when compared to 2018 or even a delay of 2 to 7 days comparing peak flowering in 2023 and 2016, suggests that temperature sum alone is not enough to trigger flowering. Other factors like the photoperiod also have a strong effect on the flowering behavior (Perrella et al., 2020).

Colonization of serpentine habitat in Wojaleite from siliceous bedrock Besides the chemical properties like low Ca levels, low Ca:Mg ratios, higher levels of heavy metals like Fe, Ni, Cr, or Co, and often a deficiency in important nutrients like P, K, or N, and physical conditions like little moisture make serpentine soils inhospitable for many plants (Brady et al., 2005). The often sparse vegetation cover increases soil temperature and further exacerbates the problem (Kruckeberg, 2002). Vegetation of serpentine sites often shows a high rate of endemics and distinct vegetation types that differ from neighboring sites. Serpentine tolerant species often show adaptations to drought stress like xeromorphic foliage and often show more developed root systems when grown on serpentine soil (Brady et al., 2005). Two common scenarios are discussed in the context of the colonization of the harsh serpentine environment: preadaptation and cross-tolerance (Brady et al., 2005). On one hand, certain individuals can be preadapted to one or more stress factors encountered on serpentine soils, by natural selection serpentine tolerant offspring would survive leading to an accumulation of serpentine tolerance alleles, while on the other hand adaptation to stress factors could have occurred in another habitat but prove to be useful for the colonization of serpentine soils, like adaptations to drought stress or to high Mg concentrations as observed in some maritime-adapted species (Brady et al., 2005). Westerbergh and Saura (1992) showed that *Silene dioica* (L.) Clairv. (Caryophyllaceae) can grow and survive on serpentine soil and tolerate high Ni concentrations whether they are from a serpentine or non-serpentine population indicating an inherent serpentine tolerance. The fact that *D. gratianopolitanus* from calcareous and siliceous origin could grow on serpentine soil also indicates an inherent serpentine tolerance as observed in *Silene dioica* and not due to specific adaptations and selection. Here no difference in fitness parameters of one of the group that could be attributed to previous adaptation was observed. The so-called refuge model also discusses the idea that for many cases of apparent substrate specificity, it is unclear whether the species restricted to certain substrates are truly adapted to those environments or if these apparent endemics are actually generalist species that are confined to particular substrates due to competitive exclusion from more favorable ones (Gankin and Major, 1964; Moore and Kadereit, 2013). *D. gratianopolitanus* which is generally seen as less competitive could have colonized the open

serpentine sites due to its inherent tolerance forming the now big and vital populations, without facing the high competition prevalent in its normal habitat. The adaptation to the drought stress experienced on calcareous bedrock could also provide a cross-tolerance facilitating this colonization. Indeed the colonization of serpentine soil originating from calcareous soils is described for members of the Alysseae tribe (Brassicaceae) (Cecchi et al., 2010) or for *Minuartia* L. (Caryophyllaceae) (Moore and Kadereit, 2013). On the other hand, the geographical location of the serpentine Cheddar Pink habitat "Wojaleite" suggests a colonization originating from the silicate group, and is further supported by the genetic assignment of Wojaleite individuals to the siliceous cluster (see Part I). I could not find clear evidence of a colonization of serpentine soil originating from siliceous soil, yet a possible preadaptation to serpentine conditions, was found in *Phacelia dubia* var. *georgiana* McVaugh an endemic inhabiting granite outcrops, in the form of tolerance to a low Ca:Mg ratio, a (Taylor and Levy, 2002).

While *D. gratianopolitanus* is no serpentine endemic the phenomenon can be found various times over the genus *Dianthus* (e.g. *Dianthus armeria* L., *Dianthus cruentus* Grisb., *Dianthus corymbosus* Sm. and *Dianthus gracilis* Sm (Pavlova et al., 2003)) further highlighting their capability to colonize harsh environments.

Summary and Outlook The Cheddar Pink from calcareous and siliceous bedrock form distinct groups that indicate adaptations to their home conditions. While differences in elemental uptake did only show small differences an adaptation in growth and flowering strategies is shown. The plants from calcareous bedrock invested more in vegetative growth, possibly facilitating vegetative reproduction and leading to higher competitiveness for space on the spatially restricted limestone outcrops, and plants with siliceous origin showed higher flowering rates and flower production allowing more gene flow and faster colonization of the more open habitats. While a shift towards earlier flowering between 2013 and 2022/23 could be shown, higher temperatures in the early spring and summer alone are likely not enough to trigger earlier flowering. Ex-situ transplant experiments provide the opportunity to test the influences of different ecological parameters under controlled conditions. On the other hand, the true environment is a complex interplay of many different factors. The absence of competition for example can be of great interest with respect to the observed differences in growth and flowering behaviour. An in situ experiment could provide further insight into the influence of not only competition but also climatic conditions. The impact of these different strategies on the genetic diversity and gene flow within a metapopulation can be assessed with the herein available genetic data and will be analyzed in the next chapter. While the competition aspect is also missing in ecological niche modeling climatic differences for the siliceous and calcareous range can be assessed. The predicted present-day conditions and ranges, as well as future prospects, are analyzed in the next chapter.

5 | Bibliography

- Alvarez, N., Thiel-Egenter, C., Tribsch, A., Holderegger, R., Manel, S., Schönswetter, P., Taberlet, P., Brodbeck, S., Gaudraul, M., Gielly, L., et al. (2009). History or ecology? Substrate type as a major driver of patial genetic structure in Alpine plants. *Ecology Letters*, 12(7):632–640.
- Anacker, B. L. (2014). The nature of serpentine endemism. *American Journal of Botany*, 101(2):219–224.
- Bothe, H. (2015). The lime–silicate question. *Soil Biology and Biochemistry*, 89:172–183.
- Brady, K. U., Kruckeberg, A. R., and Bradshaw Jr, H. D. (2005). Evolutionary ecology of plant adaptation to serpentine soils. *Annu. Rev. Ecol. Evol. Syst.*, 36(1):243–266.
- Brevik, E. C. (2013). The potential impact of climate change on soil properties and processes and corresponding influence on food security. *Agriculture*, 3(3):398–417.
- Cecchi, L., Gabbrielli, R., Arnetoli, M., Gonnelli, C., Hasko, A., and Selvi, F. (2010). Evolutionary lineages of nickel hyperaccumulation and systematics in European *Alyssaeae* (Brassicaceae): evidence from nrDNA sequence data. *Annals of Botany*, 106(5):751–767.
- Chauvier, Y., Thuiller, W., Brun, P., Lavergne, S., Descombes, P., Karger, D. N., Renaud, J., and Zimmermann, N. E. (2021). Influence of climate, soil, and land cover on plant species distribution in the European Alps. *Ecological monographs*, 91(2):e01433.
- Coyle, C., Creamer, R. E., Schulte, R. P., O’Sullivan, L., and Jordan, P. (2016). A functional land management conceptual framework under soil drainage and land use scenarios. *Environmental Science & Policy*, 56:39–48.
- Cross, A. T. and Lambers, H. (2021). Calcicole–calcifuge plant strategies limit restoration potential in a regional semi-arid flora. *Ecology and Evolution*, 11(11):6941–6961.
- Cui, H., Töpfer, J. P., Yang, Y., Vandvik, V., and Wang, G. (2018). Plastic population effects and conservative leaf traits in a reciprocal transplant experiment simulating climate warming in the Himalayas. *Frontiers in Plant Science*, 9:1069.
- Ellenberg, H. (1958). Bodenreaktion (einschließlich Kalkfrage). *Die mineralische Ernährung der Pflanze/Mineral nutrition of plants*, pages 638–708.

- Ellis, A. G. and Weis, A. E. (2006). Coexistence and differentiation of ‘flowering stones’: the role of local adaptation to soil microenvironment. *Journal of Ecology*, 94(2):322–335.
- European Commission (2011). Soil: the hidden part of the climate cycle. Luxembourg : Publications Office of the European Union https://climate.ec.europa.eu/system/files/2016-11/soil_and_climate_en.pdf. Accessed: 20. 08. 2024.
- Gankin, R. and Major, J. (1964). *Arctostaphylos myrtifolia*, its biology and relationship to the problem of endemism. *Ecology*, 45(4):792–808.
- Hamidov, A., Helming, K., Bellocchi, G., Bojar, W., Dalgaard, T., Ghaley, B. B., Hoffmann, C., Holman, I., Holzkämper, A., Krzeminska, D., et al. (2018). Impacts of climate change adaptation options on soil functions: A review of european case-studies. *Land degradation & development*, 29(8):2378–2389.
- Harvey, M.-A., Erskine, P. D., Harris, H. H., Virtue, J. I., and van der Ent, A. (2024). Plant-soil relations of selenium, molybdenum and vanadium in the Richmond District of Central Queensland, Australia. *Plant and Soil*, pages 1–21.
- Holz, I., Franzaring, J., Böcker, R., and Fangmeier, A. (2010). Eintrittsdaten phänologischer Phasen und ihre Beziehung zu Witterung und Klima: Darstellung und Auswertung phänologischer Langzeit-Beobachtungen des Deutschen Wetterdienstes in Baden-Württemberg. Hrsg.: Landesanstalt für Umwelt, Messungen und Naturschutz Baden-Württemberg (LUBW), Karlsruhe. Download: <http://www.fachdokumente.lubw.baden-wuerttemberg.de>, ID Umweltbeobachtung U96-U51-N10.
- Hopkins, A. D. (1918). *Periodical events and natural law as guides to agricultural research and practice*. Number 9. US Government Printing Office.
- Jenny, H. (1994). *Factors of soil formation: a system of quantitative pedology*. Courier Corporation.
- Jiang, Z., Liu, H., Wang, H., Peng, J., Meersmans, J., Green, S. M., Quine, T. A., Wu, X., and Song, Z. (2020). Bedrock geochemistry influences vegetation growth by regulating the regolith water holding capacity. *Nature communications*, 11(1):2392.
- Johnson, L. C., Gallart, M. B., Alsdurf, J. D., Maricle, B. R., Baer, S. G., Bello, N. M., Gibson, D. J., and Smith, A. B. (2022). Reciprocal transplant gardens as gold standard to detect local adaptation in grassland species: New opportunities moving into the 21st century. *Journal of Ecology*, 110(5):1054–1071.
- Kassambara, A. (2023). *rstatix: Pipe-Friendly Framework for Basic Statistical Tests*. R package version 0.7.2.
- Kawecki, T. J. and Ebert, D. (2004). Conceptual issues in local adaptation. *Ecology letters*, 7(12):1225–1241.

- Kinzel, H. (1983). Influence of limestone, silicates and soil pH on vegetation. In *Physiological plant ecology III: Responses to the chemical and biological environment*, pages 201–244. Springer.
- Koch, M. A., Winizuk, A., Banzhaf, P., and Reichardt, J. (2021). Impact of climate change on the success of population support management and plant reintroduction at steep, exposed limestone outcrops in the German Swabian Jura. *Perspectives in Plant Ecology, Evolution and Systematics*, 53:125643.
- Kruckeberg, A. R. (2002). The influences of lithology on plant life. *Geology and plant life: the effects of landforms and rock type on plants*, pages 160–81.
- Larson, D. W., Matthes, U., and Kelly, P. E. (2000). Cliff ecology: pattern and process in cliff ecosystems.
- Lazzaro, A., Gauer, A., and Zeyer, J. (2011). Field-scale transplantation experiment to investigate structures of soil bacterial communities at pioneering sites. *Applied and environmental microbiology*, 77(23):8241–8248.
- Lee, J. A. (1999). *The calcicole-calcifuge problem revisited*. Academic Press.
- Leimu, R. and Fischer, M. (2008). A meta-analysis of local adaptation in plants. *PloS one*, 3(12):e4010.
- Loew, O. (1901). *The Relation of Lime and Magnesia to Plant Growth: I. Liming of soils from a physiological standpoint. II. Experimental study of the relation of lime and magnesia to plant growth/by DW May*. Number 1. US Government Printing Office.
- Madlung, A. (2013). Polyploidy and its effect on evolutionary success: old questions revisited with new tools. *Heredity*, 110(2):99–104.
- Moore, A. J. and Kadereit, J. W. (2013). The evolution of substrate differentiation in *Minuartia* series *Laricifoliae* (Caryophyllaceae) in the European Alps: In situ origin or repeated colonization? *American journal of botany*, 100(12):2412–2425.
- Ostle, N., Levy, P., Evans, C., and Smith, P. (2009). UK land use and soil carbon sequestration. *Land use policy*, 26:S274–S283.
- Panchen, Z. A., Primack, R. B., Aniško, T., and Lyons, R. E. (2012). Herbarium specimens, photographs, and field observations show Philadelphia area plants are responding to climate change. *American journal of botany*, 99(4):751–756.
- Pavlova, D., Kozuharova, E., and Dimitrov, D. (2003). A floristic catalogue of the serpentine areas in the Eastern Rhodope Mountains (Bulgaria). *Polish Botanical Journal*, 48(1):21–41.

- Pearse, W. D., Davis, C. C., Inouye, D. W., Primack, R. B., and Davies, T. J. (2017). A statistical estimator for determining the limits of contemporary and historic phenology. *Nature Ecology & Evolution*, 1(12):1876–1882.
- Perrella, G., Vellutini, E., Zioutopoulou, A., Patitaki, E., Headland, L. R., and Kaiserli, E. (2020). Let it bloom: cross-talk between light and flowering signaling in *Arabidopsis*. *Physiologia plantarum*, 169(3):301–311.
- Rajakaruna, N. (2004). The edaphic factor in the origin of plant species. *International Geology Review*, 46(5):471–478.
- Rajakaruna, N., Bradfield, G. E., Bohm, B. A., and Whitton, J. (2003). Adaptive differentiation in response to water stress by edaphic races of *Lasthenia californica* (Asteraceae). *International Journal of Plant Sciences*, 164(3):371–376.
- Rauschkolb, R., Durka, W., Godefroid, S., Dixon, L., Bossdorf, O., Ensslin, A., and Scheepens, J. (2023). Recent evolution of flowering time across multiple European plant species correlates with changes in aridity. *Oecologia*, 202(3):497–511.
- Richardson, A. D., Hufkens, K., Li, X., and Ault, T. R. (2019). Testing Hopkins’ bioclimatic law with PhenoCam data. *Applications in Plant Sciences*, 7(3):e01228.
- Strobel, K. A. (2014). Substrate adaptation of *Dianthus gratianopolitanus*: Local effect or evolutionary footprint? Staatsexamens Arbeit, Ruprecht-Karls University Heidelberg.
- Sumner, E. E., Morgan, J. W., Venn, S. E., and Camac, J. S. (2022). Survival and growth of a high-mountain daisy transplanted outside its local range, and implications for climate-induced distribution shifts. *AoB Plants*, 14(2):plac014.
- Takeno, K. (2016). Stress-induced flowering: the third category of flowering response. *Journal of experimental botany*, 67(17):4925–4934.
- Taylor, S. I. and Levy, F. (2002). Responses to soils and a test for preadaptation to serpentine in *Phacelia dubia* (Hydrophyllaceae). *New Phytologist*, 155(3):437–447.
- Thomann, M., Imbert, E., Engstrand, R., and Cheptou, P.-O. (2015). Contemporary evolution of plant reproductive strategies under global change is revealed by stored seeds. *Journal of Evolutionary Biology*, 28(4):766–778.
- Unger, F. (1836). *Ueber den Einfluss des Bodens auf die Vertheilung der Gewächse: Nachgewiesen in der Vegetation des nordöstlichen Tirol’s*. Bei Rohrmann und Schweigerd.
- Warnes, G. R., Bolker, B., Lumley, T., from Randall C. Johnson are Copyright SAIC-Frederick, R. C. J. C., by the Intramural Research Program, I. F., of the NIH, Institute, N. C., and for Cancer Research under NCI Contract NO1-CO-12400., C. (2022). *gmodels: Various R Programming Tools for Model Fitting*. R package version 2.18.1.1.

- Westerbergh, A. and Saura, A. (1992). The effect of serpentine on the population structure of *Silene dioica* (Caryophyllaceae). *Evolution*, 46(5):1537–1548.
- Xiong, X., Grunwald, S., Myers, D. B., Ross, C. W., Harris, W. G., and Comerford, N. B. (2014). Interaction effects of climate and land use/land cover change on soil organic carbon sequestration. *Science of the total environment*, 493:974–982.
- Zohlen, A. and Tyler, G. (2000). Immobilization of tissue iron on calcareous soil: differences between calcicole and calcifuge plants. *Oikos*, 89(1):95–106.
- Zohlen, A. and Tyler, G. (2004). Soluble inorganic tissue phosphorus and calcicole–calcifuge behaviour of plants. *Annals of Botany*, 94(3):427–432.

Part III

Genetic variation and structure
within populations of Cheddar Pink,
and future prospects under changing
climate conditions

Abstract

In this study eleven metapopulations of *D. gratianopolitanus* originating from the calcareous as well as siliceous range were analysed using nuclear AFLP data as well as plastid haplotypes. In addition the ecological niches under the current climate and under future climate scenarios were predicted and the most influential climate variables were analysed. The genetic structure analyzed by neighbor-net inferred genotypes and genetic assignment indicate varying patterns of connectivity and degrees of isolation for the populations. While both bedrock groups showed different levels of genetic connectivity, the siliceous populations indicated stronger within-population substructuring. These patterns of connectivity could indicate recent gene flow or symbolize the remnants of past genetic connectivity. Still, the high genetic structuring between sites again highlights the need for efficient conservation strategies targeting all subpopulations conserving the genetic variation and (re-) establishing possible dispersal routes. Niche modeling indicates differing climatic conditions and limitations for *D. gratianopolitanus* from calcareous and siliceous bedrock, with the southern populations more affected by drought stress while the northern populations are limited by minimum temperatures. With higher niche breadth the siliceous group is indicated to have a wide range of suitable climate conditions, than the more specialized calcareous group. While under current climate conditions, the predicted areas exceed the present-day distribution, future predictions indicate a clear reduction of suitable areas with a trend towards higher elevations and migrations to the north.

Zusammenfassung

In dieser Studie wurden elf Metapopulationen von *D. gratianopolitanus*, die sowohl aus dem kalkhaltigen als auch aus dem silikathaltigen Bereich stammen, mit Hilfe von AFLP-Daten und Plastiden Haplotypen analysiert. Darüber hinaus wurden die ökologischen Nischen unter dem gegenwärtigen Klima und unter zukünftigen Klimaszenarien vorhergesagt und die einflussreichsten Klimavariablen analysiert. Die genetische Struktur, zeigt unterschiedliche Muster der Konnektivität und des Isolationsgrades der Populationen. Während innerhalb der beiden Substrat-Gruppen große Variationen an genetischer Konnektivität nachgewiesen wurde, zeigten die Silikat-Populationen eine stärkere genetische Substrukturierung innerhalb der Populationen. Diese Konnektivitätsmuster könnten auf einen rezenten Genfluss hindeuten oder die Überreste eines früheren genetischen Austauschs darstellen. Dennoch unterstreicht die starke genetische Strukturierung zwischen den einzelnen Standorten innerhalb einer Metapopulation erneut die Notwendigkeit effizienter Schutzmaßnahmen, die alle Teilpopulationen einbezieht, um die genetische Variation und Diversität zu erhalten und mögliche Ausbreitungswege (wieder-)herzustellen. Die Vorhersage passender Habitats deutet auf unterschiedliche klimatische Bedingungen und Einschränkungen für *D. gratianopolitanus* auf kalkhaltigem und silikathaltigem Untergrund hin, wobei die südlichen Populationen stärker von Trockenstress betroffen sind, während die nördlichen Populationen durch Mindesttemperaturen eingeschränkt werden. Die Gruppe basierend auf Silikatvorkommen weist eine breitere ökologische Nische auf als die spezialisiertere Gruppe des Kalkgesteins, was darauf hindeutet, dass sie ein breites Spektrum an geeigneten Klimabedingungen aufweist. Während die vorhergesagten Gebiete unter den derzeitigen Klimabedingungen über die heutige Verbreitung hinausgehen, deuten die Zukunftsprognosen auf eine deutliche Verringerung der geeigneten Gebiete mit einem Trend zu höheren Lagen und Wanderungen nach Norden hin.

1 | Introduction

Isolation of populations and the need for ex situ and in situ conservation in a changing environment

Natural barriers like rivers, glaciers, or mountain ranges can separate and isolate populations (Qiong et al., 2017). In addition, artificial, man-made barriers (e.g. highways, or even the Juyong-guan Great Wall) can restrict or hinder gene flow resulting in the differentiation of (sub-) populations (Su et al., 2003). Beyond that, the life history and dispersal potential of a species as well as its mating system and pollination biology also influence the genetic structure and differentiation of populations (Turner et al., 1982; Wolff et al., 1997). Habitat fragmentation and reduction of population sizes can result in a decreasing genetic variation, elevated inbreeding, and reduced fitness (Kuss et al., 2008; Putz et al., 2015). The positive correlation between population size and fitness as well as population size and genetic variation was shown for both common and rare species, as well as perennial and annuals (Leimu et al., 2006). Putz et al. (2015) studied the influence of isolation on *D. gratianopolitanus* based on selected populations from the Swiss and Franconian Jura. While morphological parameters like cushion density differed between the regions the genetic variation and reproductive traits were similar. The different levels of isolation did not seem to influence genetic variation as much as population size and density. They concluded that stronger isolation must not result in the loss of genetic variation and fitness and suggested that the protection of isolated populations contributes a great amount towards the protection of the species as a whole. Over the last years, various ex situ and in situ measures have been attempted to support and conserve *D. gratianopolitanus* populations. Besides the care and monitoring from the federal states (e.g. (Banzhaf et al., 2009)) in situ reintroduction attempts have been made. Janczyk-Weglarska et al. (2013) showed good results for the in situ re-establishment of natural Cheddar Pink populations in the “Goździk siny w Grzybnie” reserve in Poland, but also highlights the need for ex situ conservation. In Brandenburg, Germany, measures have been taken to support the remaining populations and re-establish populations at presumably preferable and suitable sites on open sandy bedrock in pine forests with overall good results after three years (Zippel et al., 2021). The higher efficiency of the planting of young plants when compared to the usage of seeds also shows the need for both in situ as well as ex situ measures. In Koch et al. (2021) 549 plants in total were reintroduced in

the Lenninger Tal and Eselsburger Tal on the Swabian Jura, accompanied by the scoring of fitness parameters and genetic background of the used plants during the cultivation in the Botanical Garden in Heidelberg. While the reintroduction experiment yielded comparable results, the genetic data showed a spatial structuring indicating only limited gene flow and an increasing isolation of subpopulations. Here, the increased need for suitable open sites to enable local dispersal and restore an active exchange within meta-population systems is proposed. The scoring of fitness parameter over the course of the experiment from 2016 to 2019 also indicated a significant shift of flowering time of three to six weeks since 1990 in response to increased temperatures, possibly leading to asynchrony of flowering and availability of suitable pollinators and a reduction of the overall flowering time. In addition to the influence on fitness parameters like the flowering time, severe climate changes will also influence the suitability of habitats and ultimately the species' distribution ranges, possibly reducing their ranges in the process leading to high extinction risks (Thomas et al., 2004; Thuiller et al., 2005). Endemic, range-restricted, and isolated species are even more prone to suffer from environmental changes, highlighting the need for appropriate monitoring and conservation efforts (Casazza et al., 2014; Dagnino et al., 2020). The endemic *Dianthus polylepis* Bien. ex Boiss., inhabits the Irano-Turanian mountain region, with a fragmented distribution of several isolated populations. Overall the climatic conditions are comparable to a continental climate with an annual mean temperature of 12-19 °C and a mean annual precipitation of 300-380mm. Here a range shift towards the north and towards higher elevations is predicted, indicating regions for possible conservation efforts (Behroozian et al., 2020).

The distribution of genetic diversity and genetic structuring within the isolated populations of *D. gratianopolitanus* is important for effective conservation strategies. The differences in growth and flowering behavior between plants from calcareous and siliceous bedrock observed in Part II might influence the genetic patterns within populations. With their preferred habitats on the open rocky outcrops the Cheddar Pink are also affected by increasing temperatures and changing climate conditions. Using genetic data the effects of isolation within populations of *D. gratianopolitanus* can be evaluated. Combined with the modeling of ecological niches and suitable distribution ranges under present-day climate conditions as well as future predictions, it can provide valuable insight for conservation efforts to design an effective conservation strategy for existing populations as well as choose suitable sites for possible reintroductions.

Contributions

The used AFLP and plastid haplotype data are subsets of the bigger datasets used in Part I and therefore include the same contribution towards the data acquisition. The following data analysis as well as ecological niche modelling was done by myself.

2 | Material and Methods

2.1 Analysis of selected (Meta-) populations using Structure, Splitstree and diversity indices

In Koch et al. (2021) AFLP data for two Cheddar Pink metapopulations, the Lenninger and Eselburger Tal from the limestone bedrock from the Swabian Alb, were analysed in the context of a reintroduction experiment to assess the genetic structure and diversity as signs of gene flow and dispersal or signs of population isolation. Both metapopulations consist of various isolated subpopulations on the slopes of long valleys that are separated by e.g. a river, wooded hilltops, streets and steep cliffs. The revealed spatial pattern of genetic diversity indicated past habitat connectivity and gene flow but also genetic uniform subpopulations, highlighting the need to protect each site in order to conserve the genetic diversity of a metapopulation.

The differences in growth and flowering between plants from calcareous and siliceous bedrock observed in Part II, as well as differing environmental conditions, could also lead to differing patterns of genetic connectivity and degrees of isolation. To compare different metapopulations with isolated subpopulation and possible barriers to gene flow additional population from calcareous and siliceous bedrock were selected. I subsampled AFLP data from the data set described in Part I section 2.3. I chose metapopulations with obvious geographic barriers to dispersal and gene flow like e.g. rivers and wooded hilltops. In addition to the six populations representing populations growing on limestone bedrock, I chose five populations from Central Germany representing populations from siliceous bedrock (see Figure 2.1). I included a study site in the Swiss Alps as a population on calcareous bedrock that showed a mixed signal in the overall STRUCTURE analysis (see Part I, Appendix Figure A.5, included Populations are marked with a star) as well as a site in Franconian Switzerland in Bavaria, the nature reserve Ehrenbürg, a site on limestone bedrock that was assigned to the northern German cluster in the STRUCTURE analysis (Appendix Figure A.6, included metapopulations are marked with a star). I also included the two populations from Koch et al. (2021), the Lenninger and Eselsburger Tal, to compare the observed patterns and genetic diversity to the published data.

For analysis of population structure, I used STRUCTURE version 2.3 (Pritchard et al., 2000) as well as genetic diversity analysis (with $n = 20$ per subset and 100 repetition).

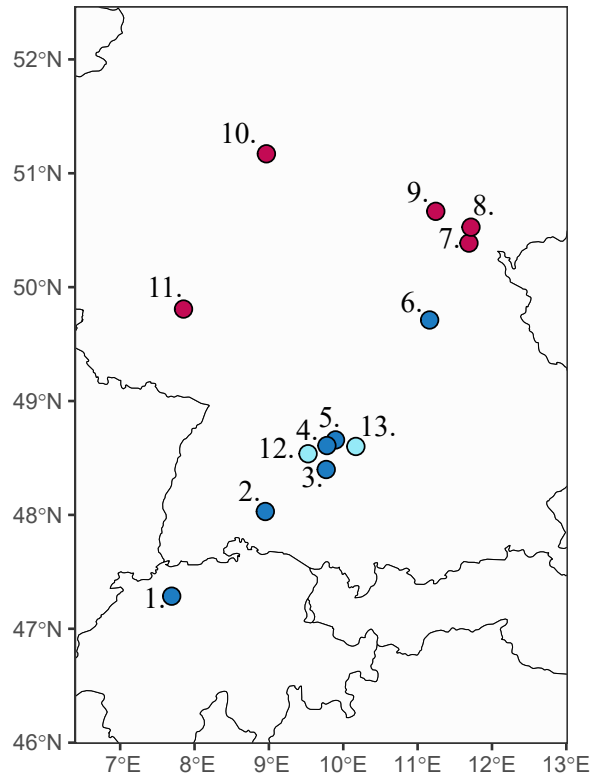


Figure 2.1: Populations from limestone (blue) and siliceous (red) bedrock. 1.) Lehnfluh and Ravellenflue (Switzerland), 2.) Danube valley near Friedingen (Baden-Württemberg), 3.) Achtal and Blaubeuren (BW), 4.) Hausener Wand, Michelsberg (BW), 5.) Eybtl (BW), 6.) nature reserve Ehrenbürg (Bavaria), 7.) Blankenberg and Höllental (Thuringia and Bavaria), 8.) nature reserve Korberfels and Bleiberg near Burgk (TH), 9.) Schwarzatal (TH), 10.) Kellerwald-Edersee (Hesse), 11.) nature reserve Gans and Rheingrafenstein (Rhineland-Palatinate). In addition the metapopulation from 12.) the Lenninger Tal and 13.) the Eselsburger Tal from Koch et al. (2021) are included.

I also calculated an AMOVA for the populations and grouped by substrate as described earlier (see Part II section 2.5). I calculated the number of molecular differences within and between sites, and visualized them using histograms and boxplots and calculated the statistical significance using `wilcox.test()` from the R stats package (R Core Team, 2023). In addition I calculated jaccard distances from AFLP data (`vegdist(method = "jaccard")`, R vegan package (Oksanen et al., 2022)) for all populations separately. Using the neighbour-net algorithm implemented in SplitsTree v.4.15.1 (Huson and Bryant, 2006) I reconstructed phylogenetic networks based on the Jaccard distance matrices and counted complete and unambiguous plastid marker haplotypes per (sub-)population.

2.2 Ecological niche modelling

To evaluate how the climate conditions influences the distribution range of *D. gratianopolitanus* and to determine whether the climate conditions differ between the calcareous and

siliceous range Ecological Niche Modelling is employed. Ecological Niche Modelling (ENM), also called Species Distribution modelling (SDM), is used to predict the potential geographic distribution of species based on their known occurrences and environmental variables like e.g. temperature, precipitation or soil data. It uses data on where a species can be found and the environmental condition it faces in these habitats to make predictions on suitable habitats. These predictions can be used to e.g. finding suitable habitats for species that possibly require protection, analysing possible differentiations of niches between species and their biogeographic patterns, evaluate the invasive potential of species, or estimate the impact of climate change on species distributions. The models rely on occurrence data of species. Presence-absence data, that include not only known occurrences of a species but specifically its absence of a region is often sparse and limited in coverage while presence-only data is more readily available. One of the most widely used methods is Maximum Entropy (Maxent), a machine learning method first introduced to Niche modelling in 2006 that solely relies on presence-only data (Phillips et al., 2006). It is simple and user-friendly either as implementation in a variety of R packages (e.g. ENMTools (Warren et al., 2021), dismo (Hijmans et al., 2017)) or in standalone programs (Steven J. Phillips, 2024). It is able to model more complex relationships between variables and is said to be robust using small sample sizes (Elith et al., 2006). In addition it outperforms other methods like linear models (GLM) and Generalized Additive Models (GAM) that rely on presence-absence data and can compete with newer ensemble methods combining predictions from single SDM models (Kaky et al., 2020).

Occurrence data and climate data preparation

The occurrence data collected during this studies runtime in Heidelberg cover the distribution range from *D. gratianopolitanus*, and is comparable to occurrence data available from e.g. GBIF (<https://www.gbif.org/>) or Atlas Flora Europaea (see General Introduction Figure 1). Due the higher confidence in the herein collected data due to personal monitoring, sampling and visiting of most of these sites and the sufficient coverage of distribution I used only our own occurrence data for ecological niche modelling. To avoid a sample bias based on different collection efforts throughout the distribution range due to accessibility and proximity to Heidelberg I filtered the samples using the R script "thin.max.R" published by the author of the R package "ENMTools" Dan Warren (Digital Supplement "S_III.2.1-thin.max.R" and <https://gist.github.com/danlwarren/271288d5bab45d2da549>). It allows to rarefy a large data set in such a way to maximize differences between the occurrence points while keeping a given number of points for further analysis. In addition I divided the dataset based on the substrate type into a limestone and siliceous dataset in order to compare climatic conditions and possible differing ecological niches between the two areas. I downloaded the climate data in the format of nineteen bioclimatic variables (bioclim) from the WorldClim database (<https://www.worldclim.org/data/bioclim.html>) at 30 arc-second resolution for the present climate conditions. Bioclimatic variables are created

by transforming monthly temperature and rainfall data into biologically more meaningful variables in order to understand the ecological significance of climate patterns. They focus on i) annual trends such as mean annual temperature or total annual precipitation to give insight into the overall climatic conditions over the course of a year, ii) seasonality such as annual range in temperature and precipitation to capture the fluctuations throughout the year and assess the response to changing environments and iii) extreme or limiting factors such as the temperature of the coldest or warmest month or the precipitation during the wettest or driest quarter to highlight the most extreme conditions faced within a year. For easier and faster processing I cropped the geographical range of bioclimatic variables to Central Europe to cover the distribution range of *D. gratianopolitanus*. To ensure no auto-correlation between the bioclimatic variables I calculated the Pearson correlation coefficients for each pair of bioclim variables using the R package "ENMTools" (Warren et al., 2021). In case of high correlation ($-0.75 \leq R \leq 0.75$) the bioclim variable with less contribution to the niche model was discarded. To get insight on the variation of the bioclimatic variables between the whole dataset, the limestone and the siliceous dataset I plotted the assumed values for each bioclim variable in a boxplot using "ggplot2" in R (Wickham, 2016), and tested for statistical significance of differences using a wilcoxon test (Constantin and Patil, 2021). Due to insufficient data on Europe-wide geological data on a meaningful scale it was not further included into this ecological niche modelling approach. In addition to present day data, future climate projections of the world climate as part of the Coupled Model Intercomparison Project 6 (CMIP6) based on different global climate models (GCMs) and different shared socio-economic pathways (SSPs) can be downloaded from the WorldClim database (<https://www.worldclim.org/data/cmip6/cmip6climate.html>). Data is available for four time intervals (2021-2040, 2041-2060, 2061-2080, 2081-2100) and four SSPs (1-2.6, 2-4.5, 3-7.0 and 5-8.5). The SSPs take into account various green house gas emission scenarios from the no-policy, worst case outcome scenario SSP5-8.5, over the middle of the road scenario SSP3-7.0 to the goal of limiting global warming to below 2 °C (SSP1-2.6) or the most likely scenario below 3 °C (SSP2-4.5). In my study I included data for end of century predictions (2081-2100) for the SSP1-2.6 to reflect the outcome pursued in the Paris Agreement from 2015 to limit the temperature increase to 1.5 °C as well as the prediction of the middle way scenario SSP3-7.0, with an estimated warming of $\sim 2.8 - 4.6^\circ\text{C}$ until the end of century. While both scenarios are unlikely, they provide a good upper and lower limit for the future outcome. Predictions of a total of fourteen different CMIP6 models are available at the WorldClim database. Compared to earlier models (e.g. CMIP5) they predict a higher temperature increase in this century and show a higher equilibrium climate sensitivity (ECS), a measure to indicate how severe future warming will be, defined by the expected long-term global warming after a doubling of CO₂ concentration in the atmosphere. As the range for likely values for ECS for CMIP6 models is given as 2.5 °C to 4 °C within the IPCC sixth assessment report (AR6) published in 2021 (Masson-Delmotte et al., 2021), I chose "GISS-E2-1-G" as model with an ECS of 2.7 °C. The respective data was downloaded with a resolution of 30 arc-seconds from WorldClim database. Models trained on the present day

distribution of *D. gratianopolitanus* and its predicted ecological niche can then be projected on other climate data to predict its niche under the changing environmental conditions and give an impression on how the species may react to future climate conditions.

Model preparation, analysis and evaluation

In order to evaluate model performance a common parameter is the Area Under the Receiver Operating Characteristic Curve (AUC). It is a measure of the model's ability to distinguish between binary classifiers like suitable and unsuitable habitats or conditions in the context of niche modelling. The AUC can be used to compare the performance of different models or scenarios. It ranges between 0 and 1 where a value of 0.5 indicates a model performance comparable to random guessing, 0.5 - 0.7 a poor performance, 0.7 - 0.9 a moderate performance and >0.9 a high model performance (Peterson et al., 2011). In order to give an estimate for the species specialization and its requirements for its habitat, I calculated niche breadth following Levins (1968) for the limestone as well as siliceous group using ENMTools (Warren et al., 2021). To compare the overlap of resource use or the overlap of suitable conditions, niche overlap measures like Schoener's D (Schoener, 1968) or Hellinger's based I (Warren et al., 2008) (modified later (Rödder and Engler, 2011)) are widely used for ENM. They range from 0, indicating no overlap between the niche models, and 1, indicating identical niche models. Rödder and Engler (2011) suggest a classification of results: 0 - 0.2 = no or very limited overlap, 0.2 - 0.4 = low overlap, 0.4 - 0.6 = moderate overlap, 0.6 - 0.8 = high overlap, 0.8 - 1.0 = very high overlap. I used a niche identity test from ENMTools to evaluate how significant the ecological niches of the two groups differed. The test pools the occurrence points of both groups and randomly reassigns them to create pseudoreplicate datasets. Models for the new occurrence distributions and niche overlap are calculated. This is repeated for $n = 100$ pseudoreplicate datasets, creating a null distribution of overlap values of the two groups with the assumption of equivalent underlying environmental distribution. When comparing the empirical niche models overlap values to the overlap distribution a significant lower empirical overlap value suggests that the niches are more divergent than expected by chance, while a value that falls within the distribution would indicate niche equivalence. By using 100 replicates and also including the niche overlap value obtained by empirical data the resolution can be calculated by $1/(100 + 1) \approx 0.01$ which can be translated to $p < 0.01$.

3 | Results

3.1 Genetic diversity and population structure within selected populations from calcareous and siliceous bedrock

Eleven study sites from Germany and Switzerland, six in the calcareous and five in the siliceous range, with sufficient population sizes and possible genetic barriers, were chosen to compare within-population genetic structuring and diversity. In addition the two metapopulations, from the Lenninger Tal and Eselsburger Tal, from Koch *et al.* (2021) are included.

The included populations ranged in number of sampled individuals with the smallest (meta-)population from the nature reserve Gans and Rheingrafenstein with 20 sampled individuals to 76 sampled individuals in the nature reserve Bleiberg near Burgk. To correct for sample sizes the AFLP summary statistic was calculated by repeated subsampling of 20 samples per population followed by the calculation of mean values and the corresponding standard deviations. Results are given in Table 3.1, Table 3.2, Table 3.3 and Table 3.4. Mean values of metapopulations per substrate type group are given Table 3.5. Due to the known difference in the genetic assignment of the metapopulation from Ehrenbürg and the Swiss populations (Lehnfluh, Ravellenflue and Holzflue), the mean values were also calculated excluding the metapopulations. The plastid marker haplotypes per populations and site are given in the Appendix Table C.1 and Table C.2.

Of the 362 AFLP fragments between $F_{\text{tot}} = 119.18$ (32.92%, 6. nature reserve Ehrenbürg) 168.93 (46.68%, 3. Achtal and Blaubeuren) are found. The mean values of the two ranges differ between 152.6 (42.15%) in the calcareous and 142.55 (39.38%) in the siliceous range. This difference is even more pronounced when excluding the nature reserve Ehrenbürg ($F_{\text{tot}} = 157.37$, 43.47%), while the site from Switzerland does not differ from the rest of the calcareous range. Yet the observed differences are not statistical significant comparing the calcareous metapopulations without Ehrenbürg to the siliceous metapopulations (Wilcox Test, $W = 29$, $p = 0.07323$). Comparing the mean values of the calcareous populations, excluding Ehrenbürg, and siliceous Between 89.94 sites (24.85%, Ehrenbürg) and 142 sites (39.23%, 2. Danube Valley) are polymorphic. The calcareous region displays a higher mean number of polymorphic sites (124.54, 34.34%; without Ehrenbürg 129.24, 35.70%) than the siliceous sites (116.63, 32.22%), also resulting in non significant differences between the calcareous metapopulations, excluding the one from Ehrenbürg, and those from

siliceous bedrock (Wilcox Test, $W = 26$, $p = 0.202$). The mean number of bands per individual ranges between 58.61 (16.19%, 8. nature reserve near Burgk) and 66.83 (18.46%, 12. Lenninger Tal), and differs between the calcareous (63.59, 17.57%, without Ehrenbürg 64.30, 17.76%) and siliceous (60.52, 16.72%) range, resulting in a weak significant difference between the calcareous (without Ehrenbürg) and siliceous metapopulations (Wilcox Test, $W = 30$, $p = 0.04798$). Yet the mean number of bands from Kellerwald Edersee (65.47) exceeds those from other siliceous and is comparable to those observed in the calcareous study sites. The calcareous group has higher numbers of rare (occurrence of $< 1\%$) and unique alleles with the highest number in Switzerland ($F_{\text{rare}} = 10.81$, $F_{\text{rare total}} = 19$, and 9 unique fragments) followed by the Eybtal ($F_{\text{rare}} = 9.48$). The lower mean number of rare alleles ($F_{\text{rare}} = 1.65$) and total number of unique alleles in populations ($F_{\text{uni in pop}} = 3$) and in the siliceous bedrock in total ($F_{\text{uni sub}} = 6$) in the siliceous group is also reflected in a lower down-weighted-marker ($DW = 8.33$), that showed a significant difference to those from calcareous bedrock ($DW = 12.71$, Wilcox Test, $W = 34$, $p = 0.005051$).

The metapopulation from Lenninger Tal is comparable to the metapopulations from the calcareous bedrock, while those from the Eselsburger Tal showed smaller mean values for total number of fragments, polymorphic sites, number of rare alleles and DW and is comparable to the metapopulation from the nature reserve Ehrenbürg. The AMOVA of genetic variation of all included populations indicate 76.17% of variation within the subpopulations, 16.05% of genetic variation originating from within populations and 7.78% between the populations ($p < 0.01$, 1023 permutation, fixation index $F_{\text{ST}} = \sim 0.238$, $F_{\text{SC}} = \sim 0.174$, $F_{\text{CT}} = \sim 0.078$). The results of the AMOVA comparing the two substrate groups shows a similar result with 76.10% of variation within the subpopulations, 22.72% of genetic variation originating from within substrate groups and 1.17% between the groups ($p < 0.01$, 1023 permutation, fixation index $F_{\text{ST}} = \sim 0.239$, $F_{\text{SC}} = \sim 0.230$, $F_{\text{CT}} = \sim 0.012$).

For 153 of the 530 included individuals of population 1-11.) unambiguous data on plastid haplotypes are available. The found haplotypes include, beside the most common ht16 and ht19, the also more frequent ht01, ht02, ht03, ht21, ht29 and ht30. ht01 and ht30 are more common in the siliceous populations while ht16 and ht29 are more common in the calcareous populations. In the analysed populations ht03 is restricted to the Swiss populations while ht02 is restricted to the siliceous Blankenberg and Höllental populations.

For each study site the summary statistic for all subpopulations, a neighbour-net using SplitsTree based on Jaccard distances, the geographic distribution of inferred genetic groups, genetic assignment using STRUCTURE as well as pairwise genetic differences between subpopulations were calculated.

1. Lehnfluh, Ravelleflue and Holzflue

The results for the Swiss study site are shown in [Figure 3.1](#) and [Figure 3.2](#). The SplitsTree analysis ([Figure 3.1 A](#)) indicates 11 groups, herein marked with different colors. The optimal number of clusters suggested for the STRUCTURE analysis according to ΔK is 2 (Di-

Table 3.1: Summary statistics of AFLP data of *D. gratianopolitanus* per region. Numbering of regions, number of investigated individuals (N), number of AFLP fragments (F_{tot}), number of polymorphic sites (F_{poly}), mean number of bands per individual (F_{bands}), number of unique alleles (F_{unique}), brackets indicate number of unique alleles unique to this site), mean number of rare alleles (F_{rare}), total number of rare alleles found in the population ($F_{rare\ total}$), frequency-down-weighted marker values (DW) and Average gene diversity over loci (Arlequin) H . Investigated populations from siliceous and volcanic bedrock. To take different sample sizes into account mean values and standard deviation for metapopulations were calculated by repeated drawing and calculation for 20 random individuals per metapopulation and calculation of mean and standard deviation. The name addition (C) indicates populations are from calcareous bedrock.

Region	N	F_{tot}	F_{poly}	F_{bands}	F_{rare}	$F_{rare\ total}$	F_{unique}	DW	H
1 Lehnfluh and Ravellenflue (C)	49	164.323 ±5.148	137.204 ±4.972	61.201 ± 1.148	10.81 ± 2.48	19	9	14.960 ± 1.830	0.094260 ± 0.045423
Braenten F1	3	82	37	61		0	0 (0)	1.56	0.080808 ± 0.063528
Braenten F2	3	66	5	64		0	0 (0)	1.84	0.020202 ± 0.018132
Holzflue	12	125	92	62		7	5 (4)	11.09	0.109848 ± 0.059647
Lehnfluh	18	153	126	61		8	3 (2)	13.11	0.104922 ± 0.055265
Ravellenflue	13	137	109	60		7	3 (1)	8.96	0.098291 ± 0.053250
2 Danube valley (south) (C)	42	168.444 ±5.127	142.0 ± 5.236	65.235 ± 0.946	4.266 ±1.187	8	3	12.980 ± 0.9355	0.099235 ± 0.047770
Kaiserstand	3	93	44	68		0	1 (0)	2.21	0.106061 ± 0.082371
Knopfmacherfels	5	99	58	65		1	2 (1)	3.48	0.074242 ± 0.047982
Schloss Bronnen	9	141	111	64		1	1 (0)	5.26	0.114057 ± 0.063985
Sperberloch	6	106	72	65		0	1 (0)	3.53	0.091414 ± 0.055756
Stiegelesfels	8	107	72	62		1	1 (1)	4.13	0.095509 ± 0.055000
Stiegelesfels Forest	11	148	116	68		5	1 (0)	8.62	0.127548 ± 0.069451
3 Achtal and Blaubeuren (C)	55	168.963 ±6.169	141.078 ± 6.594	64.679 ±1.315	5.658 ±1.946	12	8	13.555 ±1.643	0.091994 ± 0.044354
Blaufels	12	122	93	60		2	2 (1)	6.18	0.097337 ± 0.053166
Bruckfels	5	113	73	68		5	2 (0)	4.95	0.101515 ± 0.064522
Kloetzle Blei	5	77	18	68		0	0 (0)	2.76	0.030303 ± 0.021248
Obere Peilerwand	5	88	43	64		3	3 (2)	4.44	0.089394 ± 0.057173
Ruine Guenzelburg	5	89	54	58		0	0 (0)	1.23	0.068182 ± 0.044304
Rusenschloss	14	140	104	69		1	1 (0)	10.65	0.114635 ± 0.061251
Schillerstein	1	72	0	72		1	1 (1)	1.62	0.0 ± 0.0
Schneckenfels	4	88	51	60		1	1 (0)	2.19	0.084596 ± 0.058345
Sirgenstein	4	103	62	68		3	2 (1)	3.36	0.111111 ± 0.075670

Table 3.2: Summary statistics of AFLP data of *D. gratianopolitanus* per region. Numbering of regions, number of investigated individuals (N), number of AFLP fragments (F_{tot}), number of polymorphic sites (F_{poly}), mean number of bands per individual (F_{bands}), number of unique alleles (F_{unique}), brackets indicate number of unique alleles unique to this site), mean number of rare alleles (F_{rare}), total number of rare alleles found in the population ($F_{rare\ total}$), frequency-down-weighted marker values (DW) and Average gene diversity over loci (Arlequin) H . Investigated populations from siliceous and volcanic bedrock. To take different sample sizes into account mean values and standard deviation for metapopulations were calculated by repeated drawing and calculation for 20 random individuals per metapopulation and calculation of mean and standard deviation. The name addition (C) indicates populations are from calcareous bedrock.

Region	N	F_{tot}	$F_{polymorph}$	F_{bands}	F_{rare}	$F_{rare\ total}$	F_{unique}	DW	H
4 Hausener Wand (C)	46	151.127 ± 4.710	123.343 ± 4.872	66.541 ± 1.107	3.431 ± 1.441	8	1	11.460 ± 0.855	0.093942 ± 0.045273
Eckfels	3	80	29	67		1	0 (0)	1.70	0.055556 ± 0.044668
Große Hausener Wand F1	12	123	87	65		1	0 (0)	6.39	0.104683 ± 0.056972
Große Hausener Wand F2	2	75	23	64		1	0 (0)	1.40	0.083333 ± 0.087039
Jungfrauenfels F1	14	127	96	70		0	1 (0)	7.47	0.104312 ± 0.055980
Jungfrauenfels F2	3	69	21	59		2	0 (0)	1.38	0.050505 ± 0.040892
Kleine Hausener Wand	12	118	81	66		3	1 (0)	8.02	0.078053 ± 0.043171
5 Eybatal (C)	27	163.692 ± 4.947	133.767 ± 5.334	63.403 ± 0.704	9.477 ± 1.237	11	4	14.812 ± 0.934	0.085167 ± 0.041134
Donaldfels	6	98	60	62		2	1 (0)	3.43	0.098990 ± 0.060136
Drehfels	1	67	0	67		1	1 (0)	1.02	0.0 ± 0.0
Nadelfels	4	78	27	64		2	2 (1)	2.84	0.054293 ± 0.038523
Schulterfels	5	82	34	63		2	2 (0)	3.14	0.062121 ± 0.040624
Spielerwand	2	70	20	60		0	0 (0)	0.77	0.060606 ± 0.064282
West of Steinenkirch	3	92	45	69		3	1 (0)	3.62	0.101010 ± 0.078603
West of Waldhausen	6	107	72	62		3	1 (1)	5.11	0.100000 ± 0.060720
6 nature reserve Ehrenbürg (C)	28	119.184 ± 2.295	89.938 ± 2.414	58.637 ± 0.552	2.119 ± 0.721	3	1	7.918 ± 0.665	0.065447 ± 0.031830
Einsiedlerhöhle	10	100	63	58		2	0 (0)	3.63	0.060943 ± 0.034991
Forest	10	97	64	61		1	1 (1)	5.35	0.066835 ± 0.038113
Rodenstein	8	87	52	57		0	0 (0)	2.15	0.064935 ± 0.038285

Table 3.3: Summary statistics of AFLP data of *D. gratianopolitanus* per region. Numbering of regions, number of investigated individuals (N), number of AFLP fragments (F_{tot}), number of polymorphic sites (F_{poly}), mean number of bands per individual (F_{bands}), number of unique alleles (F_{unique}), brackets indicate number of unique alleles unique to this site), mean number of rare alleles (F_{rare}), total number of rare alleles found in the population (F_{rare} total), frequency-down-weighted marker values (DW) and Average gene diversity over loci (Arlequin) H . Investigated populations from siliceous and volcanic bedrock. To take different sample sizes into account mean values and standard deviation for metapopulations were calculated by repeated drawing and calculation for 20 random individuals per metapopulation and calculation of mean and standard deviation. The name addition (S) indicates metapopulation from siliceous bedrock.

	Region	N	F_{tot}	$F_{polymorph}$	F_{bands}	F_{rare}	F_{rare} total	F_{unique}	DW	H
7	Blankenberg and Höllental (S)	45	130.933 ± 4.313	104.869 ± 4.858	59.101 ± 0.916	1.329 ± 0.827	3	1	7.734 ± 0.580	0.078603 ± 0.038037
	Blankenberg	22	120	91	60		1	0 (0)	8.56	0.091631 ± 0.048053
	Hoellental	18	124	99	59		1	1 (1)	6.75	0.079224 ± 0.042381
	Papierfabrik	5	101	68	58		1	0 (0)	2.15	0.127273 ± 0.080134
8	nature reserve near Burgk (S)	76	135.830 ± 4.482	108.059 ± 4.698	58.606 ± 0.843	1.731 ± 0.903	4	1	6.779 ± 0.567	0.077207 ± 0.037378
	Bleiberg	17	122	95	59		2	0 (0)	6.30	0.083445 ± 0.044664
	Burgk	17	115	84	59		0	0 (0)	4.97	0.073084 ± 0.039446
	Eisbrücke	4	87	50	58		0	0 (0)	1.40	0.094697 ± 0.064947
	Hängesteig	38	146	118	59		2	1 (1)	13.01	0.086642 ± 0.044638
9	Schwarzatal	37	141.381 ± 3.634	111.190 ± 3.548	59.729 ± 0.850	2.257 ± 0.673	3	0	8.409 ± 0.669	0.073794 ± 0.035768
	Griesbachfels	8	88	56	55		0	0 (0)	2.07	0.060335 ± 0.035768
	Kirchfels	15	134	101	59		1	0 (0)	5.06	0.077345 ± 0.041970
	Trippstein	14	119	88	63		2	0 (0)	8.41	0.082001 ± 0.044584
10	nature reserve Kellerwald Edersee (S)	66	153.583 ± 4.863	125.011 ± 4.809	65.474 ± 1.089	1.932 ± 1.020	5	1	9.979 ± 0.711	0.091662 ± 0.044198
	Blossenbergr	31	159	135	65		4	1 (0)	16.22	0.105702 ± 0.054232
	Nelkenstieg	20	131	99	66		1	1 (0)	9.97	0.119976 ± 0.062414
	Pine forest	5	108	73	63		1	0 (0)	2.64	0.124242 ± 0.078298
	Wooghölle	8	121	82	66		0	1 (0)	3.55	0.113095 ± 0.064606
	unknown	2	72	14	65		0	0 (0)	0.62	\pm
11	nature reserve Gans and Rheingrafenstein (S)	20	151 ± 0	134 ± 0	59.700 ± 0.000	1 ± 0	1	0	8.752 ± 0	0.088027 ± 0.042483
	Gans	5	103	74	60		1	0 (0)	2.35	0.104545 ± 0.066359
	Rheingrafenstein	14	127	105	60		1	0 (0)	5.75	0.095987 ± 0.051729
	near river Nahe	1	62	0	62		0	0 (0)	0.65	0.0 ± 0.0

Table 3.4: Summary statistics of AFLP data of *D. gratianopolitanus* per region. Numbering of regions, number of investigated individuals (N), number of AFLP fragments (F_{tot}), number of polymorphic sites (F_{poly}), mean number of bands per individual (F_{bands}), number of unique alleles (F_{unique}), brackets indicate number of unique alleles unique to this site), mean number of rare alleles (F_{rare}), total number of rare alleles found in the population ($F_{rare\ total}$), frequency-down-weighted marker values (DW) and Average gene diversity over loci (Arlequin) H . Investigated populations from siliceous and volcanic bedrock. To take different sample sizes into account mean values and standard deviation for metapopulations were calculated by repeated drawing and calculation for 20 random individuals per metapopulation and calculation of mean and standard deviation. The name addition (C) indicates populations are from calcareous bedrock.

Region	N	F_{tot}	$F_{polymorph}$	F_{bands}	F_{rare}	$F_{rare\ total}$	F_{unique}	DW	H
12 Lenninger Tal (C)	64	155.97 ± 4.985	127.54 ± 5.653	66.834 ± 1.088	5.50 ± 2.05	12	5	12.377 ± 1.382	0.080482 ± 0.038924
Grasband	4	86	47	60		1	1 (1)	2.03	0.070707 ± 0.049265
Müllerfels	7	93	50	67		0	0 (0)	3.46	0.056999 ± 0.034729
Müllerfels - erster südlicher Nachbar	8	102	62	67		0	0 (0)	3.63	0.093885 ± 0.054113
Müllerfels - zweiter südlicher Nachbar	10	110	72	65		2	1 (0)	6.11	0.092088 ± 0.051481
Müllerfels - nördlicher Nachbar	2	81	27	68		0	1 (0)	0.90	0.106061 ± 0.109783
Reiterfels	8	96	54	64		2	2 (0)	4.17	0.058712 ± 0.034879
Schlatterhöhe	6	86	22	72		2	1 (1)	5.13	0.029798 ± 0.020033
Schwarze Wand	2	76	23	65		1	1 (1)	2.09	0.083333 ± 0.087039
Sylphenwand	11	130	95	68		2	1 (0)	7.52	0.086777 ± 0.048132
Sylphenwand - Nebenfels	6	114	73	71		3	2 (0)	4.63	0.091414 ± 0.055756
13 Eselsburger Tal (C)	27	129.08 ± 2.832	99.726 ± 3.241	62.211 ± 0.696	1.452 ± 0.598	2	0	8.808 ± 0.332	0.081574 ± 0.039439
Bachfelsens	5	76	30	59		1	0 (0)	2.21	0.036364 ± 0.024952
Bindstein	4	83	42	62		0	0 (0)	1.24	0.066919 ± 0.046787
Falkenstein	5	100	59	66		1	0 (0)	2.69	0.095455 ± 0.060848
Himmel und Hölle	1	46	0	46		0	0 (0)	0.19	0.0 ± 0.0
Jungfrauen	13	107	74	63		0	0 (0)	5.99	0.066822 ± 0.037062

Table 3.5: Summary statistics of AFLP data of *D. gratianopolitanus*. Mean values per substrate of origin based on metapopulation means. Number of AFLP fragments (F_{tot}), number of polymorphic sites (F_{poly}), mean number of bands per individual (F_{bands}), mean number of rare alleles (F_{rare}), total number of rare alleles found in the population ($F_{rare\ total}$), frequency-down-weighted marker values (DW) and sum of unique alleles ($F_{uni\ in\ pop.}$) in the populations and number of unique alleles ($F_{uni\ per\ sub}$) to calcareous or siliceous bedrock. In addition the statistic for the calcareous range excluding the metapopulation from Ehrenbürg, as well as the calcareous range excluding both the metapopulation from Ehrenbürg and the Swiss metapopulation is given.

	F_{tot}	$F_{polymorph}$	F_{bands}	$F_{rare\ total}$	F_{rare}	DW	$F_{uni\ in\ pop.}$	$F_{uni\ per\ subs.}$
mean calcareous	152.60 (42.15%)	124.32 (34.34%)	63.59 (17.57%)	9.38	5.34	12.11	31	69
SD, (8 populations)	± 17.55	± 18.19	± 2.63	± 5.10	± 3.11	± 2.43		
mean calc. - Ehren.	157.37 (43.47%)	129.24 (35.70%)	64.30 (17.76%)	10.29	5.80	12.71	30	68
SD, (7 populations)	± 13.02	± 13.60	± 1.97	± 4.80	± 3.06	± 1.97		
mean calc. - Ehren./ Swiss	156.21 (43.15%)	127.91 (35.33%)	64.82 (17.91%)	8.83	4.96	12.33	21	58
SD, (6 populations)	± 13.73	± 14.27	± 1.63	± 3.48	± 2.46	± 1.88		
mean siliceous	142.55 (39.38%)	116.63 (32.22%)	60.52 (16.72%)	3.20	1.65	8.33	3	6
SD, (6 populations)	± 9.36	± 11.91	± 2.38	± 1.29	± 0.41	± 0.99		

igital Supplement "S_III.1.1-CH" with "S_III.1.1.1-AFLP_Dg_CH.xlsx" to "S_III.1.1.5-evanno.txt") with overall good accordance to the neighbor-net analysis (Figure 3.1 B). While the subpopulations from Lehnfluh, Ravellenflue, and Bränten (F1) are assigned to the orange group, the subpopulation from Holzflue shows more influence of the blue cluster. The second site from Bränten (F2) is assigned to the blue group, and clusters close in the SplitsTree analysis. The three biggest sites (Lehnfluh, Ravellen, and Holzflue) are located on separate hill ridges separated by valleys and small rivers, as well as streets and cities with distances of $\sim 1.6\text{km}$ to $\sim 4\text{km}$ (Figure 3.2 A). While the geographical distribution of the neighbor-net genotypes indicates geographic structuring between the growth sites, genetic connectivity, indicated by colored lines, can be observed especially between Lehnfluh and Ravellen. A connection of Holzflue is only shown for one (light blue) SplitsTree group. Comparing the number of pairwise genetic differences (Figure 3.2 B, C) reveals significantly smaller amounts within than between the growth sites (Mann Whitney U test, $p < 0.001$) indicating isolation and only limited gene flow between those sites. The AMOVA of genetic variation indicates $\sim 85\%$ of variation within the different sites and $\sim 15\%$ of genetic variation originating from between the populations ($p < 0.001$, 1023 permutations, fixation index $F_{ST} = \sim 0.15$). Two haplotypes were found between all sites with ht03 found in the southern sites, Lehnfluh, Ravellenflue and the southern site of Bränten while ht16 is found in Holzflue and the norther part of Bränten.

2. Danube valley south, near Friedingen an der Donau

The SplitsTree results of the Danube Valley split the samples into seven groups (Figure 3.3 A). ΔK suggests $K = 2$ as optimal K (Digital Supplement "S_III.1.2-Donau" with "S_III.1.2.1-AFLP_Dg_Donau.xlsx" to "S_III.1.2.5-evanno.txt") for the genetic assignment. The STRUCTURE analysis reveals an overall strong signal of the blue with a

varying contribution of the orange cluster, without distinct patterns between the different subpopulations (Figure 3.3 B). The three northern sites (Knopfmacherfels, Sperberloch and Schloss Bronnen) are separated from the southern sites (Stiegelesfels and Forest as well as the Kaiserstand) by $\sim 1.3\text{km}$ to $\sim 2.1\text{km}$ (straight line) and $\sim 2\text{km}$ along the river Danube (Figure 3.4 A). The neighbor-net inferred groups show structuring with the red and dark green groups confined to the northern sites and the yellow group in the forest near Stiegelesfels. On the other hand, genetic connectivity can not only be found between closer sites in the north but also between the northern and southern groups. Despite the genetic exchange between the sites the number of pairwise genetic differences (Figure 3.4 B, C) differ, with significantly smaller amounts within growth sites (Mann Whitney U test, $p < 0.001$). The AMOVA result indicates $\sim 90\%$ of variation within the different subpopulations and $\sim 10\%$ of genetic variation originating from between the subpopulations ($p < 0.001$, 1023 permutations, fixation index $F_{ST} = \sim 0.10$). In most sites the common ht16 can be found while ht19 is only found in the Sperberloch.

3. Achtal and Blaubeuren

The subpopulations of the Achtal near Blaubeuren are divided into six genotype groups (Figure 3.5 A). The STRUCTURE analysis, with $K = 2$ as optimal K , as suggested by ΔK (Digital Supplement "S_III.1.3-Achtal" with "S_III.1.3.1-AFLP_Dg_Achtal.xlsx" to "S_III.1.3.5-evanno.txt"), reveals two clusters with the blue cluster contributing the most in nearly all subpopulations (Figure 3.5 B). Only the site Klötzle Blei, in the city of Blaubeuren, is mainly assigned to the orange cluster with a smaller orange signal emerging to its west at the Rusenschloss. The sites are distributed along the rocky outcrops of the river valleys of the Ach and Blau (Figure 3.6 A). Between the subpopulations, the neighbor-net genotypes indicated a high number of connections. Yet there is no complete mixing and still signs of structuring with some subpopulations only containing one genotype (e.g. Schneckenfels, Obere Peilerwand, Sirgenstein, Klötzle Blei). This differentiation is also indicated by the number of pairwise genetic differences (Figure 3.6 B, C), with significantly fewer differences within growth sites (Mann Whitney U test, $p < 0.001$). The AMOVA result also indicates $\sim 77\%$ of variation within the different sites and $\sim 23\%$ of genetic variation originating from between the populations ($p < 0.001$, 1023 permutations, fixation index $F_{ST} = \sim 0.23$). Between all subpopulations three haplotypes were found. Ht16 is found in the north western sites, ht21 spread between the Blaufels, Klötzle Blei, obere Peilerwand and southern most Schillerstein and ht29 restricted to the Sirgenstein.

4. Hausener Wand, Michelsberg

The genetic assignment using STRUCTURE identified two clusters, based on ΔK , at the Hausener Wand (Figure 3.7 B, Digital Supplement "S_III.1.4-Hausener Wand" with "S_III.1.4.1-AFLP_Dg_Hausener_Wand.xlsx" to "S_III.1.4.5-evanno.txt"). Nearly all individuals from the Jungfrauenfels (F1) are assigned to the orange cluster while the other

samples are assigned to the blue one. The two study plants from Jungfrauenfels (F1) not fully assigned to the orange cluster also differ in the neighbor-net analysis, where they are more distant from the closely clustered remaining samples from the site. The SplitsTree analysis indicates ten groups of genotypes (Figure 3.7 A) that are in good accordance with spatial distribution (Figure 3.8 A). The Hausener Wand is a rock face with single subpopulations of *D. gratianopolitanus* stretching over ~ 1.6 km. The inferred genotypes are mostly restricted to single rocky outcrops with only few evidence of dispersal events, e.g. the dark line connecting the Kleine Hausener Wand with the Große Hausener Wand. This structure is also visible at smaller distances at sites with more than one genotype, where the genotypes show a distinct spatial clustering, like the clusters at the Kleine Hausener Wand or the Jungfrauenfels (F1). The isolation of sites is also indicated by the number of pairwise genetic differences (Figure 3.8 B, C), where differences within subpopulations were significantly smaller (Mann Whitney U test, $p < 0.001$). The results of the AMOVA indicates $\sim 77\%$ of variation within the different sites and $\sim 23\%$ of genetic variation originating from between the populations ($p < 0.001$, 1023 permutations, fixation index $F_{ST} = \sim 0.23$). Ht16 is found in every site, while the Jungfrauenfels (F1) also has ht29.

5. Eybtal near Eybach

The results for the study site at the Eybtal (near Eybach) are shown in Figure 3.9 and Figure 3.10. The neighbor-net analysis (Figure 3.9 A) indicates ten groups, with three groups only including one individual. The optimal number of clusters for genetic assignment is $K = 6$ according to ΔK (Digital Supplement "S_III.1.5-Eybtal" with "S_III.1.5.1-AFLP_Dg_Eybtal.xlsx" to "S_III.1.5.5-evanno.txt"). While the two analyses are overall in good accordance, the differences between neighbor-net genotypes indicated by the STRUCTURE analysis, e.g. wine red cluster from the Schulterfels, can also be recalled in the SplitsTree analysis, where the group is separated from neighboring genotypes but also reflect the observed differences within the group. The grouping suggested by the neighbor-net analysis is in good accordance with their spatial distribution, where most genotypes are restricted to one rock outcrop on the course of the river Eyb (Figure 3.10 A). The only observed connection is between the Spielerwand and the subpopulation West of Waldhausen separated by the valley and river Eyb as well as the city of Eybach ($\sim 700 - 800$ m straight line). The missing evidence of dispersal events between the closer populations (Schulterfels, Donaldfels, Nadelfels, and the population West of Steinenkirch) and the distinct clustering of genotypes are indicating the isolation of subpopulations. The pairwise genetic differences (Figure 3.10 B, C) reveal significantly smaller amounts of differences within the growth sites as compared to between them (Mann Whitney U test, $p < 0.001$) supporting the idea of isolation and limited gene flow between the sites. The AMOVA of genetic variation indicates $\sim 78\%$ of variation within the different sites and $\sim 22\%$ of genetic variation originating from between the populations ($p < 0.001$, 1023 permutations, fixation index $F_{ST} = \sim 0.22$). While ht16 is found in the most northern but also at the Drehfels in the south. In addi-

tion three haplotypes are restricted to specific sites: ht01 at the Spielerwand, ht19 West of Waldhausen and ht30 at the Schulterfels.

6. Nature reserve Ehrenbürg

The study plants from the nature reserve Ehrenbürg are divided into seven groups by the SplitsTree analysis and into two groups, $K = 2$, by the STRUCTURE analysis (Figure 3.11). Optimal K was inferred using ΔK (Digital Supplement "S_III.1.6-Ehrenbürg" with "S_III.1.6.1-AFLP_Dg_Ehrenbuerg.xlsx" to "S_III.1.6.5-evanno.txt"). The subpopulation from the study site within the forest differs from the other two, showing two distinct neighbor-net genotypes, red and yellow, that are separated from the remaining network. Especially the yellow group shows a higher assignment to the orange cluster within the STRUCTURE analysis. As already suggested by the SplitsTree grouping the genotypes are also spatially structured, with the yellow and red genotypes restricted to the southern forest while the two green genotypes are restricted to the area around the Rodenstein (Figure 3.12 A). The light blue genotype is the most widely spread and is found in greater numbers at the Einsiedlerhöhle but has also single occurrences at the Rodenstein and in the Forest. The dark blue genotype is the other one with evidence of dispersal with most occurrences around the Rodenstein with a single occurrence at the south side of the Einsiedlerhöhle. Here pairwise genetic differences (Figure 3.12 B, C) also indicate the isolation of the different subpopulations by significantly smaller amounts of differences within the growth sites as compared to between them (Mann Whitney U test, $p < 0.001$). The AMOVA also finds the major contributor of genetic variation to be within the sites ($\sim 82\%$) and only a smaller contribution from between the population ($\sim 18\%$; $p < 0.001$, 1023 permutations, fixation index $F_{ST} = \sim 0.18$). Ht16 is the only haplotype found in all sites.

7. Blankenberg and Höllental

The study sites at Höllental and Blankenberg are near the river Seibitz and at a river loop of the river Saale, respectively. They are separated by the Saale and a wooded hilltop (~ 1.7 to ~ 2 km, straight line) or by ~ 3.6 km following valley of the course of the rivers. The Papierfabrik and Blankenberg are only separated by ~ 200 m. The neighbor-net analysis splits the study plants into five groups (Figure 3.13 A), with one group, lime green, being restricted to Blankenberg, while the others show a more mixed signal. STRUCTURE analysis with an optimal K of $K = 7$, (Figure 3.13 B, ΔK in Digital Supplement "S_III.1.7-Blankenberg_Höllental" with "S_III.1.7.1-AFLP_Dg_Bl_Hoe.xlsx" to "S_III.1.7.5-evanno.txt") shows a baseline mixed signal throughout all included samples, with a clearer division based on the assignment to the orange cluster (Blankenberg) and blue cluster (Höllental). This clear distinction is in contrast to the strong intermixing of the neighbor-net genotypes that occur in both study sites (Figure 3.14 A). While four of the five genotypes are found in Blankenberg as well as Höllental the number of occurrences differs with more occurrences of the yellow and red genotypes at Blankenberg and the Papierfabrik

while the blue and dark green have a higher rate in Höllental. While the frequency distribution of pairwise differences overlap to a higher degree the overall number of differences is also higher between different sites than within sites (Figure 3.14 B C, Mann Whitney U test, $p < 0.001$). The AMOVA of genetic variation indicates $\sim 93\%$ of variation within the different sites and $\sim 7\%$ of genetic variation originating from between the populations ($p < 0.001$, 1023 permutations, fixation index $F_{ST} = \sim 0.07$). Ht02 is present in all sites with the Papierfabrik also showing one occurrence of ht16.

8. Saale Tal from Burgk to the Bleiberg

The study site from Burgk to the nature reserve Bleiberg is downstream from Blankenberg and also follows the course of the Saale River for $\sim 5\text{km}$ covering the area between the dams Bleilochtsperre and Burgkammer. The population at Burgk is $\sim 2.5\text{km}$ downstream of the population at Hängesteig with the Eisbrücke in the middle. The Hängesteig is also $\sim 2.5\text{km}$ downstream of the population at the nature reserve Bleiberg. Bleiberg and Burgk are separated by a river loop of the Saale and a wooded hilltop ($\sim 2.9\text{km}$ straight line). The 76 included study plants are divided into twelve groups (Figure 3.15 A). Genetic assignment using STRUCTURE with $K = 3$ as optimal K suggested by ΔK (Digital Supplement "S_III.1.8-Burgk" with "S_III.1.8.1-AFLP_Dg_Burgk.xlsx" to "S_III.1.8.5-evanno.txt"). Individuals from the Bleiberg subpopulation show a higher attribution to the pink cluster mixed with the blue cluster (Figure 3.15 B). Most individuals of the next downstream subpopulation, at the Hängesteig, are mainly assigned to the blue cluster with single plants showing a higher signal of the pink cluster as well as some that show a strong signal of the orange cluster. As shown by the geographical distribution given in Figure 3.16 A, a lot of the defined genotypes are present in different subpopulations, indicating dispersal events and possible ongoing genetic exchange between the sites. While the three closer sites Hängesteig, Eisbrücke, and Burgk show genetic connectivity, two genotypes (dark green and aquamarine) are only shared between the distant Bleiberg and Burgk populations. Some genotypes are widely distributed (e.g. the wine red present in all sites) the biggest sampled site at Hängesteig also has three (rosé, dark blue, and light blue) and Burgk one unique genotype (lime green). The number of pairwise differences within and between sites also show smaller but significant differences (Figure 3.16 B, C; Mann Whitney U test, $p < 0.001$). In addition, the results of the AMOVA indicate the within-site variation to be the major source with $\sim 92\%$. Only $\sim 8\%$ of genetic variation originates from between the populations ($p < 0.001$, 1023 permutations, fixation index $F_{ST} = \sim 0.08$). Ht19 is restricted to the Bleiberg while ht16 is shared between Burgk and the Hängesteig. Ht21 has single occurrences in the Hängesteig and Eisbrücke.

9. Schwarzatal near Böhlscheiben and Schwarzburg

The Schwarzatal follows the course of the river Schwarza with the first site at Trippstein followed by the second site Kirchefels ($\sim 4.3\text{km}$ straight line) and the Griesbachfels ($\sim 950\text{m}$

straight line). The neighbor-net analysis divides the study plants into eight groups (Figure 3.17 A). The optimal K for the genetic assignment with STRUCTURE was $K = 6$ (Digital Supplement "S_III.1.9-Schwarzatal" with "S_III.1.7.1-AFLP_Dg_Schwarz.xlsx" to "S_III.1.9.5-evanno.txt"). The two populations near Böhlscheiben (Griesbach- and Kirchfels) show a higher assignment to the blue cluster, while those from Griesbachfelsen also show higher levels of the pale green cluster (Figure 3.17 B). Individuals from the Trippstein show higher levels of the orange as well as the pink cluster. The SplitsTree neighbor net is in good accordance with the spatial distribution of genotypes (Figure 3.18 A). While the dark and light blue genotypes are restricted to the Griesbachfels, the lime green, dark green, bluegreen, and light sky blue are restricted to the Kirchfels. Trippstein has two genotypes, yellow and red, with the red one also showing a single occurrence at Kirchfels. Molecular differences are fewer within sites as compared to between (Figure 3.16 B, C; Mann Whitney U test, $p < 0.001$) The AMOVA of genetic variation indicates $\sim 85\%$ of variation within the different sites and $\sim 15\%$ of genetic variation originating from between the populations ($p < 0.001$, 1023 permutations, fixation index $F_{ST} = \sim 0.15$). All three sites have haplotypes restricted to them, with ht16 at the Griesbachfels, ht01 at the Kirchfels and ht21 at the Trippstein.

10. Kellerwald-Edersee

The study site at the nature reserve Kellerwald Edersee includes the two bigger subpopulations at the Nelkenstieg and Blossenberg that are separated by the loop of the namesake river Eder ($\sim 3\text{km}$ straight line). In addition, samples from the Wooghölle, separated from the Blossenberg by the Banf Bach ($\sim 250\text{m}$ straight line) and samples from the adjoining pine forest ($\sim 650\text{m}$ straight line) are included. The study plants are divided into six genotype groups by the SplitsTree results (Figure 3.19 A). The STRUCTURE analysis reveals two genetic clusters, a mainly blue one at the Blossenberg and a higher degree of orange contribution at the Nelkenstieg (Figure 3.19 B). The optimal K was inferred using ΔK (Digital Supplement "S_III.1.10-Edersee" with "S_III.1.10.1-AFLP_Dg_Eder.xlsx" to "S_III.1.10.5-evanno.txt"). The dark- and light-green genotypes are restricted to the Nelkenstieg, while the yellow and orange ones are confined to the Blossenberg and Pine forest (Figure 3.20 A). The red and blue ones have a higher rate in Blossenberg, Wooghölle, and the Pine forest but also occur in low numbers at the Nelkenstieg, indicating possible dispersal events from Blossenberg to Nelkenstieg. Also here more molecular differences are observed between sites as compared to within (Figure 3.20 B, C; Mann Whitney U test, $p < 0.001$). The AMOVA results show the variation within sites to be the main contributor to the overall genetic variation ($\sim 88\%$) while only $\sim 12\%$ of genetic variation originates from between the populations ($p < 0.001$, 1023 permutations, fixation index $F_{ST} = \sim 0.12$). Ht01 is found at the Blossenberg and adjacent forest and ht29 is restricted to the northern Nelkenstieg. Ht30 is found at both the northern Nelkenstieg and the southern Blossenberg and Wooghölle.

11. Nature reserve Gans and Rheingrafenstein

The smallest study sites is at the nature reserve Gans and Rheingrafenstein consisting of the two rock faces at the Gans and the Rheingrafenstein separated by a short stretch of wood ($\sim 600\text{m}$ straight line) at the banks of the river Nahe. A total of 20 samples were collected and split into five genotype groups using SplitsTree (Figure 3.21 A). While all genotype groups can be found in Rheingrafenstein, only three are present at Gans. ΔK suggests $K = 3$ as optimal K (Digital Supplement "S_III.1.11-Gans" with "S_III.1.11.1-AFLP_Dg_Gans.xlsx" to "S_III.1.11.5-evanno.txt"). The STRUCTURE results indicate a mixture of the three clusters without a clear distinction between sites (Figure 3.21 B). The geographic distribution of the neighbour-net genotypes shows no clear structuring at Rheingrafenstein while the green genotype at Gans is slightly separated from the yellow and red. Despite the strong mixture of genotypes, the number of molecular differences is still lower within the sites as compared to between (Figure 3.22 B, C; Mann Whitney U test, $p < 0.001$) and the AMOVA reveals $\sim 88\%$ of variation within the different sites and $\sim 12\%$ of genetic variation originating from between the populations ($p < 0.001$, 1023 permutations, fixation index $F_{ST} = \sim 0.12$). No plastid marker haplotypes were available for this population.

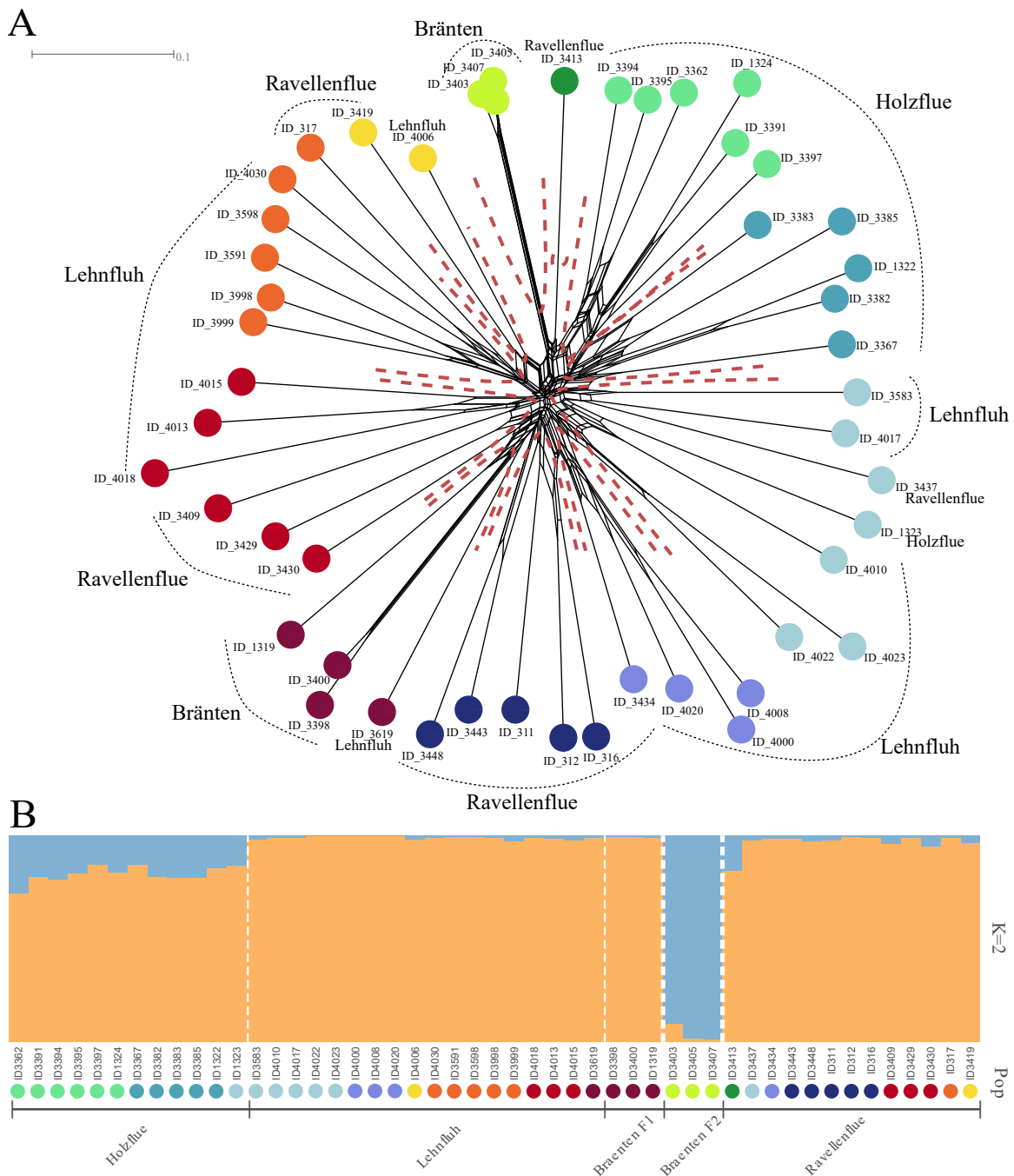
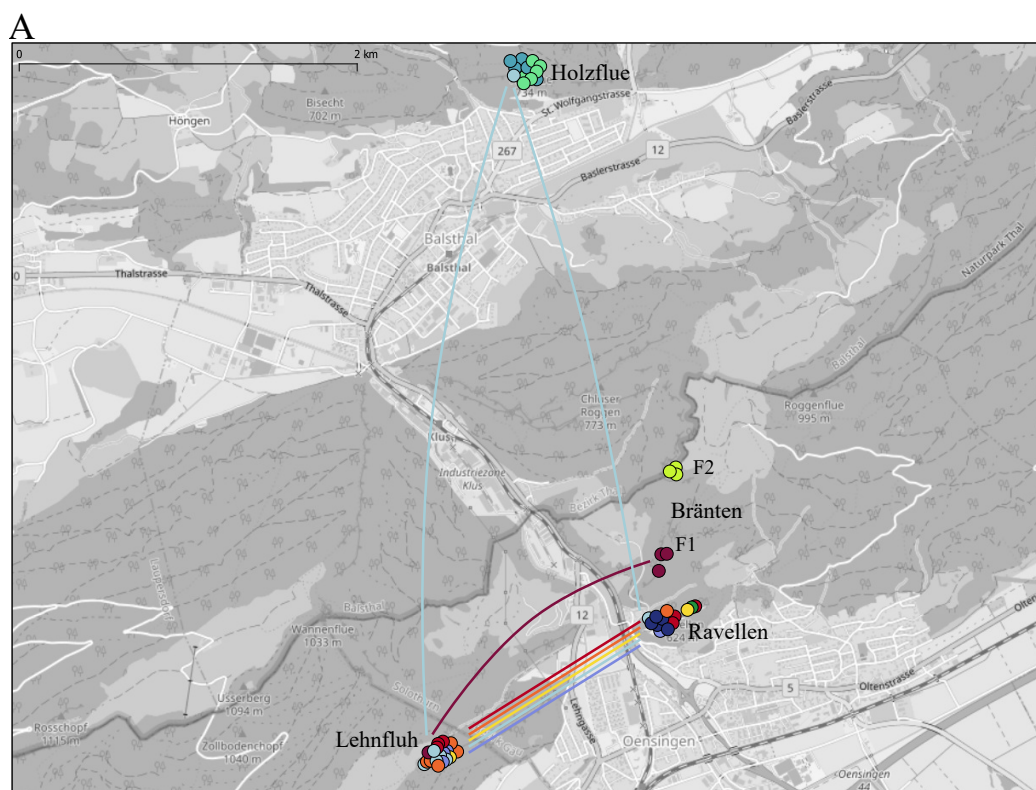


Figure 3.1: *SplitsTree* and *STRUCTURE* analysis for Populations from Oensingen and Balsthal, Switzerland. **A** *SplitsTree* analysis of AFLP data. Colors indicate resulting genotype groups, dashed lines indicate subpopulations. **B** Genetic assignment with *STRUCTURE* ($K=2$), coloured based on the *SplitsTree* analysis (A).



Molecular differences between and within growth sites

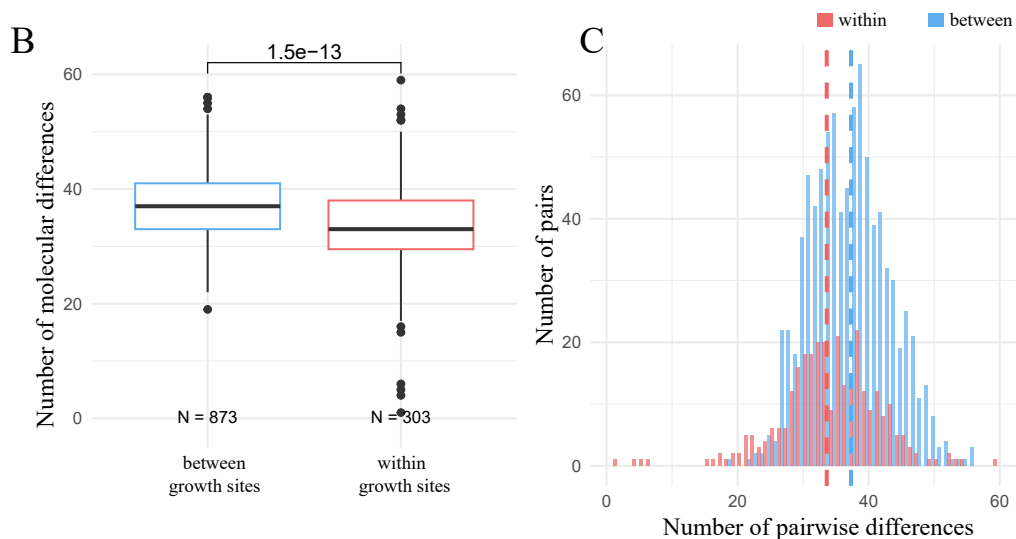


Figure 3.2: *D. gratianopolitanus* and molecular differences (AFLP fragments) for populations from Ravellenflue, Lehnfluh and Holzflue, Switzerland **A** Geographic distribution in Ravellenflue, Lehnfluh and Holzflue, coloured based on SplitsTree grouping. Coloured lines indicate possible dispersal events of the according coloured genotype. **B** Number of molecular differences between and within the growth sites, **C** Frequency distribution of molecular differences as shown in B). Dashed lines indicate mean values.

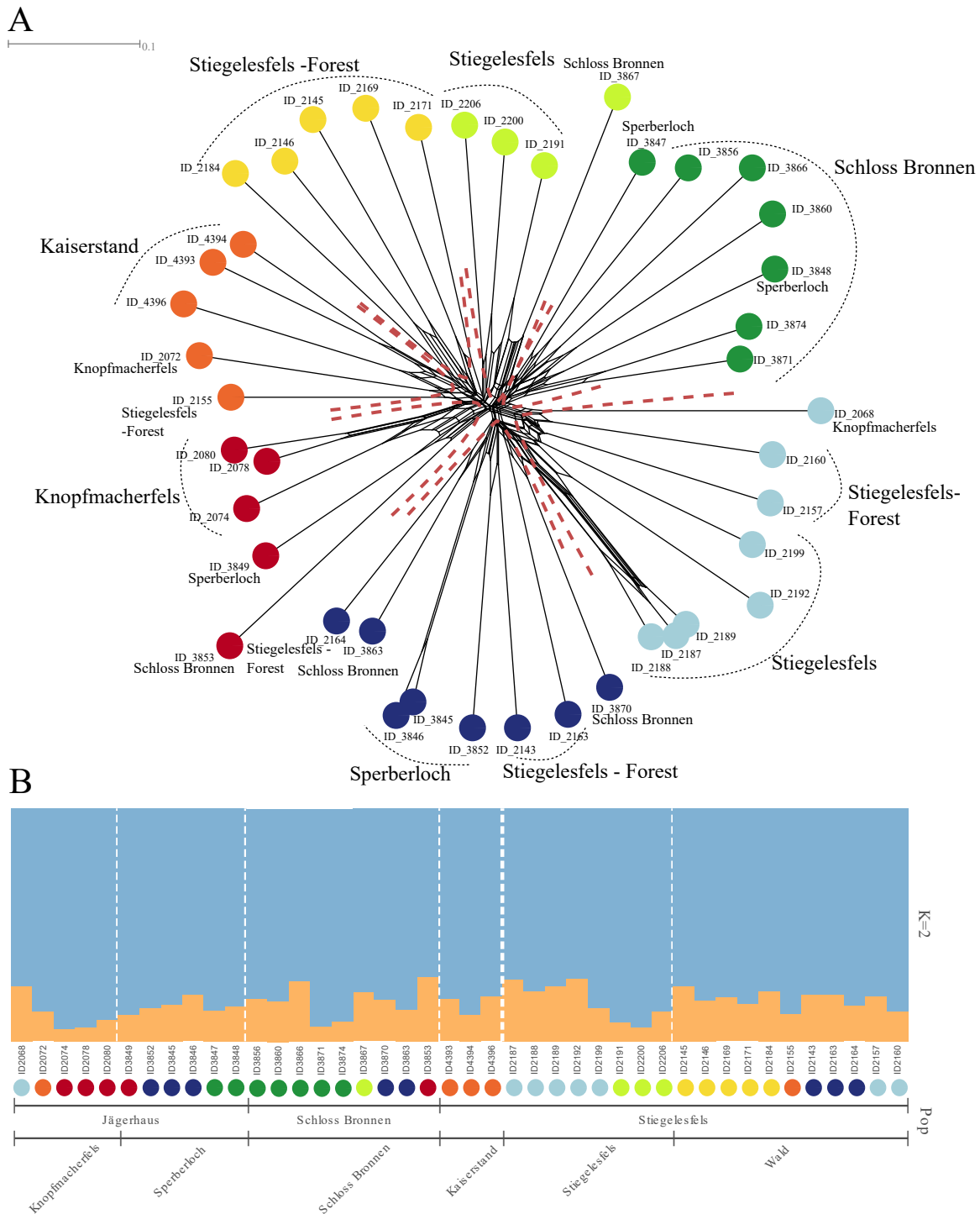
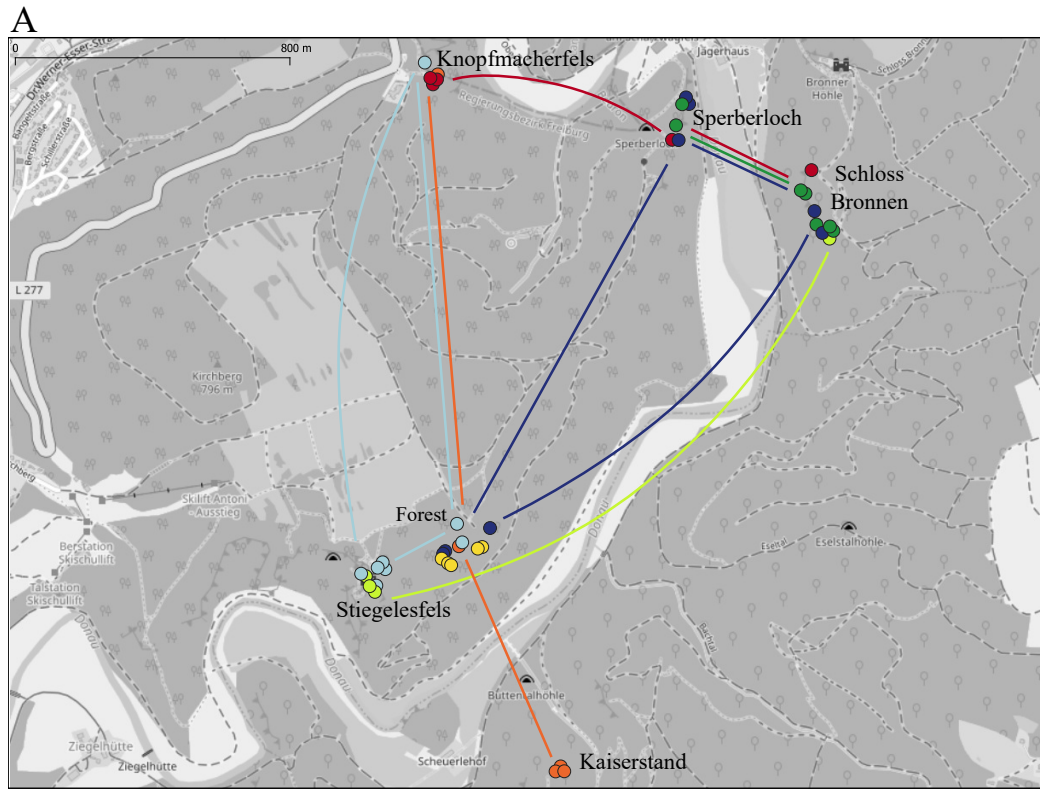


Figure 3.3: *SplitsTree* and *STRUCTURE* analysis for Populations from the Danube valley near Friedingen an der Donau. **A** *SplitsTree* analysis of AFLP data. Colors indicate resulting genotype groups, dashed lines indicate subpopulations. **B** Genetic assignment with *STRUCTURE* ($K=2$), coloured based on the *SplitsTree* analysis (A).



Molecular differences between and within growth sites

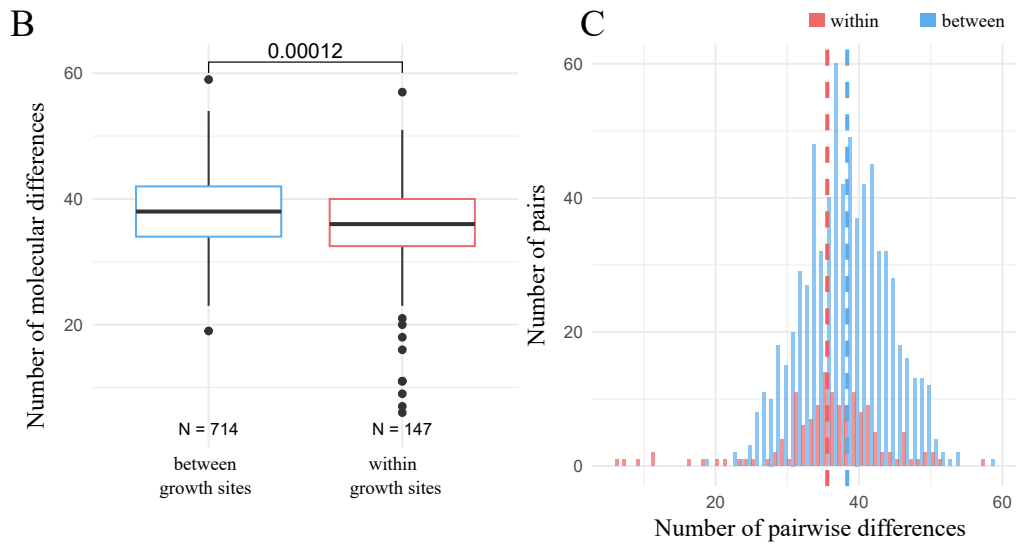


Figure 3.4: *Distribution of *D. gratianopolitanus* and molecular differences (AFLP fragments) for populations from the Danube valley near Friedingen an der Donau. A Geographic distribution in the Danube valley, coloured based on SplitsTree grouping. Coloured lines indicate possible dispersal events of the according coloured genotype. B Number of molecular differences between and within the growth sites, C Frequency distribution of molecular differences as shown in B). Dashed lines indicate mean values.*

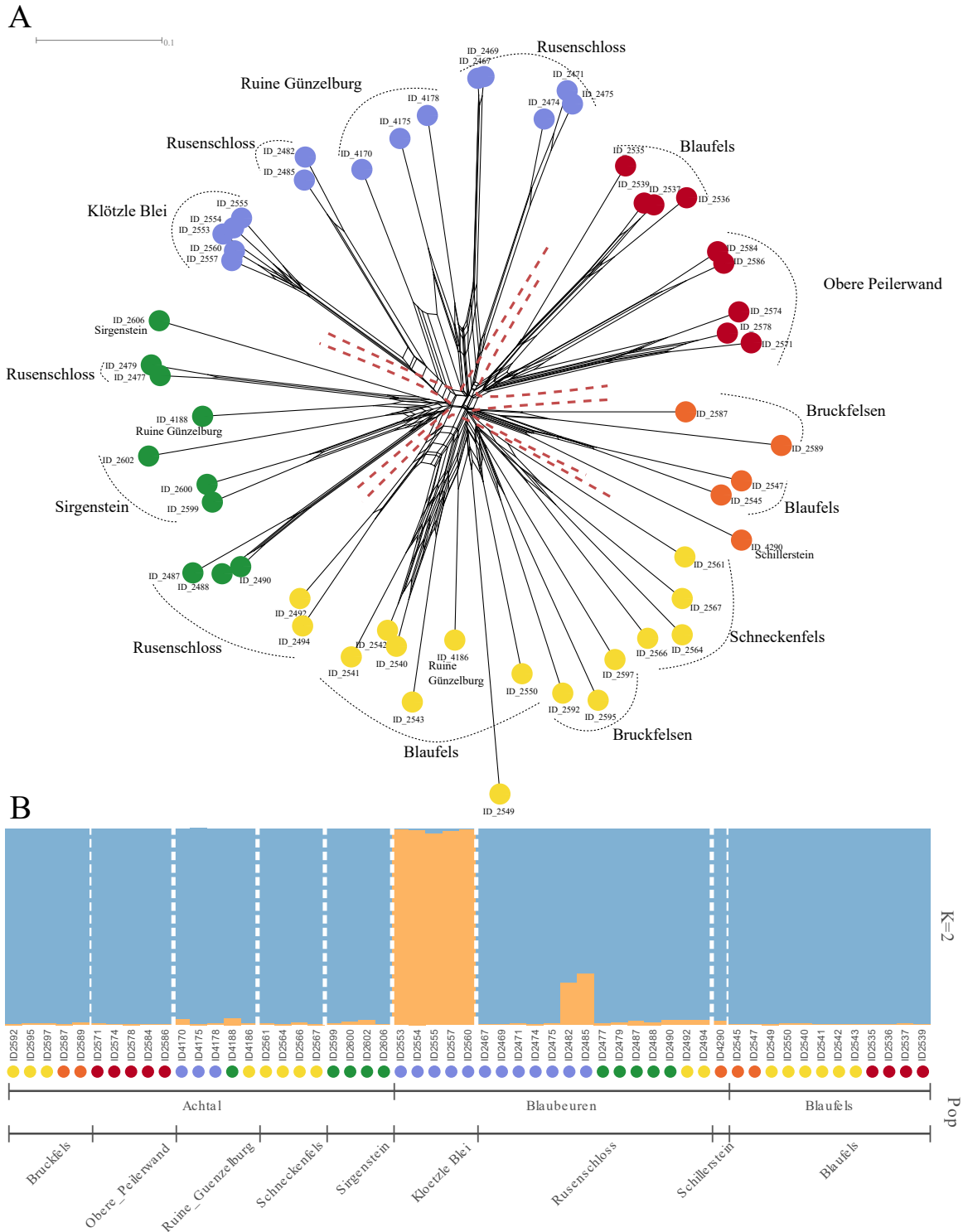
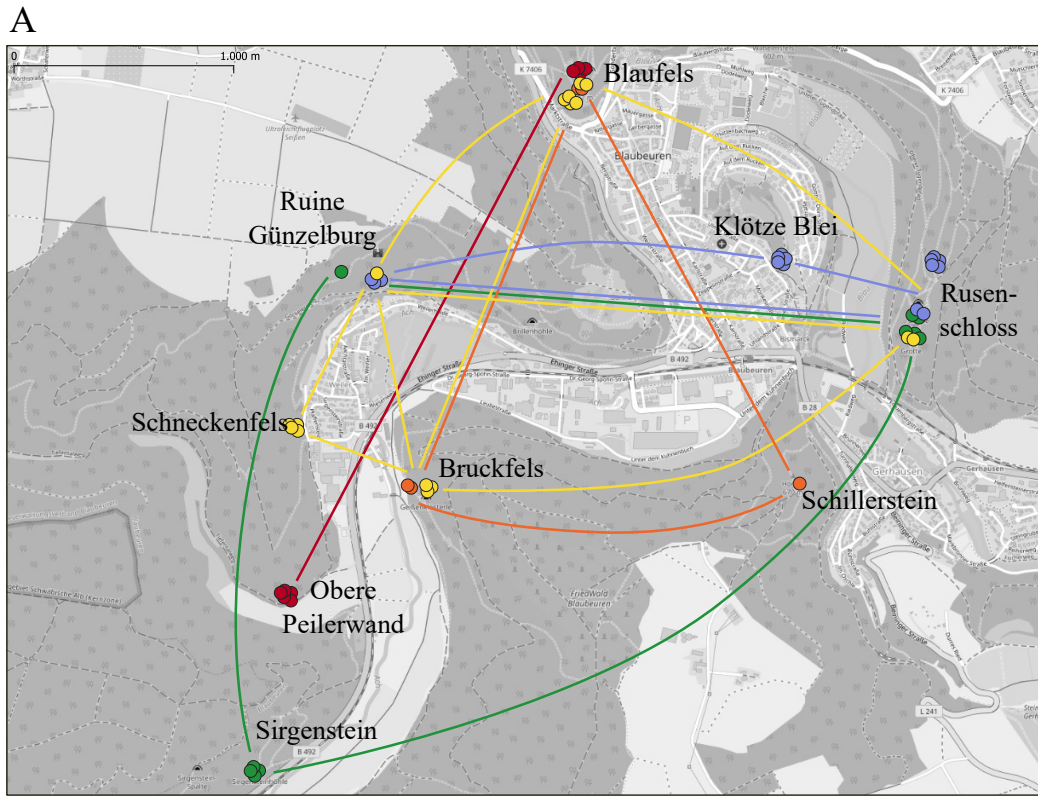


Figure 3.5: SplitsTree and STRUCTURE analysis for Populations from Achthal and Blaubeuren. **A** SplitsTree analysis of AFLP data. Colors indicate resulting genotype groups, dashed lines indicate subpopulations. **B** Genetic assignment with STRUCTURE ($K=2$), coloured based on the SplitsTree analysis (A).



Molecular differences between and within growth sites

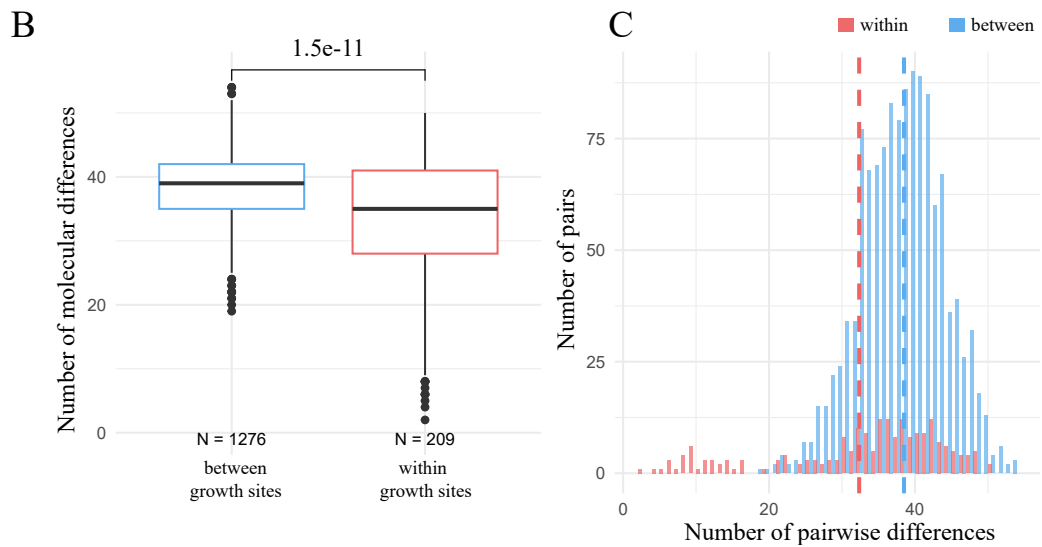
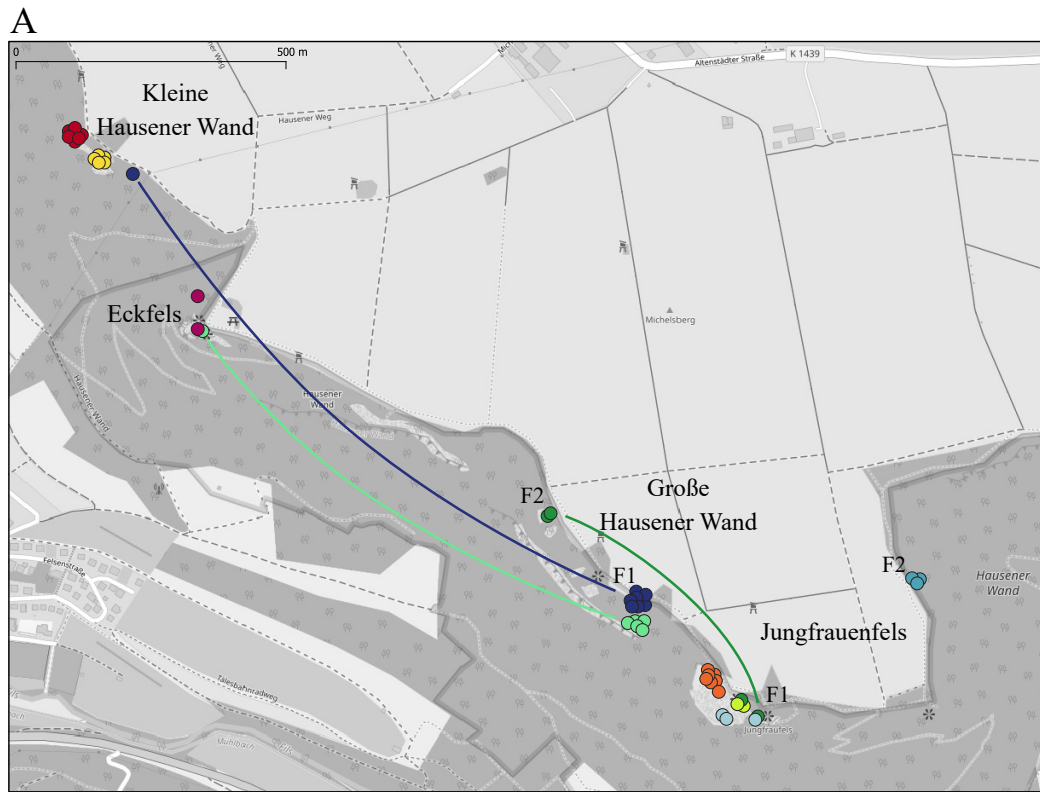


Figure 3.6: *Distribution of *D. gratianopolitanus* and molecular differences (AFLP fragments) for populations from Blaubeuren and the Aichtal.* **A** Geographic distribution in the Aichtal near Blaubeuren, coloured based on SplitsTree grouping. Coloured lines indicate possible dispersal events of the according coloured genotype. **B** Number of molecular differences between and within the growth sites, **C** Frequency distribution of molecular differences as shown in B). Dashed lines indicate mean values.



Molecular differences between and within growth sites

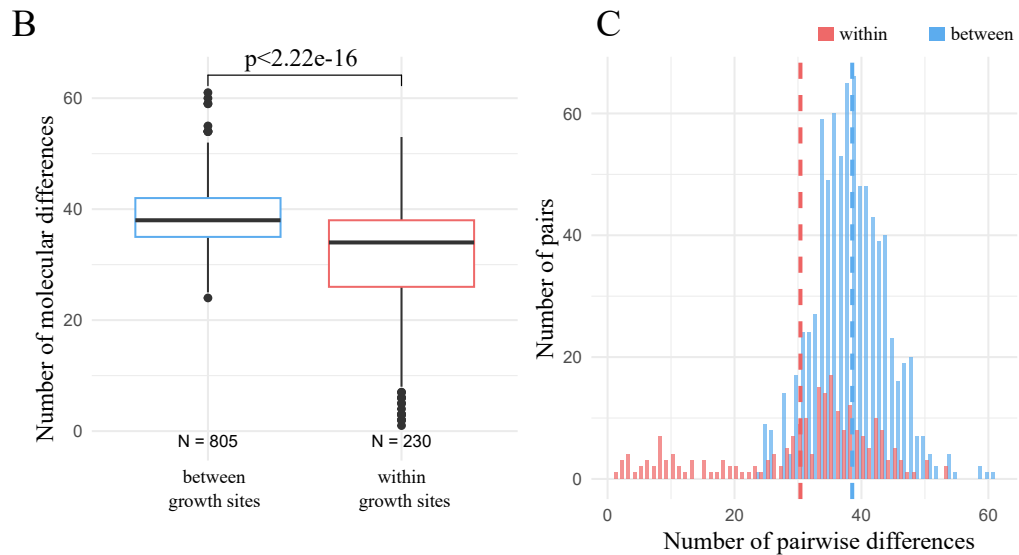


Figure 3.8: *Distribution of *D. gratianopolitanus* and molecular differences (AFLP fragments) for populations from the Hausener Wand, Michelsberg. A Geographic distribution at the Hausener Wand, coloured based on SplitsTree grouping. Coloured lines indicate possible dispersal events of the according coloured genotype. B Number of molecular differences between and within the growth sites, C Frequency distribution of molecular differences as shown in B). Dashed lines indicate mean values.*

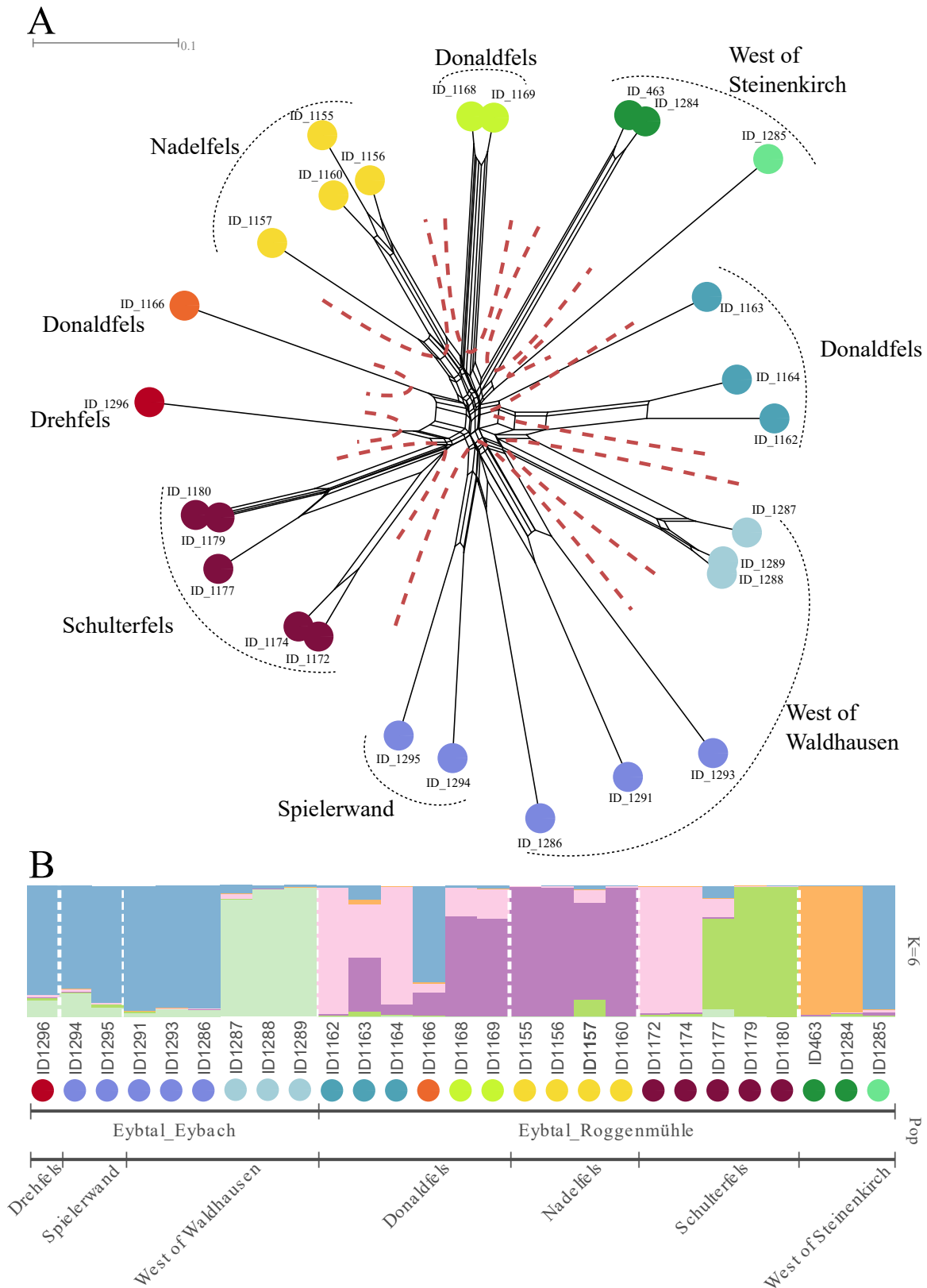
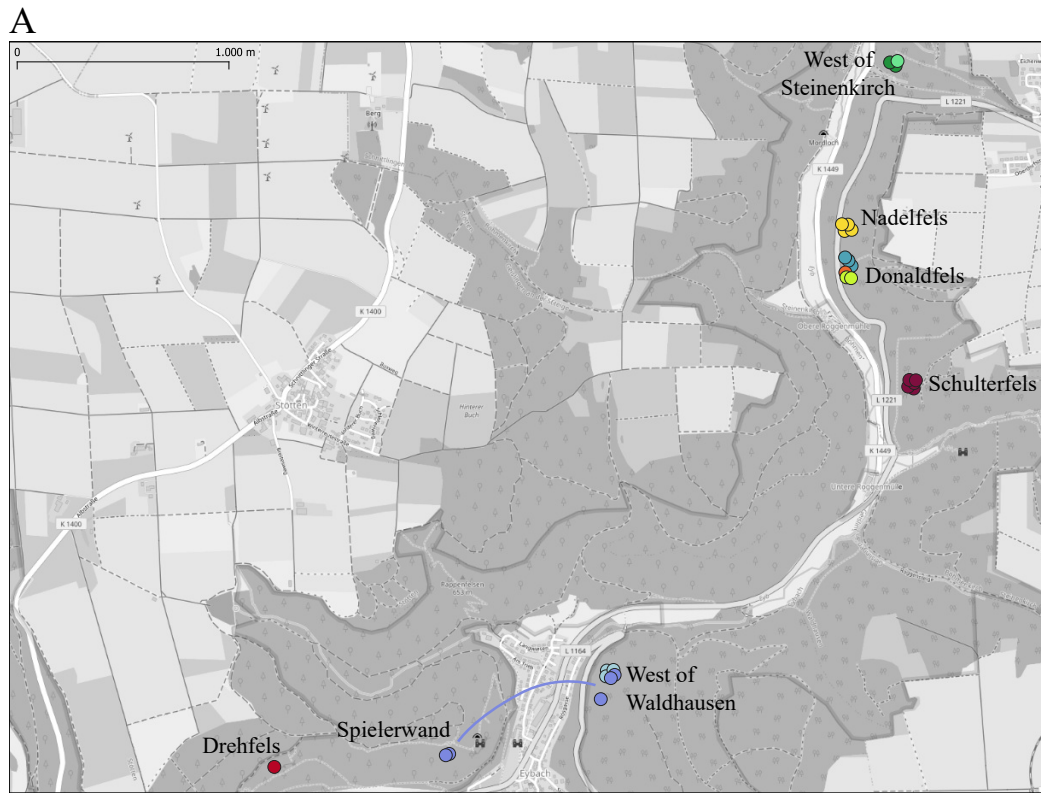


Figure 3.9: SplitsTree and STRUCTURE analysis for Populations from the Eybtal near Eybach. **A** SplitsTree analysis of AFLP data. Colors indicate resulting genotype groups, dashed lines indicate subpopulations. **B** Genetic assignment with STRUCTURE ($K=6$), coloured based on the SplitsTree analysis (A).



Molecular differences between and within growth sites

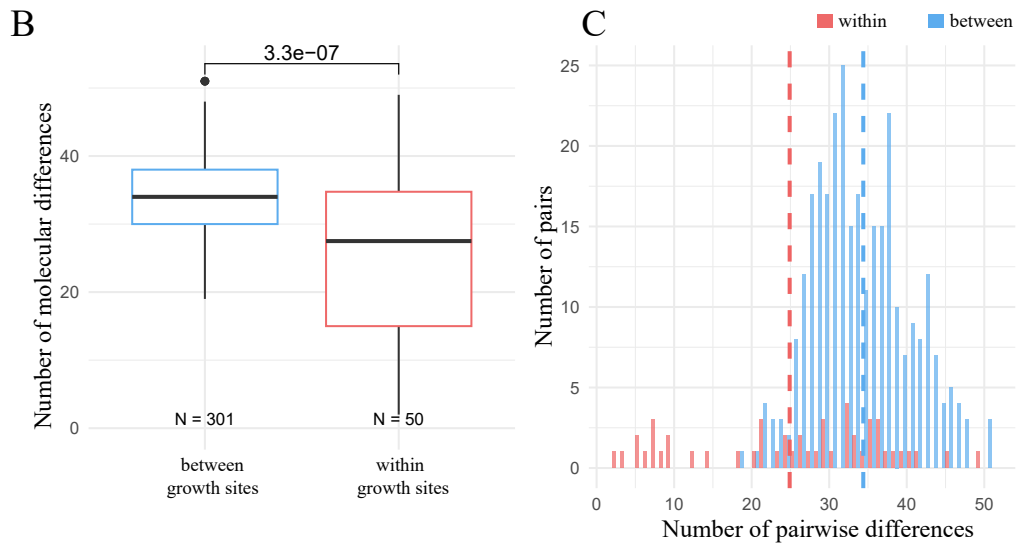


Figure 3.10: Distribution of *D. gratianopolitanus* and molecular differences (AFLP fragments) for populations from the Eybtal near Eybach. A Geographic distribution in the Eybtal, coloured based on SplitsTree grouping. Coloured lines indicate possible dispersal events of the according coloured genotype. B Number of molecular differences between and within the growth sites, C Frequency distribution of molecular differences as shown in B). Dashed lines indicate mean values.

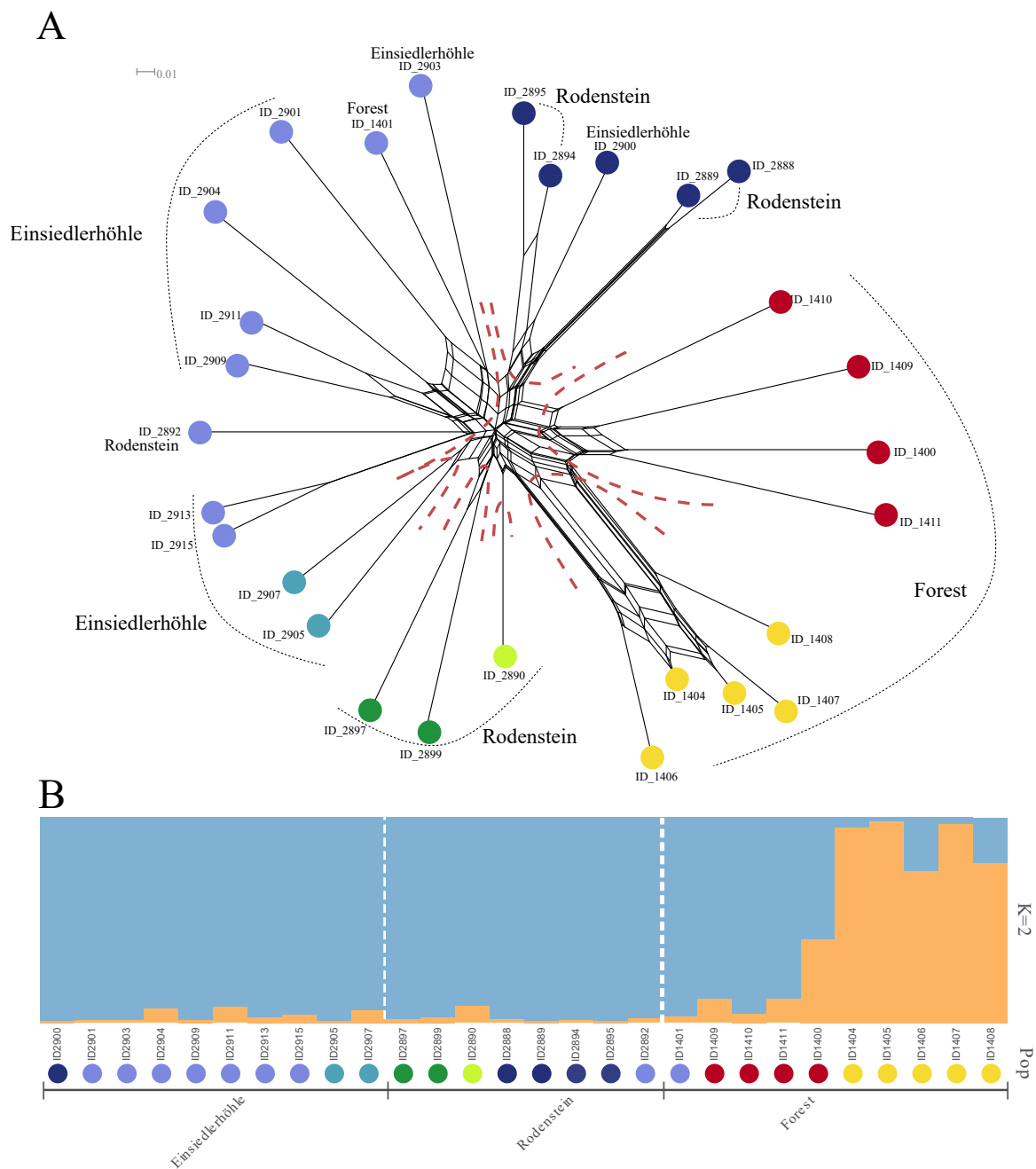
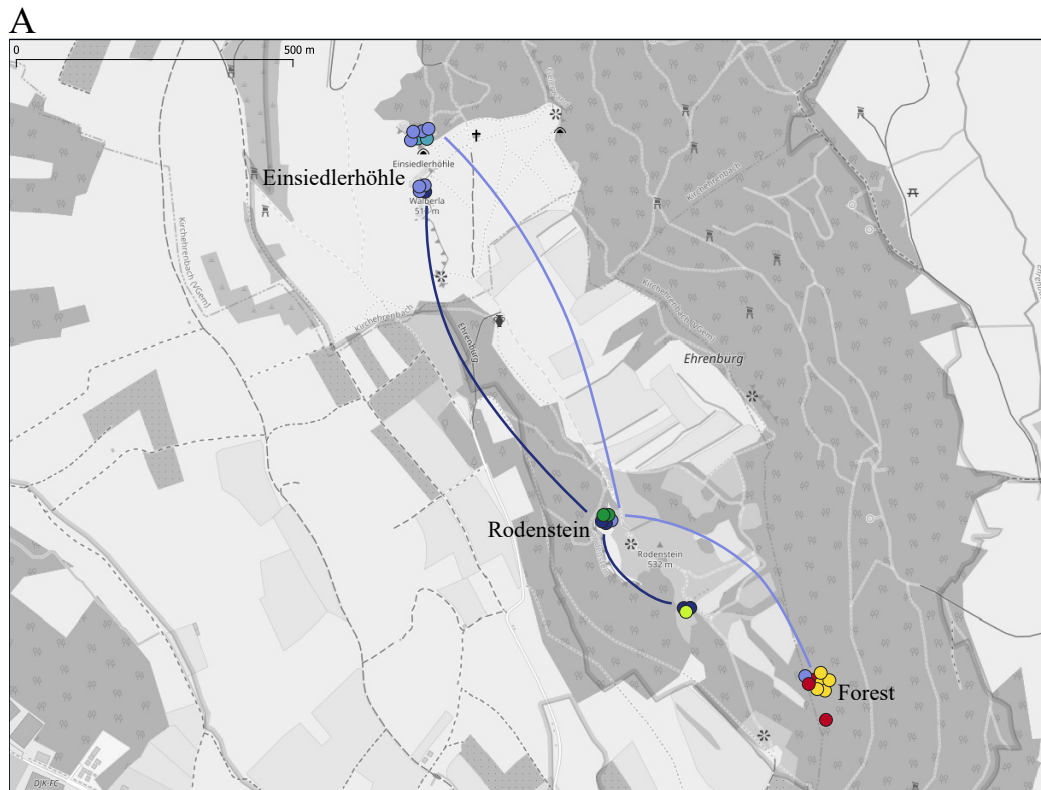


Figure 3.11: *SplitsTree* and *STRUCTURE* analysis for Populations from the nature reserve Ehrenbürg, Bavaria. **A** *SplitsTree* analysis of AFLP data. Colors indicate resulting genotype groups, dashed lines indicate subpopulations. **B** Genetic assignment with *STRUCTURE* ($K=2$), coloured based on the *SplitsTree* analysis (A).



Molecular differences between and within growth sites

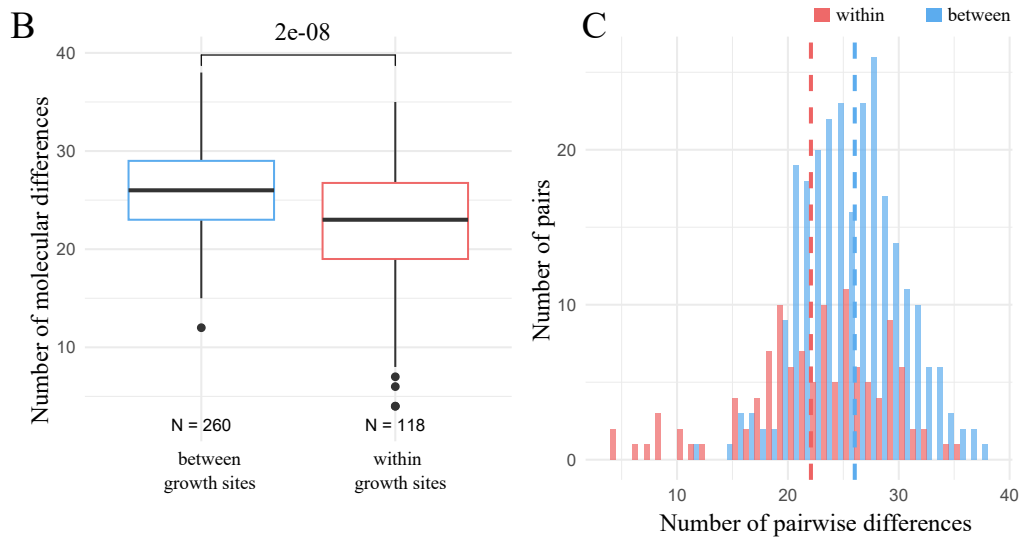


Figure 3.12: Distribution of *D. gratianopolitanus* and molecular differences (AFLP fragments) for populations from the nature reserve Ehrenbürg, Bavaria. A Geographic distribution in the nature reserve Ehrenbürg, coloured based on SplitsTree grouping. Coloured lines indicate possible dispersal events of the according coloured genotype. **B** Number of molecular differences between and within the growth sites, **C** Frequency distribution of molecular differences as shown in B). Dashed lines indicate mean values.



Molecular differences between and within growth sites

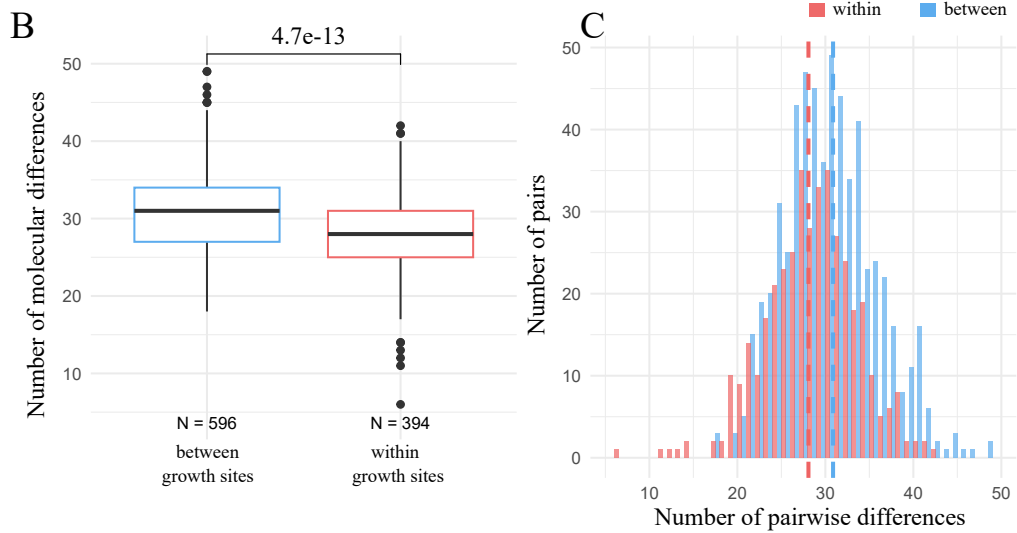


Figure 3.14: Distribution of *D. gratianopolitanus* and molecular differences (AFLP fragments) for populations from Blankenberg and Höllental. A Geographic distribution at Blankenberg and Höllental, coloured based on SplitsTree grouping. Coloured lines indicate possible dispersal events of the according coloured genotype. **B** Number of molecular differences between and within the growth sites, **C** Frequency distribution of molecular differences as shown in B). Dashed lines indicate mean values.

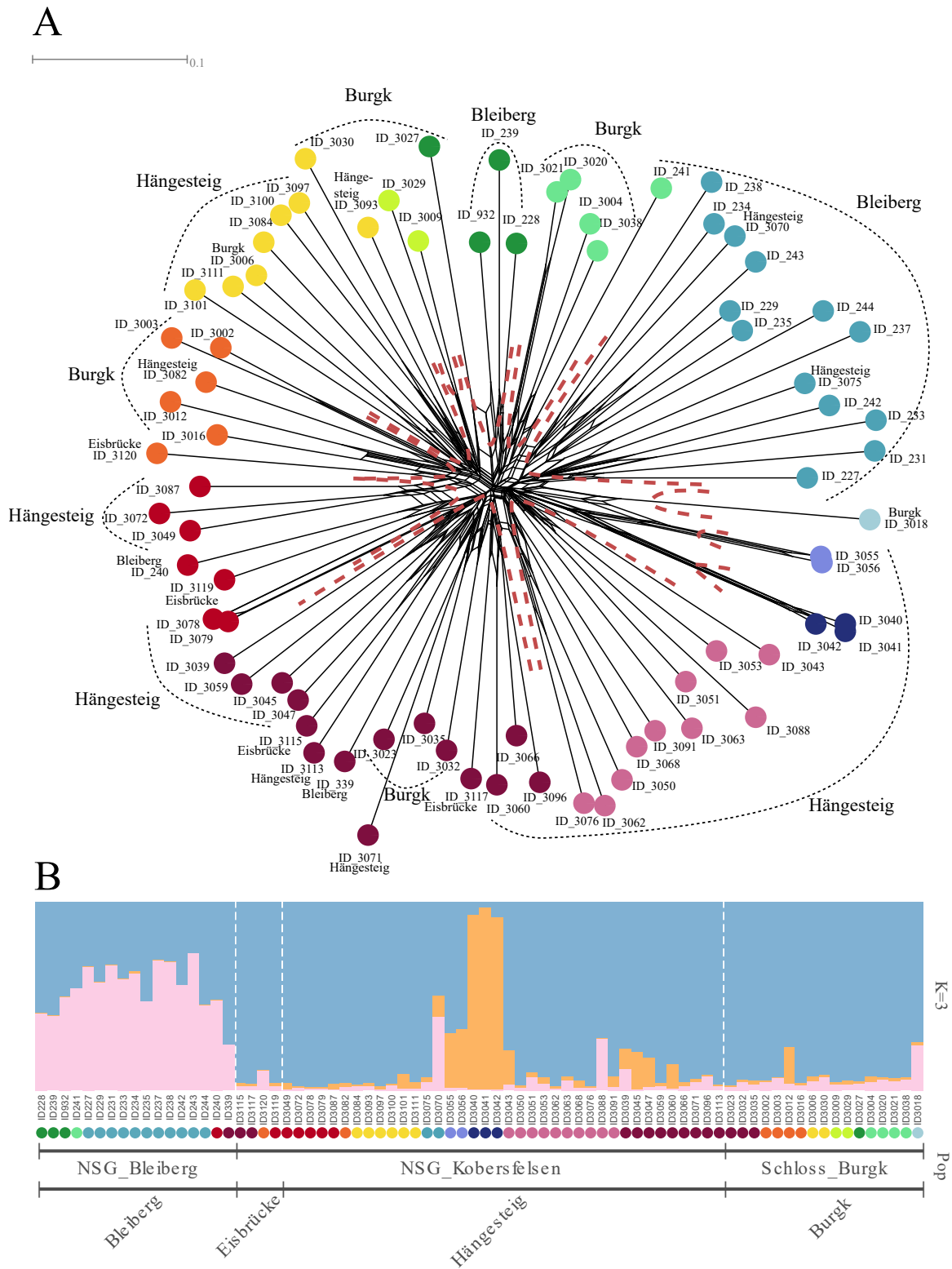
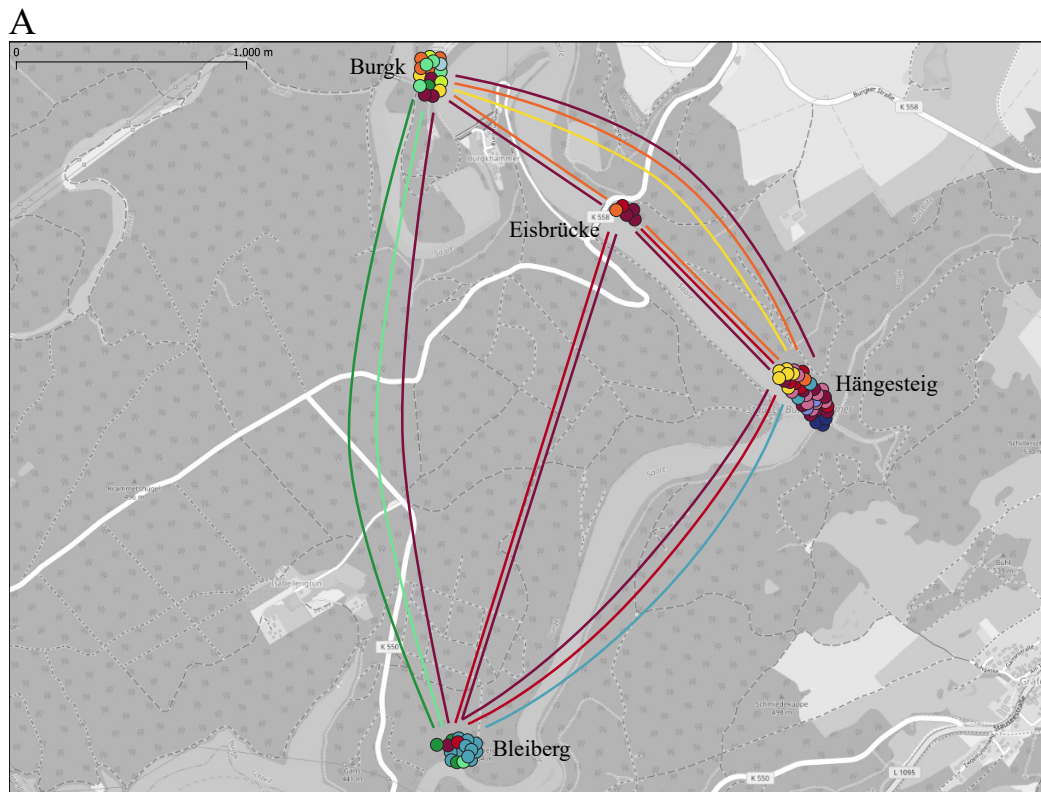


Figure 3.15: SplitsTree and STRUCTURE analysis for Populations from the nature reserve Korberfels and Bleiberg near Burgka SplitsTree analysis of AFLP data. Colors indicate resulting genotype groups, dashed lines indicate subpopulations. **B** Genetic assignment with STRUCTURE ($K=3$), coloured based on the SplitsTree analysis (A).



Molecular differences between and within growth sites

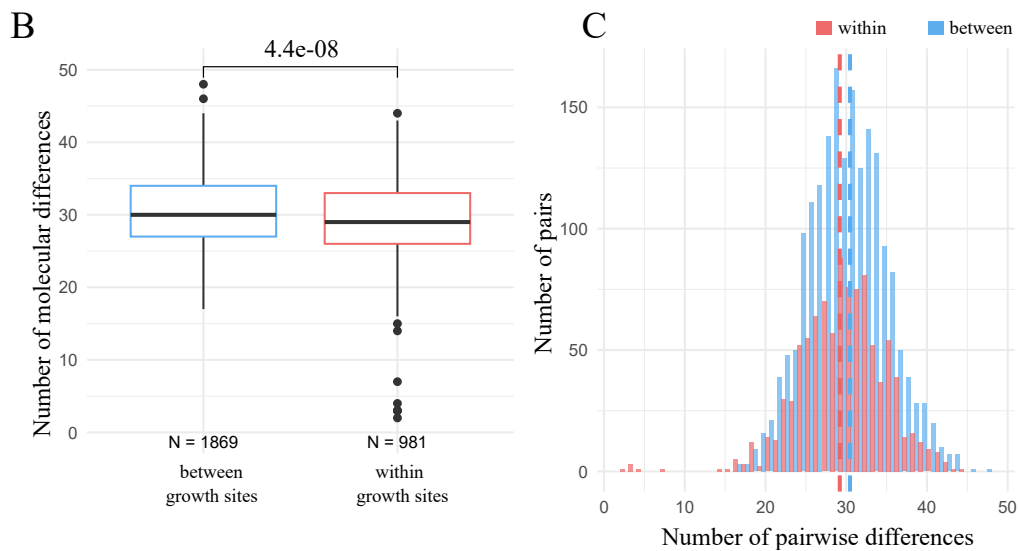


Figure 3.16: *Distribution of *D. gratianopolitanus* and molecular differences (AFLP fragments) for populations from the nature reserve Korberfels and Bleiberg near Burgk. A* Geographic distribution along the Saale Tal near Burgk, coloured based on SplitsTree grouping. Coloured lines indicate possible dispersal events of the according coloured genotype. **B** Number of molecular differences between and within the growth sites, **C** Frequency distribution of molecular differences as shown in B). Dashed lines indicate mean values.

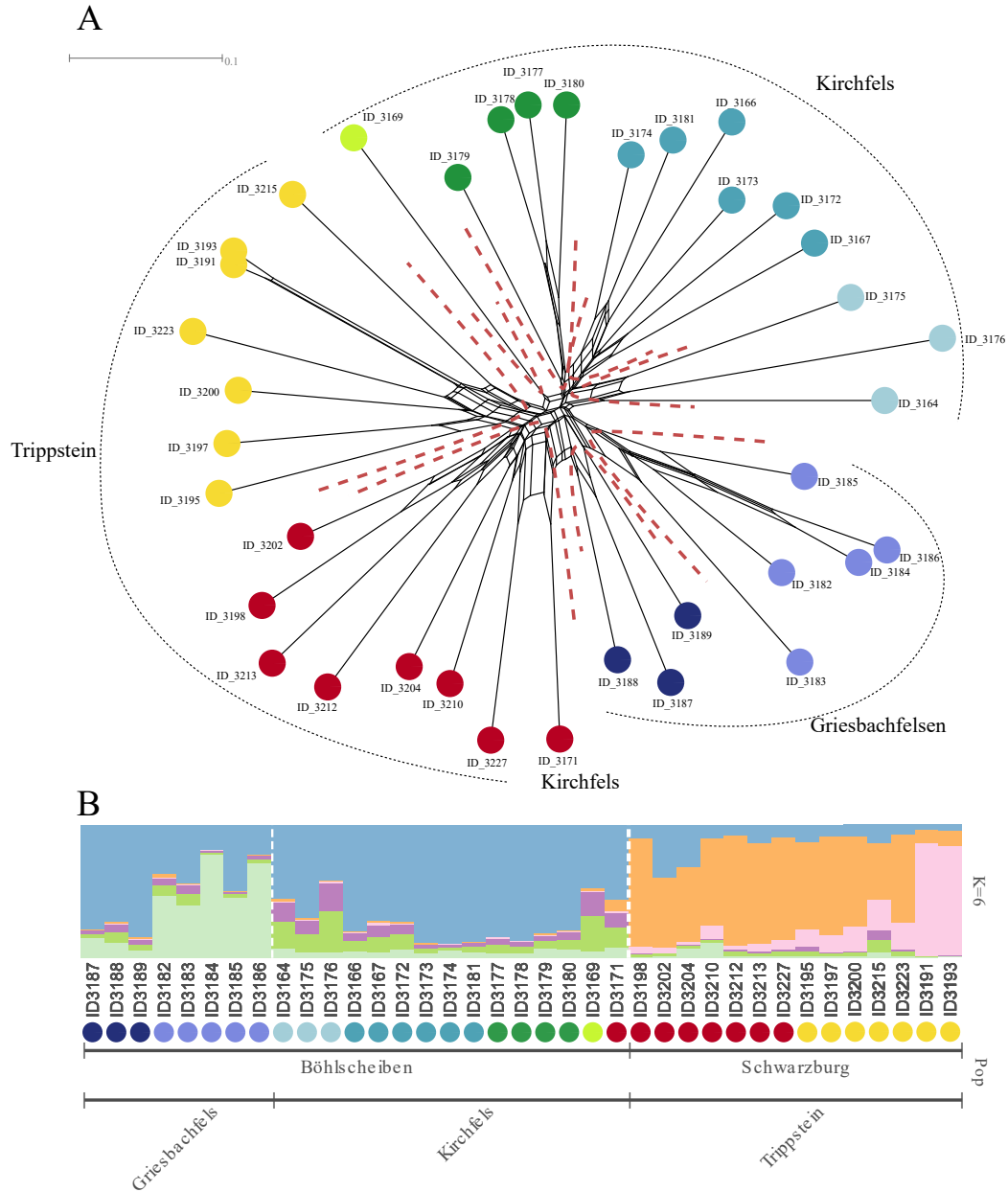
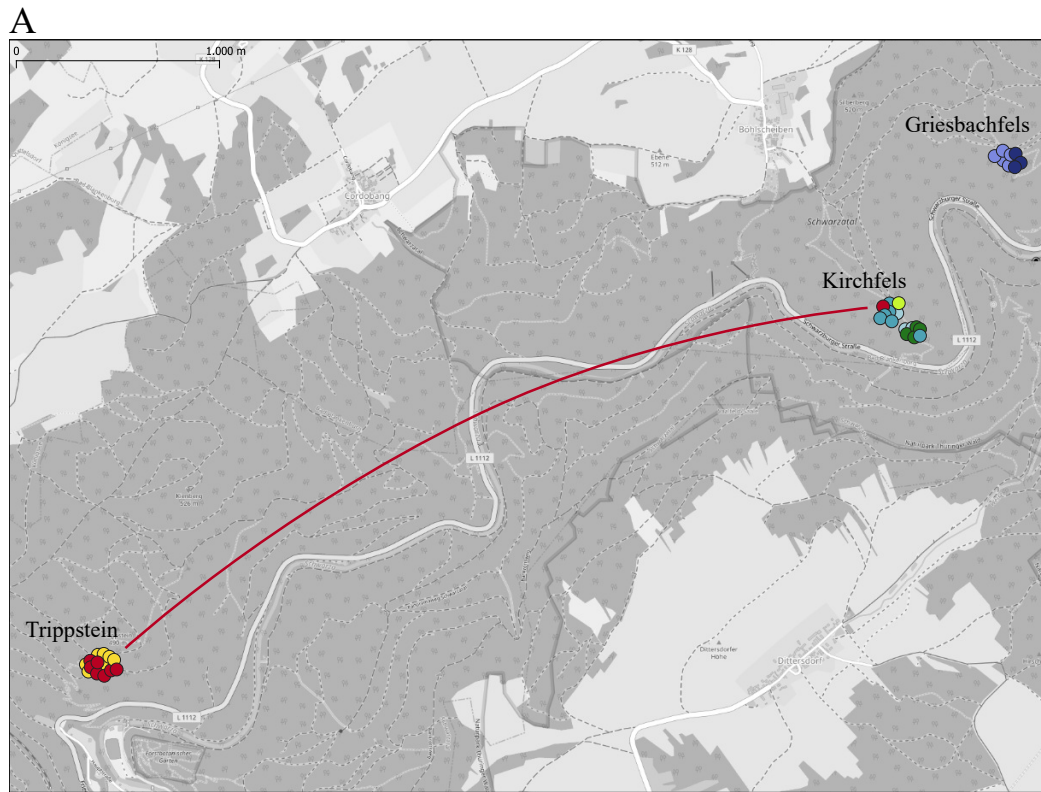


Figure 3.17: *SplitsTree* and *STRUCTURE* analysis for Populations from the Schwarztal near Böhlischeiben and Schwarzburg **A** *SplitsTree* analysis of AFLP data. Colors indicate resulting genotype groups, dashed lines indicate subpopulations. **B** Genetic assignment with *STRUCTURE* ($K=6$), coloured based on the *SplitsTree* analysis (A).



Molecular differences between and within growth sites

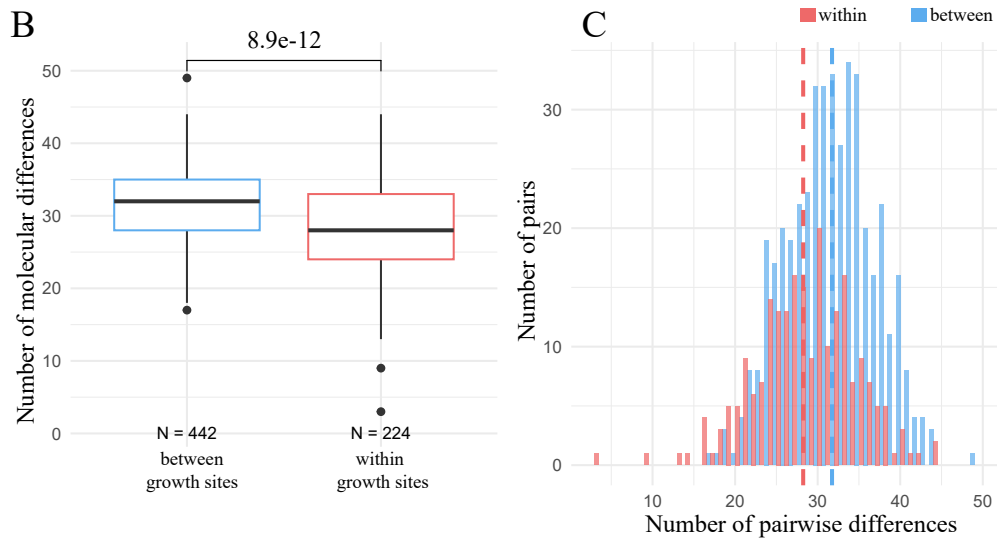


Figure 3.18: Distribution of *D. gratianopolitanus* and molecular differences (AFLP fragments) for populations from the Schwarzatal near Böhlischeiben and Schwarzburg. A Geographic distribution in the Schwarzatal, coloured based on SplitsTree grouping. Coloured lines indicate possible dispersal events of the according coloured genotype. **B** Number of molecular differences between and within the growth sites, **C** Frequency distribution of molecular differences as shown in B). Dashed lines indicate mean values.

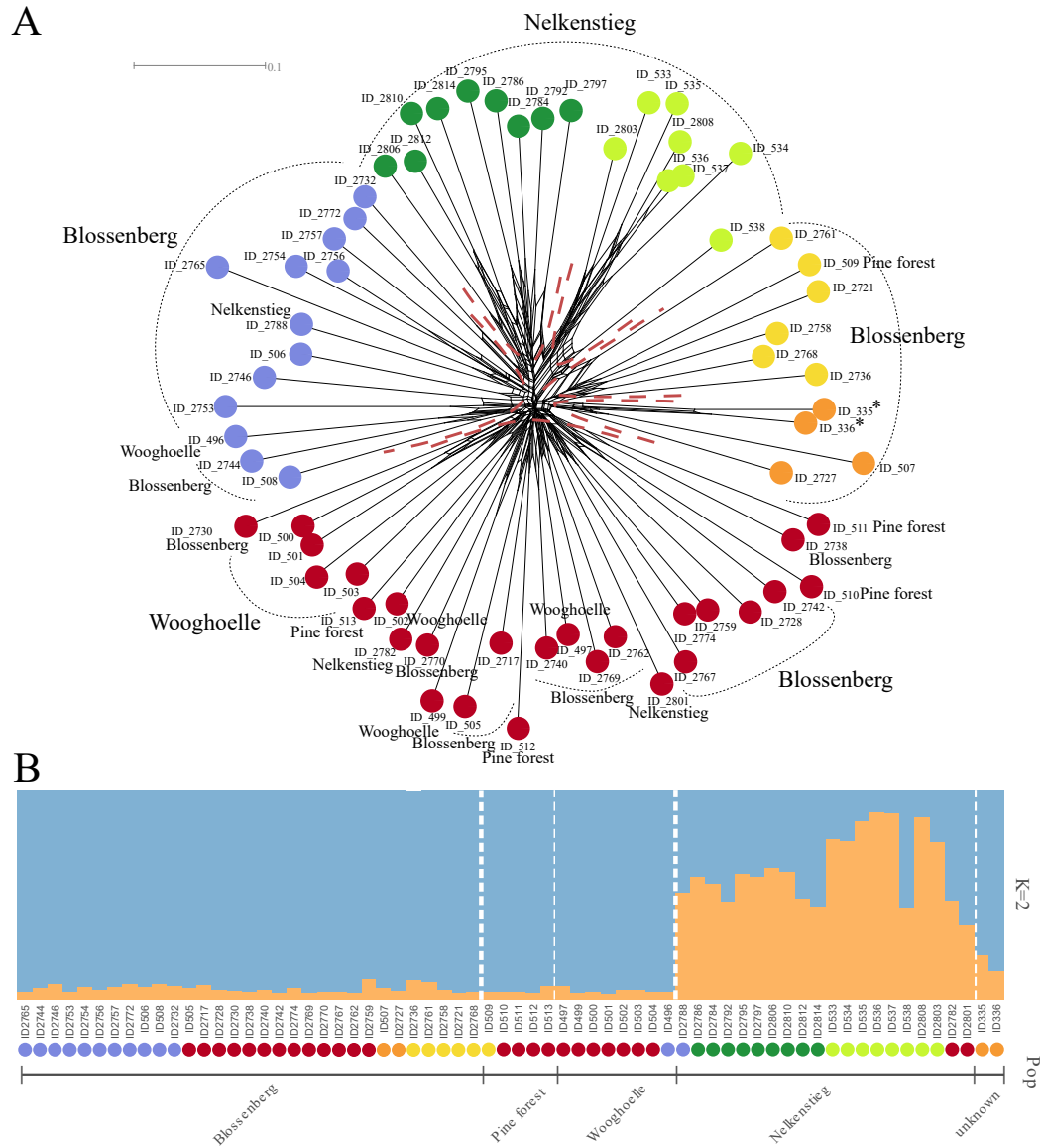
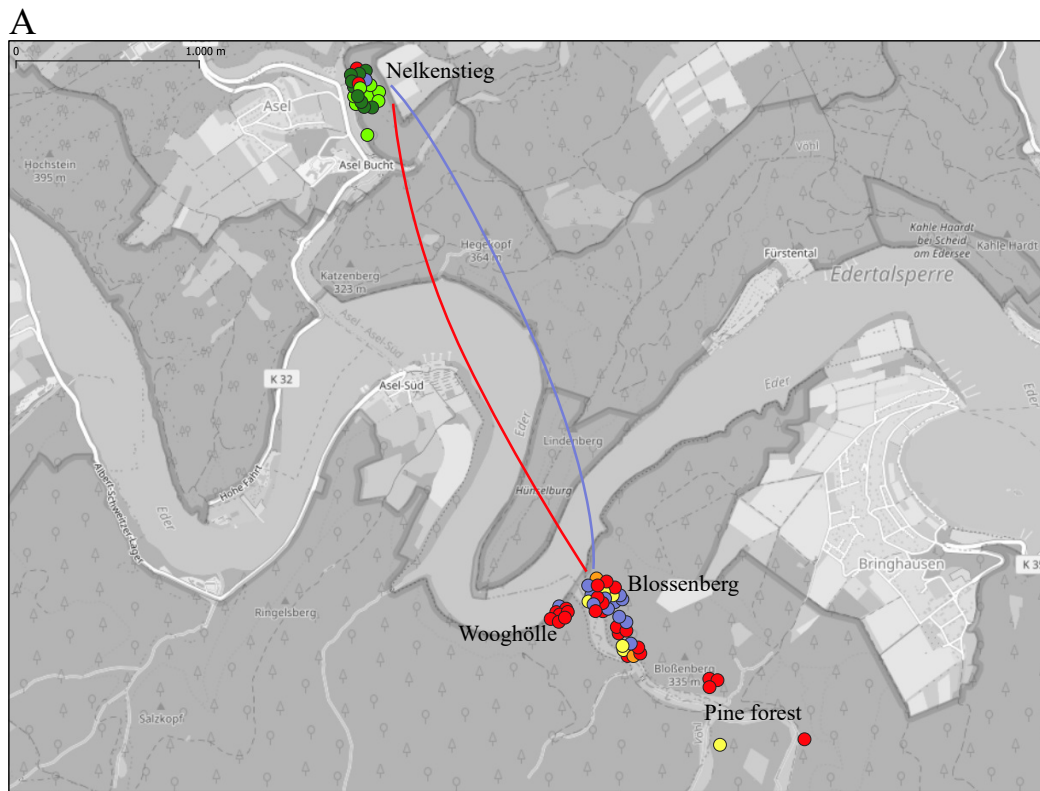


Figure 3.19: SplitsTree and STRUCTURE analysis for Populations from Kellerwald-Edersee *SplitsTree* analysis of AFLP data. Colors indicate resulting genotype groups, dashed lines indicate subpopulations. **B** Genetic assignment with *STRUCTURE* ($K=2$), coloured based on the *SplitsTree* analysis (A).



Molecular differences between and within growth sites

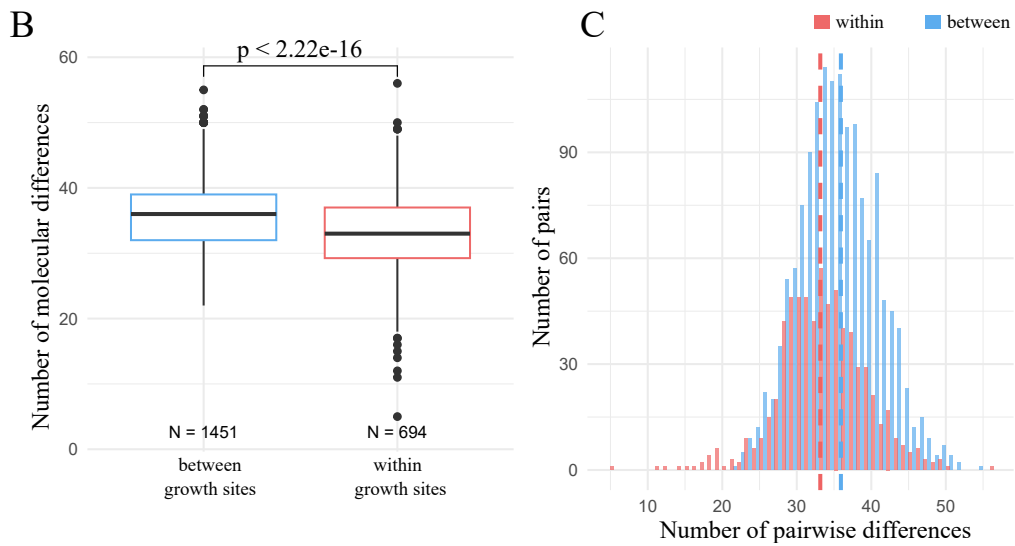


Figure 3.20: Distribution of *D. gratianopolitanus* and molecular differences (AFLP fragments) for populations from Kellerwald-Edersee. A Geographic distribution at Kellerwald-Edersee, coloured based on SplitsTree grouping. Coloured lines indicate possible dispersal events of the according coloured genotype. **B** Number of molecular differences between and within the growth sites, **C** Frequency distribution of molecular differences as shown in B). Dashed lines indicate mean values.

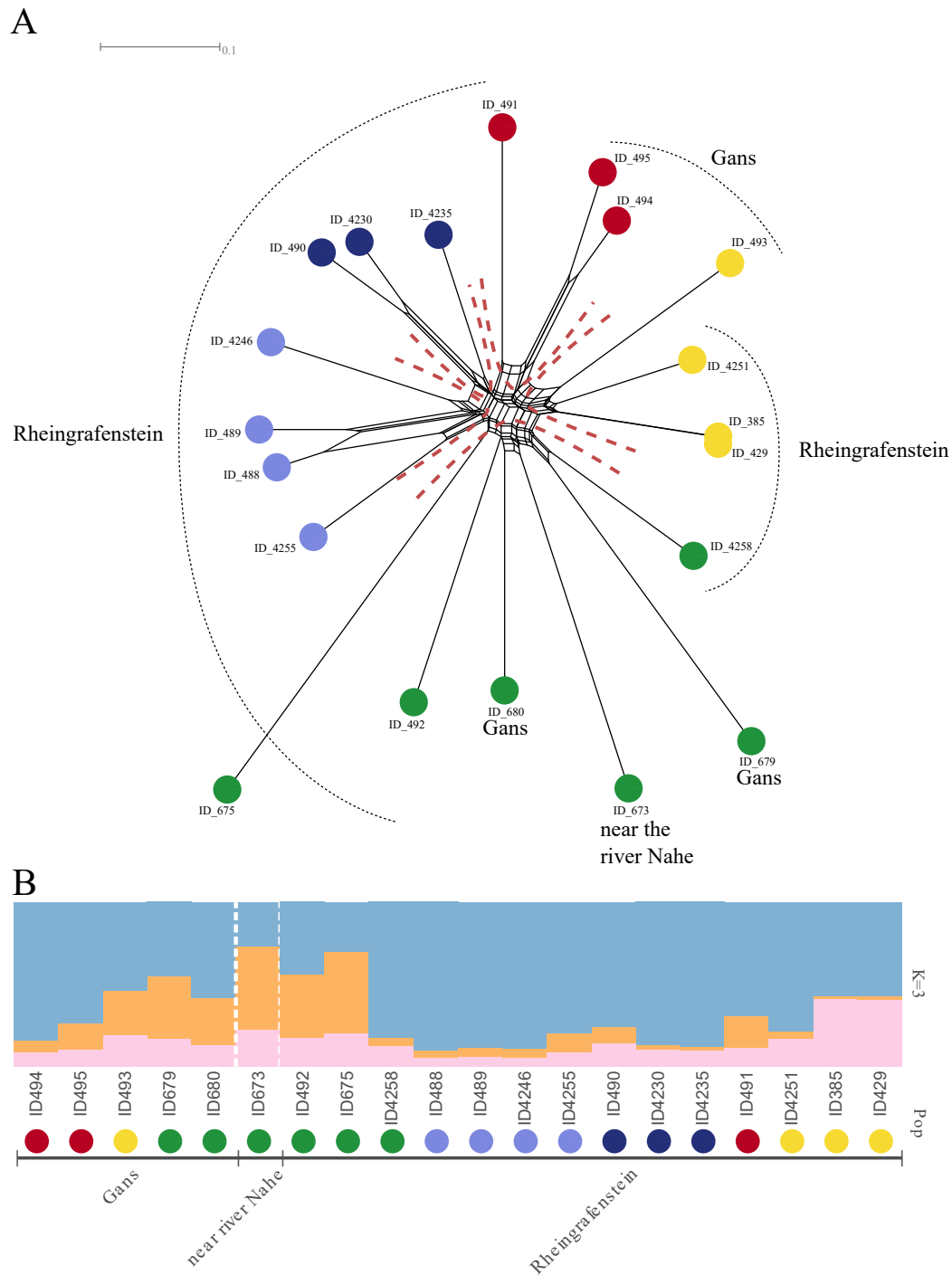


Figure 3.21: *SplitsTree* and *STRUCTURE* analysis for Populations from the nature reserve Gans and Rheingrafenstein near Bad Münster am Stein-Eberburg. **A** *SplitsTree* analysis of AFLP data. Colors indicate resulting genotype groups, dashed lines indicate subpopulations. **B** Genetic assignment with *STRUCTURE* ($K=3$), coloured based on the *SplitsTree* analysis (A).



Molecular differences between and within growth sites

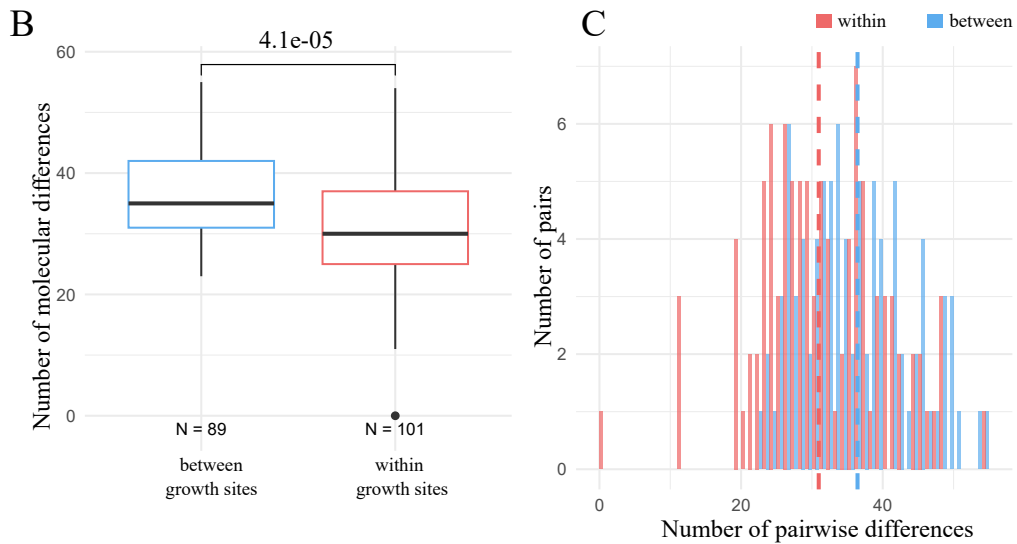


Figure 3.22: Distribution of *D. gratianopolitanus* and molecular differences (AFLP fragments) for populations from the nature reserve Gans and Rheingrafenstein near Bad Münster am Stein-Ebernburg. **A** Geographic distribution in the nature reserve Gans and Rheingrafenstein, coloured based on SplitsTree grouping. Coloured lines indicate possible dispersal events of the according coloured genotype. **B** Number of molecular differences between and within the growth sites, **C** Frequency distribution of molecular differences as shown in B). Dashed lines indicate mean values.

3.2 Ecological niches and predicted distribution range differ between the calcareous and siliceous groups

To analyse fitting environmental conditions, infer possible habitats of *D. gratianopolitanus* and compare environmental differences of calcareous and siliceous bedrock habitats species distribution range and environmental niche preferences were predicted using ENM. For model creation, 300 occurrence points were used for the whole range, 200 for the calcareous range and 96 for the siliceous+ range.

Of the 19 available bioclimatic variables nine that did not show high Pearson correlations were chosen for modelling (see Appendix [Figure C.1](#) and [Table C.3](#)). [Table 3.6](#) shows the used bioclimatic variables (Bio) for niche predictions and their contributions to the models for the whole distribution range, as well as for the calcareous and siliceous+ range. While the precipitation of the warmest quarter (Bio 18) contributed the highest for the whole distribution range (33.6%) and the calcareous range (41.4%) it is only the fourth most important variable for the siliceous+ range (10.8%). For the whole range, the temperature seasonality (Bio 4) contributed second most (24.9%) and is the second most contributing variable for the siliceous+ range (20.3%) while it is the third most important for the calcareous range (13.6%). The overall third most important variable is the precipitation of the driest month (Bio 14) with 18.4% contribution. At the same time, this is also the second most important variable for the calcareous range (23.7%) and only fifth place in the siliceous+ range (7.6%). In the siliceous+ model, the minimal temperature of the coldest month (Bio 6) contributes the most with 28.1%. In the whole and calcareous range, it is in the fourth place with 16.3% and 19.1%, respectively. The Precipitation Seasonality (Bio 15) is the third most important variable for the siliceous+ model (16.4%), while it contributes 1.1% for the whole range and 2.9% in the calcareous range model. Differences between the top three contributing bioclimatic variables are given in the Appendix [Figure C.2](#), revealing significant differences between the calcareous and siliceous+ range in Bio 4, Bio 6, Bio 14, and Bio 18. The biggest differences can be found in Bio 14 and Bio 18, both concerning the precipitation in either the driest month or warmest quarter, where the siliceous+ range receives less precipitation (Bio 14 med.: 41 mm, Bio 18 med.: 231 mm) than the calcareous region (Bio 14 med.: 61.5 mm, Bio 18 med.: 298 mm). It also faces bigger temperature differences over the year (Bio 4) and on average the colder months (Bio 6, sil+ med. -4.7 °C, cal. med. -4.1 °C) even if the high variation in the calcareous region surpasses these extremes. A comparison of all used bioclimatic variables is given in the Digital Supplement ("S_III.2.2-used_bioclims.pdf")

The niche models on present-day climate data for the whole is given in range [Figure 3.23 A](#), for the calcareous and siliceous+ in [Figure 3.24 A](#) and [B](#). Model performances for the test data were overall good ($AUC_{all} = 0.931$, $AUC_{cal} = 0.978$, $AUC_{sil+} = 0.967$) with the example receiver operating characteristic (ROC) curve for the whole distribution range given in [Figure 3.23 B](#).

While the overall present-day distribution corresponds well with the predicted range ([Fig-](#)

Bioclim Variable		%- contribution all	%- contribution lime	%- contribution sil+
Bio_18	Precipitation of Warmest Quarter	33.6	41.4	10.8
Bio_4	Temperature Seasonality (standard deviation $\times 100$)	24.9	13.6	20.3
Bio_14	Precipitation of Driest Month	18.4	23.7	7.6
Bio_6	Min Temperature of Coldest Month	16.3	10.1	28.1
Bio_8	Mean Temperature of Wettest Quarter	2.8	4.5	2.9
Bio_3	Isothermality (BIO2/BIO7) ($\times 100$)	1.3	1.5	3.6
Bio_15	Precipitation Seasonality (Coefficient of Variation)	1.1	2.9	16.4
Bio_13	Precipitation of Wettest Month	1	1.7	3.7
Bio_2	Mean Diurnal Range (Mean of monthly (max temp - min temp))	0.5	0.4	6.7

Table 3.6: Contribution of the used bioclimatic variables to the Maxent models for all *D.gratianopolitanus* (300 samples), those from calcareous bedrock (200 samples) and siliceous bedrock (96 samples).

ure 3.23 A) additional suitable regions are indicated in the South: in the Pyrenees, the Balkans and Italy, and even further in the North: in Germany Denmark, South Sweden, in Northern England and Scotland, and on the coastal line of Poland.

Separating the distribution range in the calcareous and siliceous+ regions reveals significant differences between the predicted ranges. The model prediction for the calcareous region (Figure 3.24 A) follows the actual distribution in the Swabian Alb and French Jurassic and Prealps but also includes Czech areas and areas towards the Ore Mountains, Belgium and regions towards the Sauerland. It also predicts the regions in the South, the Balkans, the Pyrenees, and Italy as well as regions in Northern England, and South Sweden as suitable habitats.

Suitable regions predicted by the siliceous+ model (Figure 3.24 B) cover a wider range of highly suitable regions, especially in Central Germany but also in Northern Denmark (North Jutland) and South Swedish regions (Öland). The overall predicted region also includes the Swabian Alb, the French Alps, and the Massif Central. The Balkans and Pyrenees are also included as suitable regions but show a weaker and narrower range than in the calcareous model. The suitable regions in the UK are focused on Scotland the coastline of Poland toward Kaliningrad is marked as suitable habitat.

The analysis of niche characteristics revealed differences between the calcareous and siliceous+ regions. The siliceous+ group shows broader niche breadths ($B2 = 0.7918$, env $B2 = 0.6929$) compared to the calcareous group ($B2 = 0.4154$, env $B2 = 0.5547$), indicating a more generalist strategy and potentially greater adaptability to environmental variations. Despite these differences in niche breadth, the two species groups showed a low ($D = 0.28$, env $D = 0.417$) to moderate ($I = 0.54$, env $I = 0.663$) niche overlap. The niche divergence was confirmed by an identity test (Figure 3.25) where niche equivalence was rejected ($p < 0.01$). In addition to the niche divergence in the geographical space, it is also observed in environmental space, where niche overlap is slightly higher (env $D = 0.417$, env $I = 0.663$) but the null hypothesis of identical niches can also be rejected ($p < 0.01$, Appendix

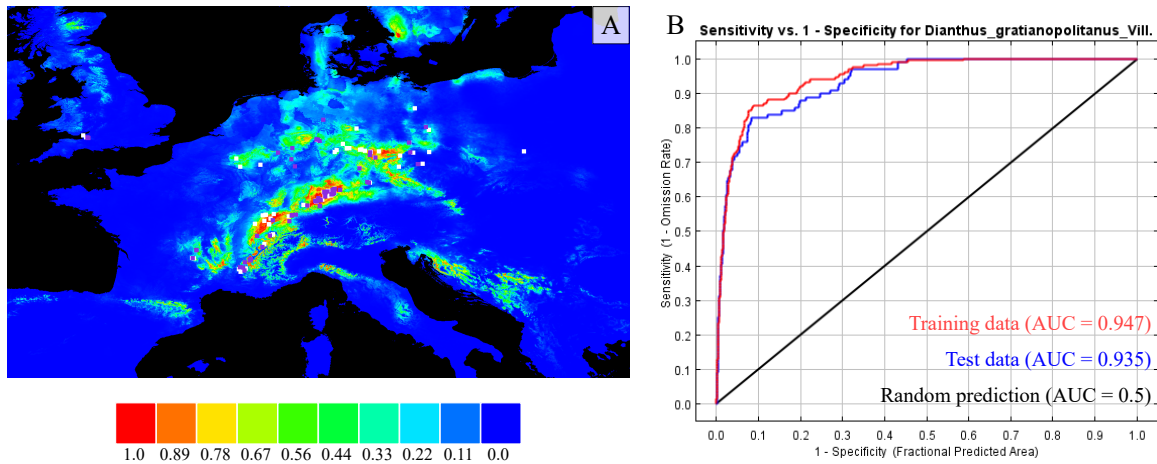


Figure 3.23: Ecological niche modelling for *D. gratianopolitanus* for present day climate data. **A** Prediction of present day niche for *D. gratianopolitanus*. Colours indicate suitability of the niche ranging from highly suitable (red) to unsuitable (blue). White dots show presence locations used for training and purple ones the test locations. **B** Model performance for training and test data.

Figure C.3).

Models were projected to future end-of-century climate scenarios for the calcareous and siliceous+ groups separately (Figure 3.24). Two scenarios were taken into account: ssp126 with a limitation of global warming to 2°C and ssp370 predicting the climate for moderate global warming. In all cases, the predicted ranges decrease significantly.

While the core regions in the Swabian Alb, the Alps, and French Prealps, as well as South Sweden, Denmark, Northern England, the Sauerland, the Ore mountains, Pyrenees and the Balkan, are still suitable for the calcareous group in ssp126 (Figure 3.24 C) the suitable region is reduced to the Alps for ssp370 (Figure 3.24 E). Only a slight signal in the Sauerland, South Sweden, and Northern England can be observed.

For the siliceous+ group, the reduction is already more severe for ssp126 (Figure 3.24 D), where only fragments of the original core range in Central Germany remain, while parts of the Alps and Prealps are predicted as suitable. While Scotland and the Balkans are indicated as suitable the strongest signal can be observed in South Sweden. For ssp370 nearly all suitable regions in Central Europe have vanished with only traces remaining in the Alps (Figure 3.24 F). South Sweden is here the region with the highest predicted suitability.

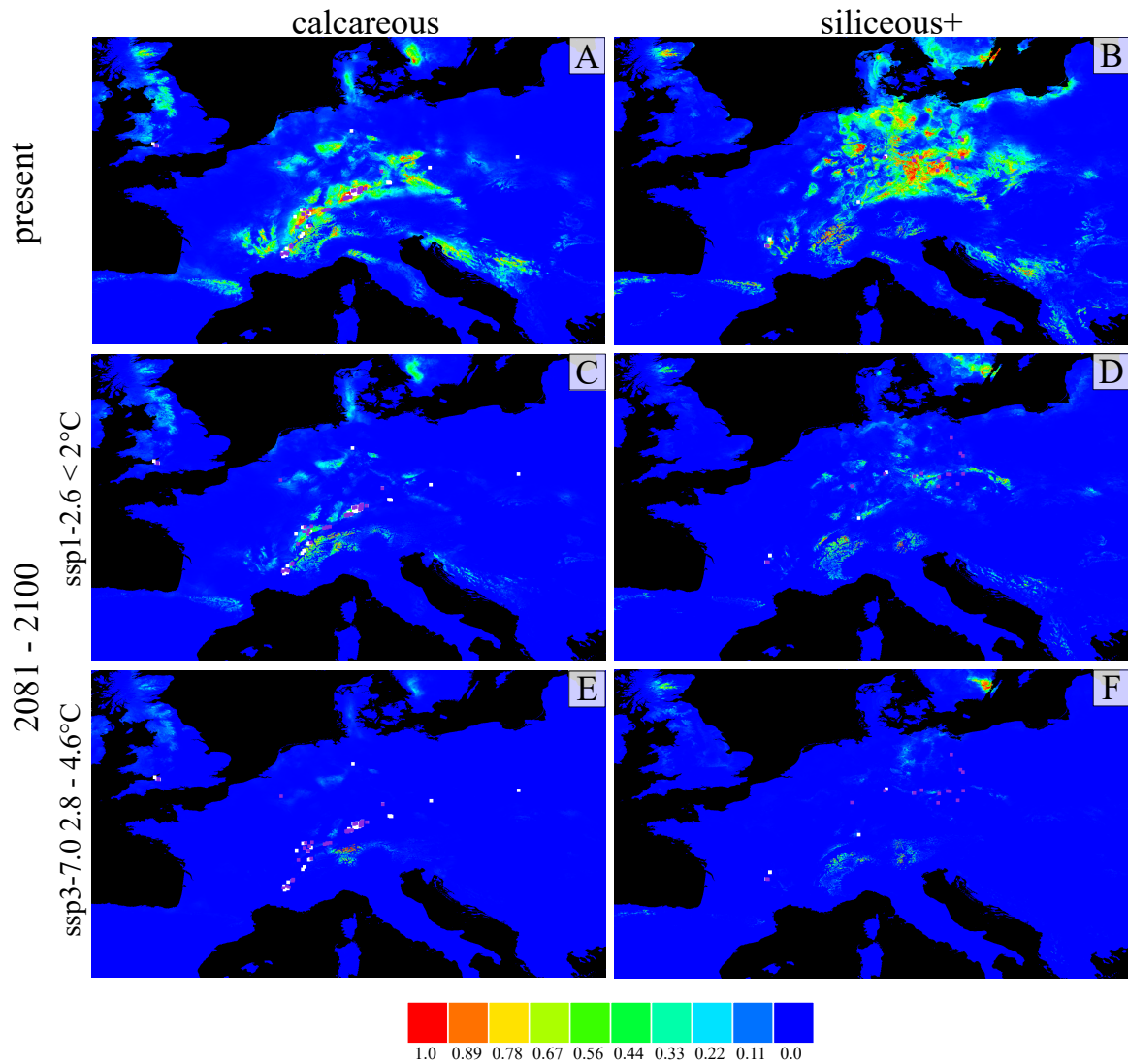


Figure 3.24: Ecological niche modelling for *D. gratianopolitanus* for present and future day climate data. Ecological niche model for present day climate for calcareous **A** and siliceous+ bedrock **B**. Prediction of future niche for calcareous bedrock **C** and siliceous bedrock **D** using climate data from *ssp1-2.6*, and predictions for calcareous bedrock **E** and siliceous bedrock **F** using climate data from *ssp3-7.0*. Colours indicate suitability of the niche ranging from highly suitable (red) to unsuitable (blue). White dots show presence locations used for training and purple ones the test locations.

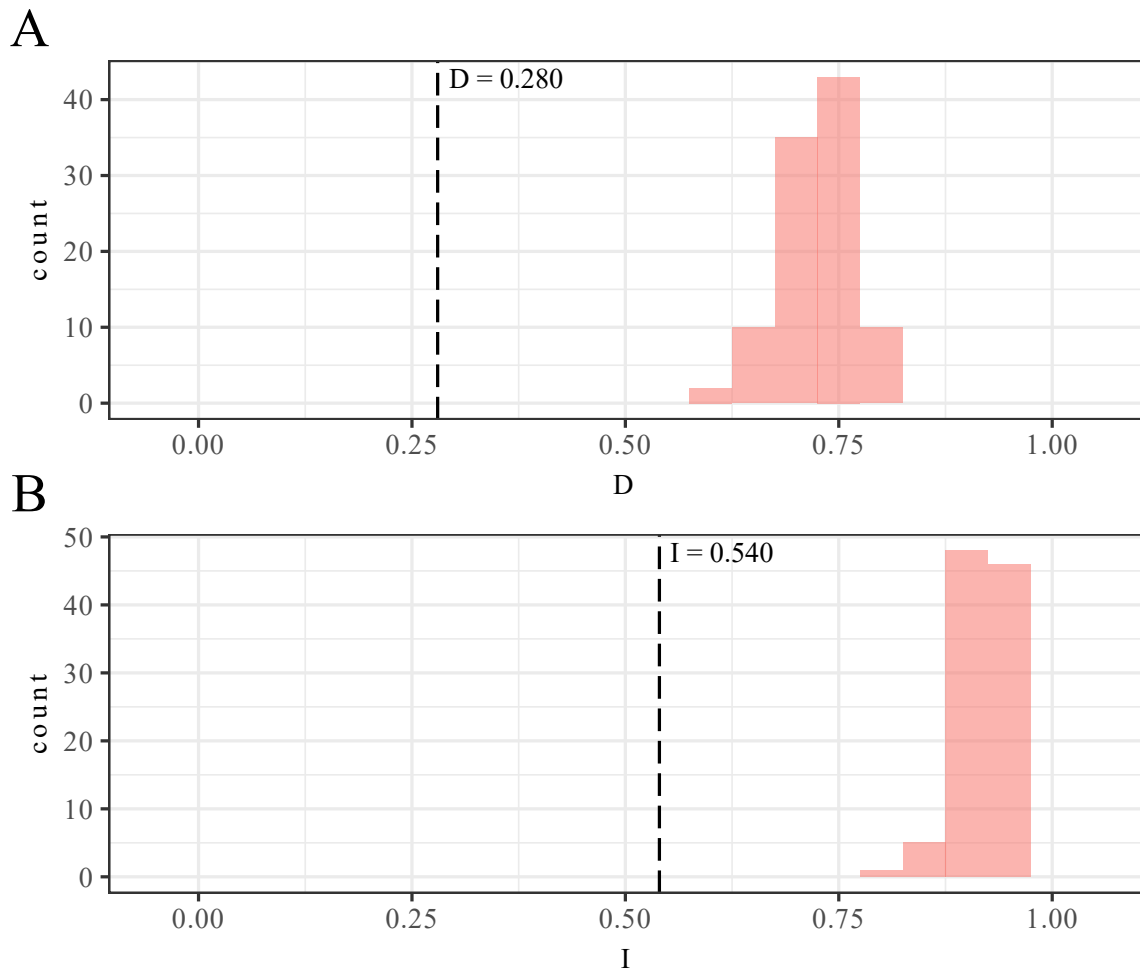


Figure 3.25: Niche identity test between *D. gratianopolitanus* from calcareous and siliceous bedrock. Expected distributions given as histogram ($N=100$) differs significantly ($p < 0.01$) from observed niche overlaps (dashed lines).

4 | Discussion

The isolation of populations can have a severe influence on their genetic variation and fitness. For *D. gratianopolitanus* spatial genetic structuring and limited gene flow could also be observed on a very local, subpopulation scale. The differences in growth and flowering behavior between populations from calcareous and siliceous bedrock might also impact the degree of isolation and genetic connectivity. In addition, they might also differ in the climatic requirements posed to their habitats. In this study, I analyzed populations from calcareous and siliceous bedrock using nuclear AFLP data and estimated the potential geographic distribution under current and future climate conditions.

Higher genetic diversity within calcareous and higher genetic structuring within siliceous metapopulations Genetic variation between populations and sites follows the trend observed in [Part I](#), where the populations from the southern calcareous regions showed higher variation when compared to those from more northern siliceous populations ([Table 3.5](#)). The calcareous populations also indicated higher levels of rare and unique alleles. The metapopulation from the Eselburger Tal and the nature reserve Ehrenbürg showed overall lower values. While it could indicate a reduction of diversity due to the isolation of the metapopulation in the Eselsburger Tal, the lower diversity observed in the metapopulation from Ehrenbürg could also be explained by the shared gene pool with northern populations that also showed a reduced variation ([Figure A.6](#)).

The metrics of genetic variation are not reflecting the number of inferred genotypes in subpopulations. Sites consisting of more than one genotype did not necessarily yield higher number of total fragments, polymorphic or mean number of bands compared to sites of comparable sizes with uniform genotypes (e.g. in Achtal Blaubeuren).

The populations from siliceous bedrock indicated higher levels of genetic substructuring although the clusters revealed by STRUCTURE did not necessarily reflect the structuring by subpopulations. While some populations showed a clearer division (e.g. [Figure 3.3](#), [Figure 3.13](#)) also higher levels of admixture are present. In the calcareous less substructuring is indicated, with the exception of the Eybtal where a more diverse pattern is shown that indicates closer genetic relationships between different sites.

Varying patterns of gene flow and genetic connectivity based on the inferred genotypes can be observed in both calcareous and siliceous bedrock populations. In both groups indications of complex genetic connectivity patterns can be observed connecting not only close

but also distant subpopulations (e.g. in the Aichtal and around Burgk). On the one hand, sparse connections covering distances of over 3km could be observed (e.g. [Figure 3.2](#), [Figure 3.18](#)) bypassing rivers, roads, or forests, they were missing between closer sites (e.g. [Figure 3.8](#)). These connections are not restricted to riverbanks but also indicate connections of more distant subpopulations separated by woody hillsides, where the genotypes are missing at closer populations along the river ([Figure 3.4](#), [Figure 3.16](#)). The maternal footprints of these connections or signs of seed dispersal indicated by shared plastid haplotypes could support some of the connections but due to lower numbers and missing coverage, a clear picture is often missing. As an example for the calcareous range the strong connection between Ravellenflue and Lehnfluh in the Swiss population indicated by shared genotypes is supported by a shared plastid haplotype that is missing from Holzfluh in other cases more common haplotypes are found at all sites without any differentiation (Ehrenbürg). In Kellerwald Edersee the potential barrier composed of the river loops of the Eder splits the plastid haplotypes found in a northern and southern group, while also indicating a shared haplotype and therefore a past seed exchange.

The genetic connectivity indicated in this study exceeds the one observed in the Lenninger Tal and Eselsburger Tal in [Koch et al. \(2020\)](#) based on both the inferred genotypes and genetic assignment. While the Lenninger and Eselsburger Tal showed more genetically uniform subpopulations the herein analyzed populations show a more diverse genetic signature, ranging from clear spatial structuring forming genetically uniform sites like at the Hausener Wand to higher levels of genetic mixture and gene flow between sites like in the Danube valley or near Burgk.

These shared genotypes could indicate recent genetic connectivity or patterns reflecting past gene flow possibly even dating back to the original colonization. Many of the analyzed sites are at cliffs and rocky outcrops along riversides. [Pott \(1996\)](#) proposed the postglacial migration following rivers for other xerotherm species in Central Europe. After this initial colonization and with increasing isolation these sites started to differentiate and accumulate site specific mutations. If the current patterns are indeed due to past genetic connectivity the shared genotypes might just reflect past genetic patterns established shortly after their colonization and during times when populations were distributed more evenly with closer connections and easier gene flow. The dispersal and migration via seeds are limited to relatively short distances as described for *Dianthus polylepsis* ([Behroozian et al., 2020](#)) and suggested for *D. gratianopolitanus* with a dispersal through animals or long-time soil seed banks seeming unlikely ([Banzhaf et al., 2009](#)). Gene flow between different subpopulations on the local scale should therefore mainly be mediated by pollen exchange. The dispersal and gene flow via pollinators like butterflies and moths could indeed cover these distances, especially in the case of *Macroglossum stellatarum* that is known to migrate from the Mediterranean area over the Alps towards Scandinavia acting as a potential long-pollen vector ([Erhardt, 1990](#)). Differences in pollinator-mediated gene flow and their influence on the genetic variation within populations were shown for the bee-pollinated *Oenothera gayleana* and the hawkmoth-pollinated *O. hartwegii* subsp. *filifolia*. The pollination by long-distance

pollinators like the hawkmoths leads to higher gene flow and lower genetic differentiation when compared to those pollinated by bees and other short-distance foragers, allowing also for long-distance dispersal between disconnected populations (Lewis et al., 2023). On the other hand forests, rivers and roads have been shown to impact some butterfly species acting as barriers hindering gene flow and possibly dispersal activity or even facilitating it along river banks (Fabritius et al., 2015; Trense et al., 2021). While the pollinators are not exclusive to *D. gratianopolitanus* a limitation of their migrations and movement can also impair gene flow between populations of *D. gratianopolitanus*.

The genetic distribution and formation of the observed patterns is influenced by many factors that are not traceable based on the herein used genetic data and would need to factor in other parameters like e.g. past land use. Yet the genetic structuring observed within the populations highlights the need for efficient conservation strategies targeting all subpopulations to 1) conserve the genetic variation within populations and 2) enable possible gene flow. In addition, the creation of new sites might facilitate gene flow in the future helping to increase the overall fitness of the entire population.

Koch et al. (2021) suggested that the missing genetic diversity within *D. gratianopolitanus* subpopulations could limit their ability to compensate for environmental changes via adaptive phenotypic plasticity. Across larger geographical scales this plasticity may vary and enable the adaptation to changing conditions.

Ecological niches indicate differences in preferred climatic conditions for different bedrock type distributions and strong reduction of predicted future ranges

While model performances indicated by AUC were overall very good they need to be treated with caution. Model performances are dependent on the available occurrence data and can be influenced by biases in sampling and lack of sufficient occurrence data (Wisz et al., 2008). The coverage of the distribution range included a majority of populations of *D. gratianopolitanus* though their restriction to the small habitats of the rocky outcrops reduces occurrences with significant distances resulting in closely clustered points and an overall occurrence point reduction after a thinning of the data set. Yet Wisz et al. (2008) showed that MAXENT is not as sensitive to smaller sample sizes compared to other algorithms supporting the predictions made for the siliceous+ group. Nevertheless, for a robust analysis, different models and their influence should be explored. Recent advances in ecological niche modeling have further highlighted the importance of edaphic factors alongside climatic variables for more accurate predictions of plant species distributions (Mod et al., 2016; Velazco et al., 2017).

In the recent niche modeling of other *Dianthus* species, the Mediterranean *D. broteri* complex (López-Jurado et al., 2019) and *D. polylepsis* (Behroozian et al., 2020) from the Irano-Turanian mountain region, environmental parameters related to the minimum temperature of the coldest quarter, diurnal temperature range, temperature, and drought stress due to the precipitation of the warmest quarter as well as mean temperatures of the warmest and driest quarter affected the predicted ranges. In my analysis of the overall distribution of *D. gratianopolitanus* the prediction is mostly influenced by the precipitation of the warmest

and driest quarter as well as the temperature seasonality. These are also the most important factors influencing the calcareous range in the south while the siliceous population to the north and east are influenced by the minimum temperature of the coldest quarter as well as the temperature and precipitation seasonality. Yet the differences in the Bioclimatic variables extracted from these habitats indicate lower levels of precipitation in the siliceous region, possibly indicating more drought stress. Crespi et al. (2023) used a k-means clustering to define main climatic regions in Germany based on data from 1971-2000. In the herein-defined zones "Southeast" and "Northwest" the southern zone has overall even higher precipitation in the summer and with both zones having a comparable number of dry days in the summer with the southern area even experiencing lower average temperatures in the winter. The herein-used classification of climatic regions covers wide ranges possibly also swamping more differentiated climatic conditions. In addition, the rocky outcrops and cliffs can provide unique micro-climates that can differ from the surrounding conditions providing more moist conditions in arid regions or even conditions that suit dry-adapted species in otherwise tropical conditions (Fitzsimons and Michael, 2017). These micro-climates would not be reflected in the study of Crespi et al. (2023) and also not in detail in the Bioclimatic variables with a spatial resolution of 30-arc-seconds ($\sim 1\text{km}$). While they are widely used for example in the niche modeling of *Dianthus polylepsis* (Behroozian et al., 2020) in the Irano-Turanian mountain region, which also shows a very fragmented, patchy, and isolated distribution, as well as in the modeling of the ploidy lines in the *D. broteri* complex (López-Jurado et al., 2019) they could be inaccurate for the modelling of species influenced by possible micro-climates.

The core range of the potential geographic distribution estimated for *D. gratianopolitanus* under current climate conditions is in good accordance with the present-day distribution, although also here the Cheddar Pink is missing from potentially suitable habitats (Figure 3.23), as observed in the field in Baden-Württemberg (Banzhaf et al., 2009). The additional predicted areas e.g. in the Pyrenees, Balkan, Italy, Scotland, Poland, Denmark, and Sweden are separated from the core range by distance as well as natural barriers like the Alps. As stated earlier the dispersal of seeds over longer distances passing over unsuitable habitats and establishing new populations is unlikely for *D. gratianopolitanus*. For the British Isles, I proposed in Part I the postglacial migration following a similar migration route to *A. scabra* (Koch et al., 2020) from the French Jura to England, by an area-wide distribution that later on fragmented, covering distances far bigger than from a proposed refugia in the South of France to the Pyrenees. A possible explanation for a missing expansion to the South could be within the low competitiveness observed in today's *D. gratianopolitanus* as it would have had to face already-established vegetation in the Mediterranean region.

The different influence of the climatic parameters on the calcareous and siliceous range can also be observed in the predicted ranges, their niche breadth and overlap, indicating significantly differing niches and a more specialized niche for the calcareous *D. gratianopolitanus*. In addition a study on alpine plants showed, that calcicolous species had lower range-filling when compared to silicolous or generalist species, meaning a lower extent at

which they fill their potential ranges (Dullinger et al., 2012). Slatyer et al. (2013) showed the general link between niche breadth and range size, which can also be seen here where the broader niche of the siliceous *D. gratianopolitanus* is reflected in its wider suitable range (Figure 3.24). Herein it is also presumed that a broader niche and range might enable a faster reaction to climate change and are therefore less vulnerable to climate change. Yet for both ssp-scenarios the end-of-century predictions for the calcareous and siliceous range result in a reduction of suitable habitats with a focus on mountain areas and a shift to the north (Figure 3.24), as observed in the predicted reaction of *D. polylepsis* (Behroozian et al., 2020). Indeed these poleward and upward range shifts are among the most frequent types reported though the true pattern might be more complicated (Lenoir and Svenning, 2015). For both bedrock groups, the ranges are predicted to undergo strong range reduction increasing the extinction risk (Thomas et al., 2004; Thuiller et al., 2005). This risk of extinction under climate change is said to be linked to a species dispersal ability and therefore its ability to shift its range with suitable habitats (Engler et al., 2009; Ozinga et al., 2009; Casazza et al., 2014). The migration capability of many range-restricted species is often limited due to their often special requirement to their environment and low dispersal ability, and the velocity of the predicted climate change will likely exceed their capabilities to migrate (Pearson, 2006). While there are predicted suitable areas for *D. gratianopolitanus* their low migration potential, special habitat needs, and low competitiveness make migration and colonization of these habitats unlikely. A combination of ex situ and in situ strategies assisted by habitat predictions and careful habitat management is needed to ensure the species' survival under changing conditions.

Yet assuming static ecological niches in time and space might distort the true potential of a species, with the risk of both an over- and underestimation of their potential to react to changing environments (see also (Atkins and Travis, 2010)). Kelly et al. (2012) showed different upper-temperature limits for the widely distributed copepod *Tigriopus californicus*, where more northern populations showed a reduced upper limit of less than 35°C while the overall limit is at 38°C. Not taking these variations into account will therefore not reflect a species's true potential and limits. The broad distribution from *D. gratianopolitanus* covers a variety of environmental conditions and might have led to local adaptations to climate as indicated in Part II to different bedrock types.

Summary The genetic structure analyzed by neighbor-net inferred genotypes and genetic assignment indicate varying patterns of connectivity and degrees of isolation. These patterns could indicate recent gene flow or symbolize the remnants of past genetic connectivity. While the calcareous populations showed higher levels of genetic variation the siliceous population revealed higher genetic substructuring in the genetic assignment. Still, the high genetic structuring between sites observed in all populations again highlights the need for efficient conservation strategies targeting all subpopulations conserving the genetic variation and (re-) establishing possible dispersal routes. Niche modeling indicates differing climatic conditions and limitations for *D. gratianopolitanus* from calcareous and siliceous bedrock,

with the southern populations more affected by drought stress while the northern populations are limited by minimum temperatures. With higher niche breadth the siliceous group is likely to have a wide range of suitable climate conditions, than the more specialized calcareous group. While under current climate conditions, the predicted areas exceed the present-day distribution, future predictions indicate a clear reduction of suitable areas with a trend towards higher elevations and migrations to the north.

5 | Bibliography

- Atkins, K. and Travis, J. (2010). Local adaptation and the evolution of species' ranges under climate change. *Journal of Theoretical Biology*, 266(3):449–457.
- Banzhaf, P., Jäger, O., and Meisterhans, U. (2009). Artenhilfsprogramm für die Pfingstnelke *Dianthus gratianopolitanus* im Regierungsbezirk Stuttgart. *Jahreshefte der Gesellschaft für Naturkunde in Württemberg*, 165:73–115.
- Behroozian, M., Ejtehadi, H., Peterson, A. T., Memariani, F., and Mesdaghi, M. (2020). Climate change influences on the potential distribution of *Dianthus polylepis* Bien. ex Boiss.(Caryophyllaceae), an endemic species in the Irano-Turanian region. *PloS one*, 15(8):e0237527.
- Casazza, G., Giordani, P., Benesperi, R., Foggi, B., Viciani, D., Filigheddu, R., Farris, E., Bagella, S., Pisanu, S., and Mariotti, M. G. (2014). Climate change hastens the urgency of conservation for range-restricted plant species in the central-northern Mediterranean region. *Biological Conservation*, 179:129–138.
- Constantin, A.-E. and Patil, I. (2021). ggsignif: R package for displaying significance brackets for 'ggplot2'. *PsyArxiv*.
- Crespi, A., Renner, K., Zebisch, M., Schauser, I., Leps, N., and Walter, A. (2023). Analysing spatial patterns of climate change: Climate clusters, hotspots and analogues to support climate risk assessment and communication in Germany. *Climate Services*, 30:100373.
- Dagnino, D., Guerrina, M., Minuto, L., Mariotti, M. G., Médail, F., and Casazza, G. (2020). Climate change and the future of endemic flora in the South Western Alps: relationships between niche properties and extinction risk. *Regional Environmental Change*, 20(4):121.
- Dullinger, S., Willner, W., Plutzer, C., Englisch, T., Schrott-Ehrendorfer, L., Moser, D., Ertl, S., Essl, F., and Niklfeld, H. (2012). Post-glacial migration lag restricts range filling of plants in the European Alps. *Global Ecology and Biogeography*, 21(8):829–840.
- Elith, J., H. Graham*, C., P. Anderson, R., Dudík, M., Ferrier, S., Guisan, A., J. Hijmans, R., Huettmann, F., R. Leathwick, J., Lehmann, A., et al. (2006). Novel methods improve prediction of species' distributions from occurrence data. *Ecography*, 29(2):129–151.

- Engler, R., Randin, C. F., Vittoz, P., Czaka, T., Beniston, M., Zimmermann, N. E., and Guisan, A. (2009). Predicting future distributions of mountain plants under climate change: does dispersal capacity matter? *Ecography*, 32(1):34–45.
- Erhardt, A. (1990). Pollination of *Dianthus gratianopolitanus* (Caryophyllaceae). *Plant Systematics and Evolution*, 170:125–132.
- Fabritius, H., Ronka, K., and Ovaskainen, O. (2015). The dual role of rivers in facilitating or hindering movements of the false heath fritillary butterfly. *Movement ecology*, 3:1–14.
- Fitzsimons, J. A. and Michael, D. R. (2017). Rocky outcrops: a hard road in the conservation of critical habitats. *Biological Conservation*, 211:36–44.
- Hijmans, R. J., Phillips, S., Leathwick, J., Elith, J., and Hijmans, M. R. J. (2017). Package ‘dismo’. *Circles*, 9(1):1–68.
- Huson, D. H. and Bryant, D. (2006). Application of phylogenetic networks in evolutionary studies. *Molecular biology and evolution*, 23(2):254–267.
- Janczyk-Weglarska, J., Weglarski, K., and Wiland-Szymanska, J. (2013). Active ex situ protection and reestablishment of *Dianthus gratianopolitanus* Vill. in the "Gozdzik siny w Grzybnie" reserve (Wielkopolska Province). *Biodiversity Research and Conservation*, 32(1):53.
- Kaky, E., Nolan, V., Alatawi, A., and Gilbert, F. (2020). A comparison between Ensemble and MaxEnt species distribution modelling approaches for conservation: A case study with Egyptian medicinal plants. *Ecological Informatics*, 60:101150.
- Kelly, M. W., Sanford, E., and Grosberg, R. K. (2012). Limited potential for adaptation to climate change in a broadly distributed marine crustacean. *Proceedings of the Royal Society B: Biological Sciences*, 279(1727):349–356.
- Koch, M. A., Mobus, J., Klockner, C. A., Lippert, S., Ruppert, L., and Kiefer, C. (2020). The Quaternary evolutionary history of Bristol rock cress (*Arabis scabra*, Brassicaceae), a Mediterranean element with an outpost in the north-western Atlantic region. *Annals of Botany*, 126(1):103–118.
- Koch, M. A., Winizuk, A., Banzhaf, P., and Reichardt, J. (2021). Impact of climate change on the success of population support management and plant reintroduction at steep, exposed limestone outcrops in the German Swabian Jura. *Perspectives in Plant Ecology, Evolution and Systematics*, 53:125643.
- Kuss, P., Pluess, A. R., Egisdottir, H. H., and Stocklin, J. (2008). Spatial isolation and genetic differentiation in naturally fragmented plant populations of the Swiss Alps. *Journal of Plant Ecology*, 1(3):149–159.

- Leimu, R., Mutikainen, P., Koricheva, J., and Fischer, M. (2006). How general are positive relationships between plant population size, fitness and genetic variation? *Journal of ecology*, 94(5):942–952.
- Lenoir, J. and Svenning, J.-C. (2015). Climate-related range shifts—a global multidimensional synthesis and new research directions. *Ecography*, 38(1):15–28.
- Levins, R. (1968). *Evolution in changing environments: some theoretical explorations*. Number 2. Princeton University Press.
- Lewis, E. M., Fant, J. B., Moore, M. J., and Skogen, K. A. (2023). Hawkmoth and bee pollinators impact pollen dispersal at the landscape but not local scales in two species of *Oenothera*. *American Journal of Botany*, 110(6):e16156.
- López-Jurado, J., Mateos-Naranjo, E., and Balao, F. (2019). Niche divergence and limits to expansion in the high polyploid *Dianthus broteri* complex. *New Phytologist*, 222(2):1076–1087.
- Masson-Delmotte, V., Zhai, P., Pirani, A., Connors, S., Péan, C., Berger, S., Caud, N., Chen, Y., Goldfarb, L., Gomis, M., Huang, M., Leitzell, K., Lonnoy, E., Matthews, J., Maycock, T., Waterfield, T., Yelekçi, O., Yu, R., and Zhou, B., editors (2021). *Climate Change 2021: The Physical Science Basis. Contribution of Working Group I to the Sixth Assessment Report of the Intergovernmental Panel on Climate Change*. Cambridge University Press, Cambridge, United Kingdom and New York, NY, USA.
- Mod, H. K., Scherrer, D., Luoto, M., and Guisan, A. (2016). What we use is not what we know: environmental predictors in plant distribution models. *Journal of Vegetation Science*, 27(6):1308–1322.
- Oksanen, J., Simpson, G. L., Blanchet, F. G., Kindt, R., Legendre, P., Minchin, P. R., O’Hara, R., Solymos, P., Stevens, M. H. H., Szoecs, E., Wagner, H., Barbour, M., Bedward, M., Bolker, B., Borcard, D., Carvalho, G., Chirico, M., De Caceres, M., Durand, S., Evangelista, H. B. A., FitzJohn, R., Friendly, M., Furneaux, B., Hannigan, G., Hill, M. O., Lahti, L., McGlinn, D., Ouellette, M.-H., Ribeiro Cunha, E., Smith, T., Stier, A., Ter Braak, C. J., and Weedon, J. (2022). *vegan: Community Ecology Package*. R package version 2.6-4.
- Ozinga, W. A., Römermann, C., Bekker, R. M., Prinzing, A., Tamis, W. L., Schaminée, J. H., Hennekens, S. M., Thompson, K., Poschlod, P., Kleyer, M., et al. (2009). Dispersal failure contributes to plant losses in NW Europe. *Ecology letters*, 12(1):66–74.
- Pearson, R. G. (2006). Climate change and the migration capacity of species. *Trends in ecology & evolution*, 21(3):111–113.
- Peterson, A. T., Soberón, J., Pearson, R. G., Anderson, R. P., Martínez-Meyer, E., Nakamura, M., and Araújo, M. B. (2011). Ecological niches and geographic distributions

- (mpb-49). In *Ecological Niches and Geographic Distributions (MPB-49)*. Princeton University Press.
- Phillips, S. J., Anderson, R. P., and Schapire, R. E. (2006). Maximum entropy modeling of species geographic distributions. *Ecological modelling*, 190(3-4):231–259.
- Pott, R. (1996). Die Entwicklungsgeschichte und Verbreitung xerothermer Vegetationseinheiten in Mitteleuropa unter dem Einfluss des Menschen. *Tuexenia: Mitteilungen der Floristisch-Soziologischen Arbeitsgemeinschaft*, 16:337–369.
- Pritchard, J. K., Stephens, M., and Donnelly, P. (2000). Inference of population structure using multilocus genotype data. *Genetics*, 155(2):945–959.
- Putz, C. M., Schmid, C., and Reisch, C. (2015). Living in isolation—population structure, reproduction, and genetic variation of the endangered plant species *Dianthus gratianopolitanus* (Cheddar pink). *Ecology and Evolution*, 5(17):3610–3621.
- Qiong, L., Zhang, W., Wang, H., Zeng, L., Birks, H. J. B., and Zhong, Y. (2017). Testing the effect of the Himalayan mountains as a physical barrier to gene flow in *Hippophae tibetana* schlect.(Elaeagnaceae). *PLoS One*, 12(5):e0172948.
- R Core Team (2023). *R: A Language and Environment for Statistical Computing*. R Foundation for Statistical Computing, Vienna, Austria.
- Rödger, D. and Engler, J. O. (2011). Quantitative metrics of overlaps in Grinnellian niches: advances and possible drawbacks. *Global Ecology and Biogeography*, 20(6):915–927.
- Schoener, T. W. (1968). The Anolis lizards of Bimini: resource partitioning in a complex fauna. *Ecology*, 49(4):704–726.
- Slatyer, R. A., Hirst, M., and Sexton, J. P. (2013). Niche breadth predicts geographical range size: a general ecological pattern. *Ecology letters*, 16(8):1104–1114.
- Steven J. Phillips, Miroslav Dudík, R. E. S. (2024). Maxent software for modeling species niches and distributions (Version 3.4.1). [http : //biodiversityinformatics.amnh.org/open_source/maxent/](http://biodiversityinformatics.amnh.org/open_source/maxent/). 2024-5-19.
- Su, H., Qu, L., He, K., Zhang, Z., Wang, J., Chen, Z., and Gu, H. (2003). The Great Wall of China: a physical barrier to gene flow? *Heredity*, 90(3):212–219.
- Thomas, C. D., Cameron, A., Green, R. E., Bakkenes, M., Beaumont, L. J., Collingham, Y. C., Erasmus, B. F., De Siqueira, M. F., Grainger, A., Hannah, L., et al. (2004). Extinction risk from climate change. *Nature*, 427(6970):145–148.
- Thuiller, W., Lavorel, S., Araújo, M. B., Sykes, M. T., and Prentice, I. C. (2005). Climate change threats to plant diversity in Europe. *Proceedings of the National Academy of Sciences*, 102(23):8245–8250.

- Trense, D., Schmidt, T. L., Yang, Q., Chung, J., Hoffmann, A. A., and Fischer, K. (2021). Anthropogenic and natural barriers affect genetic connectivity in an Alpine butterfly. *Molecular Ecology*, 30(1):114–130.
- Turner, M. E., Stephens, J. C., and Anderson, W. W. (1982). Homozygosity and patch structure in plant populations as a result of nearest-neighbor pollination. *Proceedings of the National Academy of Sciences*, 79(1):203–207.
- Velazco, S. J. E., Galvao, F., Villalobos, F., and De Marco Junior, P. (2017). Using worldwide edaphic data to model plant species niches: An assessment at a continental extent. *PLoS One*, 12(10):e0186025.
- Warren, D. L., Glor, R. E., and Turelli, M. (2008). Environmental niche equivalency versus conservatism: quantitative approaches to niche evolution. *Evolution*, 62(11):2868–2883.
- Warren, D. L., Matzke, N. J., Cardillo, M., Baumgartner, J. B., Beaumont, L. J., Turelli, M., Glor, R. E., Huron, N. A., Simões, M., Iglesias, T. L., et al. (2021). ENMTools 1.0: an r package for comparative ecological biogeography. *Ecography*, 44(4):504–511.
- Wickham, H. (2016). *ggplot2: Elegant Graphics for Data Analysis*. Springer-Verlag New York.
- Wisz, M. S., Hijmans, R., Li, J., Peterson, A. T., Graham, C., Guisan, A., and Group, N. P. S. D. W. (2008). Effects of sample size on the performance of species distribution models. *Diversity and distributions*, 14(5):763–773.
- Wolff, K., El-Akkad, S., and Abbott, R. J. (1997). Population substructure in *Alkanna orientalis* (Boraginaceae) in the Sinai Desert, in relation to its pollinator behaviour. *Molecular Ecology*, 6(4):365–372.
- Zippel, E., Rohner, M.-S., Heinken-Šmídová, A., Tschöpe, O., and Lauterbach, D. (2021). Erprobung von Ansiedlungsmaßnahmen zum Erhalt der Pfingst-Nelke (*dianthus gratianopolitanus*) bei Bad Freienwalde. *Verhandlungen des Botanischen Vereins von Berlin und Brandenburg*, 153:65–84.

Synthesis and Conclusion

Synthesis

The aim of my study was to unravel the phylogeography and evolutionary history of *D. gratianopolitanus*, its substrate evolution indicating adaptations to different substrate types and possible home-effects, and the genetic make-up and effects of isolation on metapopulation systems and possible implications for species conservation.

In [Part I](#), the lack of spatial genetic variation, the high mixing of plastid haplotypes, and the absence of distinct spatial or species structure in the plastome tree suggest postglacial gene flow, supporting a scenario of a once widespread distribution followed by secondary fragmentation. Genetic assignment reveals two distinct gene pools, in the north and south, with a third one in their contact zone. Genetic and cytological data strongly support the existence of a refugium in Southern France. While evidence for a northern German/Czech refugium is still lacking, it is possible that small, now-extinct populations in western Germany near Belgium survived and later expanded. The third genetic group identified in Baden-Württemberg could be the result of survival in unknown refugia or a contact zone where northern and southern gene pools met.

In [Part II](#), Cheddar Pink populations from calcareous and siliceous bedrock form different phenotypes that indicate adaptations to their respective environments. Although the differences in elemental uptake were minimal, variations in growth and flowering strategies were evident. Plants from calcareous bedrock focused more on vegetative growth, likely enhancing vegetative reproduction and increasing their competitiveness for space on the limited limestone outcrops. In contrast, plants from siliceous bedrock exhibited higher flowering rates, promoting gene flow and quicker colonization of the more open habitats. The plants' origin showed no influence on flowering time when comparing different geographical regions and substrates. While there was a noticeable shift towards earlier flowering between 2013 and 2022/23, the rise in early spring and summer temperatures alone does likely not suffice to trigger earlier flowering.

In [Part III](#), the analysis of genetic structure of metapopulation systems using neighbor-net inferred genotypes and genetic assignment reveals varying patterns of connectivity and degrees of isolation. These patterns may suggest recent gene flow or represent remnants of past genetic connectivity. Nonetheless, the pronounced genetic structuring observed across all populations underscores the necessity for effective conservation strategies that target all subpopulations. These strategies should aim to preserve genetic variation and (re-)establish potential dispersal routes. Ecological niche modeling highlights differing climatic conditions and constraints for *D. gratianopolitanus* on calcareous and siliceous bedrock. Southern populations are more affected by drought stress, whereas northern populations face limitations due to minimum temperatures. The siliceous group, with its broader niche breadth, appears to have a wider range of suitable climate conditions compared to the more specialized calcareous group. Although predicted areas under current climate conditions exceed the present-day distribution, future projections indicate a significant reduction in suitable areas, with a trend towards higher elevations and northward migrations.

Conclusion

The study provides a comprehensive understanding of the phylogeography, evolutionary history, and ecological adaptations of *Dianthus gratianopolitanus*. The survival in different refugia lead to a genetic differentiation but not to a distinct substrate adaptation. While the different gene pools, to the north and south, coincide with differences in bedrock type the Cheddar Pink does not show strong adaptations to the elemental composition of the different substrate types. Plants originating from a distinct bedrock type can still colonise and grow under the foreign conditions of a different bedrock type, even under the harsh conditions of serpentine soil. Indeed such possible migrations can be observed in the natural habitat, where plants originating from siliceous bedrock likely colonised the serpentine bedrock from Wojaleite, plants from calcareous bedrock colonised the siliceous habitat in the Baden-Württemberg Wutachschlucht, or plants from siliceous soil colonized limestone habitats in the Czech Republic in Střevíc or in Northern Germany at the Süntelfels. Data on element composition and fitness data is available for single individuals from these exceptional populations and can serve as interesting starting point for local, population wide adaptations. Nevertheless the observed differences in the fitness parameters indicate a genetic differentiation between the two groups, leading to differences in flowering and growth. While the plants from different origins showed a similar flowering time under the same conditions, the overall adaptation to increasing early year temperatures is evident over the years.

The fact that *D. gratianopolitanus* from siliceous bedrock differs genetically as well as in growth and flowering behaviour from the calcareous Cheddar Pink further stresses the importance of its conservation in all current areas as well as the responsibility of Germany to do so in both the calcareous but especially in the siliceous range, that has its center in Central Germany (Koch et al., 2021). In addition to the maintenance measures, such as the removal of shrubs and bushes, the number of suitable habitats should be increased to strengthen possible gene flow and dispersal to guarantee viable populations that can adapt to changing environmental conditions. Especially with changing climatic conditions the suitability of the habitats should be reassessed and the possibility to migrate to avoid the most extreme conditions, e.g. a move from the highly sun exposed southern sites to less exposed sites, need to be supported. The use of a combination of in situ and in situ conservation has been shown for *D. gratianopolitanus* (Koch et al., 2021; Janczyk-Weglarska et al., 2013; Zippel et al., 2021) and further efforts to support existing populations and establish new ones will be crucial in the conservation of the Cheddar Pink. This could also provide an interesting starting point for future studies, comparing the fitness of plants from calcareous and siliceous bedrock within the natural habitat, assessing whether the differences in growth and flowering observed in the reciprocal transplant experiment do have influence on their competitiveness and prove to be advantages in their home environment. While differences in flower as well as leaf and cushion morphology was observed in my study they did not receive further attention, but could also provide interesting insight in past evolutionary processes and adaptations.

1 | Bibliography

- Janczyk-Weglarska, J., Weglarski, K., and Wiland-Szymanska, J. (2013). Active ex situ protection and reestablishment of *Dianthus gratianopolitanus* Vill. in the "Goździk siny w Grzybnie" reserve (Wielkopolska Province). *Biodiversity Research and Conservation*, 32(1):53.
- Koch, M. A., Winizuk, A., Banzhaf, P., and Reichardt, J. (2021). Impact of climate change on the success of population support management and plant reintroduction at steep, exposed limestone outcrops in the German Swabian Jura. *Perspectives in Plant Ecology, Evolution and Systematics*, 53:125643.
- Zippel, E., Rohner, M.-S., Heinken-Šmídová, A., Tschöpe, O., and Lauterbach, D. (2021). Erprobung von Ansiedlungsmaßnahmen zum Erhalt der Pfingst-Nelke (*dianthus gratianopolitanus*) bei Bad Freienwalde. *Verhandlungen des Botanischen Vereins von Berlin und Brandenburg*, 153:65–84.

Appendix

A | Appendix - Part I

Table A.1: Permits acquired for sample collection of leaf material and cuttings of *D. gratianopolitanus*. Country, issuing authority, date of permit and licence number is given. The corresponding files as well as a more detailed overview is given in the Digital Supplement. A permission to collect serpentine substrate from the natural habitat in Wojaleite is also included.

Country	issuing authority	Date of permit	Licence number
England	Natural England	2009-10-20	20093637
Luxembourg	Le Gouvernement du Grand-Duché de Luxembourg	2010-04-21	70871 MS/sc
Switzerland	Service des forêts, de la faune et de la nature , Centre de Conservation de la faune et de la nature	2013-05-16	1882
Switzerland	Amt für Landschaft und Natur des Kantons Bern	2013-05-13	Reg.-Nr. 4.3.1.3-PG
France	Direction régionale de l'environnement , de l'aménagement et du logement , Franche-Comté	2012-07-13	PC-LT-000-566
France	Direction départementale des territoires, Le préfet de la Drôme	2012-08-01	2012-234
France	Direction régionale de l'environnement , de l'aménagement et du logement , Préfecture du Jura	2012-07-12	
France	Préfet de l'Isère	2012-07-25	2012-207-0019
France	Direction départementale des territoires, Préfet de la Haute-Savoie	2012-08-06	2012219-0004
France	Direction départementale des territoires, Le préfet de l'Ain	2012-08-07	
France	Ministère de l'écologie, du développement durable et de l'énergie	2012-07-02	12/593/EXP
France	Direction départementale des territoires, Le préfet de la Savoie	2013-01-21	2012-034
Germany	Landesverwaltungsamt Sachsen-Anhalt	2012-05-03	407.4.1-516-12-2241-Hz
Germany	Landkreis Hameln-Pyrmont, Niedersachsen	2009-09-09	411-12.2.2- Bo
Germany	Landesamt für Umwelt, Gesundheit und Verbraucherschutz Brandenburg	2013-08-21	286-2013
Germany	Landratsamt Wartburgkreis, Thüringen	2012-05-18	25.1-092-16.09-312-he-12
Germany	Stadtverwaltung Eisenach, Untere Naturschutzbehörde, Thüringen	2012-05-21	26.12/15.02-12-01
Germany	Landratsamt Saalfeld-Rudolstadt, Thüringen	2012-05-24	364.623:12_26-2.5/ra
Germany	Landratsamt Gotha, Umweltamt, Thüringen	2012-06-08	6.2.1/Reu/§45.7/2012/04
Germany	Landratsamt Saale-Orla-Kreis, Thüringen	2012-05-03	20427-2012-114
Germany	Regierung von Oberfranken, Bayern	2009-07-27	55.1-8641-4/09
Germany	Regierung von Oberfranken, Bayern	2012-04-30	55.1-8622
Germany	Struktur- und Genehmigungsdirektion Nord, Rheinland-Pfalz	2009-06-25	425-104.131.0903
Germany	Struktur- und Genehmigungsdirektion Nord, Rheinland-Pfalz	2010-06-17	425-104.133.1003
Germany	Struktur- und Genehmigungsdirektion Süd, Rheinland-Pfalz	2010-05-26	42/553-251
Germany	Regierungspräsidium Kassel, Hessen	2012-05-11	27.2-R21.1
Germany	Nationalparkamt Kellerwald-Edersee	2013-06-17	Milseburg und Habelstein R22.9
Substrate			
Germany	Regierung von Oberfranken, Bayern	2012-04-12	55.1-8622

feature number		trnL-trnF													
		1	2	3	4	5	6	7	8	9	10	11	12	13	14
alignment position		13 - 20	73	96	134 -	140	142	143	159	176	238	362	367	374	376
ht01	1 c III	G	C	T	A	-	T	A	T	A	G	G	C	G	G
ht02	2 b I	A	C	G	G	-	T	A	T	A	G	G	C	A	G
ht03	3 b I	A	C	T	G	-	T	A	T	A	G	G	C	A	G
ht04	4 d I	A	C	T	G	-	T	A	T	A	G	G	C	G	G
ht05	4 h XVII	A	C	T	G	-	T	A	T	A	G	G	C	G	G
ht06	4 h I	A	C	T	G	-	T	A	T	A	G	G	C	G	G
ht07	4 h X	A	C	T	G	-	T	A	T	A	G	G	C	G	G
ht08	4 j XIII	A	C	T	G	-	T	A	T	A	G	G	C	G	G
ht09	4 l I	A	C	T	G	-	T	A	T	A	G	G	C	G	G
ht10	4 m XIII	A	C	T	G	-	T	A	T	A	G	G	C	G	G
ht11	4 n XV	A	C	T	G	-	T	A	T	A	G	G	C	G	G
ht12	4 p I	A	C	T	G	-	T	A	T	A	G	G	C	G	G
ht13	5 a I	A	C	T	A	T	G	A	T	A	G	T	C	G	G
ht14	6 d II	A	C	T	A	-	T	A	T	A	T	G	C	G	G
ht15	7 c XIV	A	C	T	A	-	T	A	T	A	G	G	C	G	G
ht16	7 c III	A	C	T	A	-	T	A	T	A	G	G	C	G	G
ht17	7 c VII	A	C	T	A	-	T	A	T	A	G	G	C	G	G
ht18	7 c XI	A	C	T	A	-	T	A	T	A	G	G	C	G	G
ht19	7 d II	A	C	T	A	-	T	A	T	A	G	G	C	G	G
ht20	7 d III	A	C	T	A	-	T	A	T	A	G	G	C	G	G
ht21	7 d IV	A	C	T	A	-	T	A	T	A	G	G	C	G	G
ht22	7 d VI	A	C	T	A	-	T	A	T	A	G	G	C	G	G
ht23	7 g XII	A	C	T	A	-	T	A	T	A	G	G	C	G	G
ht24	7 i III	A	C	T	A	-	T	A	T	A	G	G	C	G	G
ht25	7 o XVIII	A	C	T	A	-	T	A	T	A	G	G	C	G	G
ht29	9 d I	A	C	T	G	-	T	A	A	A	G	G	C	G	G
ht30	9 d V	A	C	T	G	-	T	A	A	A	G	G	C	G	G
ht32	11 d IV	A	C	T	A	-	T	A	T	A	G	G	C	G	G
ht33	15 d I	A	A	T	G	-	T	A	T	A	G	G	C	A	G
ht34	15 e I	A	A	T	G	-	T	A	T	A	G	G	C	A	G
ht35	16 d XVI	A	C	T	A	T	G	-	T	A	G	G	A	A	G
ht37	17 d I	A	C	T	G	-	T	A	T	A	G	G	C	G	A
ht38	18 d III	A	C	T	A	-	T	A	T	A	G	G	C	G	G
ht39	19 c III	A	C	T	A	-	T	A	T	A	G	G	C	G	G
ht41	12 d XIII	A	C	T	G	-	T	A	T	C	G	G	C	A	G
ht43	12 e XIII	A	C	T	G	-	T	A	T	C	G	G	C	A	G
ht44	13 d III	A	C	T	A	-	T	A	T	A	G	G	C	G	G
ht46	14 d XX	A	C	T	A	-	T	A	T	A	G	G	C	G	G
ht47	14 d IX	A	C	T	A	-	T	A	T	A	G	G	C	G	G
ht48	14 f IX	A	C	T	A	-	T	A	T	A	G	G	C	G	G

Table A.2: SNP matrix of the plastid marker *trnL-trnF*. The alignment position refers to the alignment given in the Digital Supplement: haplotypes_ Dg_ Dm.fas

feature number		trnC-ycf6																	
		15	16	17	18	19	20	21	22	23	24	25	26	27	28	29	30	31	
alignment position		415 - 421	432	442	512	515 - 525	600	611 - 622	640	663	666	676	731	755	831	873 - 878	898	914	
ht01	1c III	G	A	C	G	G	T	G	A	C	G	G	A	G	A	G	-	T	
ht02	2b I	G	A	A	A	G	T	G	A	C	G	G	G	G	A	G	-	T	
ht03	3b I	G	A	A	A	G	T	G	A	C	G	G	G	G	A	G	-	T	
ht04	4d I	G	A	C	G	G	T	G	A	C	G	G	G	G	A	G	-	T	
ht05	4h XVII	G	A	C	G	G	T	G	A	T	G	G	G	G	A	G	-	T	
ht06	4h I	G	A	C	G	G	T	G	A	T	G	G	G	G	A	G	-	T	
ht07	4h X	G	A	C	G	G	T	G	A	T	G	G	G	G	A	G	-	T	
ht08	4j XIII	G	A	C	G	G	C	G	A	C	G	G	G	G	A	G	-	T	
ht09	4l I	G	A	C	G	G	T	G	A	C	G	A	G	G	A	G	-	G	
ht10	4m XIII	G	C	C	G	G	T	G	A	C	G	G	G	G	T	G	A	T	
ht11	4n XV	G	A	C	G	G	T	G	T	C	G	G	G	G	A	A	G	-	T
ht12	4p I	G	A	C	G	G	T	G	A	C	G	G	G	A	A	G	-	T	
ht13	5a I	G	A	C	G	A	T	G	A	C	G	G	G	G	A	G	-	T	
ht14	6d II	G	A	C	G	G	T	G	A	C	G	G	G	G	A	G	-	T	
ht15	7c XIV	G	A	C	G	G	T	G	A	C	G	G	A	G	A	G	-	T	
ht16	7c III	G	A	C	G	G	T	G	A	C	G	G	A	G	A	G	-	T	
ht17	7c VII	G	A	C	G	G	T	G	A	C	G	G	A	G	A	G	-	T	
ht18	7c XI	G	A	C	G	G	T	G	A	C	G	G	A	G	A	G	-	T	
ht19	7d II	G	A	C	G	G	T	G	A	C	G	G	G	G	A	G	-	T	
ht20	7d III	G	A	C	G	G	T	G	A	C	G	G	G	G	A	G	-	T	
ht21	7d IV	G	A	C	G	G	T	G	A	C	G	G	G	G	A	G	-	T	
ht22	7d VI	G	A	C	G	G	T	G	A	C	G	G	G	G	A	G	-	T	
ht23	7g XII	G	A	C	G	G	T	G	A	C	A	G	G	G	A	G	-	T	
ht24	7i III	G	A	C	G	G	T	G	A	C	G	G	A	G	A	A	-	T	
ht25	7o XVIII	G	A	C	G	G	T	A	A	C	A	G	G	G	A	G	-	T	
ht29	9d I	G	A	C	G	G	T	G	A	C	G	G	G	G	A	G	-	T	
ht30	9d V	G	A	C	G	G	T	G	A	C	G	G	G	G	A	G	-	T	
ht32	11d IV	G	A	C	G	G	T	G	A	C	G	G	G	G	A	G	-	T	
ht33	15d I	G	A	C	G	G	T	G	A	C	G	G	G	G	A	G	-	T	
ht34	15e I	G	A	C	G	G	T	G	A	C	G	G	G	G	A	A	-	T	
ht35	16d XVI	G	A	C	G	G	T	G	A	C	G	G	G	G	A	G	-	T	
ht37	17d I	G	A	C	G	G	T	G	A	C	G	G	G	G	A	G	-	T	
ht38	18d III	G	A	C	G	G	T	G	A	C	G	G	G	G	A	G	-	T	
ht39	19c III	G	A	C	G	G	T	G	A	C	G	G	A	G	A	G	-	T	
ht41	12d XIII	G	A	C	G	G	T	G	A	C	G	G	G	G	A	G	-	T	
ht43	12e XIII	G	A	C	G	G	T	G	A	C	G	G	G	G	A	A	-	T	
ht44	13d III	G	A	C	G	G	T	G	A	C	G	G	G	G	A	G	-	T	
ht46	14d XX	G	A	C	G	G	T	G	A	C	G	G	G	G	A	G	-	T	
ht47	14d IX	G	A	C	G	G	T	G	A	C	G	G	G	G	A	G	-	T	
ht48	14f IX	A	A	C	G	G	T	G	A	C	G	G	G	G	A	G	-	T	

Table A.3: SNP matrix of the plastid marker *trnC-ycf6*. The alignment position refers to the alignment given in the Digital Supplement: haplotypes_ Dg_ Dm.fas

feature number		trnH-psbA															
		32	33	34	35	36	37	38	39	40	41	42	43	44	45	46	47
alignment position		979	986	987- 1005	1025- 1031	1044	1047	1050	1059	1060	1067	1068	1069	1072	1122	1136	1152
ht01	1 c III	C	T	G	G	A	G	G	T	-	A	A	A	A	G	T	A
ht02	2 b I	C	T	G	G	A	G	G	T	-	A	A	A	A	G	T	A
ht03	3 b I	C	T	G	G	A	G	G	T	-	A	A	A	A	G	T	A
ht04	4 d I	C	T	G	G	A	G	G	T	-	A	A	A	A	G	T	A
ht05	4 h XVII	C	T	G	G	A	C	G	-	-	A	A	A	A	G	T	A
ht06	4 h I	C	T	G	G	A	G	G	T	-	A	A	A	A	G	T	A
ht07	4 h X	G	T	G	G	A	G	G	T	A	A	A	A	A	G	T	A
ht08	4 j XIII	C	T	G	G	A	G	G	-	A	A	A	A	A	G	T	A
ht09	4 l I	C	T	G	G	A	G	G	T	-	A	A	A	A	G	T	A
ht10	4 m XIII	C	T	G	G	A	G	G	-	A	A	A	A	A	G	T	A
ht11	4 n XV	C	T	A	G	A	G	G	T	-	A	A	A	A	G	T	A
ht12	4 p I	C	T	G	G	A	G	G	T	-	A	A	A	A	G	T	A
ht13	5 a I	C	T	G	G	A	G	G	T	-	A	A	A	A	G	T	A
ht14	6 d II	C	T	G	G	A	G	G	T	-	A	A	A	A	T	T	A
ht15	7 c XIV	C	T	G	G	A	G	G	T	-	A	A	A	A	G	T	A
ht16	7 c III	C	T	G	G	A	G	G	T	-	A	A	A	A	G	T	A
ht17	7 c VII	C	T	G	G	A	G	G	T	-	A	A	A	A	G	T	A
ht18	7 c XI	C	T	G	G	A	G	G	T	-	A	A	A	A	G	T	C
ht19	7 d II	C	T	G	G	A	G	G	T	-	A	A	A	A	T	T	A
ht20	7 d III	C	T	G	G	A	G	G	T	-	A	A	A	A	G	T	A
ht21	7 d IV	C	G	G	A	A	G	G	T	A	A	A	A	A	G	T	A
ht22	7 d VI	C	T	G	G	G	G	G	T	-	A	A	A	A	G	T	A
ht23	7 g XII	C	G	G	G	A	G	G	-	-	A	A	A	A	G	T	A
ht24	7 i III	C	T	G	G	A	G	G	T	-	A	A	A	A	G	T	A
ht25	7 o XVIII	C	T	G	G	A	G	G	T	-	T	A	A	A	G	T	A
ht29	9 d I	C	T	G	G	A	G	G	T	-	A	A	A	A	G	T	A
ht30	9 d V	C	T	G	G	A	G	G	T	A	A	A	A	C	G	T	A
ht32	11 d IV	C	G	G	A	A	G	G	T	A	A	A	A	A	G	T	A
ht33	15 d I	C	T	G	G	A	G	G	T	-	A	A	A	A	G	T	A
ht34	15 e I	C	T	G	G	A	G	G	T	-	A	A	A	A	G	T	A
ht35	16 d XVI	C	T	G	G	A	G	G	T	A	A	T	T	A	G	G	A
ht37	17 d I	C	T	G	G	A	G	G	T	-	A	A	A	A	G	T	A
ht38	18 d III	C	T	G	G	A	G	G	T	-	A	A	A	A	G	T	A
ht39	19 c III	C	T	G	G	A	G	G	T	-	A	A	A	A	G	T	A
ht41	12 d XIII	C	T	G	G	A	G	G	-	A	A	A	A	A	G	T	A
ht43	12 e XIII	C	T	G	G	A	G	G	-	A	A	A	A	A	G	T	A
ht44	13 d III	C	T	G	G	A	G	G	T	-	A	A	A	A	G	T	A
ht46	14 d XX	C	G	G	G	A	G	A	T	-	A	A	A	A	G	T	A
ht47	14 d IX	C	T	G	G	A	G	A	T	-	A	A	A	A	G	T	A
ht48	14 f IX	C	T	G	G	A	G	A	T	-	A	A	A	A	G	T	A

Table A.4: *SNP matrix of the plastid marker trnH-psbA.* The alignment position refers to the alignment given in the Digital Supplement: haplotypes_ Dg_ Dm.fas

Mean number of AFLP bands between tetraploid and hexaploid *D.gratianopolitanus* from Dios and Massif Central (France)

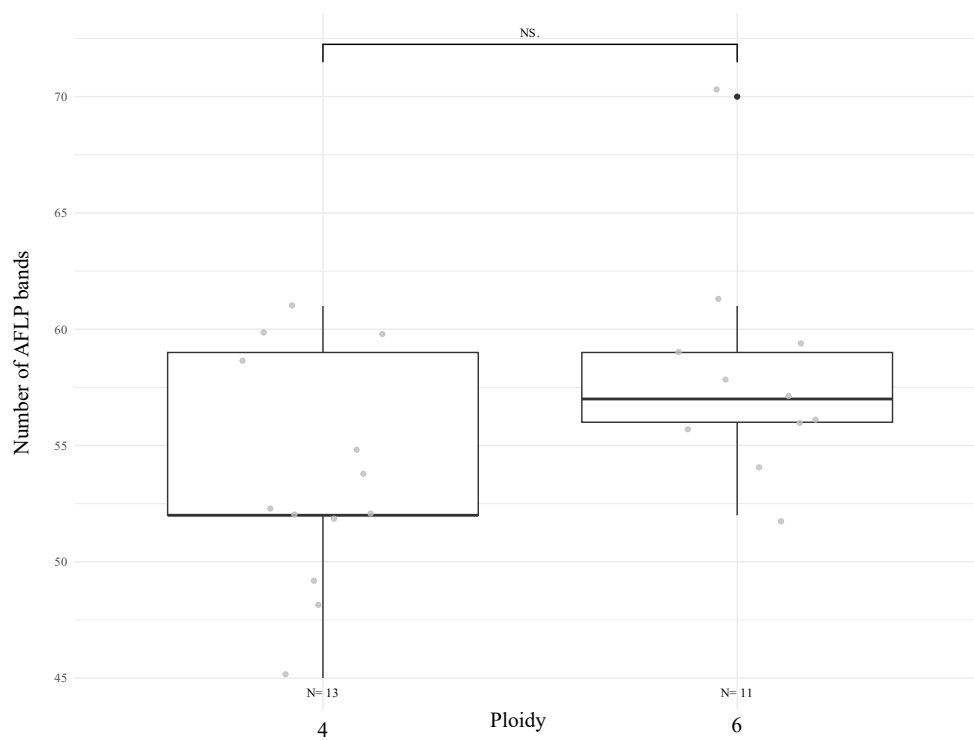
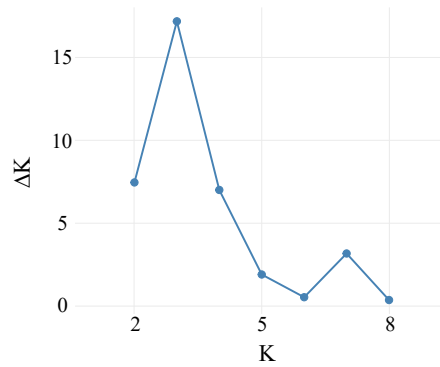


Figure A.1: *Number of AFLP bands in tetraploid and hexaploid D.gratianopolitanus from Southern France. Comparison of number of AFLP bands of individuals from Massif Central and Dios*

A



B

K	Reps	Mean LnP(K)	Stdev LnP(K)	Ln'(K)	Ln''(K)	Delta K
1	10	-122382.47	0.1059	-	-	-
2	10	-119582.03	147.458	2800.44	1099.99	7.459681
3	10	-117881.58	26.558	1700.45	456.26	17.179744
4	10	-116637.39	64.6404	1244.19	452.91	7.006604
5	10	-115846.11	120.7881	791.28	230.24	1.906149
6	10	-115285.07	442.8667	561.04	237.11	0.535398
7	10	-114486.92	203.0062	798.15	644.39	3.174238
8	10	-114333.16	1393.6976	153.76	510.87	0.366557
9	10	-113668.53	863.2908	664.63	-	-

Figure A.2: Evanno statistic for the STRUCTURE analysis of the whole distribution data set for *D. gratianopolitanus* and *D. gratianopolitanus* subsp. *moravicus*. **A** Optimal K as inferred by the evanno statistics $K = 3$ is indicated as optimal K . **B** evanno statistics for $K = 1$ to $K = 10$.

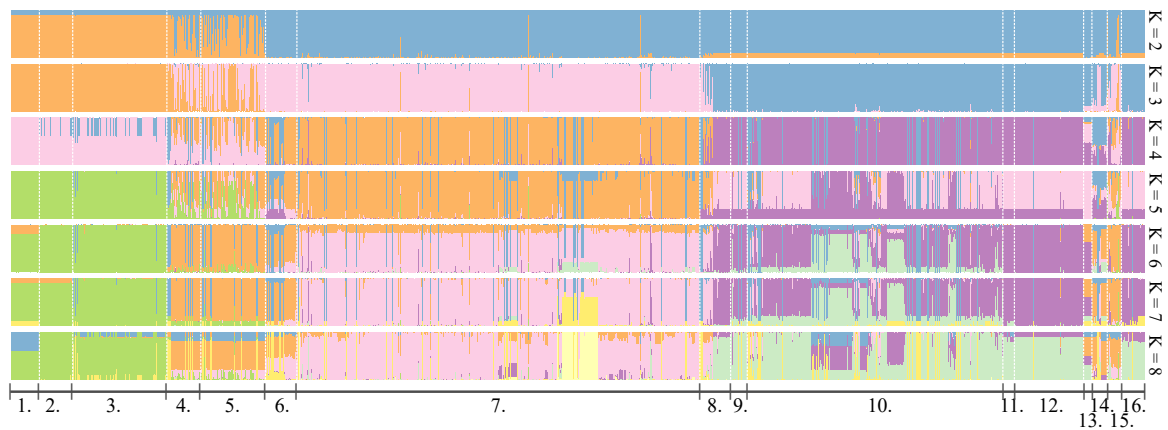


Figure A.3: STRUCTURE results for the whole distribution dataset of *D. gratianopolitanus*. Number of clusters range from $K=2$ to $K=8$. Regions are numbered: 1) Massif Central, 2) Diois, 3) French Prealps, 4) French Jurassic, 5) Switzerland, 6) Bodensee region, 7) Swabian Alb, 8) Bavarian Jurassic, 9) Bavarian Serpentine, 10) Central Germany, 11) Brandenburg, 12) Czech Republic, 13) Poland, 14) Belgium and Luxembourg, 15) United Kingdom and 16) *Dianthus moravicus* from the Czech Republic.

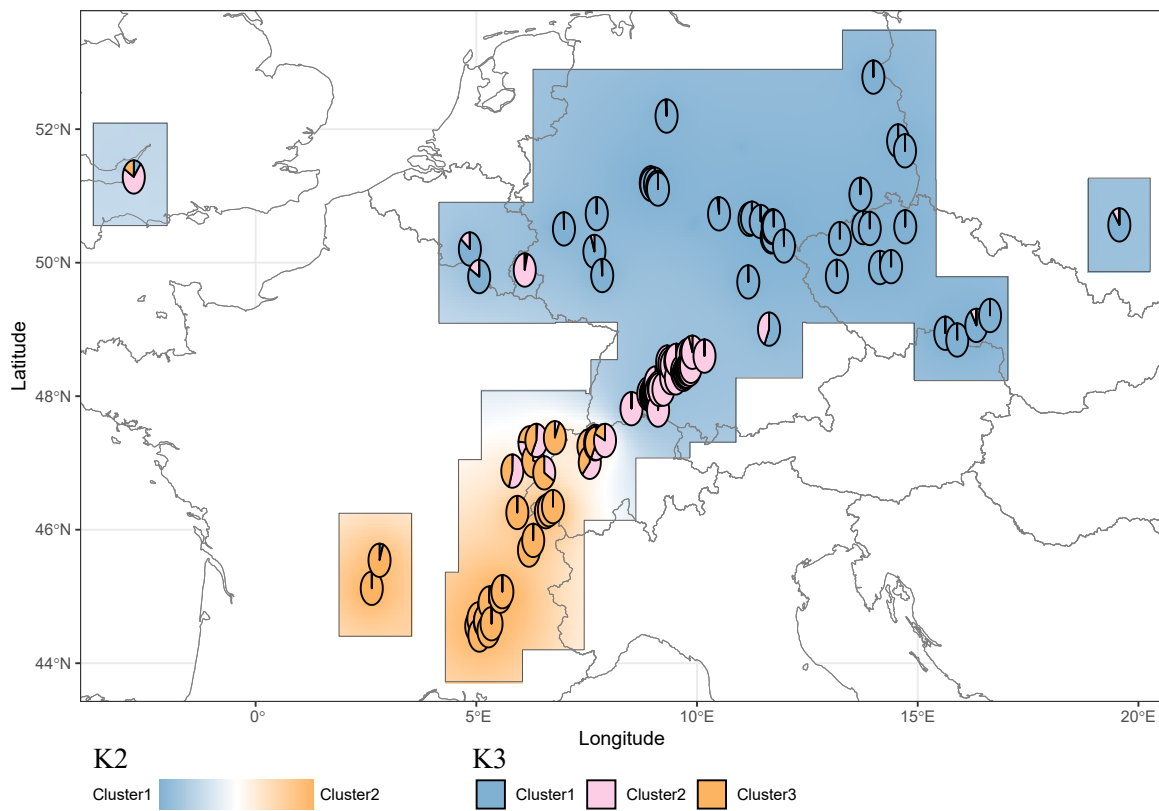


Figure A.4: Distribution of spatial AFLP genetic structure *STRUCTURE* analysis results are given for $K = 2$ as inverse distance weighted (*idw*) interpolation as background and $K=3$ as population means. A more detailed plot of genetic assignment is given in [Figure A.5](#) and [Figure A.6](#)

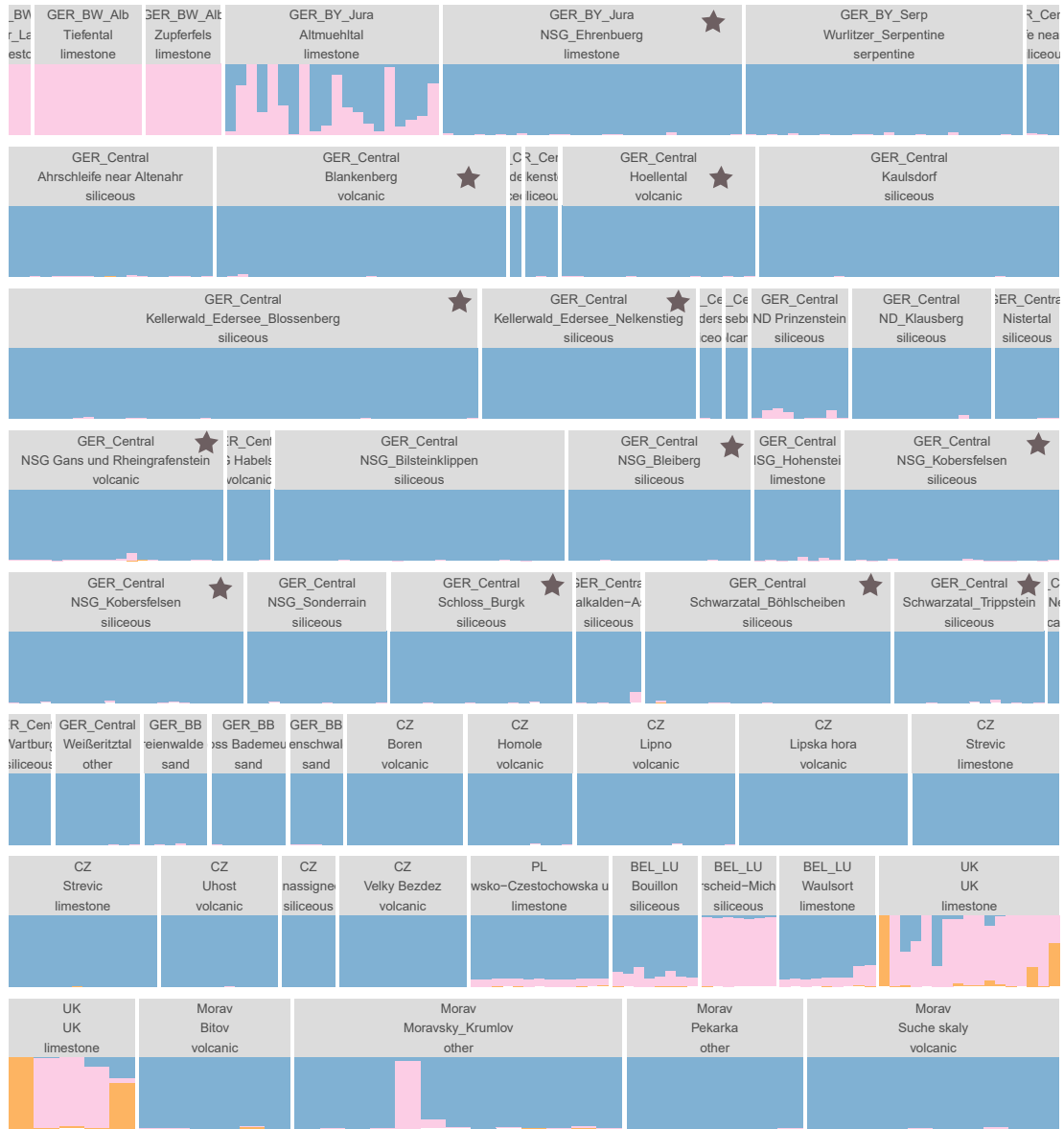


Figure A.6: Detailed STRUCTURE results for the whole distribution dataset of *D. gratianopolitanus*, $K=3$. Part 2. The stars indicate metapopulations included in the metapopulation analysis of Part III.

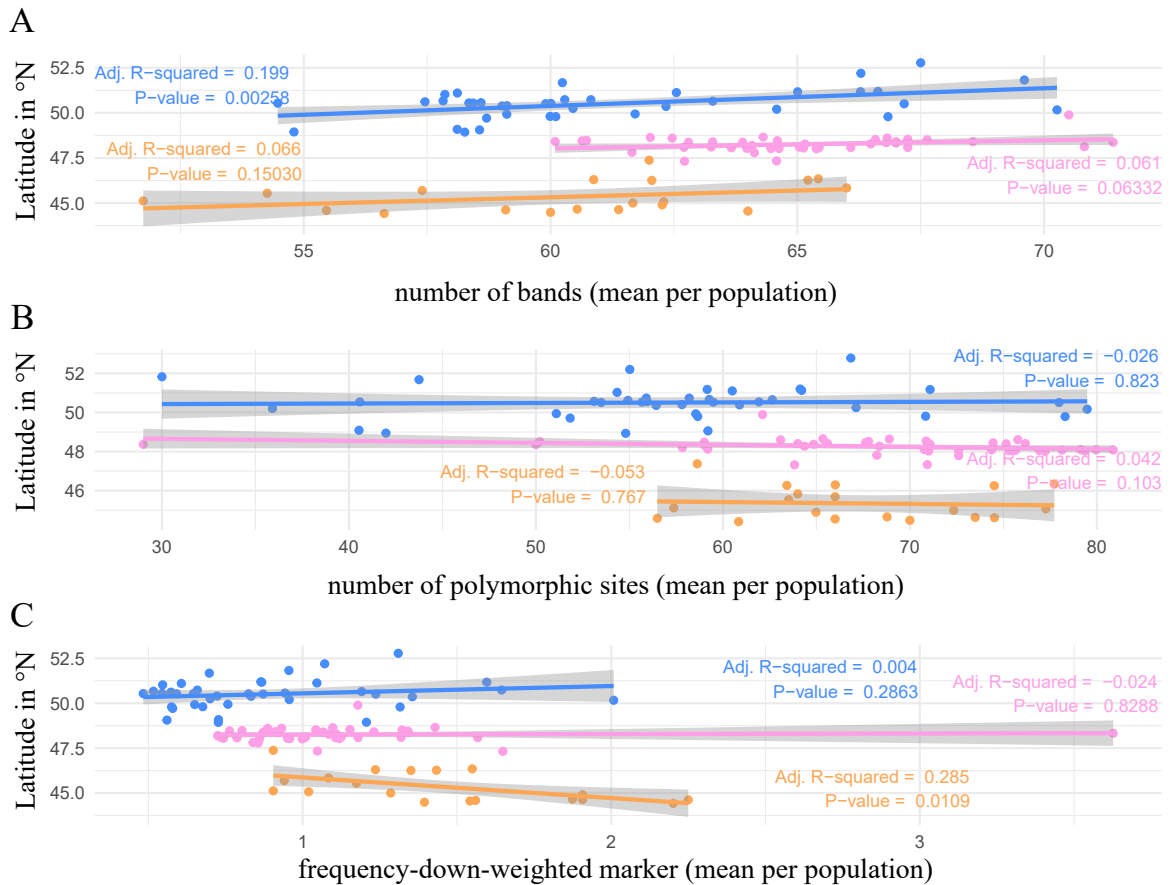


Figure A.7: Linear relationship of latitude and AFLP statistics (mean) for populations by *STRUCTURE* assignment $K=3$ To ensure sufficient sample sizes and correct for population size, mean values were calculated on basis of $n=5$ subsamples per population. Populations were grouped by structure assignment with a threshold of $> 75\%$ population mean assignment to a cluster. Three different statistics are included: **A** number of bands, **B** number of polymorphic sites and **C** frequency-down-weighted marker.

Table A.5: Ploidy and genome size of *D. gratianopolitanus* Comparison of ploidy inferred by chromosome counting (CC) and flow cytometry (FCM). Red individuals showed differences in ploidy between the methods. Due to good accordance of the genome size the FCM result was trusted.

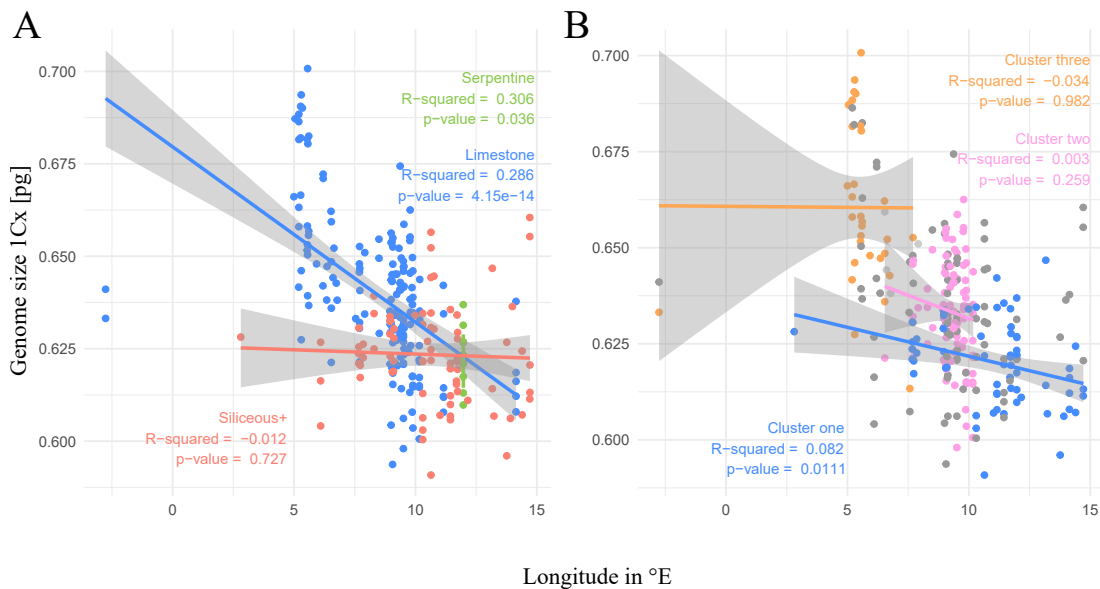
LabID	Ploidy CC	Ploidy FCM	1Cx [pg]	Population
3634	6	6	0.63	CH: Saeliflue
3437	6	6	0.65	CH: Ravellenflue
4080	6	6	0.65	CH: Le Chasseron
760	(4)	6	0.65	CZ: Lipno
3726	6	6	0.61	DE: BB: Gross Bademeusel
3988	6	6	0.63	DE: BW: NSG Wutachfluehen
975	6	6	0.63	DE: BW: Lenninger Tal: Lange Steige - Müllerfels
3849	6	6	0.63	DE: BW: Oberes Donautal - Sperberloch
3816	6	6	0.65	DE: BW: Bad Urach - Haubersloch
2467	6	6	0.63	DE: BW: Rusenschloss - Knoblauchfels
2895	6	6	0.61	DE: BY: NSG Ehrenbuerg
457	6	6	0.63	DE: BY: Wurlitzer Serpentin: Wojaleite
4272	6	6	0.62	DE: RP: ND Felsgruppe Prinzenstein
3051	6	6	0.63	DE: Th: NSG-Kobersfelsen
450	4	4	0.67	FR: Massif Central: Puy Mary
444	4	4	0.68	FR: Massif Central: Puy-de-Sancy
447	4	4	0.68	FR: Massif Central: Puy-de-Sancy
448	4	4	0.66	FR: Massif Central: Puy-de-Sancy
467	4	4	0.69	FR: Massif Central: Puy-de-Sancy
3245	6	6	0.65	FR: Massif du Jura: vallée du Doubs
1965	6	6	0.65	FR: Préalpes: Rhone-Alpes: Mont Ouzon
1890	6	6	0.70	FR: Préalpes: Rhone-Alpes: Les Moucherolles
1892	6	-	-	FR: Préalpes: Rhone-Alpes: Les Moucherolles
1222	6	6	0.64	FR: Préalpes: Rhône-Alpes: Mont Trélod
1829	6	6	0.69	FR: Rhone-Alpes: La Servelle
1712	6	6	0.64	FR: Rhone-Alpes: Le Grand Delmas
1724	6	6	0.66	FR: Rhone-Alpes: Le Grand Delmas
1730	6	6	0.66	FR: Rhone-Alpes: Le Grand Delmas
1744	6	6	0.68	FR: Rhone-Alpes: Le Grand Delmas
1755	6	6	0.69	FR: Rhone-Alpes: Le Roche Colombe
1710	6	6	0.69	FR: Rhone-Alpes: Le Veyou
1706	(6)	(4)	0.70	FR: Rhone-Alpes: Le Veyou
1810	6	6	0.69	FR: Rhone-Alpes: Rocher de l'Esqueyron
1778	4	4	0.74	FR: Rhone-Alpes: Notre Dame de Beauvoir
1787	4	4	0.69	FR: Rhone-Alpes: Notre Dame de Beauvoir
1800	4	4	0.69	FR: Rhone-Alpes: Notre Dame de Beauvoir
1766	6	6	0.67	FR: Rhone-Alpes: Montagne du Poët
440	6	6	0.63	UK: Cheddar Gorge
441	6	6	0.64	UK: Cheddar Gorge

Table A.6: Combined plastid haplotypes for *Dianthus gratianopolitanus*. Only individuals with fully known sequence or unambiguous assignment were used.

haplotype name	trnL - trnF type	trnC - ycf6 type	trnH - psbA type	number of individuals	Frequency in data set
<i>Dianthus gratianopolitanus</i>					
ht01	1	c	III	64	9,70%
ht02	2	b	I	33	5,00%
ht03	3	b	I	49	7,42%
ht04	4	d	I	3	0,45%
ht05	4	h	XVII	1	0,15%
ht06	4	h	I	4	0,61%
ht07	4	h	X	1	0,15%
ht08	4	j	XIII	1	0,15%
ht09	4	l	I	2	0,30%
ht10	4	m	XIII	6	0,91%
ht11	4	n	XV	3	0,45%
ht12	4	p	I	4	0,61%
ht13	5	a	I	4	0,61%
ht15	7	c	XIV	2	0,30%
ht16	7	c	III	179	27,12%
ht17	7	c	VII	3	0,45%
ht18	7	c	XI	1	0,15%
ht19	7	d	II	157	23,79%
ht20	7	d	III	4	0,61%
ht21	7	d	IV	48	7,27%
ht22	7	d	VI	1	0,15%
ht23	7	g	XII	8	1,21%
ht24	7	i	III	5	0,76%
ht25	7	o	XVIII	4	0,61%
ht29	9	d	I	14	2,12%
ht30	9	d	V	15	2,27%
ht32	11	d	IV	14	2,12%
ht33	15	d	I	2	0,30%
ht34	15	e	I	1	0,15%
ht35	16	d	XVI	1	0,15%
ht37	17	d	I	3	0,45%
ht38	18	d	III	2	0,30%
ht39	19	c	III	1	0,15%
ht41	12	d	XIII	2	0,30%
ht43	12	e	XIII	1	0,15%
ht44	13	d	III	7	1,06%
ht46	14	d	XX	4	0,61%
ht47	14	d	IX	2	0,30%
ht48	14	f	IX	4	0,61%
total				660	100,00%
<i>D. gratianopolitanus</i> subsp. <i>moravicus</i>					
ht14	6	d	II	4	28,57%
ht16	7	c	III	5	35,71%
ht19	7	d	II	5	35,71%
total				14	100,00%

Table A.7: Ploidy of *D. gratianopolitanus* and *Dianthus gratianopolitanus* subsp. *moravicus* Ploidy by region as inferred by Flow Cytometry

<i>Dianthus gratianopolitanus</i>				
Region	4x	6x	10x	total
BEL				
CH		19		19
CZ		15		15
FRA_Diois	4	12		16
FRA_Jura		5		5
FRA_MC	12	1		13
FRA_prealpes		20	2	22
GER_BB		4		4
GER_BW_Alb		100	2	102
GER_BW_Bodensee		10		10
GER_BY_Jura		6		6
GER_BY_Serp		12		12
GER_Central		58		58
LU		3		3
PL				
UK		2		2
total	16	267	4	287
<i>D. gratianopolitanus</i> subsp. <i>moravicus</i>				
total	16	280	4	300

**Figure A.8: Linear relationship of longitude and genome size (1Cx)** Linear regression with colors indicating **A** different substrate types and **B** > 75% assignment to a STRUCTURE cluster ($K=3$). Grey colored points indicate an ambiguous assignment to clusters.

B | Appendix - Part II

Table B.1: Analytical (spectral) lines and concentrations (in ppm) of the internal standards used in ICP OES. Several spectral lines with different wavelengths per element are used to infer the final element concentrations.

	Std-0	Std-1	Std-3	Std-4	Std-5
Al 237.3	0	0.005	0.02	0.07	0.3
Al 396.2	0	0.005	0.02	0.07	0.3
B 208.9	0	0.05	0.1	0.2	0.6
B 249.8	0	0.05	0.1	0.2	0.6
Ca 318.1	0	10	20	40	150
Cd 214.4	0	0.01	0.05	0.1	0.2
Cd 226.5	0	0.01	0.05	0.1	0.2
Cd 228.8	0	0.01	0.05	0.1	0.2
Co 228.6	0	0.005	0.01	0.02	0.05
Cr 205.6	0	0.005	0.01	0.02	0.05
Cr 267.7	0	0.005	0.01	0.02	0.05
Cu 324.8	0	0.005	0.02	0.1	0.2
Cu 327.4	0	0.005	0.02	0.1	0.2
Fe 238.2	0	0.05	0.125	0.5	2
Fe 259.9	0	0.05	0.125	0.5	2
K 766.5	0	10	50	100	150
K 769.9	0	10	50	100	150
Mg 279.1	0	2.5	5	10	50
Mn 257.6	0	0.05	0.1	0.2	1
Mn 260.6	0	0.05	0.1	0.2	1
Mo 202.0	0	0.005	0.01	0.02	0.1
Ni 221.6	0	0.025	0.1	0.4	2
Ni 231.6	0	0.025	0.1	0.4	2
P 178.3	0	1	5	10	20
P 185.9	0	1	5	10	20
P 213.6	0	1	5	10	20
Pb 220.4	0	0.025	0.1	0.4	2
Pb 283.3	0	0.025	0.1	0.4	2
Se 196.1	0	0.005	0.01	0.02	0.1
Zn 202.5	0	0.1	0.3	1	3
Zn 206.2	0	0.1	0.3	1	3
Zn 213.9	0	0.1	0.3	1	3

Table B.2: Summary of elemental differences between substrate of origin as well as treatment groups. Mdn give the medians in $\mu\text{g/g}$, p -value of Mann-Whitney U test, effect size r calculated based on Wilcoxon results as well as its respective confidence interval (95% CI). Significant results ($p < 0.05$) are highlighted.

	substrate of origin		treatment groups	
	calcareous x siliceous	limestone x porphyry	limestone x serpentine	porphyry x serpentine
Ca	Mdn:15307.69 x 16423.4 $p = 0.19168$ 0.100 95% CI [0.005, 0.24]	Mdn: 19802.88 x 17339.53 $p = 0.08647$ 0.161 95% CI [0.01, 0.34]	Mdn: 19802.88 x 9214.95 $p < 0.0001$ 0.776 95% CI [0.7, 0.83]	Mdn: 17339.53 x 9214.95 $p < 0.0001$ 0.75 95% CI [0.67, 0.81]
Cd	Mdn: 0.6 x 0.59 $p = 0.42171$ 0.060 95% CI [0.003, 0.21]	Mdn: 0.47 x 3.21 $p < 0.0001$ 0.862 95% CI [0.84, 0.86]	Mdn: 0.47 x 0.42 $p = 0.29035$ 0.099 95% CI [0.004, 0.26]	Mdn: 3.21 x 0.42 $p < 0.0001$ 0.86 95% CI [0.84, 0.86]
Co	Mdn: 0.33 x 0.26 $p = 0.88775$ 0.011 95% CI [0.003, 0.18]	Mdn: 0 x 0.32 $p < 0.0001$ 0.688 95% CI [0.62, 0.75]	Mdn: 0 x 0.93 $p < 0.0001$ 0.85 95% CI [0.82, 0.86]	Mdn: 0.32 x 0.93 $p < 0.0001$ 0.56 95% CI [0.41, 0.69]
Cu	Mdn: 8.55 x 6.9 $p = 0.00366$ 0.222 95% CI [0.08, 0.36]	Mdn: 7.37 x 12.3 $p < 0.0001$ 0.531 95% CI [0.39, 0.66]	Mdn: 7.37 x 6.36 $p = 0.09289$ 0.157 95% CI [0.007, 0.35]	Mdn: 12.33 x 6.36 $p < 0.0001$ 0.63 95% CI [0.5, 0.74]
Fe	Mdn: 28.91 x 28.855 $p = 0.46613$ 0.056 95% CI [0.004, 0.21]	Mdn: 29.21 x 33.73 $p = 0.00381$ 0.271 95% CI [0.09, 0.43]	Mdn: 29.21 x 27.27 $p = 0.17468$ 0.127 95% CI [0.006, 0.32]	Mdn: 33.73 x 27.27 $p < 0.0001$ 0.38 95% CI [0.2, 0.53]
K	Mdn: 15281.4 x 15078.99 $p = 0.21251$ 0.095 95% CI [0.003, 0.230]	Mdn: 15656.68 x 18399.54 $p = 0.00020$ 0.348 95% CI [0.16, 0.5]	Mdn: 15656.68 x 13038.64 $p = 0.00058$ 0.32 95% CI [0.14, 0.49]	Mdn: 18399.54 x 13038.64 $p < 0.0001$ 0.59 95% CI [0.47, 0.7]
Mg	Mdn: 3890.87 x 3355.18 $p = 0.32709$ 0.075 95% CI [0.005, 0.22]	Mdn: 3448.34 x 2564.13 $p < 0.0001$ 0.449 95% CI [0.29, 0.59]	Mdn: 3448.34 x 6766.67 $p < 0.0001$ 0.76 95% CI [0.68, 0.82]	Mdn: 2564.13 x 6766.67 $p < 0.0001$ 0.85 95% CI [0.82, 0.86]
Mn	Mdn: 107.56 x 98 $p = 0.37011$ 0.069 95% CI [0.005, 0.22]	Mdn: 69.8 x 210.09 $p < 0.0001$ 0.795 95% CI [0.73, 0.84]	Mdn: 69.8 x 100.26 $p < 0.0001$ 0.48 95% CI [0.33, 0.61]	Mdn: 210.09 x 100.26 $p < 0.0001$ 0.61 95% CI [0.48, 0.72]
Mo	Mdn: 2.94 x 1.99 $p < 0.0001$ 0.310 95% CI [0.18, 0.45]	Mdn: 3.23 x 2.99 $p = 0.58835$ 0.051 95% CI [0.004, 0.23]	Mdn: 3.23 x 1.74 $p < 0.0001$ 0.51 95% CI [0.36, 0.66]	Mdn: 2.99 x 1.74 $p < 0.0001$ 0.50 95% CI [0.34, 0.62]
Ni	Mdn: 2.57 x 2.64 $p = 0.95054$ 0.005 95% CI [0.003, 0.170]	Mdn: 2.45 x 2.01 $p < 0.0001$ 0.577 95% CI [0.42, 0.7]	Mdn: 2.45 x 24.15 $p < 0.0001$ 0.86 95% CI [0.84, 0.86]	Mdn: 2.01 x 24.15 $p < 0.0001$ 0.86 95% CI [0.85, 0.86]
P	Mdn: 2509.1 x 2525.16 $p = 0.57035$ 0.043 95% CI [0.003, 0.19]	Mdn: 2259.34 x 2601.96 $p < 0.0001$ 0.396 95% CI [0.23, 0.55]	Mdn: 2259.34 x 2712.08 $p = 0.00082$ 0.31 95% CI [0.15, 0.49]	Mdn: 2601.96 x 2712.08 $p = 0.77907$ 0.026 95% CI [0.003, 0.22]
S	Mdn: 2086.97 x 1364.58 $p < 0.0001$ 0.383 95% CI [0.25, 0.5]	Mdn: 1759.43 x 1858.29 $p = 0.14763$ 0.136 95% CI [0.008, 0.31]	Mdn: 1759.43 x 1601.33 $p = 0.91650$ 0.010 95% CI [0.002, 0.21]	Mdn: 1858.29 x 1601.33 $p = 0.12952$ 0.14 95% CI [0.01, 0.32]
Zn	Mdn: 161.6 x 193.5 $p = 0.42184$ 0.061 95% CI [0.003, 0.2]	Mdn: 149.16 x 477.96 $p < 0.0001$ 0.846 95% CI [0.82, 0.86]	Mdn: 148.16 x 103.91 $p < 0.0001$ 0.39 95% CI [0.21, 0.52]	Mdn: 477.96 x 103.91 $p < 0.0001$ 0.86 95% CI [0.84, 0.86]

Table B.3: Summary of elemental differences between substrate of origin within each treatment group. Mdn give the medians in $\mu\text{g/g}$, p -value of Mann-Whitney U test, effect size r calculated based on Wilcoxon results as well as its respective confidence interval (95% CI). Significant results ($p < 0.05$) are highlighted.

	limestone treatment calcareous x siliceous	porphyry treatment calcareous x siliceous	serpentine treatment calcareous x siliceous
Ca	Mdn: 19731.48 x 20374.99 $p = 0.20561$ 0.168 95% CI [0.009, 0.41]	Md: 17339.53 x 17303.84 $p = 0.82252$ 0.030 95% CI [0.004, 0.32]	Md: 7945.83 x 9803.32 $p = 0.01085$ 0.34 95% CI [0.01, 0.54]
Cd	Md: 0.47 x 0.43 $p = 0.55853$ 0.077 95% CI [0.004, 0.33]	Md: 3.15 x 3.67 $p = 0.29031$ 0.14 95% CI [0.01, 0.39]	Md: 0.53 x 0.39 $p = 0.38228$ 0.116 95% CI [0.007, 0.38]
Co	Md: -0.14 x -0.09 $p = 0.12313$ 0.20 95% CI [0.01, 0.45]	Md: 0.33 x 0.30 $p = 0.18864$ 0.174 95% CI [0.008, 0.43]	Md: 0.92 x 0.97 $p = 0.89799$ 0.017 95% CI [0.004, 0.32]
Cu	Md: 8.19 x 6.08 $p = 0.00246$ 0.40 95% CI [0.18, 0.6]	Md: 12.29 x 13.45 $p = 0.76080$ 0.040 95% CI [0.004, 0.31]	Md: 6.92 x 5.27 $p = 0.00252$ 0.40 95% CI [0.15, 0.61]
Fe	Md: 27.63 x 31.10 $p = 0.07800$ 0.23 95% CI [0.02, 0.47]	Md: 34.44 x 31.71 $p = 0.88534$ 0.019 95% CI [0.004, 0.31]	Md: 27.34 x 27.05 $p = 0.76692$ 0.039 95% CI [0.004, 0.31]
K	Md: 15656.68 x 15105.18 $p = 0.24868$ 0.15 95% CI [0.01, 0.39]	Md: 18425.93 x 18334.65 $p = 0.77305$ 0.038 95% CI [0.004, 0.31]	Md: 13853.21 x 10888.69 $p = 0.03055$ 0.29 95% CI [0.03, 0.54]
Mg	Md: 3794.47 x 3269.16 $p = 0.00989$ 0.34 95% CI [0.10, 0.57]	Md: 2485.85 x 2653.85 $p = 0.97444$ 0.004 95% CI [0.004, 0.30]	Md: 7205.61 x 6407.72 $p = 0.70059$ 0.051 95% CI [0.007, 0.31]
Mn	Md: 71.34 x 68.89 $p = 0.64220$ 0.062 95% CI [0.004, 0.31]	Md: 234.08 x 175.92 $p = 0.03055$ 0.29 95% CI [0.05, 0.52]	Md: 105.38 x 95.70 $p = 0.47092$ 0.095 95% CI [0.004, 0.34]
Mo	Md: 4.52 x 2.07 $p = 0.00021$ 0.49 95% CI [0.28, 0.68]	Md: 3.35 x 2.74 $p = 0.34451$ 0.125 95% CI [0.006, 0.37]	Md: 1.86 x 1.31 $p = 0.00021$ 0.49 95% CI [0.25, 0.68]
Ni	Md: 2.39 x 2.60 $p = 0.11634$ 0.21 95% CI [0.01, 0.48]	Md: 2.04 x 1.96 $p = 0.17820$ 0.18 95% CI [0.01, 0.43]	Md: 24.14 x 24.48 $p = 0.72448$ 0.047 95% CI [0.004, 0.34]
P	Md: 2227.86 x 2372.38 $p = 0.25531$ 0.151 95% CI [0.004, 0.39]	Md: 2594.37 x 2602.33 $p = 0.92342$ 0.013 95% CI [0.004, 0.3]	Md: 2712.08 x 2671.51 $p = 0.70059$ 0.051 95% CI [0.004, 0.3]
S	Md: 2086.97 x 1327.84 $p = 0.00016$ 0.50 95% CI [0.28, 0.69]	Md: 2068.66 x 1742.51 $p = 0.17836$ 0.18 95% CI [0.01, 0.44]	Md: 2134.25 x 1241.45 $p = 0.00010$ 0.52 95% CI [0.3, 0.71]
Zn	Md: 143.38 x 158.76 $p = 0.25531$ 0.15 95% CI [0.01, 0.39]	Md: 458.25 x 521.85 $p = 0.81008$ 0.032 95% CI [0.004, 0.32]	Md: 99.67 x 110.30 $p = 0.47092$ 0.095 95% CI [0.004, 0.36]

Table B.4: Summary of element accumulation rate differences between substrate of origin between as well as within each treatment group. Mdn give the medians, p -value of Mann-Whitney U test, effect size r calculated based on Wilcoxon results as well as its respective confidence interval (95% CI). Significant results ($p < 0.05$) are highlighted.

	substrate of origin		treatment groups	
	calcareous x siliceous	limestone x porphyry	limestone x serpentine	porphyry x serpentine
total accumulation ratio	Mdn: 1.97 x 1.96 $p = 0.65070$ 0.035	Mdn: 2.05 x 2.09 $p = 0.30903$ 0.095	Mdn: 2.05 x 1.85 $p < 0.0001$ 0.72	Mdn: 2.09 x 1.85 $p < 0.0001$ 0.67
macro element acc. ratio	95% CI [0.002, 0.190] Mdn: 1.97 x 1.97 $p = 0.68455$ 0.031	95% CI [0.006, 0.280] Mdn: 2.05 x 2.09 $p = 0.53117$ 0.059	95% CI [0.61, 0.79] Mdn: 2.05 x 1.86 $p < 0.0001$ 0.72	95% CI [0.56, 0.76] Mdn: 2.09 x 1.86 $p < 0.0001$ 0.66
micro element acc. ratio	95% CI [0.004, 0.170] Mdn: 1.73 x 1.75 $p = 0.62413$ 0.037	95% CI [0.003, 0.250] Mdn: 1.63 x 2.79 $p < 0.0001$ 0.86	95% CI [0.63, 0.79] Mdn: 1.63 x 1.63 $p = 0.59227$ 0.050	95% CI [0.53, 0.75] Mdn: 2.79 x 1.63 $p < 0.0001$ 0.86
		limestone calcareous x siliceous	porphyry calcareous x siliceous	serpentine calcareous x siliceous
total accumulation rate	Mdn: 2.06 x 2.03 $p = 0.64220$ 0.062	Mdn: 2.09 x 2.09 $p = 0.98722$ 0.002	Mdn: 1.86 x 1.84 $p = 0.55331$ 0.079	95% CI [0.004, 0.340]
macro element acc. rate	95% CI [0.006, 0.330] Mdn: 2.07 x 2.04 $p = 0.66532$ 0.057	95% CI [0.004, 0.300] Mdn: 2.09 x 2.09 $p = 0.97444$ 0.004	95% CI [0.004, 0.340] Mdn: 1.86 x 1.84 $p = 0.59700$ 0.070	95% CI [0.004, 0.330]
micro element acc. rate	95% CI [0.004, 0.320] Mdn: 1.60 x 1.64 $p = 0.21141$ 0.17	95% CI [0.004, 0.300] Mdn: 2.74 x 2.80 $p = 0.86011$ 0.023	95% CI [0.004, 0.330] Mdn: 1.63 x 1.63 $p = 0.86011$ 0.023	95% CI [0.004, 0.310]
	95% CI [0.01, 0.41]	95% CI [0.004, 0.320]	95% CI [0.004, 0.310]	

Table B.5: Summary of fitness differences between substrate of origin between as well as within each treatment group. Mdn give the medians, p -value of Mann-Whitney U test, effect size r calculated based on Wilcoxon results as well as its respective confidence interval (95% CI). Significant results ($p < 0.05$) are highlighted.

	substrate of origin		treatment groups	
	calcareous x siliceous	limestone x porphyry	limestone x serpentine	porphyry x serpentine
number of flowers	Mdn: 1 x 5 $p < 0.00031$ 0.28 95% CI [0.13, 0.42]	Mdn: 2 x 3 $p = 0.54214$ 0.058 95% CI [0.003, 0.240]	Mdn: 2 x 6 $p = 0.00978$ 0.25 95% CI [0.06, 0.42]	Mdn: 3 x 6 $p = 0.02718$ 0.21 95% CI [0.04, 0.38]
size in April in cm ²	Mdn: 25.85 x 19.17 $p < 0.0001$ 0.34 95% CI [0.19, 0.47]	Mdn: 19.98 x 20.79 $p = 0.54698$ 0.057 95% CI [0.004, 0.260]	Mdn: 19.98 x 26.46 $p < 0.0001$ 0.48 95% CI [0.34, 0.63]	Mdn: 20.79 x 26.46 $p < 0.0001$ 0.38 95% CI [0.19, 0.54]
size in August in cm ²	Mdn: 36.66 x 27.99 $p < 0.0001$ 0.34 95% CI [0.19, 0.48]	Mdn: 29.54 x 30.50 $p = 0.77554$ 0.027 95% CI [0.004, 0.21]	Mdn: 29.54 x 40.67 $p < 0.0001$ 0.42 95% CI [0.26, 0.57]	Mdn: 30.5 x 40.67 $p < 0.0001$ 0.40 95% CI [0.23, 0.54]
growth factor	Mdn: 1.47 x 1.43 $p = 0.36526$ 0.070 95% CI [0.004, 0.220]	Mdn: 1.47 x 1.45 $p = 0.34279$ 0.090 95% CI [0.005, 0.270]	Mdn: 1.47 x 1.43 $p = 0.40721$ 0.079 95% CI [0.003, 0.260]	Mdn: 1.45 x 1.43 $p = 0.81804$ 0.022 95% CI [0.003, 0.230]
fresh weight in g	Mdn: 6.45 x 4.10 $p < 0.0001$ 0.40 95% CI [0.27, 0.52]	Mdn: 4.65 x 4.30 $p = 0.72912$ 0.033 95% CI [0.003, 0.220]	Mdn: 4.65 x 6.95 $p < 0.0001$ 0.46 95% CI [0.3, 0.6]	Mdn: 4.30 x 6.95 $p < 0.0001$ 0.48 95% CI [0.31, 0.61]
dry weight in g	Mdn: 2.33 x 1.68 $p < 0.0001$ 0.34 95% CI [0.19, 0.47]	Mdn: 1.75 x 1.75 $p = 0.47772$ 0.067 95% CI [0.003, 0.21]	Mdn: 1.75 x 2.45 $p < 0.0001$ 0.42 95% CI [0.25, 0.56]	Mdn: 1.75 x 2.45 $p < 0.0001$ 0.42 95% CI [0.25, 0.57]
water loss (factor)	Mdn: 0.37 x 0.39 $p = 0.01065$ 0.20 95% CI [0.05, 0.34]	Mdn: 0.38 x 0.38 $p = 0.90247$ 0.012 95% CI [0.003, 0.21]	Mdn: 0.38 x 0.37 $p = 0.45453$ 0.071 95% CI [0.005, 0.26]	Mdn: 0.38 x 0.37 $p = 0.40963$ 0.078
		limestone	porphyry	serpentine
		calcareous x siliceous	calcareous x siliceous	calcareous x siliceous
number of flowers		Mdn: 1 x 3 $p = 0.00803$ 0.35 95% CI [0.09, 0.59]	Mdn: 1 x 5 $p = 0.04291$ 0.27 95% CI [0.04, 0.51]	Mdn: 3 x 10 $p = 0.07212$ 0.24 95% CI [0.3, 0.49]
size in April in cm ²		Mdn: 24.10 x 17.82 $p = 0.00403$ 0.38 95% CI [0.13, 0.60]	Mdn: 23.18 x 17.02 $p = 0.00344$ 0.39 95% CI [0.15, 0.60]	Mdn: 27.23 x 24.48 $p = 0.02737$ 0.30 95% CI [0.03, 0.56]
size in August in cm ²		Mdn: 33.83 x 24.92 $p = 0.00521$ 0.37 95% CI [0.13, 0.59]	Mdn: 32.71 x 23.09 $p = 0.00223$ 0.41 95% CI [0.15, 0.64]	Mdn: 42.25 x 35.77 $p = 0.04343$ 0.27 95% CI [0.03, 0.5]
growth factor		Mdn: 1.47 x 1.45 $p = 0.62092$ 0.066 95% CI [0.003, 0.320]	Mdn: 1.50 x 1.38 $p = 0.72913$ 0.046 95% CI [0.004, 0.32]	Mdn: 1.44 x 1.43 $p = 0.64674$ 0.062 95% CI [0.005, 0.32]
fresh weight in g		Mdn: 5.75 x 6.60 $p = 0.00113$ 0.44 95% CI [0.19, 0.64]	Mdn: 5.30 x 3.55 $p = 0.00142$ 0.43 95% CI [0.2, 0.63]	Mdn: 7.55 x 6.05 $p = 0.00080$ 0.45 95% CI [0.19, 0.65]
dry weight in g		Mdn: 2.15 x 1.56 $p = 0.00263$ 0.40 95% CI [0.15, 0.62]	Mdn: 1.86 x 1.35 $p = 0.02607$ 0.30 95% CI [0.04, 0.53]	Mdn: 3.10 x 2.08 $p = 0.00298$ 0.40 95% CI [0.14, 0.63]
water loss (factor)		Mdn: 0.37 x 0.38 $p = 0.14347$ 0.20 95% CI [0.01, 0.44]	Mdn: 0.36 x 0.42 $p = 0.00918$ 0.35 95% CI [0.09, 0.57]	Mdn: 0.37 x 0.38 $p = 0.70188$ 0.052 95% CI [0.004, 0.320]

Table B.6: Correlation of element accumulation rate to Size in April, Size in August and the growth factor

	overall correlation	substrate of origin		treatment		
		calcareous	siliceous	limestone	porphyry	serpentine
size in April ~						
tot_acc_corr	-0.277 p < 0.0001	-0.275 p = 0.008	-0.324 p = 0.005	-0.030 p = 0.826	0.043 p = 0.754	-0.315 p = 0.019
tot_Macro_corr	-0.278 p < 0.0001	-0.278 p = 0.007	-0.324 p = 0.005	-0.031 p = 0.822	0.042 p = 0.759	-0.316 p = 0.019
tot_Micro_corr	-0.119 p = 0.126	-0.092 p = 0.380	-0.169 p = 0.151	-0.006 p = 0.965	0.054 p = 0.691	-0.049 p = 0.725
size in August~						
tot_acc_corr	-0.218 p = 0.005	-0.231 p = 0.026	-0.246 p = 0.035	-0.124 p = 0.364	0.175 p = 0.197	-0.275 p = 0.042
tot_Macro_corr	-0.217 p = 0.005	-0.232 p = 0.025	-0.244 p = 0.036	-0.124 p = 0.362	0.177 p = 0.192	-0.277 p = 0.041
tot_Micro_corr	-0.135 p = 0.083	-0.125 p = 0.232	-0.166 p = 0.156	-0.059 p = 0.664	0.051 p = 0.710	-0.005 p = 0.969
growth factor ~						
tot_acc_corr	0.039 p = 0.614	0.019 p = 0.854	0.073 p = 0.539	-0.176 p = 0.196	0.189 p = 0.163	0.068 p = 0.620
tot_Macro_corr	0.042 p = 0.590	0.022 p = 0.836	0.076 p = 0.521	-0.175 p = 0.196	0.193 p = 0.155	0.067 p = 0.627
tot_Micro_corr	-0.035 p = 0.653	-0.041 p = 0.696	-0.026 p = 0.826	-0.109 p = 0.424	0.019 p = 0.889	0.119 p = 0.388

Table B.7: Correlation of leaf element concentration and number of flowers in flowering plants

number of flowers~ (in flowering plants)	overall correlation	origin		treatment		
		calcareous	siliceous	limestone	porphyry	serpentine
Ca	-0.357 p < 0.0001	-0.372 p = 0.003	-0.354 p = 0.003	-0.336 p = 0.029	-0.231 p = 0.141	-0.340 p = 0.019
Cd	-0.132 p = 0.133	-0.118 p = 0.360	-0.155 p = 0.205	-0.066 p = 0.676	-0.206 p = 0.190	-0.157 p = 0.292
Co	0.146 p = 0.095	0.166 p = 0.196	0.131 p = 0.282	-0.051 p = 0.746	-0.034 p = 0.830	0.080 p = 0.593
Cu	-0.026 p = 0.767	-0.004 p = 0.973	-0.066 p = 0.592	-0.120 p = 0.451	0.224 p = 0.154	-0.025 p = 0.869
Fe	-0.117 p = 0.184	-0.033 p = 0.797	-0.225 p = 0.063	-0.062 p = 0.696	-0.104 p = 0.513	0.014 p = 0.927
K	-0.083 p = 0.346	0.091 p = 0.480	-0.309 p = 0.010	0.206 p = 0.190	0.173 p = 0.274	-0.274 p = 0.062
Mg	-0.003 p = 0.975	-0.142 p = 0.272	0.211 p = 0.081	-0.251 p = 0.109	0.039 p = 0.808	-0.436 p = 0.002
Mn	0.015 p = 0.869	0.093 p = 0.471	-0.109 p = 0.371	-0.091 p = 0.567	0.059 p = 0.709	0.059 p = 0.693
Mo	-0.234 p = 0.007	-0.228 p = 0.075	-0.269 p = 0.026	-0.196 p = 0.213	-0.129 p = 0.415	-0.229 p = 0.121
Ni	0.198 p = 0.023	0.086 p = 0.504	0.343 p = 0.004	-0.003 p = 0.987	0.388 p = 0.011	-0.106 p = 0.480
P	0.060 p = 0.499	0.137 p = 0.288	-0.065 p = 0.595	0.120 p = 0.449	0.031 p = 0.844	-0.057 p = 0.704
S	-0.056 p = 0.525	-0.058 p = 0.654	-0.079 p = 0.516	0.096 p = 0.545	-0.022 p = 0.892	-0.177 p = 0.234
Zn	-0.131 p = 0.137	-0.126 p = 0.329	-0.139 p = 0.256	-0.288 p = 0.064	0.034 p = 0.832	-0.227 p = 0.125

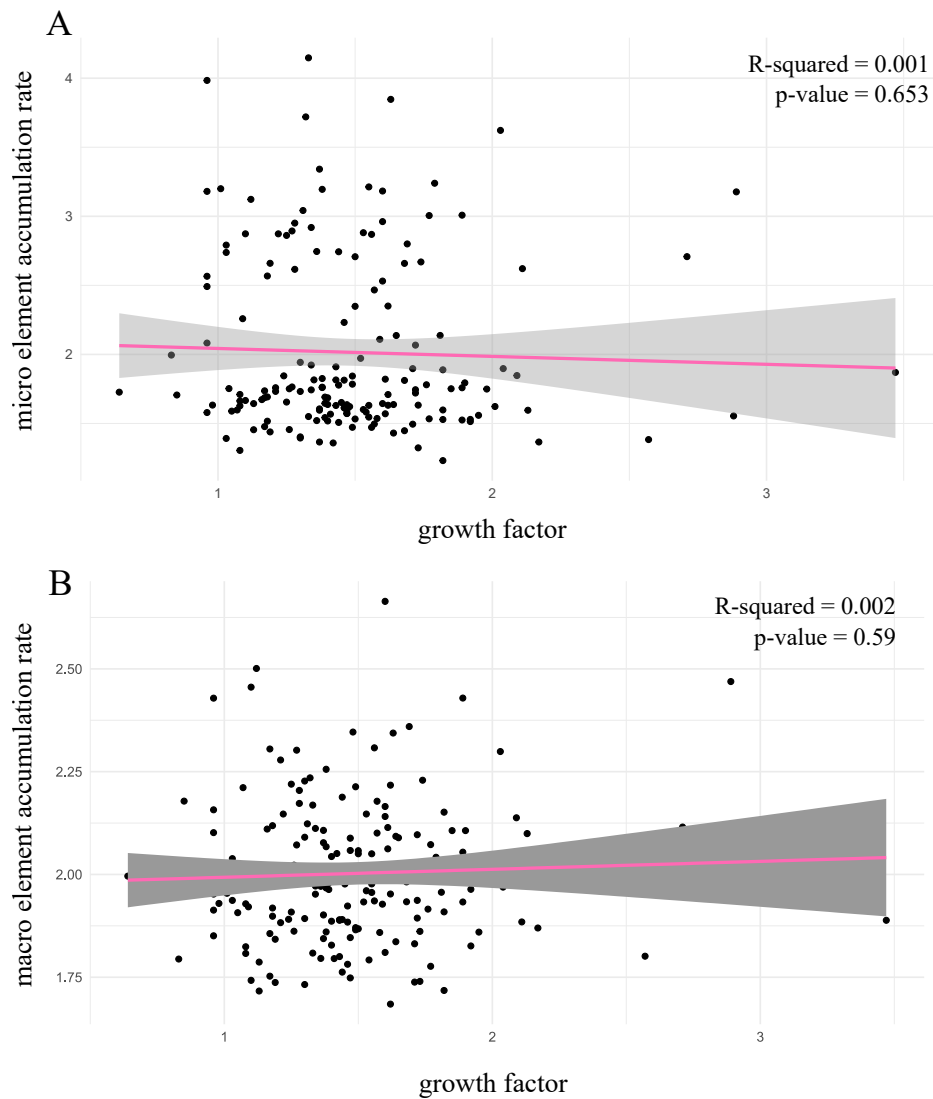


Figure B.1: *Linear regression of element accumulation rate with growth rate between April 2013 and August 2013. A Relationship of micro element accumulation rate and B Relationship of macro element accumulation rate and growth factor.*

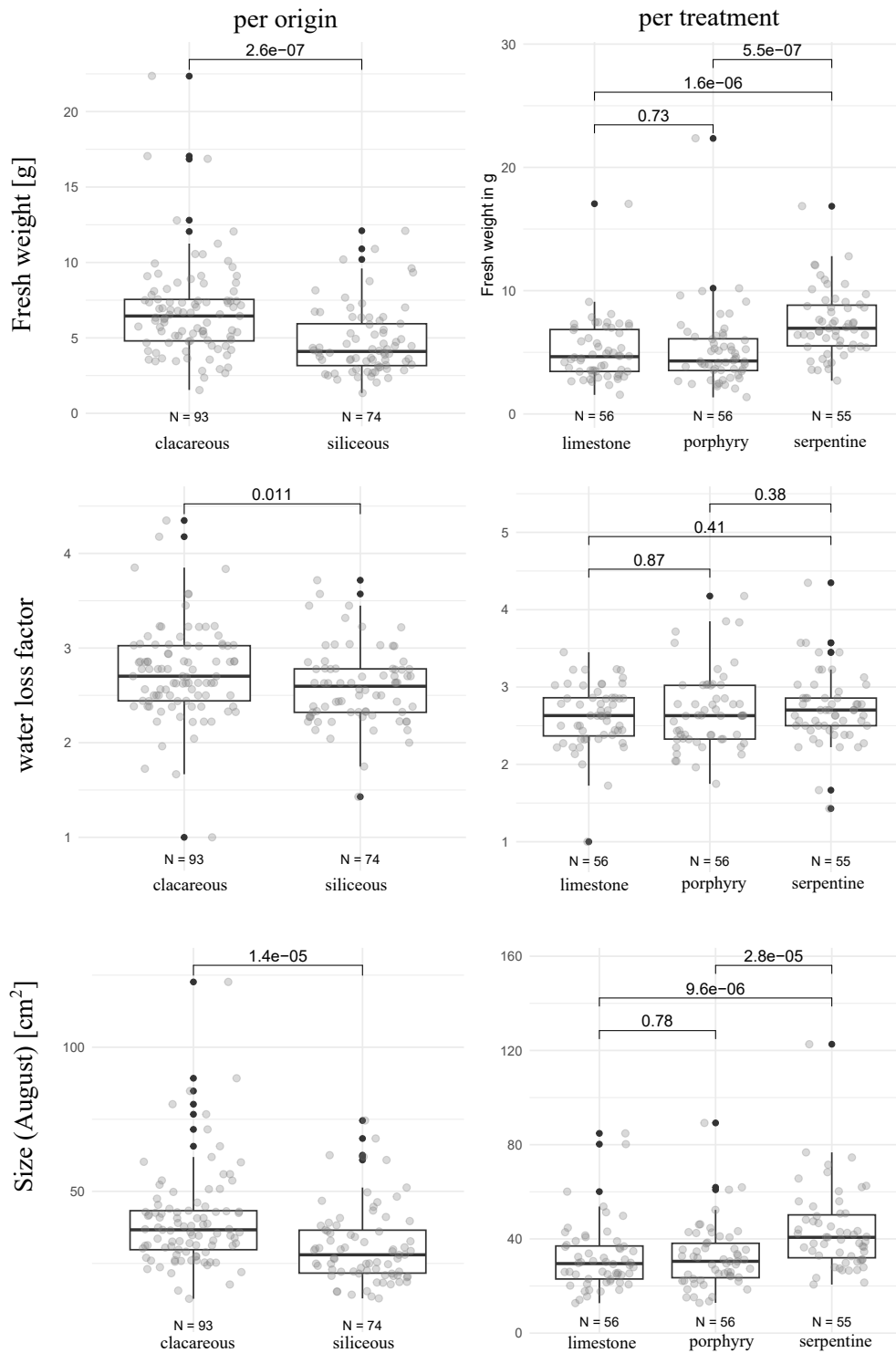


Figure B.2: Comparison of fresh weight, water loss factor, and cushion size in August based on plant origin and treatment groups. Fresh weight was measured for above ground plant material at the experiment end in August 2013. The water loss factor indicates the times the dry weight is contained within the fresh weight and allows an estimation of the water content in the fresh plant material.

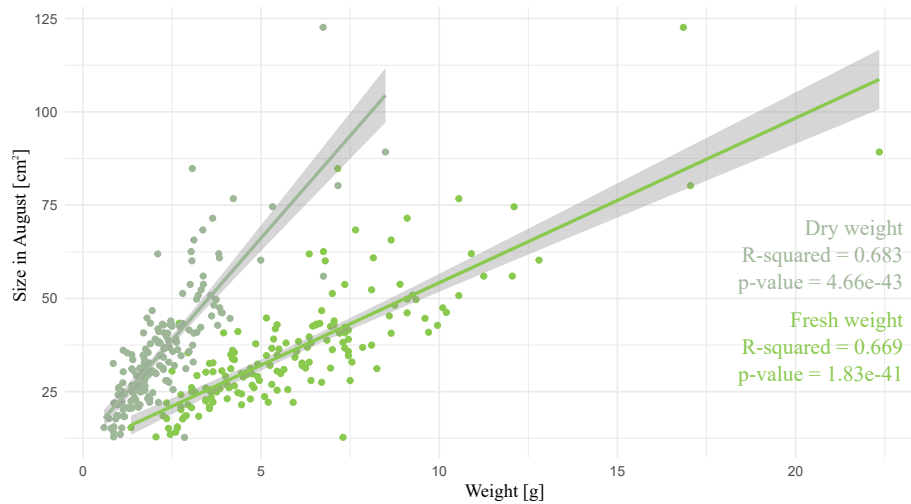


Figure B.3: *Linear regression of cushion size and above ground plant material weight at the end of the experiment in August* Weight is given for fresh and dried plant material. Adjusted R-squared and p-value are given.

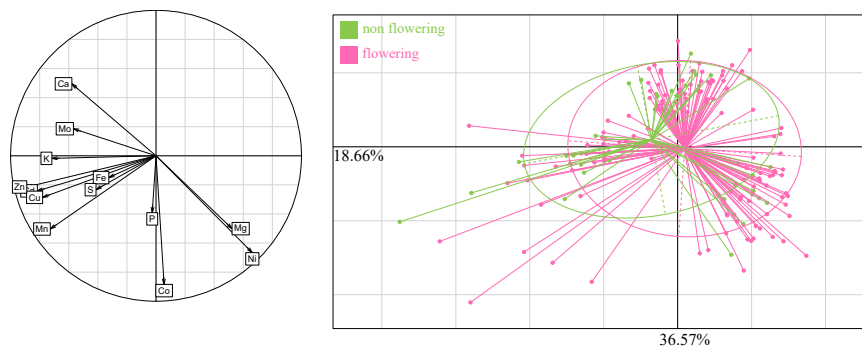


Figure B.4: *Principal component analysis of element concentrations comparing floriferous and non floriferous plants.* All plants in the transplant experiment were included. Correlation circle and biplot with representation of floriferous (pink) and non floriferous (green) plants.

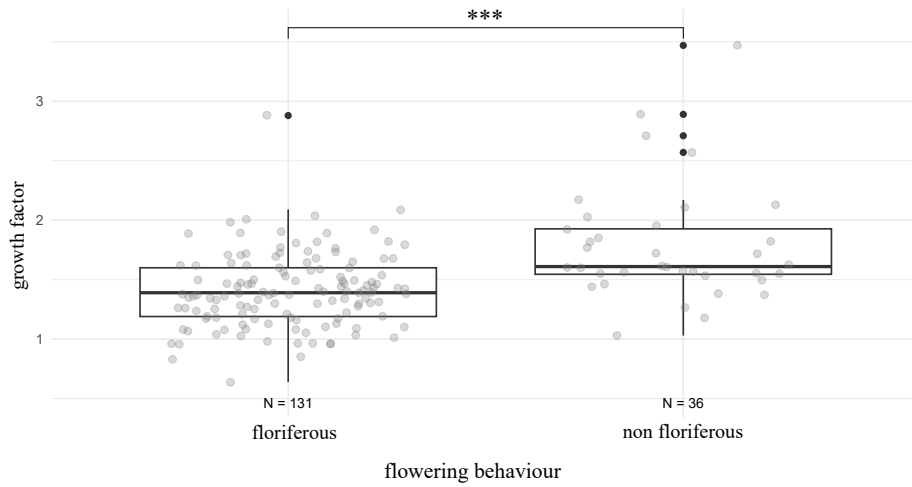


Figure B.5: Growth behaviour of floriferous and non floriferous plants. Comparing the growth factor (Size in April / Size in August) for flowering and non flowering plants.

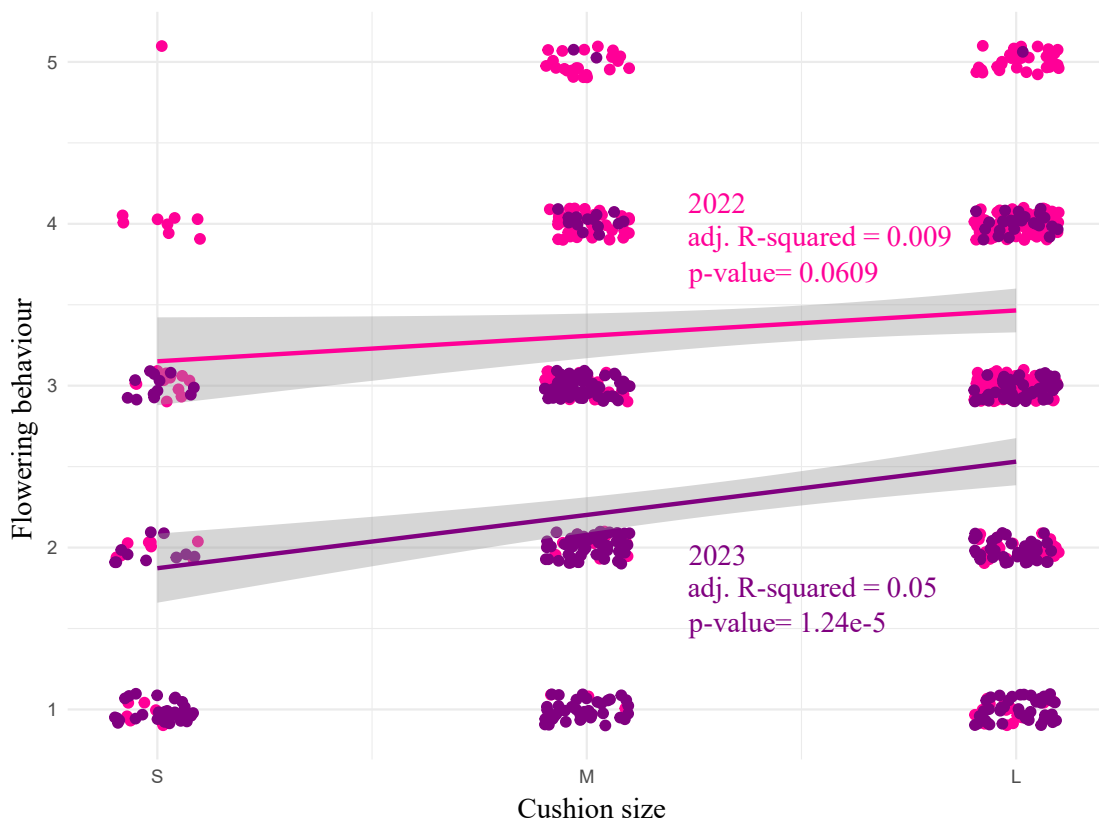


Figure B.6: Linear regression and relationship of flowering number categories and cushion size category for flowering *D. gratianopolitanus* in 2022 and 2023

Table B.8: Flowering time in 2022 and 2023. Start of flowering as opening of the first flower, maximum flowering as date with most flowering plants, end of flowering as wilthing of the last flower, and start date for temp. sum as date where the back calculated cumulative temperature sum reaches 865°C.

(a) Flowering time of <i>D.gratianopolitanus</i> in 2022.				
region	N	start of flowering	maximum flowering	end of flowering
all	286	09.04.2022	13.05.2022	10.06.2022
<i>D.g. ssp. morav</i>	17	14.04.2022	10.05.2022	05.06.2022
CZ	15	14.04.2022	03.05.2022	01.06.2022
GER_Cen	76	09.04.2022	13.05.2022	10.06.2022
UK	2	26.04.2022	26.04.2022	27.05.2022
LU	3	13.04.2022	20.04.2022	30.05.2022
GER_BW	101	19.04.2022	13.05.2022	10.06.2022
CH	19	19.04.2022	13.05.2022	01.06.2022
FRA_Jura	25	19.04.2022	13.05.2022	01.06.2022
FRA_Diois	15	19.04.2022	06.05.2022	03.06.2022
FRA_MC	13	13.04.2022	06.05.2022	01.06.2022
(b) Flowering time of <i>D.gratianopolitanus</i> in 2023.				
region	N	start of flowering	maximum flowering	end of flowering
all	269	13.04.2023	26.05.2023	16.06.2023
<i>D.g. ssp. morav</i>	14	15.04.2023	09.05.2023	09.06.2023
CZ	14	15.04.2023	10.05.2023	09.06.2023
GER_Cen	70	13.04.2023	26.05.2023	16.06.2023
UK	2	03.05.2023	05.05.2023	09.06.2023
LU	3	24.04.2023	02.05.2023	02.06.2023
GER_BW	100	24.04.2023	26.05.2023	16.06.2023
CH	16	05.05.2023	19.05.2023	13.06.2023
FRA_Jura	25	24.04.2023	22.05.2023	12.06.2023
FRA_Diois	14	28.04.2023	22.05.2023	09.06.2023
FRA_MC	11	02.05.2023	15.05.2023	16.06.2023

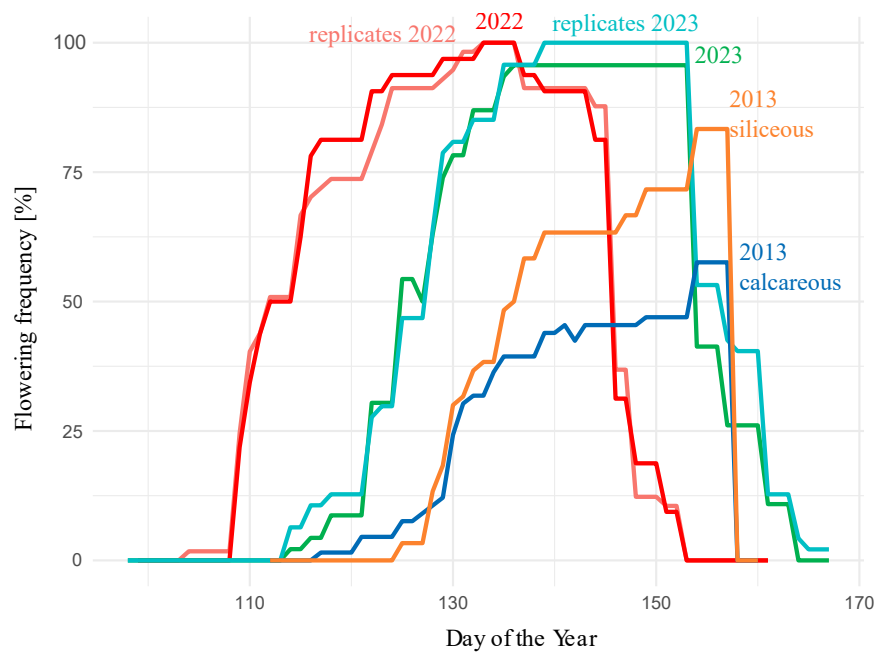


Figure B.7: Flowering time comparison 2013, 2022 and 2023. Plants from the transplant experiment 2013 were subsetted from the years 2022 and 2023. Plants from 2013 were divided by home bedrock and the corresponding home substrate treatment.

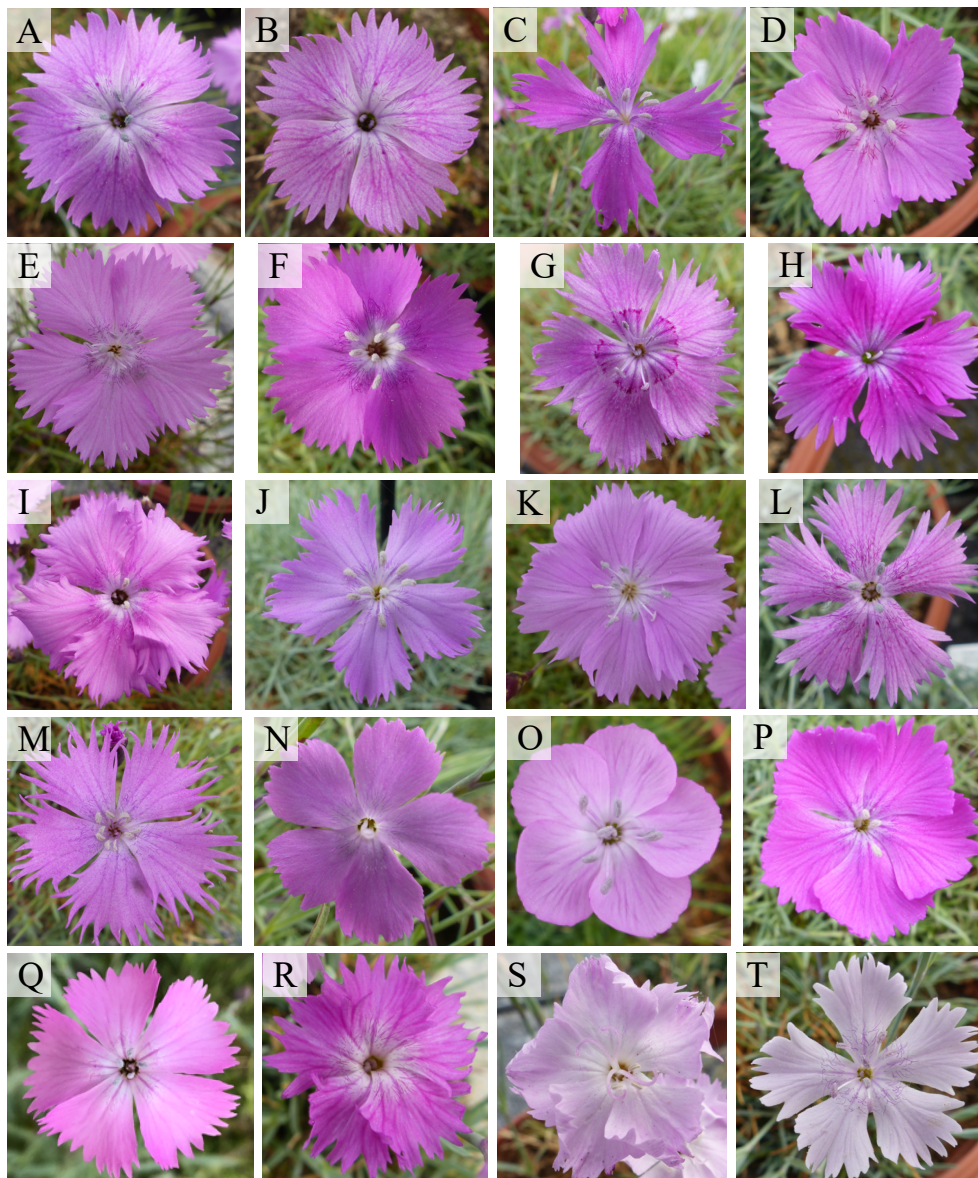


Figure B.8: Morphological differences in *Dianthus gratianopolitanus* flowers Pictures were taken during the flowering period 2024 in the Botanical Garden Heidelberg. **A,B** Kellerwald Edersee, nature reserve Sonderrain, Hesse; **C** Velky Bezdez, Czech Republic; **D** Le Chasseron, Switzerland; **E** Holzflue, Switzerland; **F** Strevic, Czech Republic; **G** Knoblauchfels near Blaubeuren, Baden-Württemberg; **H** Groß Bademeusel, Brandenburg; **I** Bad Urach, Baden-Württemberg; **J** Cheddar Gorge, England; **K** Danube Valley, Bandfelsen, Baden-Württemberg; **L** Wojaleite, Wurlitzer Serpentine, Bavaria; **M** Lenninger Tal, Schlatterhöhe, Baden-Württemberg; **N** nature reserve Bleiberg, Thuringia; **O** Le Grand Delmas, Dios, France; **P** Danube Valley, Hausener Zinnen, Baden-Württemberg; **Q** Wartburg, Thuringia; **R** Lenningertal, Sylphenwand, Baden-Württemberg; **S** Lenningertal, Sylphenwand, Baden-Württemberg; **T** Wartburg, Thuringia;

C | Appendix - Part III

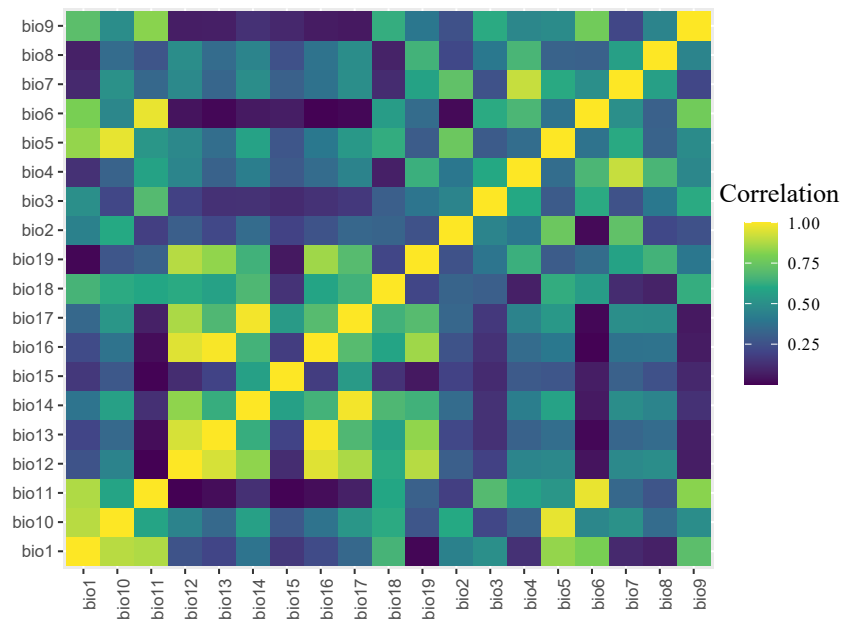


Figure C.1: Heatmap of all bioclim variables highlighting correlations. Marked in yellow and light green are values either < -0.75 or > 0.75 , where the bioclimatic variable with the smaller contribution to the niche model using all *D. gratianopolitanus* is excluded from the final modeling step. Detailed values are given in [Table C.3](#).

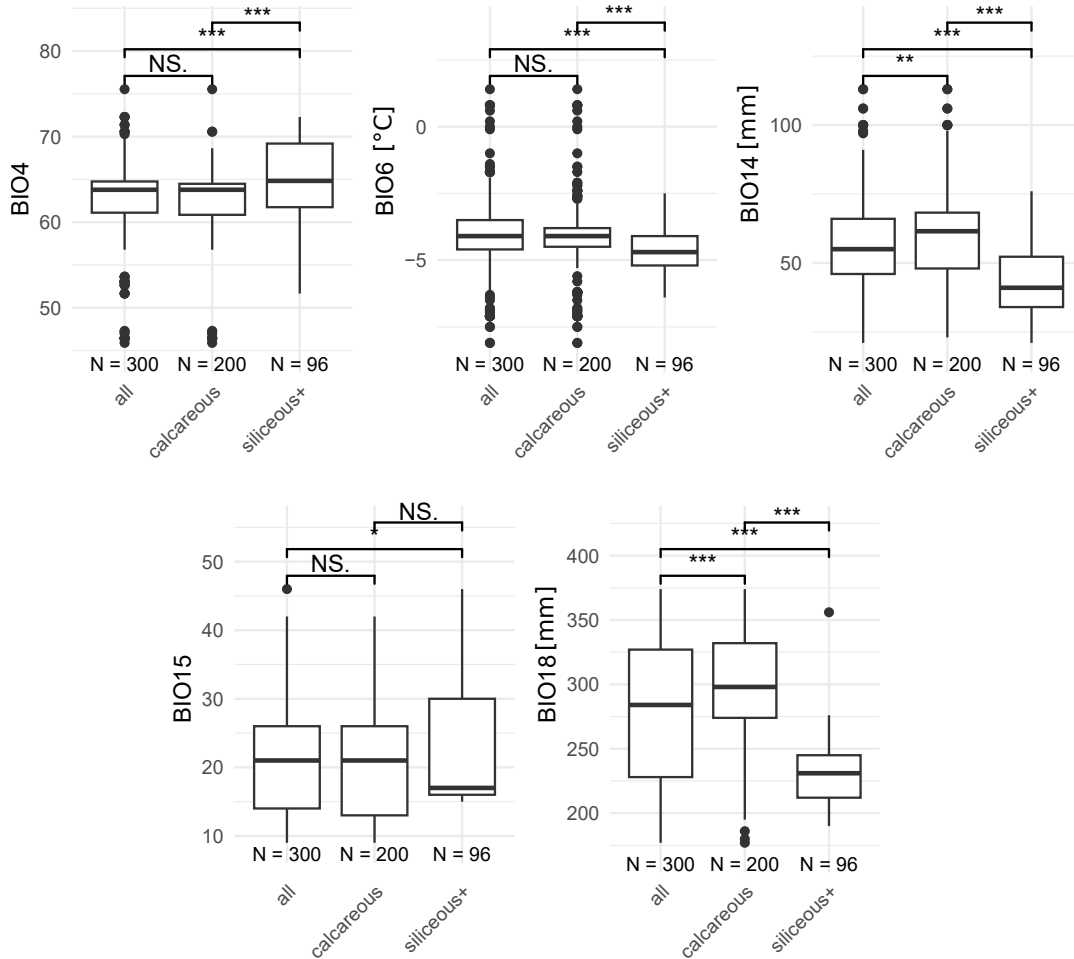


Figure C.2: Differences of the top three most contributing bioclim variables between the substrate types. Statistical significance is given for Wilcox test with Bonferroni correction. BIO4 (Temperature Seasonality, calculated by Standard Deviation (SD) of temperature ($^{\circ}\text{C} * 100$), BIO6 (Min Temperature of Coldest Month), BIO14 (Precipitation of Driest Month), BIO15 (Precipitation Seasonality, as Coefficient of Variation (%)), and BIO18 (Precipitation of Warmest Quarter).

Table C.1: Plastid marker haplotypes in *D. gratianopolitanus* populations from calcareous bedrock. Only cases where unambiguous data was available was used. Here only the most common haplotypes (see Appendix Table A.6) were found.

	ht01	ht02	ht03	ht16	ht19	ht21	ht29	ht30
CH	0	0	18	5	0	0	0	0
Braenten F1	0	0	1	0	0	0	0	0
Braenten F2	0	0	0	1	0	0	0	0
Holzflue	0	0	0	4	0	0	0	0
Lehnfluh	0	0	9	0	0	0	0	0
Ravellenflue	0	0	8	0	0	0	0	0
Donautal_S	0	0	0	6	4	0	0	0
Kaiserstand	0	0	0	1	0	0	0	0
Knopfmacherfels	0	0	0	2	0	0	0	0
Schloss_Bronnen	0	0	0	2	0	0	0	0
Sperberloch	0	0	0	0	4	0	0	0
Stiegelesfels	0	0	0	1	0	0	0	0
Achtal_Blaubeuren	0	0	0	4	0	11	5	0
Blaufels	0	0	0	1	0	7	0	0
Bruckfels	0	0	0	1	0	0	0	0
Kloetzle Blei	0	0	0	0	0	1	0	0
Obere_Peilerwand	0	0	0	0	0	2	0	0
Ruine_Guenzelburg	0	0	0	1	0	0	0	0
Schillerstein	0	0	0	0	0	1	0	0
Schneckenfels	0	0	0	1	0	0	0	0
Sirgenstein	0	0	0	0	0	0	5	0
Michelsberg_Hausener_Wand	0	0	0	6	0	0	5	0
Eckfels	0	0	0	1	0	0	0	0
Große Hausener Wand F1	0	0	0	1	0	0	0	0
Große Hausener Wand F2	0	0	0	1	0	0	0	0
Jungfrauenfels F1	0	0	0	1	0	0	5	0
Jungfrauenfels F2	0	0	0	1	0	0	0	0
Kleine Hausener Wand	0	0	0	1	0	0	0	0
Eybtal	3	0	0	7	6	0	0	2
Donaldfels	0	0	0	2	0	0	0	0
Drehfels	0	0	0	2	0	0	0	0
Nadelfels	0	0	0	1	0	0	0	0
Schulterfels	0	0	0	0	0	0	0	2
Spielerwand	3	0	0	0	0	0	0	0
West of Steinenkirch	0	0	0	2	0	0	0	0
West of Waldhausen	0	0	0	0	6	0	0	0
NSG_Ehrenbuerg	0	0	0	4	0	0	0	0
Einsiedlerhöhle	0	0	0	1	0	0	0	0
Forest	0	0	0	2	0	0	0	0
Rodenstein	0	0	0	1	0	0	0	0

Table C.2: Plastid marker haplotypes in *D. gratianopolitanus* populations from siliceous bedrock. Only cases where unambiguous data was available was used. Here only the most common haplotypes (see Appendix Table A.6) were found.

	ht01	ht02	ht03	ht16	ht19	ht21	ht29	ht30
Blankenberg_Hoellental	0	16	0	1	0	0	0	0
Blankenberg	0	7	0	0	0	0	0	0
Hoellental	0	5	0	0	0	0	0	0
Papierfabrik	0	4	0	1	0	0	0	0
Burgk	0	0	0	5	7	2	0	0
Bleiberg	0	0	0	0	7	0	0	0
Burgk	0	0	0	1	0	0	0	0
Eisbrücke	0	0	0	0	0	1	0	0
Hängesteig	0	0	0	4	0	1	0	0
Schwarzatal	8	0	0	1	0	5	0	0
Griesbachfels	0	0	0	1	0	0	0	0
Kirchfels	8	0	0	0	0	0	0	0
Trippstein	0	0	0	0	0	5	0	0
Kellerwald_Edersee	20	0	0	0	0	0	2	10
Blossenbergl	16	0	0	0	0	0	0	3
Nelkenstieg	0	0	0	0	0	0	2	3
Pine forest	4	0	0	0	0	0	0	0
Wooghoelle	0	0	0	0	0	0	0	4

Table C.3: Pairwise Pearson correlation of bioclim variables. Marked in yellow are values either < -0.75 or > 0.75 , where the bioclimatic variable with the smaller contribution to the niche model using all *D. gratianopolitanus* is excluded from the final modeling step.

pearson corr.	bio_1	bio_10	bio_11	bio_12	bio_13	bio_14	bio_15	bio_16	bio_17	bio_18	bio_19	bio_2	bio_3	bio_4	bio_5	bio_6	bio_7	bio_8	bio_9
bio_9	0.7072	0.4867	0.8195	0.0675	0.0718	-0.1308	0.0986	0.0613	-0.0542	-0.6229	0.3967	0.2483	0.6099	-0.4648	0.4808	0.7699	-0.2100	-0.4492	1.0000
bio_8	0.0775	0.3540	-0.2634	-0.4884	-0.3541	-0.4504	0.2507	-0.3812	-0.4871	0.0824	-0.6482	0.2157	-0.3983	0.6627	0.3192	-0.3086	0.5643	1.0000	-0.4492
bio_7	0.1027	0.5060	-0.3370	-0.4738	-0.3287	-0.4902	0.3110	-0.3771	-0.4923	-0.1127	-0.5766	0.7215	-0.2534	0.9091	0.6071	-0.4953	1.0000	0.5643	-0.2100
bio_6	0.7929	0.4643	0.9670	0.0408	-0.0114	-0.0575	-0.0695	-0.0013	-0.0126	-0.5494	0.3531	-0.0180	0.6104	-0.6678	0.3795	1.0000	-0.4953	-0.3086	0.7699
bio_5	0.8344	0.9638	0.5253	-0.4663	-0.3590	-0.5740	0.2690	-0.4015	-0.5351	-0.6214	-0.2906	0.7528	0.2884	0.3579	1.0000	0.3795	0.6071	0.3192	0.4808
bio_4	-0.1295	0.3166	-0.5771	-0.4542	-0.3146	-0.4274	0.2818	-0.3544	-0.4487	0.0747	-0.6341	0.3972	-0.6024	1.0000	0.3579	-0.6678	0.9091	0.6627	-0.4648
bio_3	0.4955	0.2101	0.6886	0.1875	0.1307	0.1330	-0.1110	0.1350	0.1576	-0.3012	0.3898	0.4494	1.0000	-0.6024	0.2884	0.6104	-0.2534	-0.3983	0.6099
bio_2	0.4370	0.6031	0.1798	-0.3030	-0.2152	-0.3541	0.1930	-0.2568	-0.3354	-0.3229	-0.2539	1.0000	0.4494	0.3972	0.7528	-0.0180	0.7215	0.2157	0.2483
bio_19	0.0103	-0.2685	0.3089	0.8843	0.8304	0.6441	-0.0524	0.8495	0.6932	0.2092	1.0000	-0.2539	0.3898	-0.6341	-0.2906	0.3531	-0.5766	-0.6482	0.3967
bio_18	-0.6564	-0.6107	-0.5938	0.6092	0.5709	0.6735	-0.1394	0.5847	0.6469	1.0000	0.2092	-0.3229	-0.3012	0.0747	-0.6214	-0.5494	-0.1127	0.0824	-0.6229
bio_17	-0.3385	-0.5276	-0.0762	0.8680	0.6769	0.9824	-0.5408	0.6938	1.0000	0.6469	0.6932	-0.3354	0.1576	-0.4487	-0.5351	-0.0126	-0.4923	-0.4871	-0.0542
bio_16	-0.2277	-0.3793	-0.0239	0.9500	0.9914	0.6509	0.1740	1.0000	0.6938	0.5847	0.8495	-0.2568	0.1350	-0.3544	-0.4015	-0.0013	-0.3771	-0.3812	0.0613
bio_15	0.1546	0.2754	0.0051	-0.1176	0.1968	-0.5692	1.0000	0.1740	-0.5408	-0.1394	-0.0524	0.1930	-0.1110	0.2818	0.2690	-0.0695	0.3110	0.2507	0.0986
bio_14	-0.3851	-0.5664	-0.1290	0.8277	0.6265	1.0000	-0.5692	0.6509	0.9824	0.6735	0.6441	-0.3541	0.1330	-0.4274	-0.5740	-0.0575	-0.4902	-0.4504	-0.1308
bio_13	-0.2055	-0.3399	-0.0236	0.9357	1.0000	0.6265	0.1968	0.9914	0.6769	0.5709	0.8304	-0.2152	0.1307	-0.3146	-0.3590	-0.0114	-0.3287	-0.3541	0.0718
bio_12	-0.2553	-0.4485	-0.0001	1.0000	0.9357	0.8277	-0.1176	0.9500	0.8680	0.6092	0.8843	-0.3030	0.1875	-0.4542	-0.4663	0.0408	-0.4738	-0.4884	0.0675
bio_11	0.8730	0.5830	1.0000	-0.0001	-0.0236	-0.1290	0.0051	-0.0239	-0.0762	-0.5938	0.3089	0.1798	0.6886	-0.5771	0.5253	0.9670	-0.3370	-0.2634	0.8195
bio_10	0.8873	1.0000	0.5830	-0.4485	-0.3399	-0.5664	0.2754	-0.3793	-0.5276	-0.6107	-0.2685	0.6031	0.2101	0.3166	0.9638	0.4643	0.5060	0.3540	0.4867
bio_1	1.0000	0.8873	0.8730	-0.2553	-0.2055	-0.3851	0.1546	-0.2277	-0.3385	-0.6564	0.0103	0.4370	0.4955	-0.1295	0.8344	0.7929	0.1027	0.0775	0.7072

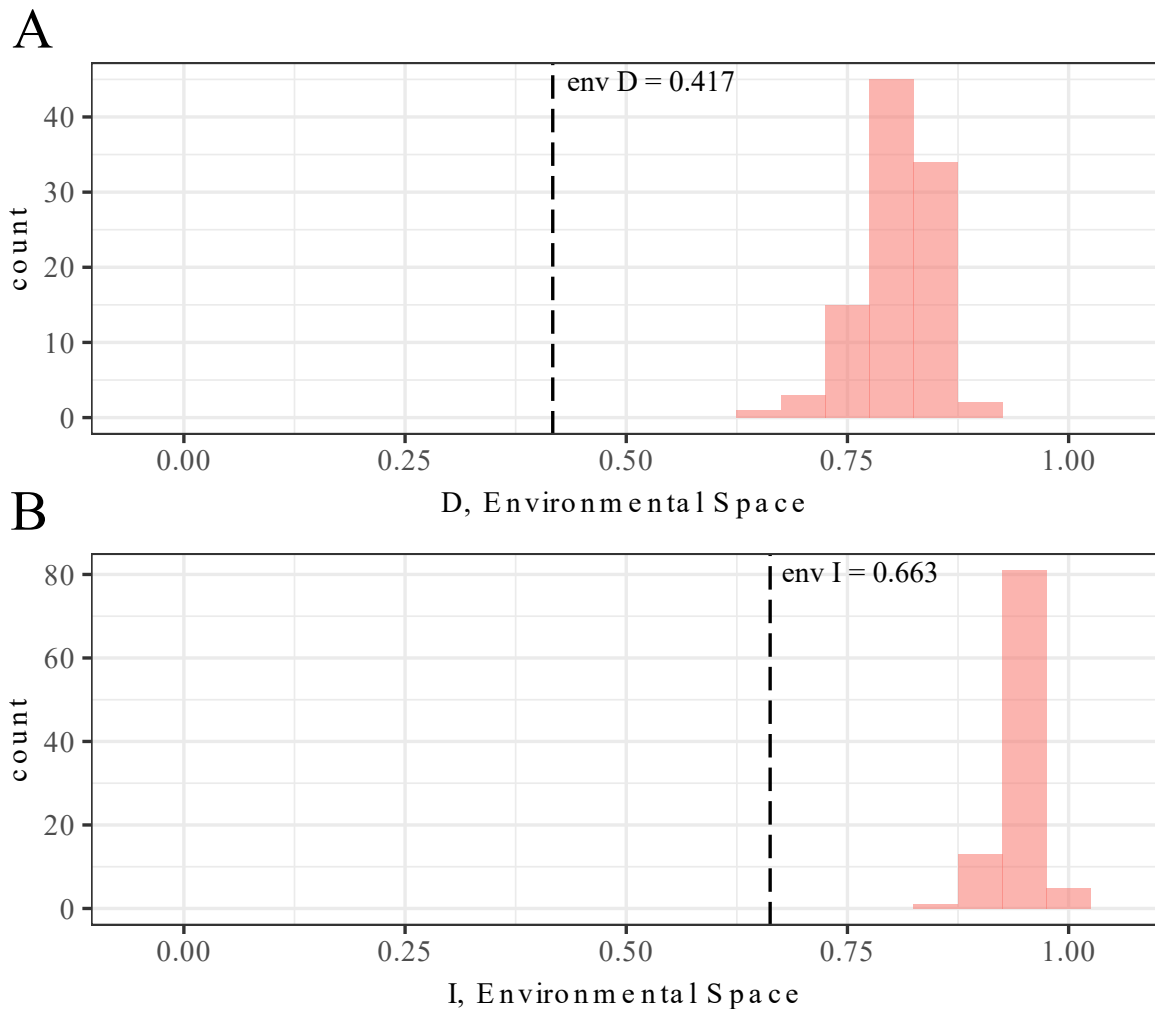


Figure C.3: Niche identity test in environmental space between *D. gratianopolitanus* from calcareous and siliceous bedrock. Expected distributions given as histogram ($N=100$) differs significantly ($p < 0.01$) from observed niche overlaps (dashed lines).

D | Digital Supplement

The following is a list of files and folders included in the digital supplement.

A digital version of this thesis:

Dissertation_Dianthus_gratianopolitanus_Alexandra_Schöne_2024.pdf

Part I:

An overview of all sampled *Dianthus*, as well as the availability of data is given in S_I.0-Dianthus.Summary.xlsx. The permits for the collection of plants and leaf material are given in the folder /S_I.1-Permits.

For the AFLP data (/S_I.2-AFLP) the AFLP matrix for *D. gratianopolitanus* S_I.2.1 and other *Dianthus* species S_I.2.2, as well as the AFLP statistics for the populations S_I.2.3 and structure evanno results S_I.2.4 and S_I.2.5 are included .

For the cp marker data (/S_I.3-Plastid marker) the overview of haplotypes per individual for *D. gratianopolitanus* S_I.3.1 and other *Dianthus* species S_I.3.2, the SNP matrix S_I.3.3 and alignment S_I.3.4, as well as the GenBank accession numbers per plastid marker variation S_I.3.5 are included.

For the plastomes (/S_I.4-Plastomes), the RAxML tree S_I.4.1 used for the generation of the treePL divergence time estimation is given.

/PartI

/S_I.0-Dianthus.Summary.xlsx

/S_I.1-Permits

/S_I.1-Permits/S_I.1.00-Permits_overview.xlsx

/S_I.1-Permits/S_I.1.1-England_20093637.pdf

/S_I.1-Permits/S_I.1.2-Luxembourg_70871_MS.sc.pdf

/S_I.1-Permits/S_I.1.3-Switzerland_1882.pdf

/S_I.1-Permits/S_I.1.4-Switzerland_4313.pdf

/S_I.1-Permits/S_I.1.5-France_Doubs_PC-LT-000-566.pdf

/S_I.1-Permits/S_I.1.6-France_Drome_2012-234 .pdf

/S_I.1-Permits/S_I.1.7-France_Jura.pdf

/S_I.1-Permits/S_I.1.8-France_Isere_2012-207-0019.pdf

/S_I.1-Permits/S_I.1.9-France_Haute-Savoie_2012219-0004.pdf

/S_I.1-Permits/S_I.1.10-France_Ain.pdf

/S_I.1-Permits/S_I.1.11-France_12-593-EXP.pdf

/S_I.1-Permits/S_I.1.12-France_Savoie_2012-034.pdf

/S_I.1-Permits/S_I.1.13-Germany_Sachen-Anhalt_407.4.1_516_12_2241_Hx.pdf

/S_I.1-Permits/S_I.1.14-Germany_Niedersachsen_411.12.2.2.Bo.pdf

/S_I.1-Permits/S_I.1.15-Germany_Brandenburg_286_2013.pdf

/S_I.1-Permits/S_I.1.16-Germany_Thuringia_25.1-092-16.09-312-he-12.pdf

/S_I.1-Permits/S_I.1.17-Germany_Thuringia_26.12-15.02-12-01.pdf
 /S_I.1-Permits/S_I.1.18-Germany_Thuringia_364.623-12_26-2.5-ra.pdf
 /S_I.1-Permits/S_I.1.19-Germany_Thuringia_6.2.1-Reu.pdf
 /S_I.1-Permits/S_I.1.20-Germany_Thuringia_20427-2012-114.pdf
 /S_I.1-Permits/S_I.1.21-Germany_Bavaria_55.1-8641-4-09.pdf
 /S_I.1-Permits/S_I.1.22-Germany_Bavaria_55.1-8622.pdf
 /S_I.1-Permits/S_I.1.23-Germany_RP_425-104.131.0903.pdf
 /S_I.1-Permits/S_I.1.24-Germany_RP_425-104.133.1003.pdf
 /S_I.1-Permits/S_I.1.25-Germany_RP_42-553-251.pdf
 /S_I.1-Permits/S_I.1.26-Germany_Hesse_27.2-R21.1 Milseburg und Habelstein.pdf
 /S_I.1-Permits/S_I.1.27-Germany_Hesse_R22.9.pdf

/S_I.2-AFLP
 /S_I.2-AFLP/S_I.2.1-AFLP.Dg.morav.xlsx
 /S_I.2-AFLP/S_I.2.2-AFLP.additional.species.xlsx
 /S_I.2-AFLP/S_I.2.3-AFLP_Stats_populations.xlsx
 /S_I.2-AFLP/S_I.2.4-evanno.pdf
 /S_I.2-AFLP/S_I.2.5-evanno.txt

/S_I.3-Plastid marker
 /S_I.3-Plastid marker/S_I.3.1-plastid_marker_Dg_Dgm.xlsx
 /S_I.3-Plastid marker/S_I.3.2-plastid_marker_additional_species.xlsx
 /S_I.3-Plastid marker/S_I.3.3-Datamatrix_Indel_SNPs.xlsx
 /S_I.3-Plastid marker/S_I.3.4-haplotypes_Dg_Dm.fas
 /S_I.3-Plastid marker/S_I.3.5-Genbank_accessions_and_haplotype_combinations.xlsx

/S_I.4-Plastomes
 /S_I.4-Plastomes/S_I.4.1-Raxml_tree.pdf

Part II:

In the folder /S_II.1-Substrate an overview of of element concentration and fitness data is given for all plants included in the experiment as well as for leaf material sampled from natural sites (S_II.1.0). The permit for the collection of substrate from Wojaleite in Bavaria (S_II.1.1), results for ICP-OES of the soil samples (S_II.1.2), the ICP-OES and fitness data for plants in the transplant experiment (S_II.1.3), and the differences between the replicates (S_II.1.4) are given. The flowering behaviour of individual plants are given in (S_II.1.5) and the differences in elemental concentration and fitness data between flowering and non flowering plants are given in (S_II.1.6).

The folder /S_II.2-Flowering 22 23 includes the temperature measurement in the greenhouses 2022 (S_II.2.1), the flowering documentation in 2022 (S_II.2.2) and 2023 (S_II.2.3).

/PartII

```
/S_II.1-Substrate
/S_II.1-Substrate/S_II.1.0-Transplant_experiment_overview_all_leafmaterial.xlsx
/S_II.1-Substrate/S_II.1.1-Permit_Substrate-Germany_Bavaria_55.1-8622.pdf
/S_II.1-Substrate/S_II.1.2-Substrat_ICP-OES.xlsx
/S_II.1-Substrate/S_II.1.3-Transplant_experiment_overview_plants.xlsx
/S_II.1-Substrate/S_II.1.4-replicates_summary_table.xlsx
/S_II.1-Substrate/S_II.1.5-Aufbluehzeiten_Mittelwert_Herkunft_T-Substrat.xlsx
/S_II.1-Substrate/S_II.1.6-Stats_flowering_vs_nonflowering.xlsx
```

```
/S_II.2-Flowering 22 23
/S_II.2-Flowering 22 23/S_II.2.1-BoGa_Temp_Messung_2022.xlsx
/S_II.2-Flowering 22 23/S_II.2.2-Dianthus_Blütendoku_2022.xlsx
/S_II.2-Flowering 22 23/S_II.2.3-Dianthus_Blütendoku_2023.xlsx
```

Part III:

The folder /S_III.1-Metapopulations includes the AFLP data used for the Structure analysis and calculation of the jaccard distances S_III.1.X.1, the nexus file for spiltstree generation S_III.1.X.2, the structure results for $K = 2$ to $K = 9$ S_III.1.X.3, and the respective evanno results S_III.1.X.4 and S_III.1.X.5 for all eleven populations. The folder /S_III.2-ENM includes the R script S_III.2.1-thin.max.R and the overview of differences observed in the distribution range of the Cheddar pink between the used bioclimatic variables /S_III.2-ENM/S_III.2.2-used_bioclims.pdf

```
/PartIII
```

```
/S_III.1-Metapopulations
```

```
/S_III.1-Metapopulations/S_III.1.1-CH
/S_III.1.1-CH/S_III.1.1.1-AFLP_Dg_CH.xlsx
/S_III.1.1-CH/S_III.1.1.2-splistree_AFLP_Dg_CH.nxs
/S_III.1.1-CH/S_III.1.1.3-CH_structure_overview.svg
/S_III.1.1-CH/S_III.1.1.4-evanno.png
/S_III.1.1-CH/S_III.1.1.5-evanno.txt
```

```
/S_III.1-Metapopulations/S_III.1.2-Donau
S_III.1.2-Donau/S_III.1.2.1-AFLP_Dg_Donau_S.xlsx
S_III.1.2-Donau/S_III.1.2.2-splitstree_AFLP_Dg_Donau.nxs
S_III.1.2-Donau/S_III.1.2.3-Donau_Structure_overview.svg
S_III.1.2-Donau/S_III.1.2.4-evanno.png
S_III.1.2-Donau/S_III.1.2.5-evanno.txt
```

/S_III.1-Metapopulations/S_III.1.3-Achtal

S_III.1.3-Achtal/S_III.1.3.1-AFLP_Dg_Achtal.xlsx

S_III.1.3-Achtal/S_III.1.3.2-splitstree_AFLP_Dg_Achtal.nxs

S_III.1.3-Achtal/S_III.1.3.3-Achtal_Structure_overview.svg

S_III.1.3-Achtal/S_III.1.3.4-evanno.png

S_III.1.3-Achtal/S_III.1.3.5-evanno.txt

/S_III.1-Metapopulations/S_III.1.4-Hausener Wand

S_III.1.4-Hausener Wand/S_III.1.4.1-AFLP_Dg_Hausener_Wand.xlsx

S_III.1.4-Hausener Wand/S_III.1.4.2-splitstree_AFLP_Dg_Hausener_Wand.nxs

S_III.1.4-Hausener Wand/S_III.1.4.3-Hausener_Wand_Structure_overview.svg

S_III.1.4-Hausener Wand/S_III.1.4.4-evanno.png

S_III.1.4-Hausener Wand/S_III.1.4.5-evanno.txt

/S_III.1-Metapopulations/S_III.1.5-Eybtal

S_III.1.5-Eybtal/S_III.1.5.1-AFLP_Dg_Eybtal.xlsx

S_III.1.5-Eybtal/S_III.1.5.2-splitstree_AFLP_Dg_Eybtal.nxs

S_III.1.5-Eybtal/S_III.1.5.3-Eybtal_Structure_overview.svg

S_III.1.5-Eybtal/S_III.1.5.4-evanno.png

S_III.1.5-Eybtal/S_III.1.5.5-evanno.txt

/S_III.1-Metapopulations/S_III.1.6-Ehrenbürg

S_III.1.6-Ehrenbürg/S_III.1.6.1-AFLP_Dg_Ehrenbuerg.xlsx

S_III.1.6-Ehrenbürg/S_III.1.6.2-splitstree_AFLP_Dg_Ehrenbuerg.nxs

S_III.1.6-Ehrenbürg/S_III.1.6.3-Ehrenbürg_Structure_overview.svg

S_III.1.6-Ehrenbürg/S_III.1.6.4-evanno.png

S_III.1.6-Ehrenbürg/S_III.1.6.5-evanno.txt

/S_III.1-Metapopulations/S_III.1.7-Blankenberg_Höllental

S_III.1.7-Blankenberg_Höllental/S_III.1.7.1-AFLP_Dg_Bl_Hoe.xlsx

S_III.1.7-Blankenberg_Höllental/S_III.1.7.2-splitstree_AFLP_Dg_Blank_Hoelle.nxs

S_III.1.7-Blank_Höller/S_III.1.7.3-Blank_Höller_Structure_overview.svg

S_III.1.7-Blankenberg_Höllental/S_III.1.7.4-evanno.png

S_III.1.7-Blankenberg_Höllental/S_III.1.7.5-evanno.txt

/S_III.1-Metapopulations/S_III.1.8-Burgk

S_III.1.8-Burgk/S_III.1.8.1-AFLP_Dg_Burgk.xlsx

S_III.1.8-Burgk/S_III.1.8.2-splitstree_AFLP_Dg_Burgk.nxs

S_III.1.8-Burgk/S_III.1.8.3-Burgk_Structure_overview.svg

S_III.1.8-Burgk/S_III.1.8.4-evanno.png

S_III.1.8-Burgk/S_III.1.8.5-evanno.txt

/S_III.1-Metapopulations/S_III.1.9-Schwarzatal

S_III.1.9-Schwarzatal/S_III.1.9.1-AFLP_Dg_Schwarz.xlsx

S_III.1.9-Schwarzatal/S_III.1.9.2-splitstree_AFLP_Dg_Schwarzatal.nxs

S_III.1.9-Schwarzatal/S_III.1.9.3-Schwarzatal_Structure_overview.svg

S_III.1.9-Schwarzatal/S_III.1.9.4-evanno.png

S_III.1.9-Schwarzatal/S_III.1.9.5-evanno.txt

/S_III.1-Metapopulations/S_III.1.10-Edersee

S_III.1.10-Edersee/S_III.1.10.1-AFLP_Dg_Eder.xlsx

S_III.1.10-Edersee/S_III.1.10.2-splitstree_AFLP_Dg_Eder.nxs

S_III.1.10-Edersee/S_III.1.10.3-Edersee_Structure_overview.svg

S_III.1.10-Edersee/S_III.1.10.4-evanno.png

S_III.1.10-Edersee/S_III.1.10.5-evanno.txt

/S_III.1-Metapopulations/S_III.1.11-Gans

S_III.1.11-Gans/S_III.1.11.1-AFLP_Dg_Gans.xlsx

S_III.1.11-Gans/S_III.1.11.2-splitstree_AFLP_Dg_Gans.nxs

S_III.1.11-Gans/S_III.1.11.3-Gans_Structure_overview.svg

S_III.1.11-Gans/S_III.1.11.4-evanno.png

S_III.1.11-Gans/S_III.1.11.5-evanno.txt

/PartIII

/S_III.2-ENM

/S_III.2-ENM/S_III.2.1-thin.max.R

/S_III.2-ENM/S_III.2.2-used_bioclimes.pdf

E | Lists

List of Figures

1	Distribution area of <i>Dianthus gratianopolitanus</i> and <i>D. gratianopolitanus</i> subsp. <i>moravicus</i> adapted from the digital map generated by Atlas Flora Europaeae (version year 1999) (Jalas, 1988).	5
2	A Drawing of <i>Dianthus gratianopolitanus</i> from Hess et al. (1976); B flowering <i>D. gratianopolitanus</i> in Kellerwald-Edersee, Hesse; C Klausberg near Hemfurth, Hesse; D Blossenberg, Kellerwald-Edersee, Hesse; E Bilsteinklippen, Bad Wildungen, Hesse, Photos B-E from Florian Michling 2013; F Bourscheid-Michelau, Luxembourg; G Near Blankenberg, Thuringia; , H Wartburg, Thuringia; I, J Danube valley, Baden-Württemberg, K,L Ehrenbürg, Bavaria; M Lenninger Tal, Baden-Württemberg; N Near Blankenberg, Thuringia; O Wutachflüh, Baden-Württemberg; P Massif Central, France; Photos F-P from Botanical Garden Heidelberg April 2024	8
3	A <i>Dianthus gratianopolitanus</i> subsp. <i>moravicus</i> Drawing of plant from type locality, adapted from Kovanda (1982), (Orig. A. Chrtkova); B <i>Dianthus gratianopolitanus</i> subsp. <i>moravicus</i> from Bitov, CZ; C <i>Dianthus gratianopolitanus</i> subsp. <i>moravicus</i> from Ivancice, Pictures taken April 2024 in the Botanical Garden Heidelberg	9
2.1	Sample locations included in the genetic analysis. Grid size indicates 4 MTB, MTB = Messtischblatt = ordnance survey map 10 x 10 km, colors indicate sample locations from <i>D. gratianopolitanus</i> and <i>D. gratianopolitanus</i> subsp. <i>moravicus</i> from the Czech Republic.	23
3.1	Distribution of spatial AFLP genetic structure STRUCTURE analysis results are given for K = 2 as inverse distance weighted (idw) interpolation as background and K=3 as region mean for the different regions. Numbers indicate regions according to Table 3.1.	38

3.2	Linear relationship of longitude and AFLP statistics (mean) for populations and corresponding boxplots. To ensure sufficient sample sizes and correct for population size, mean values were calculated on basis of $n = 5$ subsamples per population. Colors refer to the respective STRUCTURE cluster were populations were grouped by the structure assignment with a threshold of $> 75\%$ population mean assignment to a cluster. Three different statistics are included: A number of bands, B number of polymorphic sites and C frequency-down-weighted marker.	45
3.3	Mantel correlogram (a) and mantel test results (b) for AFLP data Jaccard-distances for AFLP data was used as genetic distance matrix, ten geographic distance classes were adjusted to contain the same amount of pairwise comparisons, upper distance class limit is given. Calculation of Mantel correlation coefficients was done using Spearman correlation, p-values were adjusted for multiple testing using the Holm method.	46
3.4	TCS network based on plastid marker haplotypes. Network is calculated based on a total of 47 SNPs, single nucleotide gaps and longer indels. Lines represent one mutational step, small circles indicate intermediate (unsampled or extinct) haplotypes. * Additional haplotypes were assigned to the nodes of ht16, ht20 and ht21 due to missing resolution of the SNP matrix . Haplotypes unique to the Southern France regions are indicated by dashed circle outlines. While ht20 is not exclusive to France the ht38 and ht44 are. Dashed lines indicate divergence time estimates in mya from Figure 3.6 . Representatives of Group 6 were missing from the plastome tree. Geographical distribution is given in Figure 3.5	47
3.5	Distribution of plastid marker haplotypes over Europe. Haplotypes are grouped and colored based on their position in the TCS network (Figure 3.4). Regions are numbered based on Table 3.3 . Size reflects sampling sizes.	47
3.6	Time calibrated phylogenetic tree and divergence time estimates of 15 <i>D. gratianopolitanus</i> and 20 additional <i>Dianthus</i> using plastome sequences. Divergence times are indicated by blue bars and given in million years ago (Myr). The maximum-likelihood tree was constructed using RAxM-ng and dated using treePL. Colored blocks indicate position in the TCS network based on the inferred haplotype. Geographical occurrence of haplotypes is given in A including the reduced outline of the TCS network. B Complete phylogenetic tree including outgroup branches. The <i>Dianthus</i> clade is given in more detail in C	48
3.7	Comparison of genome size by ploidy level. Comparison of A tetra- and hexaploids from the whole distribution range, B tetra- and hexaploids from the French Massif Central and Diois region including significance from Mann-Whitney U test	49

- 3.8 **Linear relationship of latitude and genome size (1Cx) and corresponding boxplots.** **A** Linear regression. Colors indicate bedrock types (limestone, serpentine and siliceous+ including siliceous, volcanic and sandy bedrock. Adjusted R^2 and corresponding p-values are given. **B** Corresponding boxplots comparing genome size based on substrate types. Statistical significance (Mann-Whitney U test with Bonferroni correction)for pairwise comparisons are given. 49
- 3.9 **Linear relationship of latitude and genome size (1Cx) and corresponding boxplots.** **A** Linear regression. Colors indicate the assignment to a Structure cluster ($K = 3$). Grey colored points indicate either no available Structure data or no possible assignment to a cluster to more than 75%. Adjusted R^2 and corresponding p-values are given. **B** Corresponding boxplots comparing genome size based on structure clusters. Statistical significance (Mann-Whitney U test with Bonferroni correction)for pairwise comparisons are given. 50
- 2.1 **A:** Plant sampling and outline of transplant experiment. Limestone substrate was triassic shell limestone from the quarry in Nussloch, the porphyry as well as serpentine substrate were collected from quarries in Wojaleite. Plants were acclimatized on potting soil for a minimum of 6 months prior to the transfer of cuttings to the treatment soils. Duration of the transplant experiment was from May 2012 to August 2013. **B:** Pot arrangement per individual. From left to right: limestone, porphyry and serpentine. Replicates are arranged accordingly in a second row. **C:** Arrangement in the greenhouse at the start of the experiment in May 2012 (Photos: Florian Michling) 78
- 3.1 **Element concentrations of treatment soils including ground serpentine.** **A:** Total element concentration. **B:** Plant available (exchangeable) element concentrations. The corresponding table is given in [Table 3.2](#). 87
- 3.2 **Principal component analysis of element concentrations in the transplant experiment grouped by treatment and substrate of origin** **A** total element concentrations, **B** macro element concentrations and **C** micro element concentrations with correlation circle, biplot of the first two axes with point classes as representation of the three treatments (limestone (blue), porphyry (purple), serpentine (orange)) and as representation of substrate of origin (calcareous (blue) and siliceous (purple)). Centroids indicate the mean position of the groups and the respective ellipsoid each groups variability. . . . 90

3.3	Principal component analysis of element concentrations within each treatment grouped by substrate of origin A within the limestone treatment, B the porphyry treatment and C the serpentine treatment with correlation circle and biplot of the first two axes with point classes as representation of substrate of origin (calcareous (blue) and siliceous (purple)). Centroids indicate the mean position of the groups and the respective ellipsoid each groups variability.	91
3.4	Element accumulation rate by origin and treatment group. Micro element accumulation ratio (Cd, Co, Cu, Fe, Mn, Mo, Ni, Zn), Macro element accumulation ratio (Ca, K, Mg, P, S) and total accumulation ratio indicate the ratio by which an individual accumulated elements within a treatment compared to how much it accumulated over all treatments.	93
3.5	Signs of withering and chlorosis based on substrate of origin and treatment group. Numbers indicate the number of plants showing signs of A withering, categorized as either healthy or withered and B chlorosis categorized as either healthy or showing signatures of mild or severe chlorosis, grouped by treatment and substrate of origin.	95
3.6	Flowering of <i>D. gratianopolitanus</i> in the flowering period 2013. A Summary of number of flowering and non flowering plants per origin in each treatment. B Number of flowers per flowering plant of calcareous and siliceous origin. C Number of flowers per flowering plant in each treatment. D Correlation of number of flowers per plant and cushion size at the start of the flowering period in April 2013.	99
3.7	Half monthly temperature sum for the years 2013, 2022 and 2023 as well as in green house data for 2022. The half-monthly sum for the crucial months during spring and early summer documented at the weather station at Berliner Straße (LUBW) as well as in house temperature is given. Due to the frost-free cultivation within the green houses, the data from LUBW was corrected to 4°C for all temperature measurements > 4°C.	101
3.8	Flowering frequency of <i>D. gratianopolitanus</i> per region in 2022 and 2023. The flowering frequency (percentage of flowering plants per region) of Cheddar Pink cultivated in the Botanical Garden in Heidelberg grouped by origin region as well as <i>D. gratianopolitanus</i> subsp. <i>moravicus</i> plants is given at the corresponding day of the year. Overall flowering started on the 9 th April in 2022 (99 th day of the year) and on the 13 th April 2023 (103 rd day of the year) and reached its peak on the 13 rd May 2022 and 26 th May 2023, respectively. The regions of Luxembourg and the United Kingdom are represented by only 3 (LU) and 2 (UK) plants, hindering a meaningful results but still indicating the same overall trend. A detailed overview is given in the Appendix Table B.8	102

- 3.9 **Flowering start of *D. gratianopolitanus* per region in 2022 and 2023.** The flowering start was scored for each individual cultivated in the Botanical Garden in Heidelberg during the flowering period in 2022 and 2023. Points indicate individual start of flowering, with the color indicating the origin substrate of the plant. The variation of within region starting date varies for up to 34 days in 2022 and 43 days in 2023 (e.g. in Central Germany) and no significant differences between regions and substrates were found. 103
- 3.10 **Categorical number of flowers per region.** The flowering categories range from 1 - indicating only few flowers to 5 with exceptional high number of flowers. The numbers in each stacked barplot segment indicate the number of individuals in each category. The change in flowering between the years 2022 and 2023 is influenced by horticultural measures in fall 2022. 104
- 3.11 **Categorical cushion size per region.** The cushion size categories range from S indicating a small cushion to L indicating cushions that reach over the pot edges. The numbers in each stacked barplot segment indicate the number of individuals in each category. The change in cushion size between the years 2022 and 2023 is influenced by horticultural measures in fall 2022. 105
- 3.12 **Categorical number of flowers per cushion size.** The flowering categories range from 1 - indicating only few flowers to 5 with exceptional high number of flowers and the cushion size categories range from S indicating a small cushion to L indicating cushions that reach over the pot edges. The numbers in each stacked barplot segment indicate the number of individuals in each category. 105
- 3.13 **Flowering time comparison 2013, 2022 and 2023 for plants from calcareous and siliceous bedrock.** Plants from the transplant experiment 2013 were extracted from the years 2022 and 2023. Plants from 2013 were grouped by home bedrock and the corresponding home substrate treatment. . 106
- 3.14 **Cumulative temperature sum between start of the year and maximum flowering of *D. gratianopolitanus*.** Maximum flowering was taken from [Figure 3.13](#) and the 4°C corrected climate data from the weather station at Berliner Straße was used for calculations. The cumulative sum of mean daily temperature values was calculated and plotted for 2013, 2022 and 2023. The in [Koch et al. \(2021\)](#) observed convergence at a temperature sum of 865°C the therein resulting starting date, February 6th, as well as the in my study observed temperature sum of 825°C at the convergence of the lines from 2013 and 2023 and corresponding date, March 25th, are indicated by dashed lines. 107

2.1	Populations from limestone (blue) and siliceous (red) bedrock. 1.) Lehnfluh and Ravellenflue (Switzerland), 2.) Danube valley near Friedingen (Baden-Württemberg), 3.) Achtal and Blaubeuren (BW), 4.) Hausener Wand, Michelsberg (BW), 5.) Eybtal (BW), 6.) nature reserve Ehrenbürg (Bavaria), 7.) Blankenberg and Höllental (Thuringia and Bavaria), 8.) nature reserve Korberfels and Bleiberg near Burgk (TH), 9.) Schwarzatal (TH), 10.) Kellerwald-Edersee (Hesse), 11.) nature reserve Gans and Rheingrafenstein (Rhineland-Palatinate). In addition the metapopulation from 12.) the Lenninger Tal and 13.) the Eselsburger Tal from Koch et al. (2021) are included.	130
3.1	SplitsTree and STRUCTURE analysis for Populations from Oensingen and Balsthal, Switzerland. A SplitsTree analysis of AFLP data. Colors indicate resulting genotype groups, dashed lines indicate subpopulations. B Genetic assignment with STRUCTURE (K=2), coloured based on the SplitsTree analysis (A).	148
3.2	Distribution of <i>D. gratianopolitanus</i> and molecular differences (AFLP fragments) for populations from Ravellenflue, Lehnfluh and Holzflue, Switzerland A Geographic distribution in Ravellenflue, Lehnfluh and Holzflue, coloured based on SplitsTree grouping. Coloured lines indicate possible dispersal events of the according coloured genotype. B Number of molecular differences between and within the growth sites, C Frequency distribution of molecular differences as shown in B). Dashed lines indicate mean values.	149
3.3	SplitsTree and STRUCTURE analysis for Populations from the Danube valley near Friedingen an der Donau. A SplitsTree analysis of AFLP data. Colors indicate resulting genotype groups, dashed lines indicate subpopulations. B Genetic assignment with STRUCTURE (K=2), coloured based on the SplitsTree analysis (A).	150
3.4	Distribution of <i>D. gratianopolitanus</i> and molecular differences (AFLP fragments) for populations from the Danube valley near Friedingen an der Donau. A Geographic distribution in the Danube valley, coloured based on SplitsTree grouping. Coloured lines indicate possible dispersal events of the according coloured genotype. B Number of molecular differences between and within the growth sites, C Frequency distribution of molecular differences as shown in B). Dashed lines indicate mean values.	151
3.5	SplitsTree and STRUCTURE analysis for Populations from Achtal and Blaubeuren. A SplitsTree analysis of AFLP data. Colors indicate resulting genotype groups, dashed lines indicate subpopulations. B Genetic assignment with STRUCTURE (K=2), coloured based on the SplitsTree analysis (A).	152

-
- 3.6 **Distribution of *D. gratianopolitanus* and molecular differences (AFLP fragments) for populations from Blaubeuren and the Achtal.** **A** Geographic distribution in the Achtal near Blaubeuren, coloured based on SplitsTree grouping. Coloured lines indicate possible dispersal events of the according coloured genotype. **B** Number of molecular differences between and within the growth sites, **C** Frequency distribution of molecular differences as shown in B). Dashed lines indicate mean values. 153
- 3.7 **SplitsTree and STRUCTURE analysis for Populations from the Hausener Wand, Michelsberg.** **A** SplitsTree analysis of AFLP data. Colors indicate resulting genotype groups, dashed lines indicate subpopulations. **B** Genetic assignment with STRUCTURE (K=2), coloured based on the SplitsTree analysis (A). 154
- 3.8 **Distribution of *D. gratianopolitanus* and molecular differences (AFLP fragments) for populations from the Hausener Wand, Michelsberg.** **A** Geographic distribution at the Hausener Wand, coloured based on SplitsTree grouping. Coloured lines indicate possible dispersal events of the according coloured genotype. **B** Number of molecular differences between and within the growth sites, **C** Frequency distribution of molecular differences as shown in B). Dashed lines indicate mean values. 155
- 3.9 **SplitsTree and STRUCTURE analysis for Populations from the Eybtal near Eybach.** **A** SplitsTree analysis of AFLP data. Colors indicate resulting genotype groups, dashed lines indicate subpopulations. **B** Genetic assignment with STRUCTURE (K=6), coloured based on the SplitsTree analysis (A). 156
- 3.10 **Distribution of *D. gratianopolitanus* and molecular differences (AFLP fragments) for populations from the Eybtal near Eybach.** **A** Geographic distribution in the Eybtal, coloured based on SplitsTree grouping. Coloured lines indicate possible dispersal events of the according coloured genotype. **B** Number of molecular differences between and within the growth sites, **C** Frequency distribution of molecular differences as shown in B). Dashed lines indicate mean values. 157
- 3.11 **SplitsTree and STRUCTURE analysis for Populations from the nature reserve Ehrenbürg, Bavaria.** **A** SplitsTree analysis of AFLP data. Colors indicate resulting genotype groups, dashed lines indicate subpopulations. **B** Genetic assignment with STRUCTURE (K=2), coloured based on the SplitsTree analysis (A). 158

3.12	Distribution of <i>D. gratianopolitanus</i> and molecular differences (AFLP fragments) for populations from the nature reserve Ehrenbürg, Bavaria. A Geographic distribution in the nature reserve Ehrenbürg, coloured based on SplitsTree grouping. Coloured lines indicate possible dispersal events of the according coloured genotype. B Number of molecular differences between and within the growth sites, C Frequency distribution of molecular differences as shown in B). Dashed lines indicate mean values.	159
3.13	SplitsTree and STRUCTURE analysis for Populations from Blankenberg and Höllental A SplitsTree analysis of AFLP data. Colors indicate resulting genotype groups, dashed lines indicate subpopulations. B Genetic assignment with STRUCTURE (K=7), coloured based on the SplitsTree analysis (A).	160
3.14	Distribution of <i>D. gratianopolitanus</i> and molecular differences (AFLP fragments) for populations from Blankenberg and Höllental. A Geographic distribution at Blankenberg and Höllental, coloured based on SplitsTree grouping. Coloured lines indicate possible dispersal events of the according coloured genotype. B Number of molecular differences between and within the growth sites, C Frequency distribution of molecular differences as shown in B). Dashed lines indicate mean values.	161
3.15	SplitsTree and STRUCTURE analysis for Populations from the nature reserve Korberfels and Bleiberg near Burgk A SplitsTree analysis of AFLP data. Colors indicate resulting genotype groups, dashed lines indicate subpopulations. B Genetic assignment with STRUCTURE (K=3), coloured based on the SplitsTree analysis (A).	162
3.16	Distribution of <i>D. gratianopolitanus</i> and molecular differences (AFLP fragments) for populations from the nature reserve Korberfels and Bleiberg near Burgk. A Geographic distribution along the Saale Tal near Burgk, coloured based on SplitsTree grouping. Coloured lines indicate possible dispersal events of the according coloured genotype. B Number of molecular differences between and within the growth sites, C Frequency distribution of molecular differences as shown in B). Dashed lines indicate mean values.	163
3.17	SplitsTree and STRUCTURE analysis for Populations from the Schwarzatal near Böhlischeiben and Schwarzburg A SplitsTree analysis of AFLP data. Colors indicate resulting genotype groups, dashed lines indicate subpopulations. B Genetic assignment with STRUCTURE (K=6), coloured based on the SplitsTree analysis (A).	164

- 3.18 **Distribution of *D. gratianopolitanus* and molecular differences (AFLP fragments) for populations from the Schwarzatal near Böhlscheiben and Schwarzburg.** **A** Geographic distribution in the Schwarzatal, coloured based on SplitsTree grouping. Coloured lines indicate possible dispersal events of the according coloured genotype. **B** Number of molecular differences between and within the growth sites, **C** Frequency distribution of molecular differences as shown in B). Dashed lines indicate mean values. 165
- 3.19 **SplitsTree and STRUCTURE analysis for Populations from Kellerwald-Edersee****A** SplitsTree analysis of AFLP data. Colors indicate resulting genotype groups, dashed lines indicate subpopulations. **B** Genetic assignment with STRUCTURE (K=2), coloured based on the SplitsTree analysis (A). . . 166
- 3.20 **Distribution of *D. gratianopolitanus* and molecular differences (AFLP fragments) for populations from Kellerwald-Edersee.** **A** Geographic distribution at Kellerwald-Edersee, coloured based on SplitsTree grouping. Coloured lines indicate possible dispersal events of the according coloured genotype. **B** Number of molecular differences between and within the growth sites, **C** Frequency distribution of molecular differences as shown in B). Dashed lines indicate mean values. 167
- 3.21 **SplitsTree and STRUCTURE analysis for Populations from the nature reserve Gans and Rheingrafenstein near Bad Münster am Stein-Ebernburg.****A** SplitsTree analysis of AFLP data. Colors indicate resulting genotype groups, dashed lines indicate subpopulations. **B** Genetic assignment with STRUCTURE (K=3), coloured based on the SplitsTree analysis (A). 168
- 3.22 **Distribution of *D. gratianopolitanus* and molecular differences (AFLP fragments) for populations from the nature reserve Gans and Rheingrafenstein near Bad Münster am Stein-Ebernburg.****A** Geographic distribution in the nature reserve Gans and Rheingrafenstein, coloured based on SplitsTree grouping. Coloured lines indicate possible dispersal events of the according coloured genotype. **B** Number of molecular differences between and within the growth sites, **C** Frequency distribution of molecular differences as shown in B). Dashed lines indicate mean values. 169
- 3.23 **Ecological niche modelling for *D. gratianopolitanus* for present day climate data.** **A** Prediction of present day niche for *D. gratianopolitanus*. Colours indicate suitability of the niche ranging from highly suitable (red) to unsuitable (blue). White dots show presence locations used for training and purple ones the test locations. **B** Model performance for training and test data. 172

3.24 **Ecological niche modelling for *D. gratianopolitanus* for present and future day climate data.** Ecological niche model for present day climate for calcareous **A** and siliceous+ bedrock **B**. Prediction of future niche for calcareous bedrock **C** and siliceous bedrock **D** using climate data from ssp1-2.6, and predictions for calcareous bedrock **E** and siliceous bedrock **F** using climate data from ssp3-7.0. Colours indicate suitability of the niche ranging from highly suitable (red) to unsuitable (blue). White dots show presence locations used for training and purple ones the test locations. 173

3.25 **Niche identity test between *D. gratianopolitanus* from calcareous and siliceous bedrock.** Expected distributions given as histogram (N=100) differs significantly ($p < 0.01$) from observed niche overlaps (dashed lines). . . . 174

A.1 **Number of AFLP bands in tetraploid and hexaploid *D. gratianopolitanus* from Southern France.** Comparison of number of AFLP bands of individuals from Massif Central and Diois 200

A.2 **Evanno statistic for the STRUCTURE analysis of the whole distribution data set for *D. gratianopolitanus* and *D. gratianopolitanus* subsp. *moravicus*.** **A** Optimal K as inferred by the evanno statistics K = 3 is indicated as optimal K. **B** evanno statistics for $K = 1$ to $K = 10$ 201

A.3 **STRUCTURE results for the whole distribution dataset of *D. gratianopolitanus*.** Number of clusters range from K=2 to K=8. Regions are numbered: 1) Massif Central, 2) Diois, 3) French Prealps, 4) French Jurassic, 5) Switzerland, 6) Bodensee region, 7) Swabian Alb, 8) Bavarian Jurassic, 9) Bavarian Serpentine, 10) Central Germany, 11) Brandenburg, 12) Czech Republic, 13) Poland, 14) Belgium and Luxembourg, 15) United Kingdom and 16) *Dianthus moravicus* from the Czech Republic. 201

A.4 **Distribution of spatial AFLP genetic structure** STRUCTURE analysis results are given for K = 2 as inverse distance weighted (idw) interpolation as background and K=3 as population means. A more detailed plot of genetic assignment is given in [Figure A.5](#) and [Figure A.6](#) 202

A.5 **Detailed STRUCTURE results for the whole distribution dataset of *D. gratianopolitanus*, K=3.** Part 1. The stars indicate metapopulations included in the metapopulation analysis of [Part III](#). 203

A.6 **Detailed STRUCTURE results for the whole distribution dataset of *D. gratianopolitanus*, K=3.** Part 2. The stars indicate metapopulations included in the metapopulation analysis of [Part III](#). 204

A.7	Linear relationship of latitude and AFLP statistics (mean) for populations by STRUCTURE assignment K=3 To ensure sufficient sample sizes and correct for population size, mean values were calculated on basis of n=5 subsamples per population. Populations were grouped by structure assignment with a threshold of > 75% population mean assignment to a cluster. Three different statistics are included: A number of bands, B number of polymorphic sites and C frequency-down-weighted marker.	205
A.8	Linear relationship of longitude and genome size (1Cx) Linear regression with colors indicating A different substrate types and B > 75% assignment to a STRUCTURE cluster (K=3). Grey colored points indicate an ambiguous assignment to clusters.	208
B.1	Linear regression of element accumulation rate with growth rate between April 2013 and August 2013. A Relationship of micro element accumulation rate and B Relationship of macro element accumulation rate and growth factor.	216
B.2	Comparison of fresh weight, water loss factor, and cushion size in August based on plant origin and treatment groups. Fresh weight was measured for above ground plant material at the experiment end in August 2013. The water loss factor indicates the times the dry weight is contained within the fresh weight and allows an estimation of the water content in the fresh plant material.	217
B.3	Linear regression of cushion size and above ground plant material weight at the end of the experiment in August Weight is given for fresh and dried plant material. Adjusted R-squared and p-value are given.	218
B.4	Principal component analysis of element concentrations comparing floriferous and non floriferous plants. All plants in the transplant experiment were included. Correlation circle and biplot with representation of floriferous (pink) and non floriferous (green) plants.	218
B.5	Growth behaviour of floriferous and non floriferous plants. Comparing the growth factor (Size in April / Size in August) for flowering and non flowering plants.	219
B.6	Linear regression and relationship of flowering number categories and cushion size category for flowering <i>D. gratianopolitanus</i> in 2022 and 2023	219
B.7	Flowering time comparison 2013, 2022 and 2023. Plants from the transplant experiment 2013 were subsetted from the years 2022 and 2023. Plants from 2013 were divided by home bedrock and the corresponding home substrate treatment.	221

B.8	Morphological differences in <i>Dianthus gratianopolitanus</i> flowers Pictures were taken during the flowering period 2024 in the Botanical Garden Heidelberg. A,B Kellerwald Edersee, nature reserve Sonderrain, Hesse; C Velky Bezdez, Czech Republic; D Le Chasseron, Switzerland; E Holzflue, Switzerland; F Strevic, Czech Republic; G Knoblauchfels near Blaubeuren, Baden-Württemberg; H Groß Bademeusel, Brandenburg; I Bad Urach, Baden-Württemberg; J Cheddar Gorge, England; K Danube Valley, Bandfelsen, Baden-Württemberg; L Wojaleite, Wurlitzer Serpentine, Bavaria; M Lenninger Tal, Schlatterhöhe, Baden-Württemberg; N nature reserve Bleiberg, Thuringia; O Le Grand Delmas, Dios, France; P Danube Valley, Hausener Zinnen, Baden-Württemberg; Q Wartburg, Thuringia; R Lenningertal, Sylphenwand, Baden-Württemberg; S Lenningertal, Sylphenwand, Baden-Württemberg; T Wartburg, Thuringia;	222
C.1	Heatmap of all bioclim variables highlighting correlations. Marked in yellow and light green are values either < -0.75 or > 0.75 , where the bioclimatic variable with the smaller contribution to the niche model using all <i>D. gratianopolitanus</i> is excluded from the final modeling step. Detailed values are given in Table C.3	224
C.2	Differences of the top three most contributing bioclim variables between the substrate types. Statistical significance is given for Wilcox test with Bonferroni correction. BIO4 (Temperature Seasonality, calculated by Standard Deviation (SD) of temperature ($^{\circ}\text{C} * 100$), BIO6 (Min Temperature of Coldest Month), BIO14 (Precipitation of Driest Month), BIO15 (Precipitation Seasonality, as Coefficient of Variation (%)), and BIO18 (Precipitation of Warmest Quarter).	225
C.3	Niche identity test in environmental space between <i>D. gratianopolitanus</i> from calcareous and siliceous bedrock. Expected distributions given as histogram (N=100) differs significantly ($p < 0.01$) from observed niche overlaps (dashed lines).	228

List of Tables

1	Ecological indicator values for <i>D. gratianopolitanus</i> after Ellenberg (Ellenberg et al., 1992) and Landolt (Landolt, 1977). Table adapted from (Banzhaf et al., 2009)	6
2.1	<i>Dianthus</i> species included in plastome analysis List of species, their sample origin, Lab-internal LabID and official HEID-number under which they can be found in the database of the Botanic garden Heidelberg (gartenbank.cos.uni-heidelberg.de)	32

2.2	Species and GenBank accession numbers List of additional species from the genus <i>Dianthus</i> as well as representatives from the family Caryophyllaceae used as outgroup for the plastome analysis and their corresponding accession numbers.	32
3.1	Summary statistics of AFLP data of <i>D. gratianopolitanus</i> per region. Numbering of regions, number of investigated individuals per region (N), number of AFLP fragments (F_{tot}), number of polymorphic sites (F_{poly}), mean number of bands per individual (F_{bands}), number of unique alleles (F_{unique}), mean number of rare alleles (F_{rare}), total number of rare alleles found in the population ($F_{\text{rare total}}$), frequency-down-weighted marker values (DW) and Average gene diversity over loci (Arlequin) H . To take different sample sizes into account mean values and standard deviation were calculated by repeated subsampling. * Minimum subsample size was set to $n = 13$ the number of individuals from Poland.	39
3.2	Analysis of Molecular Variance (AMOVA) for genetic variation in <i>D. gratianopolitanus</i> based on AFLP data Significance test were performed in Arlequin v.3.5.2.2. with 1023 permutations ($p < 0.01$). Fixation indices were calculated: $F_{\text{SC}} = 0.13080$, $F_{\text{ST}} = 0.17036$, $F_{\text{CT}} = 0.04552$. . .	39
3.3	Summary on found plastid haplotypes per region. For each region the number of analysed individuals (N), number of different haplotypes ($N_{\text{ht_total}}$), number ($N_{\text{ht_unique}}$) and name of plastid haplotypes unique to this region as well as the gene diversity (Arlequin) is given. Especially the three French regions, from the Massif Central (MC), Diois and the prealps show high amounts of unique haplotypes and high gene diversity. One haplotype (ht14) is restricted to <i>D. gratianopolitanus</i> subsp. <i>moravicus</i>	41
3.4	AMOVA of plastid haplotypes Analysis of molecular variance calculated using Arlequin for (a) by regions, (b) by bedrock type	42
2.1	List of individuals included in analysis List of <i>Dianthus gratianopolitanus</i> with lab-internal LabID, sampling origin and substrate of origin. Table adapted from (Strobel, 2014). The geographic locations are given in Figure 2.1.	76
3.1	pH measurement of the treatment soils pH measurement of the used treatment soils including ground serpentine and measurement of unfiltered and filtered solutions. All samples show neutral to slightly alkaline reaction, with the only exception in the slightly acidic reaction of the filtered ground serpentine.	86

3.2 **Mean Element Concentrations in Treatment Soil** Total element concentration and plant available (exchangeable) element concentrations measured for all treatment soils as well as ground serpentine soil. The number of replicates N per treatment soil is given in brackets. The corresponding plot is given in [Figure 3.1](#). 88

3.3 **Mean element concentration in leaf material.** Results are grouped either by origin: with calcareous ($n = 31 * 3 = 93$, plants from the calcareous range in all three treatments) or siliceous origin ($n = 26 * 3 = 78$), or per treatment with the limestone ($n = 57$), porphyry ($n = 57$) and serpentine treatment ($n = 57$). 89

3.4 **Growth behaviour of plants in the experiment, based on origin and treatment groups).** a) Mean cushion sizes measured in April and August 2013, b) Mean fresh and dry weight of above ground plant matter harvested at the end of the experiment in 2013. 97

3.5 **Flowering frequency overview based on origin bedrock and treatment group.** The total number of plants as well as the number and percentage of flowering and non flowering *D. gratianopolitanus* grouped by substrate of origin and treatment is given. The result is also given in [Figure 3.6 A](#) . . . 98

3.1 **Summary statistics of AFLP data of *D. gratianopolitanus* per region.** Numbering of regions, number of investigated individuals (N), number of AFLP fragments (F_{tot}), number of polymorphic sites (F_{poly}), mean number of bands per individual (F_{bands}), number of unique alleles (F_{unique}), brackets indicate number of unique alleles unique to this site), mean number of rare alleles (F_{rare}), total number of rare alleles found in the population ($F_{rare total}$), frequency-down-weighted marker values (*DW*) and Average gene diversity over loci (Arlequin) H. Investigated populations from siliceous and volcanic bedrock. To take different sample sizes into account mean values and standard deviation for metapopulations were calculated by repeated drawing and calculation for 20 random individuals per metapopulation and calculation of mean and standard deviation. The name addition (C) indicates populations are from calcareous bedrock. 137

- 3.2 **Summary statistics of AFLP data of *D. gratianopolitanus* per region.** Numbering of regions, number of investigated individuals (N), number of AFLP fragments (F_{tot}), number of polymorphic sites (F_{poly}), mean number of bands per individual (F_{bands}), number of unique alleles (F_{unique} , brackets indicate number of unique alleles unique to this site), mean number of rare alleles (F_{rare}), total number of rare alleles found in the population ($F_{\text{rare total}}$), frequency-down-weighted marker values (DW) and Average gene diversity over loci (Arlequin) *H*. Investigated populations from siliceous and volcanic bedrock. To take different sample sizes into account mean values and standard deviation for metapopulations were calculated by repeated drawing and calculation for 20 random individuals per metapopulation and calculation of mean and standard deviation. The name addition (C) indicates populations are from calcareous bedrock. 138
- 3.3 **Summary statistics of AFLP data of *D. gratianopolitanus* per region.** Numbering of regions, number of investigated individuals (N), number of AFLP fragments (F_{tot}), number of polymorphic sites (F_{poly}), mean number of bands per individual (F_{bands}), number of unique alleles (F_{unique} , brackets indicate number of unique alleles unique to this site), mean number of rare alleles (F_{rare}), total number of rare alleles found in the population ($F_{\text{rare total}}$), frequency-down-weighted marker values (DW) and Average gene diversity over loci (Arlequin) *H*. Investigated populations from siliceous and volcanic bedrock. To take different sample sizes into account mean values and standard deviation for metapopulations were calculated by repeated drawing and calculation for 20 random individuals per metapopulation and calculation of mean and standard deviation. The name addition (S) indicates metapopulation from siliceous bedrock. 139
- 3.4 **Summary statistics of AFLP data of *D. gratianopolitanus* per region.** Numbering of regions, number of investigated individuals (N), number of AFLP fragments (F_{tot}), number of polymorphic sites (F_{poly}), mean number of bands per individual (F_{bands}), number of unique alleles (F_{unique} , brackets indicate number of unique alleles unique to this site), mean number of rare alleles (F_{rare}), total number of rare alleles found in the population ($F_{\text{rare total}}$), frequency-down-weighted marker values (DW) and Average gene diversity over loci (Arlequin) *H*. Investigated populations from siliceous and volcanic bedrock. To take different sample sizes into account mean values and standard deviation for metapopulations were calculated by repeated drawing and calculation for 20 random individuals per metapopulation and calculation of mean and standard deviation. The name addition (C) indicates populations are from calcareous bedrock. 140

3.5	Summary statistics of AFLP data of <i>D. gratianopolitanus</i>. Mean values per substrate of origin based on metapopulation means. Number of AFLP fragments (F_{tot}), number of polymorphic sites (F_{poly}), mean number of bands per individual (F_{bands}), , mean number of rare alleles (F_{rare}), total number of rare alleles found in the population ($F_{\text{rare total}}$), frequency-down-weighted marker values (DW) and sum of unique alleles (F_{uni} in pop.) in the populations and number of unique alleles (F_{uni} per sub) to calcareous or siliceous bedrock. In addition the statistic for the calcareous range excluding the metapopulation from Ehrenbürg, as well as the calcareous range excluding both the metapopulation from Ehrenbürg and the Swiss metapopulation is given.	141
3.6	Contribution of the used bioclimatic variables to the Maxent models for all <i>D.gratianopolitanus</i> (300 samples), those from calcareous bedrock (200 samples) and siliceous bedrock (96 samples).	171
A.1	Permits acquired for sample collection of leaf material and cuttings of <i>D. gratianopolitanus</i>. Country, issuing authority, date of permit and licence number is given. The corresponding files as well as a more detailed overview is given in the Digital Supplement. A permission to collect serpentine substrate from the natural habitat in Wojaleite is also included.	196
A.2	SNP matrix of the plastid marker <i>trnL-trnF</i>. The alignment position refers to the alignment given in the Digital Supplement: haplotypes_ Dg_ Dm.fas	197
A.3	SNP matrix of the plastid marker <i>trnC-ycf6</i>. The alignment position refers to the alignment given in the Digital Supplement: haplotypes_ Dg_ Dm.fas	198
A.4	SNP matrix of the plastid marker <i>trnH-psbA</i>. The alignment position refers to the alignment given in the Digital Supplement: haplotypes_ Dg_ Dm.fas	199
A.5	Ploidy and genome size of <i>D. gratianopolitanus</i> Comparison of ploidy inferred by chromosome counting (CC) and flow cytometry (FCM). Red individuals shwed differences in ploidy between the methods. Due to good accordance of the genome size the FCM result was trusted.	206
A.6	Combined plastid haplotypes for <i>Dianthus gratianopolitanus</i>. Only individuals with fully known sequence or unambiguous assignment were used.	207
A.7	Ploidy of <i>D. gratianopolitanus</i> and <i>Dianthus gratianopolitanus</i> subsp. <i>moravicus</i> Ploidy by region as inferred by Flow Cytometry	208
B.1	Analytical (spectral) lines and concentrations (in ppm) of the internal standards used in ICP OES. Several spectral lines with different wavelengths per element are used to infer the final element concentrations.	210

B.2	Summary of elemental differences between substrate of origin as well as treatment groups. Mdn give the medians in $\mu\text{g/g}$, p-value of Mann-Whitney U test, effect size r calculated based on Wilcoxon results as well as its respective confidence interval (95% CI). Significant results ($p < 0.05$) are highlighted.	211
B.3	Summary of elemental differences between substrate of origin within each treatment group. Mdn give the medians in $\mu\text{g/g}$, p-value of Mann-Whitney U test, effect size r calculated based on Wilcoxon results as well as its respective confidence interval (95% CI). Significant results ($p < 0.05$) are highlighted.	212
B.4	Summary of element accumulation rate differences between substrate of origin between as well as within each treatment group. Mdn give the medians, p-value of Mann-Whitney U test, effect size r calculated based on Wilcoxon results as well as its respective confidence interval (95% CI). Significant results ($p < 0.05$) are highlighted.	213
B.5	Summary of fitness differences between substrate of origin between as well as within each treatment group. Mdn give the medians, p-value of Mann-Whitney U test, effect size r calculated based on Wilcoxon results as well as its respective confidence interval (95% CI). Significant results ($p < 0.05$) are highlighted.	214
B.6	Correlation of element accumulation rate to Size in April, Size in August and the growth factor	215
B.7	Correlation of leaf element concentration and number of flowers in flowering plants	215
B.8	Flowering time in 2022 and 2023. Start of flowering as opening of the first flower, maximum flowering as date with most flowering plants, end of flowering as wilthing of the last flower, and start date for temp. sum as date where the back calculated cumulative temperature sum reaches 865°C	220
C.1	Plastid marker haplotypes in <i>D. gratianopolitanus</i> populations from calcareous bedrock. Only cases where unambiguous data was available was used. Here only the most common haplotypes (see Appendix Table A.6) were found.	226
C.2	Plastid marker haplotypes in <i>D. gratianopolitanus</i> populations from siliceous bedrock. Only cases where unambiguous data was available was used. Here only the most common haplotypes (see Appendix Table A.6) were found.	227
C.3	Pairwise Pearson correlation of bioclim variables. Marked in yellow are values either < -0.75 or > 0.75 , where the bioclimatic variable with the smaller contribution to the niche model using all <i>D. gratianopolitanus</i> is excluded from the final modeling step.	227

Acknowledgements - Danksagung

First of all, I would like to thank my doctoral supervisor Prof. Dr. Marcus Koch for giving me the opportunity to work on this fascinating project and for the chance to grow with it. Many thanks to Prof. Dr. Alex Widmer and Dr. Mike Thiv for their participation in my Thesis Advisory Committee and for helpful discussions and suggestions. Furthermore, I would like to thank Dr. Mike Thiv for taking on the role of second referee. I would also like to thank Prof. Dr. Rüdiger Hell and Prof. Dr. Thomas Rausch for their participation in my examination committee.

I am extremely thankful for the entire AG Koch, for creating an open, fun, and supportive atmosphere. I thank Dr. Christiane Kiefer for her support, encouragement, and proofreading. With her ability to cheer everyone up and the nice chats in between it is always a pleasure to work with her; Dr. Nora Walden for her support in the preparation for the conferences, which helped me greatly to present the project to a broader audience and Dr. Markus Kiefer for the technical support and help with Linux and R. A big thank you and the credit for the laboratory work and goes to Anna Loreth. I want to thank Dr. Peter Sack for helping with every concern regarding the Botanical Garden Heidelberg, for cheering up every day at work, and for the fun and instructive conversations during the many field trips to the Pyrenees, the Emsland, Austria, and the Vanoise National Park. Many thanks to my fellow PhD students, Laura Kellermann, Jonas Bleilevens, Johanna Möbus, Sarina Jabbusch, and Eric Stein for the fun times, their open ears and friendship, and the daily walks to the Botanical Garden. Thanks to you, the PhD time was always fun even during stressful times. I will also always cherish the time we spent on the trip to the Vanoise National Park! I would like to thank the whole team of the Botanical Garden in Heidelberg, especially Jonas Silbermann for taking care of the *Dianthus* cultivated in the greenhouses and the help with the flowering documentation in 2022 and 2023. I am grateful for the support from external institutions and cooperation partners, among other things for granting the permits to collect the plants and leaf material at the beginning of the project, providing the climate data for Heidelberg, and for the help with the substrate experiment from the Team of Ute Krämer.

I would like to thank Arnulf, Max, and Ella for the weekly distractions, and Max, Georg, and Anna for the constant encouragement, support, and years of friendship. I am very

grateful to my family, my mother Heide, my father Wini and Ina and my brothers Jonas and Fabi as well as Juli, Emmi and Thea. Thank you for your continuous support, patience and encouragement during these many years of study. Finally, I would like to thank my husband Moritz, who supports me in everything, always has my back, and has provided encouragement, motivation, and a kick in the butt at the right moments. None of this would have been possible without you.

Affidavit

Sworn Affidavit according to § 8 of the doctoral degree regulations of the Combined Faculty of Mathematics, Engineering and Natural Sciences at Heidelberg University

1. The thesis I have submitted entitled

.....
.....

is my own work.

2. I have only used the sources indicated and have not made unauthorized use of services of a third party. Where the work of others has been quoted or reproduced, the source is always given.

3. I have not yet presented this thesis or parts thereof to a university as part of an examination or degree.

4. I confirm that the declarations made above are correct.

5. I am aware of the importance of a sworn affidavit and the criminal prosecution in case of a false or incomplete affidavit.

I affirm that the above is the absolute truth to the best of my knowledge and that I have not concealed anything.

Place and Date

Signature

Infobox: Bitte denken Sie daran, dass eine Eidesstattliche Erklärung ohne Seitenzahl und ohne im Inhaltsverzeichnis zu erscheinen in die bestehende Arbeit aufgenommen wird. Einige Hochschulen sehen anstelle der Eidesstattlichen Erklärung eine Ehrenwörtliche Erklärung vor. Hier sollten Sie sich über die jeweiligen Vorgaben Ihrer Hochschule bzw. Ihrer Fakultät informieren.